Epigenetic Regulation of Postnatal Subventricular Zone Development

A thesis submitted to the Department of Physiology, Anatomy and Genetics, in partial fulfilment of the requirements for the degree of

Doctor of Philosophy

by

Bin Sun

St Peter's College, University of Oxford, United Kingdom

Trinity 2015

For my family

ABSTRACT

Epigenetic Regulation of Postnatal Subventricular Zone Development

Sun, Bin. St Peter's College

Submitted for D.Phil. Trinity 2015.

The postnatal/adult subventricular zone (SVZ) harbours neural stem cells (NSC), which produce neurons that migrate to the olfactory bulbs. SVZ NSC share several biological features with glia, especially reactive astrocytes. However, it is not clear how SVZ NSC simultaneously maintain self-renewal stem cell properties and the potential for generating daughter cells that differentiate into neurons.

Multiple cyclin-dependent kinase inhibitors (CDKIs), including p16, p19 and p21 have been identified as indispensable for maintaining stem cell potential, in both cyclin dependent and independent manners. However, how these CDKIs are coordinated remains poorly defined. One possible regulator of CDKIs is the canonical Polycomb Repressive Complex 2 (PRC2) that consists of Eed, Suz12, and Ezh2. Ezh2 functions to methylate lysine 27 of histone 3 (H3K27me3) and consequently suppresses target gene expression. Whereas PRC2 serves to balance self-renewal versus differentiation and neuron versus glial fate choices in early and late embryogenesis, respectively, our understanding of its role in the neonatal and adult SVZ is incomplete. In this thesis, I discovered that the PRC2 core subunit Eed, but not Ezh2, was expressed in SVZ NSC. Eed directly repressed p16 and p19, but indirectly fine-tuned p21 expression in SVZ NSC. Conditional deletion or knockdown of Eed in vivo led to loss of constitutive SVZ stemness and blocked NSC activation. This was partly due to selective activation of the PRC2 targets, Cdkn2a and Gata6; in contrast Ezh2 loss of function only activated Cdkn2a but not Gata6. In the SVZ, Gata6 overexpression was sufficient to limit the neurogenic ability of NSC and also inhibited p21 post-transcriptional expression. I also showed that although reactive astrocytes in the cerebral cortex can acquire stem cell properties in response to brain injury, Eed was not involved in this process. Taken together, I identified novel and divergent regulation of SVZ CDKIs by separate subcomponents of PRC2, and showed that these are essential for SVZ NSC maintenance. Whilst this regulatory pathway was specific in the neurogenic niche it had little influence on parenchymal astrocytes.

In a relatively small side project, I screened and identified several long non-coding RNAs (lncRNA) that were highly expressed in the adult rodent SVZ. The lncRNA *Paupar*, which is transcribed upstream from the *Pax6* antisense strand, was enriched in the postnatal SVZ and regulated Pax6 and Ezh2 expression. In vivo, *Paupar* knockdown showed it is necessary for stem cell maintenance and thus regulates postnatal neurogenesis.

To conclude, I discovered two interacting epigenetic regulators that control postnatal SVZ NSC and neurogenesis.

ACKNOWLEDGEMENT

My D.Phil time in Oxford has been a precious and pleasant experience. I have endeavoured to cope with challenges from every aspect, e.g. science, language, life, etc. My family, supervisor, friends and colleagues are continually around to guide and encourage me whenever I met difficulties, and make me through these 4 years.

First, I would like to thank my supervisor, Prof. Francis Szele, from the very beginning when he accepted me into the lab. Francis is a great supervisor and gives comprehensive guidance, and at the same time allows developing my independence in research. Discussions with Francis have inspired many new thoughts in science and career. In addition, as a group leader, Francis is always trying to create a harmonious working environment, and stimulate new collaborative ideas.

Meanwhile, Dr. Eunhyuk Chang, a former senior graduate student in Szele lab, acted as my day-by-day mentor when I first joined the lab. Ms. Kate Milne, Ms. Anna Gerhartl, Ms. Jie Yao and Mr. Xinheng Zhang are young scientists who I enjoyed the supervising and also from whom I have learned a lot as well. Dr. Christopher Young, Dr. Rachel James, Dr. Rod Walker, Dr. Tracy Lane, Dr. James Hillis, Dr. Osama Aldalahmah, Dr. Istvan Adorjan, Dr. Julie Davies, Dr. Keith Vance, Ms. Abeer Al-shammari, Mr. Martin Ducker, Ms. Yichen Li, and Ms. Mayara Vieira are nice colleagues to work with. They are constantly willing to share their experience in scientific research and have improved me intellectually. Prof. Zoltan Molnar, Prof. Richard Wade-Martins, Prof. Shankar Srinivas and Prof. Matthew Wood are always kind to allow me to work in their facilities, which made lots of experiments happen. Prof. Neil Brockdorf offered many valuable suggestions to develop the project, too.

I also want to express gratitude to Prof. Magdalena Götz, Prof. Alexander Tarakhovsky, Prof. Rick Livesey, Dr. Francois Guillemot, Prof. Colin Akerman, Prof.

Stuart Orkin, Dr. Huafeng Xie, Prof. Xin Lu and Prof. Xiaohua Shen for their technical support and sharing reagents, including various transgenic mice and constructs. The staff in Department of Biomedical Services also provided tremendous help with my animal colony management and surgery advice. A few names I want to acknowledge include Ms. Denise Jelfs, Ms. Angela Cooke, Ms. Laura Thomas, Mr. James Ward, Mr. Simon Whitfield, and Mr. Richard Maxwell, without whom my experiments would not have been carried out successfully. Thanks to FS and MD for their proofreading of the thesis.

The China Scholarship Council was generous to fund my studies and living expenses in Oxford for three years, and gave me the opportunity to work in this country and I really appreciate it. The Henry Lester Trust also financially supported my study and I want to thank Mr. James Adams in the trust for his assistance.

Finally, I am grateful for my family. My parents are always understanding and supportive of my studies in a foreign country. I have to apologize to them that I could not be available anytime they needed me. Also I would love to thank myself for striving to the last minute no matter what problems arose. It is a pity that my grandmother (1923-2013) is unable to hear my joy from this journey. May she rest in peace.

AUTHORSHIP STATEMENT

I primarily designed the project in this thesis under the supervision of Prof. Francis Szele.

In Chapter 3, Ms. Kate Milne helped to characterize the Ezh2 antibody and Ms. Anna Gerhartl helped with the analysis of Ezh2 expression in SVZ cell types. Anna also quantified the Ezh2 in GFAP+ and Sox2+ cells in the SVZ. The MCAO surgery was performed by Dr. Christopher Young.

In Chapter 4, Kate helped to confirm the loss of Ezh2 by immunohistochemistry in cKO SVZs and also analysed the phenotypes in P14 Ezh2 cKO mice. Anna helped with the immunohistochemistry in P75 Ezh2 cKO SVZ.

In Chapter 5, Dr. Isabelle Comte performed the cortical lesion surgery and carried out the microarray analysis along with Dr. Edward Kang and Ms. Gwendolyn Goings.

In Chapter 6, Dr. Keith Vance carried out qPCR for *Paupar* expression and in *Paupar* knockdown neurospheres. He also performed the CHART-Seq and the bioinformatics analysis.

All other experimental procedures, quantifications and analyses were done by me with experimental advice from colleagues in the department.

TABLE OF CONTENTS

Word count: ~42,885

LIST OF FIGURES

Chapter 1

Chapter 2

Chapter 3

Chapter 4

Chapter 5

Chapter 6

Chapter 7

Appendices

LIST OF TABLES

Chapter 1

Chapter 2

Chapter 6

Appendices

ABBREVIATIONS

Ara-C	Cytosine-β-D-arabinofuranoside
BLBP	brain lipid binding protein
BMP	bone morphogenetic protein
BrdU	5-bromo-2'-deoxyuridine
cc	corpus callosum
CDKI	cyclin-dependent kinase inhibitor
ChIP	chromatin-immunoprecipitation
cKO	conditional knockout
CSC	cancer stem cells
CSF	cerebrospinal fluid
DAPI	4',6-diamidino-2-phenylindole
Dcx	doublecortin
DIV	day in vitro
dpe	days post electroporation
dpi	days post injury
Eed	embryonic ectoderm development
EGF	epidermal growth factor
EGFR	epidermal growth factor receptor
ESC	embryonic stem cell
Ezh2	enhancer of zeste homolog 2
FACS	fluorescence-activated cell sorting
FBS	fetal bovine serum
FGF	fibroblast growth factor
GCL	granule cell layer
GFAP	glial fibrillary acidic protein
GFP	green fluorescent protein
GL	glomerular layer

Glast	glutamate aspartate transporter
H3K27me3	histone 3 lysine 27 trimethylation
HDAC	histone deacetylases
iPSC	induced pluripotent stem cell
ISH	in *situ* hybridization
KD	knockdown
lncRNA	long non-coding RNA
LRC	label retaining cells
LV	lateral ventricle
MCAO	middle cerebral artery occlusion
miR	microRNA
NeuN	neuronal nuclei
NSC	neural stem cells
OB	olfactory bulb
PBS	phosphate buffered saline
PBST	phosphate buffered saline with Tween
PCR	polymerase chain reaction
PDGF	platelet-derived growth factor
PFA	paraformaldehyde
PHi3	phosphorylated histone H3
PRC	polycomb repressive complex
PSA-NCAM	polysialylated neural cell adhesion molecule
qPCR	quantitative PCR
RBP	RNA binding protein
RMS	rostral migratory stream
RNAi	RNA interference
SD	standard deviation
SEZ	subependymal zone
SGZ	subgranular zone

Shh	sonic hedgehog
shRNA	short hairpin RNA
str	striatum
SVZ	subventricular zone
TBI	traumatic brain injury
TMX	tamoxifen
TrxG	Trithorax group
UTR	untranslated region

Chapter 1

Introduction

1.1 Stem cells in adult brains

1.1.1 Postnatal and adult subventricular zone

The subventricular zone (SVZ, also known as subependymal zone, SEZ), lines the lateral ventricles and is a mitotically active area containing neural stem cells (Figure 1.1) (Doetsch et al. 1999; Spassky et al. 2005; Ihrie and Alvarez-Buylla 2011). It consists of three main cell types, each with different morphologies, markers and cellular behaviours (Ming and Song 2011). Initial stem/progenitor cells (B cells) are astrocyte-like. They divide and give rise to transit amplifying cells (C cells) that divide rapidly and generate neuroblasts (A cells), which migrate as the rostral migratory stream (RMS) to the olfactory bulb (OB), where they normally differentiate into granule or periglomerular interneurons (Ihrie and Alvarez-Buylla 2011). Fluorescence-activated cell sorting (FACS) has shown that SVZ cell subtypes can be isolated according to the combined expression of cell markers: niche astrocytes ($GFAP^+EGFR^-CD24^-$), stem cell astrocytes ($GFAP^+EGFR^+CD24^-$), transit amplifying cells ($GFAP^-EGFR^+CD24^-$), and neuroblasts ($GFAP^-EGFR^-CD24^{low}$) (Pastrana et al. 2009). Other cell markers that identify SVZ cell subtypes include brain lipid binding protein (BLBP) for stem cell astrocytes; the basic helix-loop-helix (bHLH) transcription factor Mash1 for progenitors; and doublecortin (Dcx), a microtubule-associated protein, for migratory neuroblasts (Ihrie and Alvarez-Buylla 2011).

The RMS is the major neuronal migratory region in the postnatal mammalian brain. After their generation in the SVZ, neuroblasts migrate rostrally in a stream to feed into the olfactory bulb. Both intrinsic and extrinsic signals guide the neuroblasts in highly directed neuronal "chains" (Ghashghaei et al. 2007). For example, poly-sialated neural cell adhesion molecule (PSA-NCAM) is required to form migratory

chains in the RMS (Ono et al. 1994). In NCAM-deficient mice, the neuroblast migration is disrupted with accumulated cells in the RMS as a consequence (Tomasiewicz et al. 1993). On the other hand, localized neuronal injury in adult brain has been proven to induce neurogenesis and ectopic neuronal migration towards the site of injury showing that homeostatic directional cues can be altered or superseded (Goings et al. 2004; Ramaswamy et al. 2005; Sundholm-Peters et al. 2005). To some

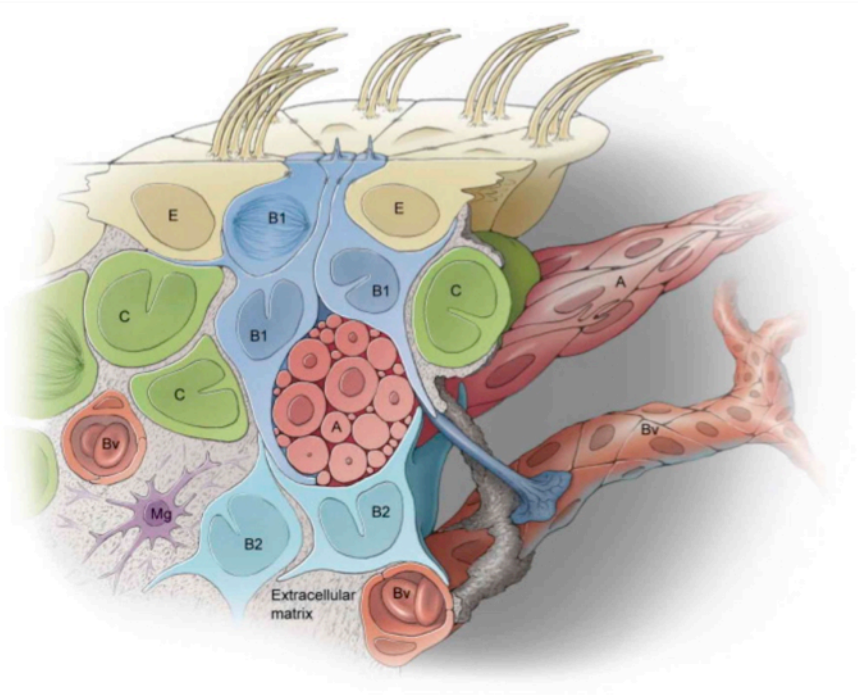

Figure 1. 1 Cytoarchitecture of the adult SVZ

Multiciliated ependymal cells (E) line the lateral ventricle. Astrocyte-like NSC (B1) locate in the centre of pinwheel structures formed by ependymal cells. The apical primary cilium of NSC is in contact with the lateral ventricle and basal process contact blood vessels (Bv). Niche astrocytes (B2) on the other hand are away from the lateral ventricle. NSC can generate transit amplifying cells (C), which will produce neuroblasts (A). Microglia (Mg) can also be found in the SVZ. (Figure adapted from Ihrie and Alvarez-Buylla 2011)

extent, migration in the model of brain injury shares common mechanisms to that in the RMS. After cortical lesion, the expression of PSA-NCAM increased in the SVZ, which suggests the involvement of this adhesion molecule in modulating neuronal migration (Szele and Chesselet 1996; Macas et al. 2006). Moreover, how neuroblasts move through brain extracellular matrix (ECM) after stroke has been studied. The migration of neuroblasts was found to decrease after the application of matrix metalloproteinase (MMP) inhibitors GM6001 and FN-439 (Lee et al. 2006a; Kang et al. 2008). Studies about blood vessels demonstrated that neuroblasts migrate along them as scaffolds, towards the ischemic region (Kojima et al. 2010). However, it is currently unclear what the entire signal networks are and how they respond to brain injuries for regulating neural progenitor migration in adult mammalian brain.

1.1.2 Subventricular zone in human brain

The stem cell population in the postnatal and adult SVZ serves as a potential therapeutic tool for brain repair. However, for a long time, the existence of neurogenesis in the adult human SVZ has been questioned (Curtis et al. 2007; Sanai et al. 2007). From the perspective of cytoarchitecture, the human SVZ can be divided into four layers: (1) ependymal layer; (2) hypocellular gap, astrocytic processes primarily constitute this layer with the processes entering the ependymal layer; (3) astrocytic ribbon formed by cell bodies of astrocytes; and (4) transitional zone where a large amount of myelin is found (Figure 1.2) (Sanai et al. 2004; Quinones-Hinojosa et al. 2006; Quinones-Hinojosa and Chaichana 2007). Migratory neuroblasts have been found in the anterior human SVZ, though no obvious migratory chains exist (Quinones-Hinojosa et al. 2006; Wang et al. 2011). Neurogenesis in the human SVZ

seems to be limited to early neonatal ages, namely 18 months, but disappears in the healthy adult human brain (Sanai et al. 2011). On the other hand, the adult human SVZ can generate self-renewable and multipotent neurospheres in vitro and may also be a source of cancer stem cells giving rise to glioblastomas in vivo (Lim et al. 2007; Quinones-Hinojosa and Chaichana 2007; Sandberg et al. 2014). These studies, taken together indicate that homeostatic neurogenic ability may be restrained in the human SVZ niche.

Evaluation of the nuclear bomb test-derived ^{14}C in genomic DNA provides another approach for neurogenesis study in human brain. Birth date analysis suggested no newborn neurons generated in the human OB postnatally, supporting previous data (Sanai et al. 2011; Wang et al. 2011; Bergmann et al. 2012). Instead, postnatal-born interneurons could be identified in the striatum, but it is elusive whether these newborn cells were generated locally or originated from the SVZ (Ernst et al. 2014).

A non-RMS migratory stream has also been described in human brain, which added new neurons into the prefrontal cortex, instead of to the OB (Sanai et al. 2011). Although the OB is the primary destination of SVZ neurogenesis in rodents, lobus parolfactorius in the striatum receives most newborn neurons in songbirds (Alvarez-Buylla et al. 1994; Kaslin et al. 2008). Hence, it seems adult neurogenesis is refined during evolution and may be closely relevant to specific behaviours in individual species. The role of neurogenesis in human prefrontal cortex remains to be assessed.

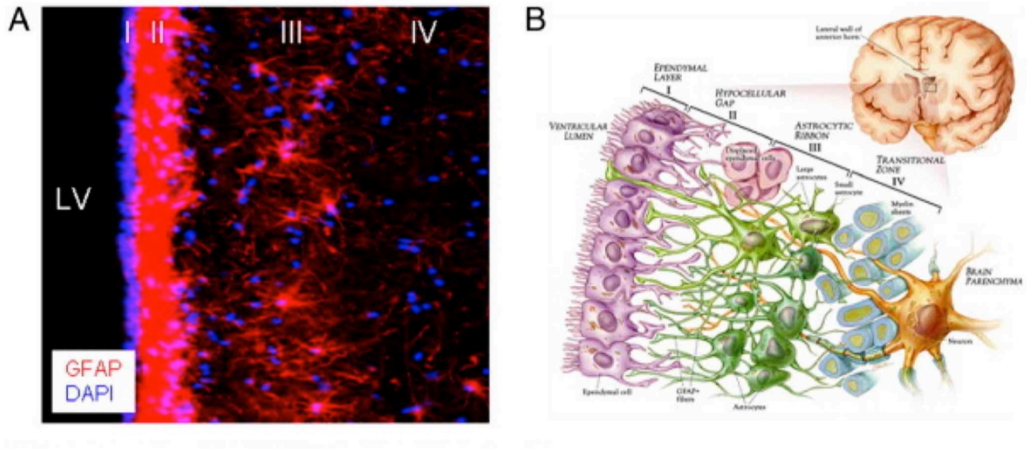

Figure 1. 2 Cytoarchitecture of the adult human SVZ

(A) GFAP+ cell ribbon can be found in the human SVZ. (B) Schematic structure of the human SVZ, which can be divided into four layers: ependymal layer, hypocellular gap, astrocytic ribbon and transitional zone. (Figure adapted from Quinones-Hinojosa and Chaichana 2007)

1.1.3 Molecular regulation of neurogenesis in SVZ

Extensive research in rodents has demonstrated regulation of SVZ neurogenesis via several molecular levels and families. Multiple aspects of the overall process of neurogenesis are under tight control to guarantee the proper number, type and placement of newborn neurons in the OB: stem cell maintenance, cell cycle, fate choices, cell migration, cell death, differentiation, etc.

NSC maintenance Both intracellular and extracellular signalling is reported to maintain SVZ NSC. Transcription factors are able to control gene expression directly: either to repress differentiation related genes or to promote self-renewal related genes. The zinc finger protein Ars2, cyclin-dependent kinase inhibitor p21 and E2f3 isoforms are all required to directly modulate Sox2 expression to maintain the stem

cell identity in the SVZ (Andreu-Agullo et al. 2012; Julian et al. 2013; Marques-Torrejon et al. 2013). Extracellular molecules from the neurogenic niche endothelial cells, ependymal cells and choroid plexus, on the other hand, function in a non-cell autonomous manner. Notch ligand, Dll1 controls NSC asymmetric division and balances the activated versus quiescent NSC populations (Kawaguchi et al. 2013). Neurotrophin-3 and thyroid hormone also function in SVZ NSC maintenance through TrkC or Sox2, respectively (Lopez-Juarez et al. 2012; Delgado et al. 2014). Though several upstream regulators of Sox2 have been documented, the complete role of Sox2 itself is relatively unknown in the postnatal and adult SVZ. Lessons from another neurogenic niche, the hippocampal subgranular zone (SGZ) study suggested Sox2 promotes sonic hedgehog signalling to maintain the SGZ NSC population (Favaro et al. 2009). SVZ NSC possess a primary cilium that senses signals in the cerebrospinal fluid (CSF). Igf1 in the CSF stimulates NSC proliferation in the developing forebrain and is upregulated in glioblastoma patients (Lehtinen et al. 2011). Similar effects could also be found in the SGZ NSC (Falcao et al. 2012; Ziegler et al. 2015). Sonic hedgehog, BMP, EGF, FGF and retinoic acid in the CSF all contribute to NSC as well (Lehtinen and Walsh 2011; Falcao et al. 2012).

Fate choice During SVZ neurogenesis, neuronal versus glial and neuronal subtypes must be determined in the NSC lineage progression. Transcription factors such as Pax6, Mash1 and Olig2 play essential roles in lineage commitment. Although Pax6 was believed to govern SVZ-derived dopaminergic neuron specification in the OB, recent work highlighted its role in driving general neurogenesis against gliogenesis (Kohwi et al. 2005; Weinandy et al. 2011; Ninkovic et al. 2013). Meanwhile, Olig2 contributes to both oligodendrocyte and astrocyte differentiation in the postnatal SVZ (Marshall et al. 2005; Cai et al. 2007). Interestingly, despite

multipotency, neurospheres cultured from the SVZ express Olig2 in all cells and Olig2 is also present in a large proportion of transit amplifying cells in vivo (Hack et al. 2004; Parras et al. 2004). Thus it needs to be investigated whether Olig2 is involved in OB neuronal subtype specification as during embryonic interneuron development (Zhou and Anderson 2002). Recent studies highlighted the extracellular ligands in the niche, which initiate the sequential expression of transcription factors. PDGFα receptor, for example, is expressed by SVZ NSC and is required for oligodendrocyte differentiation, and PDGFα signalling works to balance neuron versus oligodendrocyte numbers generated (Jackson et al. 2006).

1.1.4 SVZ in response to brain injury

After traumatic brain injury, increased cell proliferation and neuroblast numbers are found in the SVZ (Szele and Chesselet 1996; Yoshiya et al. 2003; Ramaswamy et al. 2005; Kim and Szele 2008). But in these studies, one unaddressed question is whether this is due to activation of SVZ NSC or increased proliferation in transit amplifying cells and neuroblasts. Indeed, neurosphere culture work did not support the hypothesis that SVZ NSC is activated after traumatic injury (Dizon et al. 2006). Since both NSC and transit amplifying cells are able to form neurospheres, it is likely that neuroblasts are the main source for the increased proliferation (Pastrana et al. 2011). This is consistent with the observation that neuroblast emigration towards lesion is induced after injury with no alteration in the rate of OB neurogenesis (Sundholm-Peters et al. 2005). SVZ neuroblast emigration has been reported in other injuries, such as the MCAO model of stroke (Young et al. 2011). From the therapeutic perspective, the response in neuroblasts seems to be more important for their migratory feature, however the evidence suggests that the emigrated neuroblasts do not generate

significant numbers of functionally relevant neurons but eventually undergo cell death in the lesion area. Nevertheless SVZ neuroblasts seem to limit damage and when neurogenesis is halted lesions get worse.

The difficulties in human postmortem studies hamper our understanding of neurogenesis after human brain injury. In adult human, though neurogenesis is very limited, there are reports showing increased SVZ cell proliferation in ischemic brains, but it is uncertain whether any neuroblast that then emigrate towards the ischemic area are therapeutically beneficial (Sanai et al. 2004; Macas et al. 2006; Marti-Fabregas et al. 2010). In non-human primates, it seems such emigration towards injury also exists and neuroblasts are still added to the OB with increased neurogenesis (Tonchev et al. 2005; Koketsu et al. 2006; Tonchev et al. 2007). Controversial results have also been described for the existence of cortical neurogenesis after stroke (Jin et al. 2006; Huttner et al. 2014; Inta and Gass 2015). Clearly the role and contribution of the human SVZ to brain injury repair should be assessed further.

1.2 Stem cell potential in glial cells after brain injury

Somatic stem cells that self-renew and are multipotent, have been proposed as a promising therapeutic tool for disease treatment. In the adult brain, stem cell populations only reside in limited regions, namely the SVZ, the SGZ and possibly around the hypothalamic third ventricle (Ihrie and Alvarez-Buylla 2011; Lee et al. 2012; Robins et al. 2013). Although lifelong neurogenesis continues in these areas, their therapeutic contribution to brain repair is still being challenged. This is because neural progenitors/neuroblasts are largely restricted in the neurogenic niche and the cells migrating towards the injury areas are not sufficient to replace the local loss of neurons (Young et al. 2011). Both internal genetic programming and external signalling together limit regeneration from the neurogenic niches.

The development of induced pluripotent stem cell (iPSC) technology seems to provide an alternative option. By introducing the Yamanaka factors (Oct3/4, Sox2, c-Myc and Klf4), fully differentiated somatic cells can be reprogrammed into a stem cell-like pluripotent state (Takahashi and Yamanaka 2006). It is reported that fibroblasts can also be directly converted into neurons with specific induced genes (Ambasudhan et al. 2011; Liu et al. 2012; Xue et al. 2013). Intriguingly, the clinical application of iPSC has started in the treatment of age-related macular degeneration, while the final outcome still waits to be evaluated (Kamao et al. 2014). Tumorigenicity and immunogenicity are the two main concerns regarding iPSC-based therapies. Though it is been long believed that iPSC are immune tolerated by the donor from whom the cells are derived, there is evidence that iPSC could actually induce immune response (Okita et al. 2011; Zhao et al. 2011). Thus, the safety of iPSC needs to be further verified for therapeutic purposes.

Instead, the search for endogenous stem cell populations in the adult brain, especially after injury, demonstrates new potential sources for cell replacement. Like SVZ/SGZ NSC, they are primarily glial cells, but distributed more broadly around the brain. In particular, parenchymal astrocytes, NG2 cells (oligodendrocyte precursor cells) and ependymal cells are the most encouraging for brain repair.

1.2.1 Parenchymal astrocytes

Astrocytes constitute a large proportion of central nervous system cells and have a high diversity across the brain (Freeman 2010). Cell markers like GFAP, S100β, Glast and Aldh1l1 are widely used to identify astrocytes in the brain, but their expression level varies among different types of astrocytes. GFAP, for instance, is highly expressed in radial glia, SVZ NSC and astrocytes in the corpus callosum, while it is low or undetectable in cortical and striatal astrocytes (Ihrie and Alvarez-Buylla 2011; Robel et al. 2011). Although at early postnatal ages astrocytes expand through local proliferation, mature astrocytes in the adult intact brain are quiescent and relatively stable (Robel et al. 2011; Ge et al. 2012).

Since parenchymal astrocytes and SVZ NSC share several biological features, genetic manipulation is being used in an attempt to modify non-SVZ astrocytes for regenerative purposes. Sox2 is a pluripotent transcription factor expressed by stem cells. Interestingly, Sox2 is equally expressed by both SVZ NSC and parenchymal astrocytes (Beckervordersandforth et al. 2010; Magnusson et al. 2014). Overexpression of Sox2 in the parenchymal astrocytes in vivo however activates the neurogenic program outside the stem cell niche (Niu et al. 2013; Su et al. 2014; Niu et al. 2015). A dose-response effect of Sox2 has been documented in regulating cortical

and retinal neurogenesis, but it is not well understood in the SVZ NSC and other

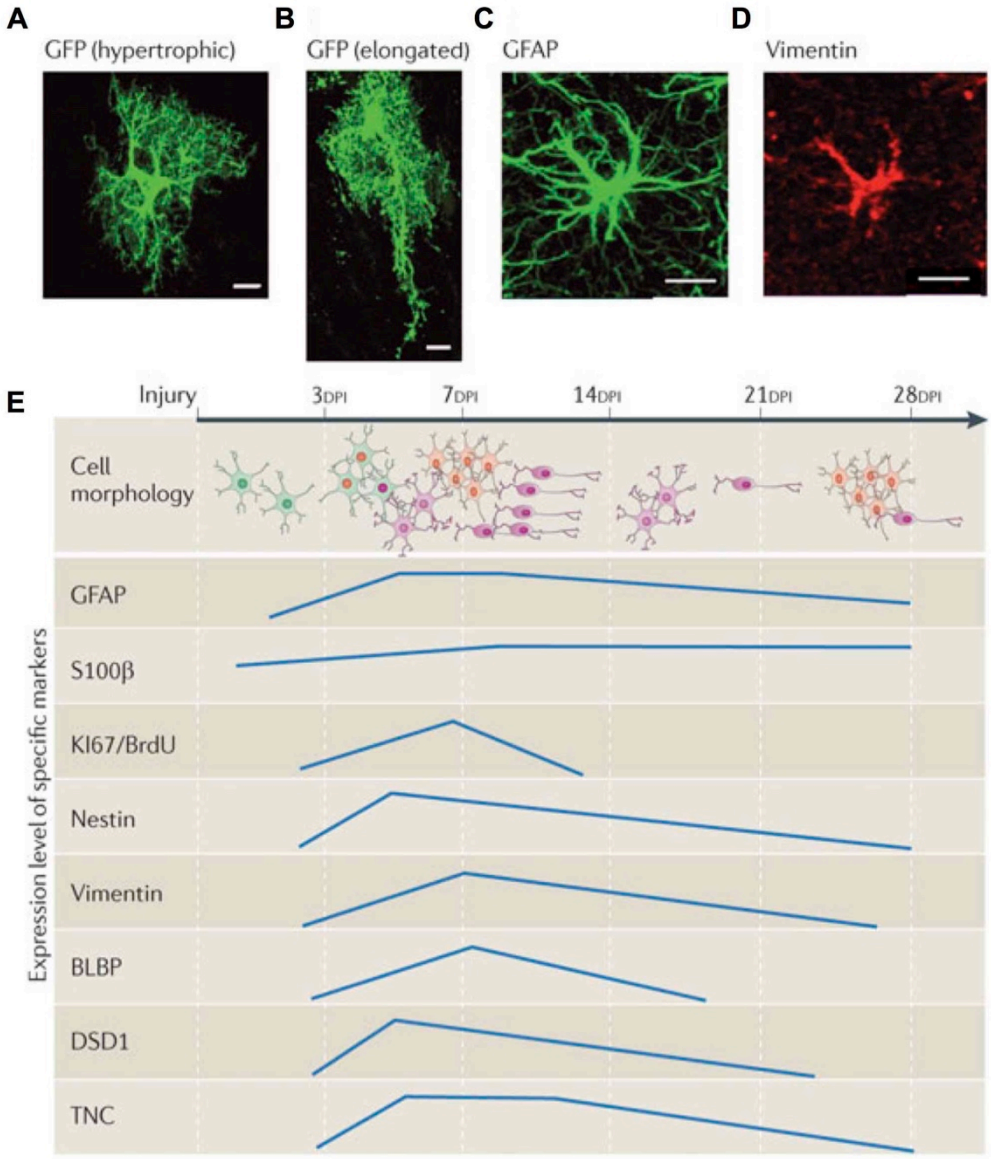

Figure 1. 3 The characteristics of reactive astrocytes

(A-D) The morphology of reactive astrocytes can be characterised by hypertrophy, elongation and the expression of GFAP and Vimentin. (E) Cell marker expression in reactive astrocytes after brain injury. Reactive astrocytes are proliferative and express high levels of immature cell markers, including Nestin and Vimentin, mainly in the first week post injury. (Figure adapted from Robel et al. 2011)

astrocytes (Taranova et al. 2006; Hagey and Muhr 2014). One possibility is distinct posttranscriptional regulation of Sox2 protein in these two cell types, which determines their neurogenic capacity. Other genes are also able to trigger the entry into neurogenic program in astrocytes, such as Mash1, NeuroD1 and Notch signalling (Guo et al. 2013; Ding et al. 2014; Magnusson et al. 2014). Of note, most work used injections to deliver virus and a minor brain injury can be caused by this method, which may potentially alter the external environment of parenchymal astrocytes. Genetic deletion of the Notch signalling gene RBP-Jκ circumvented this issue but was still able to generate neuroblasts from mature astrocytes in the striatum, suggesting genetic manipulation can truly enhance the plasticity in mature parenchymal astrocytes (Magnusson et al. 2014). For clinical practice, small molecules have been discovered for cell reprogramming (Hou et al. 2013; Federation et al. 2014). There is evidence that the small molecule isoxazole could activate neuronal gene expression in malignant astrocytes in vitro, but it remains mysterious whether administration of these small molecules in vivo is sufficient to drive the neurogenic ability in parenchymal astrocytes (Federation et al. 2014).

Without genetic or chemical manipulation, astrocytes can also be activated in response to brain injury. These reactive astrocytes become hypertrophic and upregulate many markers, like GFAP, Nestin, Vimentin and BLBP, which are more frequently found in SVZ NSC (Figure 1.3) (Robel et al. 2011). In addition to the morphological and marker changes, they re-enter the cell cycle and proliferate for a certain period after injury (Figure 1.3). Though reactive astrocytes more resemble SVZ NSC, unfortunately they are unipotent in vivo, only giving rise to more astrocytes and limiting the possibility of direct local neurogenesis (Shimada et al. 2012). Nevertheless, a series of recent studies illustrated that reactive astrocytes self-

renew and are multipotent in vitro (Buffo et al. 2008; Shimada et al. 2012; Grande et al. 2013; Sirko et al. 2013). They could form neurospheres in culture, albeit at a lower frequency than SVZ NSC and they also gave rise to neurons (Sirko et al. 2013). It is not clear yet which mechanisms contribute to this turning-on of stem cell properties in reactive astrocytes in vitro, but it seems to be brain injury type specific and the Sonic Hedgehog pathway may be involved in this process (Sirko et al. 2013).

1.2.2 NG2 cells

NG2 cells are generally considered as oligodendrocyte precursor cells (Nishiyama et al. 2009). They are both self-renewable and can produce mature oligodendrocytes in the adult brain and spinal cord (Nishiyama et al. 2009; Barnabe-Heider et al. 2010), however, the multipotency in NG2 cells has not been confirmed. In vitro, NG2 cells are able to differentiate into neurons, at least at postnatal ages (Belachew et al. 2003). In vivo, their neurogenic ability seems to diminish and lineage-tracing studies indicate they produce oligodendrocytes with a small population of astrocytes (Nishiyama et al. 2009; Barnabe-Heider et al. 2010; Robel et al. 2011). So fate choices seem quite restricted in NG2 cells of both healthy and injured brains. Nonetheless with the aid of genetic manipulation, this lineage commitment can be modified, suggesting plasticity of NG2 cells. The same transcription factors used for astrocyte reprogramming, NeuroD1 and Sox2, are also capable of initiating the neurogenic program in NG2 cells (Guo et al. 2013; Heinrich et al. 2014). In particular, NeuroD1 induced glutamatergic and GABAergic neuronal differentiation (Guo et al. 2013). Compared to non-specific reprogramming towards neurons, this method generated defined neuronal subtypes that could be more advantageous for cell replacement in the injured brain.

1.2.3 Ependymal cells

Unlike the SVZ NSC, which is neurogenic after birth, adult ependymal cells are believed to be postmitotic or at least quiescent in healthy brains (Spassky et al. 2005; Mirzadeh et al. 2008). In both rodent and human adult forebrains, ependymal cells possess multiple motile cilia that control the flow of CSF (Spassky et al. 2005; Quinones-Hinojosa et al. 2006; Young et al. 2012). They form a "pinwheel structure" with SVZ NSC and are involved in niche formation for SVZ neurogenesis through membrane contact molecules like Ank3 (Mirzadeh et al. 2008; Paez-Gonzalez et al. 2011). From the developmental perspective, both ependymal cells and SVZ NSC are derived from radial glia (Spassky et al. 2005; Kriegstein and Alvarez-Buylla 2009). Ank3 and the transcription factor Foxj1 are reported to direct radial glia to become ependymal cells, while the homeobox gene Six3 is important for maturation (Jacquet et al. 2009; Lavado and Oliver 2011; Paez-Gonzalez et al. 2011). More detailed functions (for instance, CSF regulation and CSF brain barrier) and developmental mechanisms of ependymal cells remain to be discovered.

Activation and regeneration in ependymal cells have been illustrated in brain and spinal cord injuries. Stroke, for instance, induced ependymal proliferation and drove the cells towards a neurogenic lineage (Zhang et al. 2007b; Gleason et al. 2008; Carlen et al. 2009). Nevertheless, the neuroblasts transformed from ependymal cells were reported to migrate along the RMS, which challenges the therapeutic importance for the ependymal activation (Carlen et al. 2009). Moreover, in some studies no ependymal proliferation could be detected, while instead GFAP was upregulated in ependymal cells after MCAO stroke, suggesting inconsistency in response to brain injury (Young et al. 2012). In spinal cord injury, ependymal cells exhibited self-

renewal and multipotency in vitro, however like reactive astrocytes in the brain, these activated ependymal cells were unable to generate new neurons in vivo (Barnabe-Heider et al. 2010). On the molecular level, Notch signalling was found to be essential in ependymal quiescence maintenance in the SVZ (Carlen et al. 2009). On the other hand, work in paediatric ependymoma, the third most common brain tumour in children, showed upregulation of Notch1 and repression of the Notch inhibitor Fbxw7, indicating the involvement of Notch signalling in the progression of paediatric ependymoma (Mack and Taylor 2009; Puget et al. 2009). This opposite effect may result from the heterogeneity in ependymal cells. It remains to be determined whether Notch is only involved in the activation of ependymal cells or can also regulate the neuronal differentiation ability.

1.3 Epigenetic regulation of neurogenesis

"Epigenetics, in a broad sense, is a bridge between genotype and phenotype—a phenomenon that changes the final outcome of a locus or chromosome without changing the underlying DNA sequence" (Goldberg et al. 2007).

Since C. H. Waddington proposed the term "epigenetics" in 1942 (Waddington 2012), several epigenetic mechanisms (Goldberg et al. 2007) have been discovered including DNA methylation (Goll and Bestor 2005), histone post-translational modification (Kouzarides 2007) and noncoding RNAs (ncRNA) (Mattick and Makunin 2006; Zaratiegui et al. 2007; Dinger et al. 2008), etc (Figure 1.4). Epigenetic mechanisms affect multiple cell behaviours, organ development and tumorigenesis by regulating gene expression.

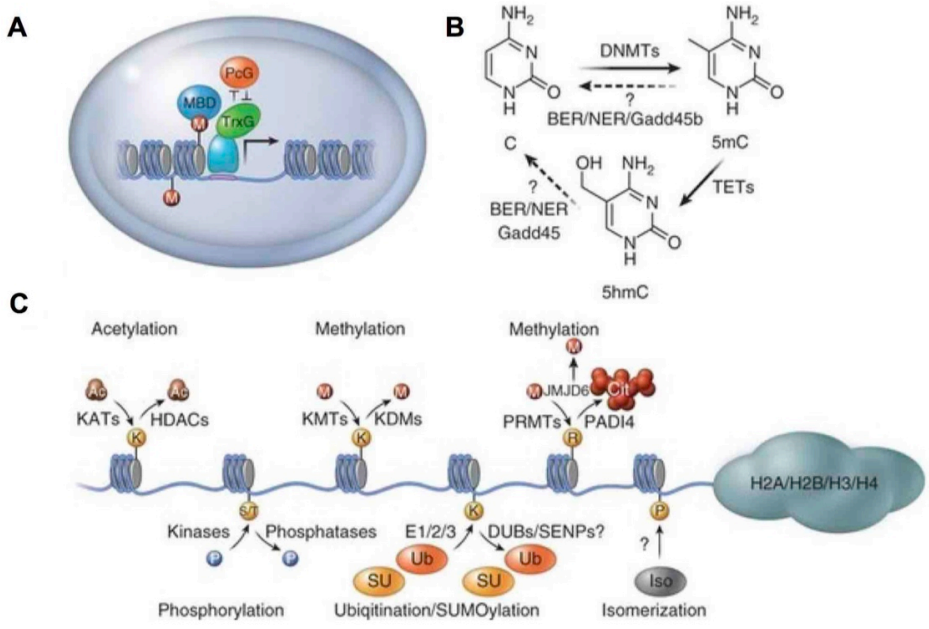

Figure 1. 4 A summary of epigenetic mechanisms

(A) PcG and TrxG complexes act antagonistically to modulate histone methylation, while methyl-CpG-binding domain proteins (MBD) bind to DNA with methylated CpGs to control gene expression. (B) DNA methyltransferase (DNMT) produces 5mC in DNA while TET oxidizes 5mC to 5hmC. Base and nucleotide excision repair (BER/NER) machineries and Gadd45b possibly function for DNA demethylation. (C)

Histones can be modified posttranscriptionally in different manners, including methylation, phosphorylation, ubiqitination, etc. And different enzymes catalyse these diverse modifications. (Figure adapted from Hirabayashi and Gotoh 2010)

1.3.1 DNA modification

Two major DNA modifications, methylation (5mC) and hydroxymethylation (5hmC) have been described. They are catalysed by DNA methyltransferases (DNMT) and enzymes of the TET family, respectively (Kohli and Zhang 2013). DNA methylation locates predominantly at CpG islands and represses gene expression, while 5hmC is considered as the initiation of DNA demethylation (Piccolo and Fisher 2014).

In brain development, 5hmC is associated with activation of genes relevant to neural development. Loss of Tet2/Tet3 led to a defect in cortical neuronal differentiation (Hahn et al. 2013). Tet3 also promotes the expression of CyclinD1 in embryonic NSC (Lv et al. 2014). In adult SGZ, 5hmC guarantees the activation of NSC proliferation related genes and drives hippocampal neurogenesis for learning and memory (Zhang et al. 2013b). Finally, in human brain cancer, 5hmC is reduced in malignant glioma and correlated with poor survival (Orr et al. 2012; Bian et al. 2014).

1.3.2 Histone modification

Compared to DNA modification, more types of histone modification are known (Guibert and Weber 2013). These include different amino acid sites and covalent residues, such as methylation, acetylation, phosphorylation, ubiqitination and so on (Bannister and Kouzarides 2011). These posttranscriptional modifications work through direct transcriptional or chromatin structural regulation to modify the global transcriptome (Figure 1.5).

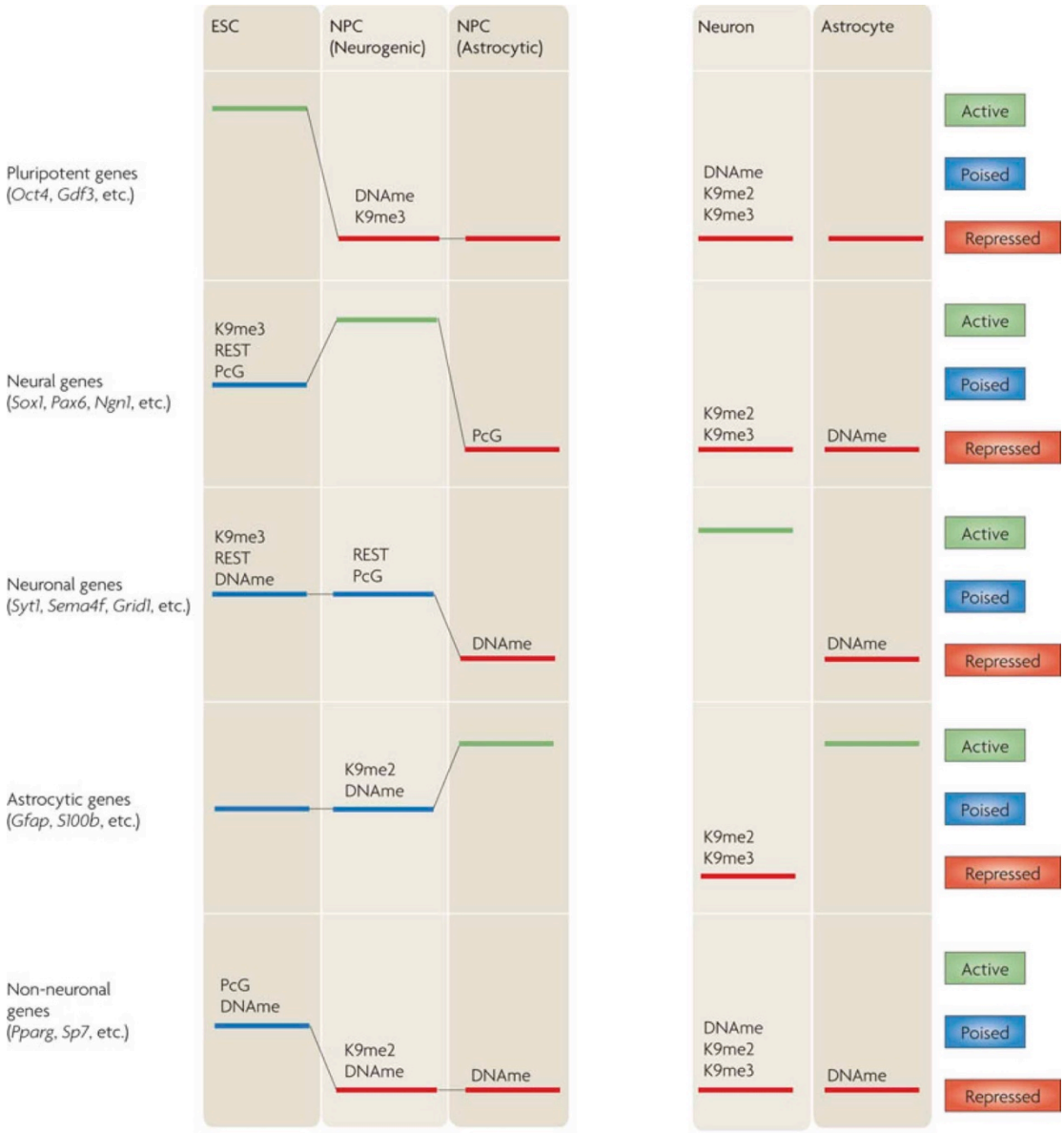

Figure 1. 5 A summary of 5mC and histone methylation in neural development

During lineage progression, transcription factors have diverse 5mC and histone methylations for proper expression. For instance, pluripotent genes are repressed by both DNA and histone methylations after embryonic stem cells (ESC) differentiate into neural restricted stem cells. The poised state refers to promoters bound by inactive RNA polymerase II and the genes are not actively transcribed, but can be rapidly upregulated. Examples are neuronal and astrocytic genes in NSC/NPC. During neural differentiation, the repressive transcriptional factor REST associates with H3K27me3 and H3K9me3 to suppress relevant genes. (Figure adapted from Hirabayashi and Gotoh 2010)

For example, the Trithorax group (TrxG) methylates lysine 4 in histone 3 (H3K4) and contributes to active chromatin (Ringrose and Paro 2004). It thereby controls the neurogenic transcription factor Dlx2 (Petryniak et al. 2007). The depletion of TrxG member Mll1 represses Dlx2 and decreases neuronal differentiation (Lim et al. 2009). Dlx2 is also under control of the H3K27me3 demethylase Jmjd3 for the active state to promote neuronal fate (Park et al. 2014). On the other hand, Polycomb Repressive Complex 1 (PRC1) antagonizes TrxG through ubiquitylating lysine 119 of histone H2A (H2AK119ub) and its component Bmi1 is essential for SVZ NSC self-renewal (Molofsky et al. 2003; Ringrose and Paro 2004; Fasano et al. 2009; He et al. 2009a; Margueron and Reinberg 2011; Yadirgi et al. 2011). HDAC3, a histone deacetylase is required for cell cycle progression in NSC (Jiang and Hsieh 2014). When inhibitors of histone deacetylase were added to neurosphere cultures, more neuronal, instead of oligodendrocyte, differentiation was reported along with increased expression of NeuroD (Siebzehnrubl et al. 2007). Recently SVZ NSC, but not ependymal cells, were shown to highly express the histone acetyltransferase querkopf (Qkf) (Sheikh et al. 2012).

Aberrant global histone modifications have been reported in glioblastomas. H3K27me3 was lost in glioblastoma cancer stem cells at the *MASH1* locus, in contrast to the H3K27me3 and H3K4me3 bivalent domain in NSC. The activation of MASH1 consequently stimulated WNT signalling and induced cancer expansion (Rheinbay et al. 2013). Similar changes in histone modifications can also be found in other loci, such as *OLIG1, OLIG2, KLF4, DLX1, DLX2,* etc (Rheinbay et al. 2013).

1.3.3 Histone variants

Besides covalent modifications, histone variants also add to the diversity of chromatin. Nonallelic variants of histones are distinguished from major histones in sequence and length. Take H2A for example. There are variants including H2A.Z, H2A.X, H2AvD, etc. Meanwhile, three H3 variants exist, H3.3, CenH3 and H3.4 (Kamakaka and Biggins 2005). Besides their sequence differences, the histone variants perform distinct biological functions. For instance, H2A.X can repress gene expression, while H2A.Z will activate transcription (Kamakaka and Biggins 2005). In neurogenesis, H2A.X was reported to inhibit SVZ NSC proliferation and this process is under the control of $GABA_A$ signalling (Andang et al. 2008; Fernando et al. 2011).

Recent studies highlighted the importance of histone variants, especially H3.3 in glioblastoma. H3.3K27M mutations could be identified in over 70% of human diffuse intrinsic pontine gliomas (DIPG) and correlated with worse overall survival (Khuong-Quang et al. 2012; Wu et al. 2012). This specific mutation inhibits H3K27me3 through interaction with the methyltransferase Ezh2 and modulates the gene expression profile in glioblastoma (Chan et al. 2013; Lewis et al. 2013; Voigt and Reinberg 2013; Funato et al. 2014). OLIG2, as a downstream gene, is upregulated in DIPG patents, while CDK6 is downregulated, both of which correspond to the altered global H3K27me3 distribution (Chan et al. 2013). Interestingly, it is reported that tumours with H3.3K27M express higher level of NG2, which is consistent with the observation that oligodendrocyte precursor cells are the origin of gliomas in *p53/Nf1* mutants (Yadavilli et al. 2015). Application of the Jmjd3 inhibitor, GSK-J4 is sufficient to reduce cell growth in DIPG tumours harbouring H3.3K27M, but not in other genetic backgrounds, which provides a potential therapeutic method for this type of glioma (Gupta et al. 2014).

1.3.4 Chromatin remodelling

Chromatin remodelling is the organization of chromatin to modify the accessibility of transcriptional regulation proteins to DNA. SWI/SNF complex (also known as BAF complex), for example, is an ATP-dependent chromatin regulator. Several BAF subunits together form the SWI/SNF complex in mammalian cells (Tang et al. 2010). The diversity of BAF subunits is essential in neural development. During lineage progression from neural progenitors to neurons, the SWI/SNF complex undergoes a subunit switch: BAF45A and BAF53A in progenitors are switched to BAF45B/C and BAF53B during neuronal differentiation. In postmitotic neurons, the complex recruits the calcium-response factor CREST for synaptic development (Riccio 2010). During embryonic neurogenesis, BAF170 controls proper cortical size by limiting proliferation in intermediate progenitors (Tuoc et al. 2013). However, in the adult SVZ, another SWI/SNF complex subunit, Brg1, interacts with Pax6 to drive neurogenesis versus gliogenesis (Ninkovic et al. 2013).

In addition, the NuRD/Mi-2/CHD complex is another family of proteins that carries out ATP-dependent chromatin remodelling (Wang et al. 2007). This complex reads modified histone tails and primarily represses transcription (Wang et al. 2007). CHD5 is a tumour suppressor gene present in active H3K4me3 domains (Paul et al. 2013). It cooperates with the repressive H3K27me3 mark to regulate neuronal differentiation in cortical neurogenesis (Egan et al. 2013). CHD7, on the other hand, activates the expression of Sox4 and Sox11 in the adult SVZ resulting in increased neurogenesis (Feng et al. 2013; Feng and Liu 2013).

1.4 Polycomb repressive complex 2

Polycomb repressive complex 2 (PRC2) mediated gene silencing by post-translational histone modification is widely involved in both embryonic development and adult functions. The canonical PRC2 mechanism is conserved from Drosophila to mammals. It consists of the enzymes Ezh2 (Histone-lysine N-methyltransferase), Suz12, RbAp46/48, and Eed (Margueron and Reinberg 2011). Among them, Ezh2 di/trimethylates Lysine 27 of histone H3, which allows polycomb repressive complex 1 (PRC1) to bind and monoubiquitylate Lysine 119 of histone H2A (H2AK119ub). Consequently, the elongation of mRNA transcription for the genes with these chromatin modifications cannot continue and expression is thereby suppressed (Margueron and Reinberg 2011). Studies in embryonic stem cells (ESC) have revealed that PRC2 targets many developmental regulators, which have significant overlaps with those of Oct4, Sox2 and Nanog, like *Hox* genes, *Dlx*, and *Tbx* families (Boyer et al. 2006; Bracken et al. 2006; Lee et al. 2006b). PRC2 is not, however, necessary for the maintenance of ESC pluripotency (Chamberlain et al. 2008).

In vivo work in mouse epidermal development has shown that Ezh2 and H3K27me3 were highly expressed in embryonic and young postnatal basal progenitors and PRC2 controlled the proliferation and differentiation of these cells (Ezhkova et al. 2009; Ezhkova et al. 2011). In late cortical development, PRC1 and PRC2 control the temporal transition of precursor cell fate choice from neurons to astrocytes by targeting the transcription factor Neurog1 (Hirabayashi et al. 2009). Studies in other systems have described the involvement of PRC2 in B cell development, cortical organization, etc (Su et al. 2003; Pereira et al. 2010). Loss of Ezh2 disrupted the temporal order of cortical layer generation (Pereira et al. 2010). In the postnatal/adult brain, Ezh2 was reported to be expressed in SVZ NSC and

astrocytes (Hwang et al. 2014). However this contradicts a study in the SGZ, which indicated quiescent NSC do not express Ezh2 and in vitro analysis also suggested Ezh2 could not be found in astrocytes (Sher et al. 2012; Zhang et al. 2014). On the other hand, Hwang et al reported that Ezh2 could repress Olig2 during NSC differentiation in vitro, which is required for neuronal fate (Hwang et al. 2014). There is contrasting evidence that Ezh2 promotes oligodendrocytes and should be turned off during neuronal differentiation (Sher et al. 2012). Clearly, the importance of Ezh2 and PRC2 in SVZ neurogenesis needs further investigation.

In humans, mutations in EZH2 are related to an overgrowth disease, Weaver syndrome (Tatton-Brown et al. 2011; Gibson et al. 2012; Tatton-Brown et al. 2013). Similar symptoms could also be identified in EED mutation carriers (Cohen et al. 2015). EZH2 mutations were found mainly in the SET sequence, a domain shared by lysine methyltransferases such as MLL1 (Tatton-Brown et al. 2013). It is not clear what is the effect of these missense mutations on the enzymatic activity of EZH2, but it seems cell proliferation cannot be suppressed at the proper developmental stage, which phenocopies EZH2 overexpression in somatic cancer cells (Kleer et al. 2003).

Besides the role of histone methylation, PRC2 and its subunits also process non-canonical functions. There is evidence that in addition to histone tails, EZH2 is able to methylate GATA4 directly to modulate the latter's transcriptional activity (He et al. 2012). Moreover, EZH2 can cooperate with PAF to improve β-catenin signalling, which is independent of histone methylation (Jung et al. 2013). Transcriptional activation is also observed in which Ezh2 activates NF-κB target genes (Tan et al. 2014).

1.5 Long non-coding RNAs

1.5.1 Introduction to long non-coding RNAs

A large proportion (~95%) of the human genome is identified as non-coding elements such as regions expressing non-coding RNA, introns, pseudogenes, etc (Lander et al. 2001). Long non-coding RNAs (lncRNAs) are transcripts longer than 200 nucleotides (nt) and without any known protein coding sequence. Except for the difference in protein coding ability, lncRNAs share a number of features of mRNA, e.g. length and 3'-polyadenylation. According to the genomic organization, lncRNAs can be categorized into 5 groups (Figure 1.6): (1&2) sense or antisense of another transcript locus; (3) bidirectional, opposite strands of a protein coding gene with the same transcription starting region; (4) intronic, the whole sequence existing in the intron; and (5) intergenic, within genomic intervals between two genes (Mercer et al. 2009; Ponting et al. 2009).

The functionality for most lncRNAs is still in question. One criterion to predict biological importance has relied on the evolutionary sequence conservation of DNA/RNA among species. The poor conservation of lncRNAs suggests low evolutionary pressure and selection. This is primarily considered as evidence to support the notion that lncRNAs are transcriptional noise instead of biological regulators (Ponting et al. 2009; Ponting and Belgard 2010). However, although it is an essential player in X chromosome inactivation, lncRNA *Xist* has been documented to have relatively poor sequence conservation (Hendrich et al. 1993; Nesterova et al. 2001). So it is important to note that the functionality and sequence conservation may not correspond to each other in some cases. On the other hand, the analysis of conservation in functional sequence or structure of lncRNAs may be more important.

Take *Xist* for example. Despite the low sequence conservation, tandem repeats, a PRC2 targeting region could be found in *Xist* from different species (Nesterova et al. 2001; Zhao et al. 2008).

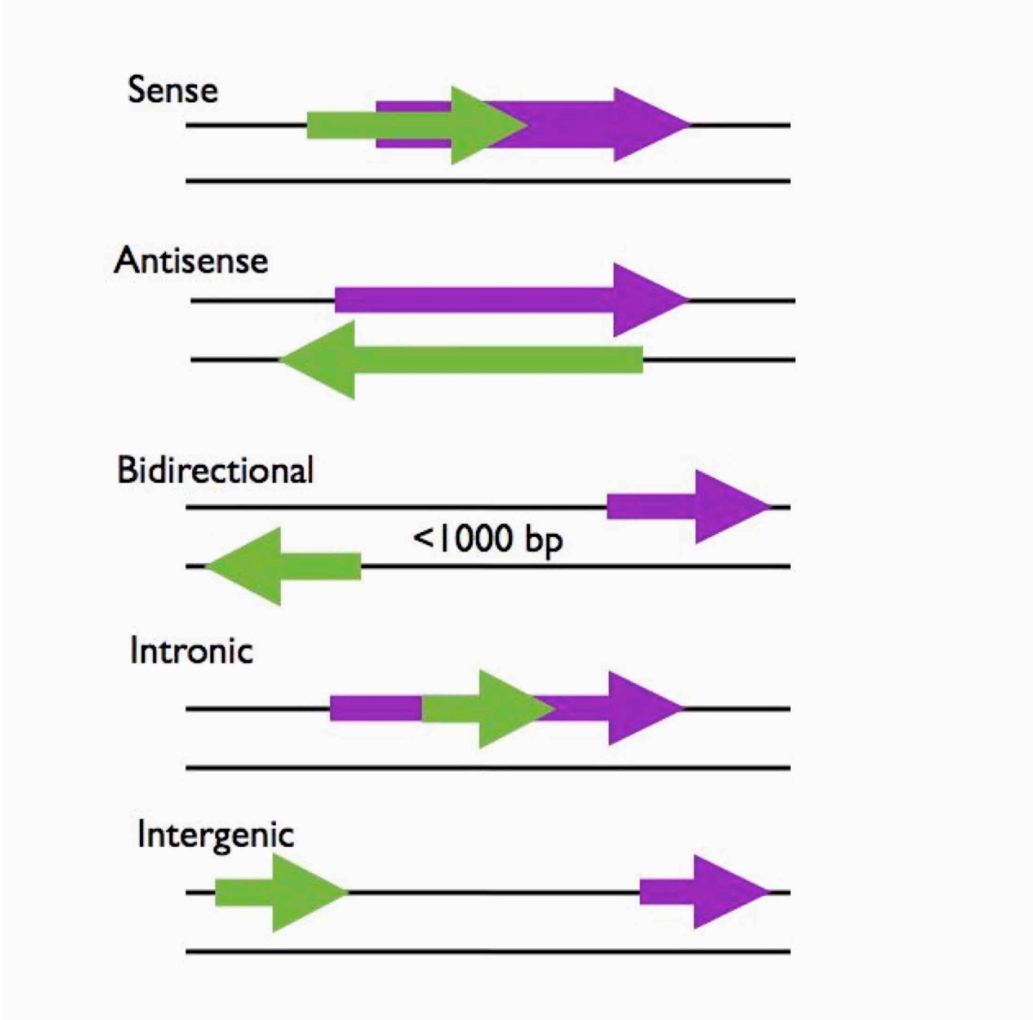

Figure 1. 6 Locations of lncRNAs in the genome

Base on their locations in genome, lncRNAs can be categorized into five types: (1) The lncRNA (green) overlaps with the sense strand of a protein coding gene (purple); (2) The lncRNA is antisense to a protein coding gene; (3) The lncRNA and its neighbouring protein coding gene (with less than 1000bp in distance) are bidirectional. And the genes are in opposite strands; (4) The lncRNA entirely locates in the intron of another gene; and (5) The lncRNA is not within any protein coding gene. (Figure adapted from mcmanuslab.ucsf.edu)

A number of lncRNAs serve as hosts for microRNAs (Royo and Cavaille 2008; Bassett et al. 2014). LncRNA *H19*, for instance, can produce miR-675; while miR-770 can be transcribed from lncRNA *Gtl2* (Royo and Cavaille 2008). The functions of lncRNAs can be diverse depending on their subcellular locations. It has been reported that cytoplasmic lncRNA can work as competing endogenous RNA to fine-tune the binding of miRNA with its target mRNA (Cesana et al. 2011; Xia et al. 2014). Nuclear lncRNA, in turn, is able to regulate transcription directly and this regulation can be divided, based on the downstream gene locus, into in *cis* and in *trans* effects. Transcription factors or other regulatory proteins, like histone modifiers, as well as other RNAs, can be recruited by some lncRNAs. Meanwhile, lncRNA can

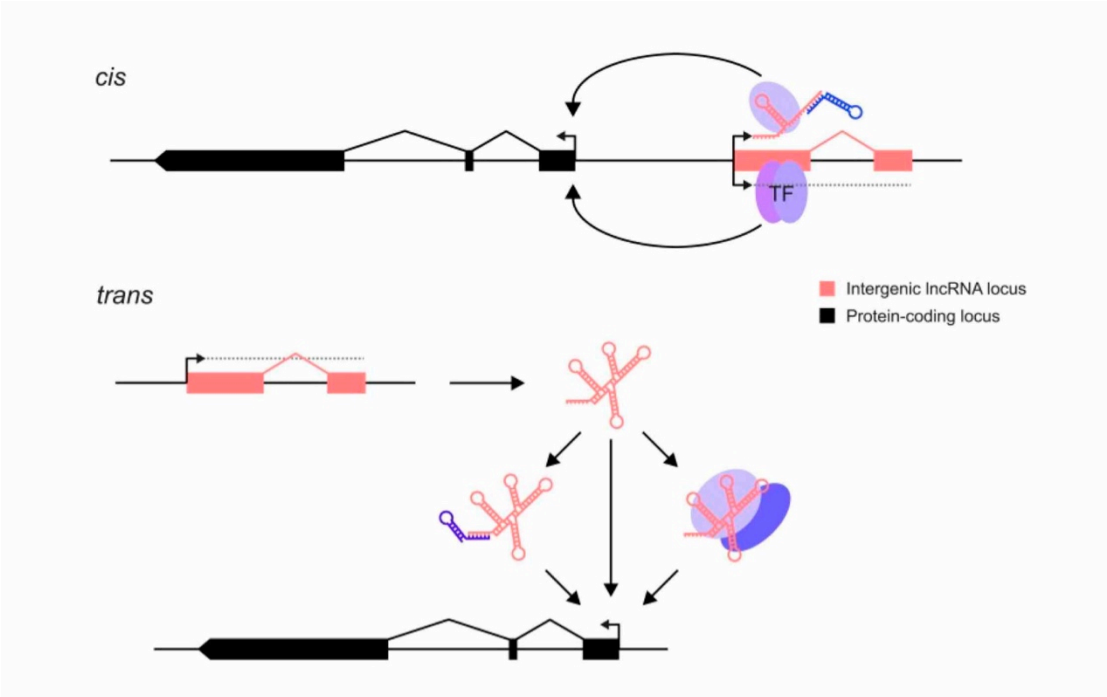

Figure 1. 7 LncRNA regulatory mechanisms

LncRNA (pink) can recruit the regulatory proteins (purple) and other RNA (blue) to bind with regulatory regions of neighbouring genes in *cis* to regulate the latter's expression. For instance, *Xist* functions in *cis* to inactivate genes in X chromosome with PRC2. Meanwhile the in *trans* model implies transcribed lncRNA binds with proteins/RNA to a distal gene or directly associates with the regulatory region of a distal gene. LncRNAs are thought to work through either one or both mechanisms. (Figure adapted from Bassett et al. 2014)

bind double strand DNA and modulate transcriptional activity (Figure 1.7) (Bassett et al. 2014). Another regulation model is through lncRNA locus interaction with other local or distal protein coding genes. In this model, the lncRNA locus functions as an enhancer while roles of the transcribed RNA are less understood (Vance and Ponting 2014). Interestingly, a recent study described double mechanisms in regulating HOXA expression (Yin et al. 2015). *Haunt*, is a lncRNA transcribed upstream of the *HOXA* locus. The authors discovered that the lncRNA *Haunt* repressed the expression of HOXA genes while the *Haunt* genomic locus activated HOXA genes as an enhancer (Figure 1.8) (Lin et al. 2015; Yin et al. 2015). This study demonstrated that lncRNA may act in multiple ways and the orchestration of these different mechanisms may control downstream gene expression.

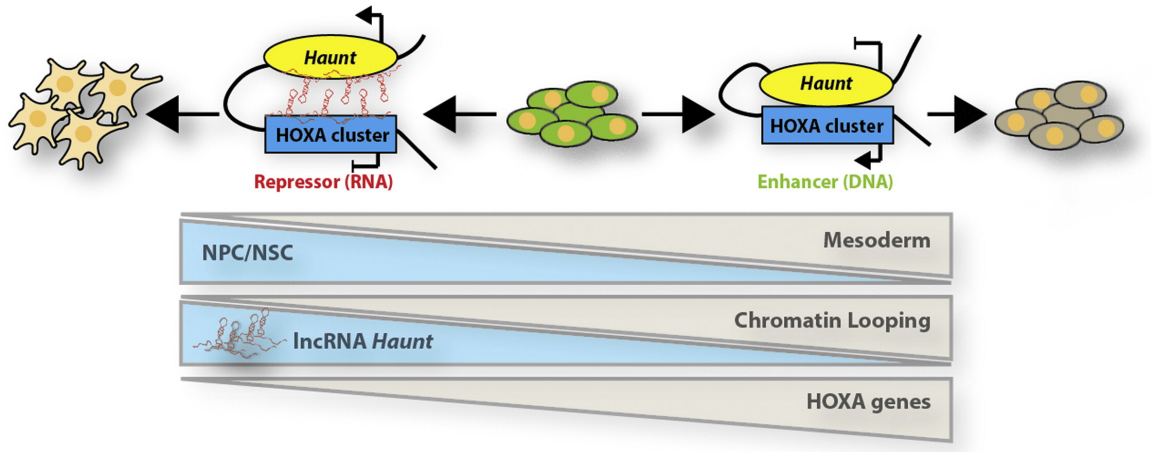

Figure 1. 8 Working mechanisms for lncRNA *Haunt*

A schematic summary for lncRNA *Haunt* working mechanisms. On the one hand, lncRNA *Haunt* can repress HOXA expression during neural differentiation; on the other hand, *Haunt* locus can activate HOXA expression as an enhancer in mesoderm development. (Figure adapted from Lin et al. 2015)

The distinct roles of lncRNA and its genomic locus in transcription raised another essential question in the research of lncRNA: which loss of function method should be chosen? Complete deletion of the lncRNA locus may disrupt the regulatory DNA sequences, such as enhancers. In this case, any phenotype observed can result from either loss of the enhancer or the lncRNA. Rescuing expression of the same lncRNA from another allele would then be necessary. RNA interference (RNAi) by shRNA or siRNA is a rapid and efficient technology to target the lncRNA of interest. Nevertheless, RNAi works posttranscriptionally, which may not be suitable for nuclear lncRNA (Bassett et al. 2014). Moreover, the stability of knockdown by RNAi should also be taken into consideration. A comprehensive analysis with different technologies would therefore be a major priority to explore the functions of lncRNAs.

1.5.2 LncRNA regulation in development

Several potential biological functions of lncRNAs have been investigated. Nonetheless, in many models no or only subtle phenotypes could be identified after mutation of lncRNAs with high expression in relevant tissues, such as *Visc-2*, *Malat1* and *Neat1* (Table 1.1) (Bassett et al. 2014; Oliver et al. 2014). Of note, one lncRNA *Fendrr* was shown to be indispensable in early embryonic development (Grote et al. 2013; Sauvageau et al. 2013). Loss of *Fendrr* disrupted the H3K27me3 mark in cardiac differentiation related transcription factors due to improper recruitment of PRC2 and TrxG complexes (Grote et al. 2013). Importantly, the authors found RNAi with shRNA was unable to cause any phenotype, consistent with the notion that *Fendrr* functions as an intranuclear lncRNA. Instead a replacement of the first exon with a stop signal sequence was used as the loss-of-function model and a rescue knockin line was included as well, which together supported that the phenotypes were

Table 1. 1 List of lncRNAs which have been studied

lncRNA name	Organism	Mutation strategy	Reported animal phenotype	RNA-based rescue?	Reference
Xist	*Mus musculus*	~15 kb replaced with a *neo* expression cassette	Females inheriting paternal allele were embryonic lethal; males fully viable	No	(***Marahrens et al., 1997***)
Xist	*Mus musculus*	Inversion of Exon 1 to intron 5	Embryonic lethality of paternally inherited allele	No	(***Senner et al., 2011***)
H19	*Mus musculus*	Replacement by *neo* cassette	Slightly increased growth	No	(***Ripoche et al., 1997***)
roX	*Drosophila melanogaster*	Deletions of *roX1* or *roX2*	None, except when in combination: male-specific reduction in viability	Yes	(***Meller and Rattner, 2002***)
Kcnq1ot1	*Mus musculus*	Promoter deletion	Growth deficiency for paternally inherited mutation	No	(***Fitzpatrick et al., 2002***)
Airn	*Mus musculus*	Premature transcriptional termination	Growth deficiency for paternally inherited mutation	No	(***Sleutels et al., 2002***)
Evf2	*Mus musculus*	Premature transcriptional termination	None	N/A	(***Bond et al., 2009***)
BC1	*Mus musculus*	Replacement of promoter and exon by *PgkNeo* cassette	Vulnerable to epileptic fits after auditory stimulation	No	(***Zhong et al., 2009***)
Neat1	*Mus musculus*	3 kb Promoter and 5′ deletion	None	N/A	(***Nakagawa et al., 2011***)
Tsx	*Mus musculus*	2 kb Promoter and exon 1 deletion	Smaller testes and less fearful (males)	No	(***Anguera et al., 2011***)
Malat1	*Mus musculus*	Deletion	None	N/A	(***Eissmann et al., 2012***)
Malat1	*Mus musculus*	*lacZ* insertion and premature transcriptional termination	None	N/A	(***Nakagawa et al., 2012***)
Malat1	*Mus musculus*	3 kb Promoter and 5′ deletion	None	N/A	(***Zhang et al., 2012***)
Hotair	*Mus musculus*	Deletion	Spine and wrist malformations	No	(***Li et al., 2013***)
Hotdog* and *Twin of Hotdog	*Mus musculus*	Large (28 Mb) translocation by inversion	Loss of *Hoxd* expression in the cecum	N/A	(***Delpretti et al., 2013***)
Fendrr	*Mus musculus*	Replacement of exon 1 with transcriptional stop signal	Embryonic lethal around E13.75	Yes (majority of embryos)	(***Grote et al., 2013***)
Fendrr	*Mus musculus*	Locus replacement with *lacZ* cassette	Perinatal lethality	No	(***Sauvageau et al., 2013***)
Peril	*Mus musculus*	Locus replacement with *lacZ* cassette	Perinatal lethality	No	(***Sauvageau et al., 2013***)
Mdgt	*Mus musculus*	Locus replacement with *lacZ* cassette	Reduced viability and reduced growth	No	(***Sauvageau et al., 2013***)
15 other lncRNA loci	*Mus musculus*	Locus replacement with *lacZ* cassette	None	N/A	(***Sauvageau et al., 2013***)

(Table adapted from Bassett et al. 2014)

caused by lncRNA *Fendrr* (Grote et al. 2013). Knockout with another approach, replacement of *Fendrr* locus with a lacZ cassette also led to lethality in mice (Sauvageau et al. 2013). Nevertheless, a further characterization suggested different phenotypes: developmental defects could be noticed in lung and gut as well as heart (Sauvageau et al. 2013). One possible explanation for this difference is the method used by the latter group may disrupt the potential regulatory DNA sequence in the *Fendrr* locus and similar to lncRNA *Haunt* mentioned above, the genomic locus function might then be neglected. These two studies together again illustrate the importance of proper methods and interpretation in lncRNA function research.

1.5.3 The interaction between lncRNA and PRC2

It has been recognized that PRC2 can interact with a number of lncRNAs to silence target gene expression, which reveals an essential role of lncRNA in PRC2 recruitment (Brockdorff 2013). Early examples like *Xist* and *HOTAIR* were found to associate with PRC2 and repress transcription in *cis* or in *trans*, respectively, although the interaction between *Xist* and PRC2 was recently challenged by super-resolution microscopy (Rinn et al. 2007; Zhao et al. 2008; Cerase et al. 2014). A current study further characterized the role of a non-core subunit in PRC2, Jarid2 during this interaction. It was shown that several lncRNAs, such as Meg3 transcribed from the imprinted *Dlk1-Dio3* locus, indirectly bound with PRC2 via Jarid2 at some genomic sites and meanwhile Meg3 was also able to work as the platform to recruit PRC2/Jarid2 complex at other sites (Kaneko et al. 2013). In spite of these examples, there is no common binding sequence or structure described to predict other potential PRC2 associated lncRNAs. This may be due to our incomplete understanding of these

molecules and/or poor sequence conservation in lncRNAs. The sticky aspect of lncRNA should also be taken into account, which can produce non-specific binding.

In addition to recruiting mechanisms, PRC2 and lncRNAs can regulate each other's expression. H3K27me3 could be found at the promoters of lncRNAs with low expression and thereby set distinct expression profiles of lncRNA in different cell lineages. Loss of Ezh2 could induce misexpression of lncRNAs, for instance FT31040 and FT319969 (Wu et al. 2010). Less is known about the role of lncRNA in PRC2 component expression. Small non-coding RNAs, like miR-101, miR-214 have been reported to regulate Ezh2 expression posttranscriptionally (Juan et al. 2009; Kottakis et al. 2011). MiR-214, for instance, locates within a host lncRNA, Dnm3os. Another transcript miR-199a from the same locus seems to play an insignificant role in repressing Ezh2 (Juan et al. 2009).

1.6 Investigation of PRC2 and lncRNA in SVZ neurogenesis

Though a number of studies have been carried out to investigate the roles of epigenetic regulators in SVZ neurogenesis, our understanding is still incomplete with the following questions unanswered: (1) How do SVZ NSC coordinate maintenance of quiescence versus activation? (2) What mechanisms distinguish SVZ NSC from other parenchymal astrocytes? (3) Do SVZ NSC and reactive astrocytes share the same mechanisms for activation?

In my thesis, the primary aim was to study the roles of PRC2 and lncRNA in regulating postnatal SVZ neurogenesis. Firstly, considering the diversity of the PRC2 complex, the expression of two core components, Ezh2 and Eed in individual SVZ cell types was examined. Meanwhile, the global H3K27me3 distribution was analyzed in postnatal and adult brains as well as in injured brains. Secondly, a comparison of the biological functions of Ezh2 and Eed in the postnatal/adult SVZ was carried out. To perform these loss-of-function studies, two techniques were used, inducible knockout and in vivo knockdown by electroporation. Following my investigation into the biological functions of PRC2, the downstream molecular mechanisms were examined. Thirdly, cerebral cortex lesions were used to study the function of PRC2 in cortical astrocyte activation. Finally, the expression of lncRNAs in the adult SVZ was screened and the function of a candidate lncRNA, Paupar was studied by loss-of-function in the postnatal SVZ.

Overall, my thesis revealed that PRC2 and lncRNA contribute to normal SVZ neurogenesis and therefore that they can be therapeutic targets for regenerative purposes after brain injury.

Chapter 2

Material and methods

2.1 Animals

Species and ages of mice used for the neurosphere assay, electroporation and traumatic brain injury are indicated elsewhere in each chapter.

$Ezh2^{fl/fl}$ mice were obtained from Prof. Rick Livesey's lab in University of Cambridge (Su et al. 2003; Pereira et al. 2010; Ezhkova et al. 2011), $Eed^{fl/fl}$ mice from Dr. Stuart Orkin's lab in Harvard University (Neff et al. 2012; Xie et al. 2013), Nestin-CreERT2 mice from Dr. Xin Lu's lab in University of Oxford (Lagace et al. 2007), and GLAST-CreERT2 mice from Dr. François Guillemot's lab in the MRC National Institute for Medical Research (Mori et al. 2006), and Ai9 reporter mice from Dr. Colin Akerman's lab in University of Oxford.

To obtain GLAST-$CreERT2^{Cre/+}$;$Ezh2^{fl/fl}$ mice, $Ezh2^{fl/fl}$ mice were mated with GLAST-$CreERT2^{Cre/+}$ mice to get GLAST-$CreERT2^{Cre/+}$;$Ezh2^{fl/+}$ mice. GLAST-$CreERT2^{Cre/+}$;$Ezh2^{fl/+}$ mice were then mated with $Ezh2^{fl/fl}$ to obtain GLAST-$CreERT2^{Cre/+}$;$Ezh2^{fl/fl}$. In the postnatal experiments, male GLAST-$CreERT2^{Cre/+}$;$Ezh2^{fl/fl}$ were mated with female $Ezh2^{fl/fl}$ to get litters with GLAST-$CreERT2^{Cre/+}$;$Ezh2^{fl/fl}$ (conditional knockout, cKO) and $Ezh2^{fl/fl}$ (littermate control).

To obtain Nestin-$CreERT2^{Cre/+}$;$Eed^{fl/fl}$ mice, $Eed^{fl/fl}$ mice were mated with Nestin-$CreERT2^{Cre/+}$ mice to get Nestin-$CreERT2^{Cre/+}$;$Eed^{fl/+}$ mice. Nestin-$CreERT2^{Cre/+}$;$Eed^{fl/+}$ mice were then mated with $Eed^{fl/fl}$ to obtain Nestin-$CreERT2^{Cre/+}$;$Eed^{fl/fl}$. In the postnatal experiments, male Nestin-$CreERT2^{Cre/+}$;$Eed^{fl/fl}$ were mated with female $Eed^{fl/fl}$ to get litters with Nestin-$CreERT2^{Cre/+}$;$Eed^{fl/fl}$ (conditional knockout, cKO) and $Eed^{fl/fl}$ (littermate control).

To obtain GLAST-$CreERT2^{Cre/+}$;$Eed^{fl/fl}$ mice, $Eed^{fl/+}$ mice were mated with GLAST-$CreERT2^{Cre/Cre}$ mice to get GLAST-$CreERT2^{Cre/+}$;$Eed^{fl/+}$ mice. GLAST-

CreERT2$^{Cre/+}$;Eed$^{fl/+}$ mice were then mated with Eed$^{fl/fl}$ to obtain GLAST-CreERT2$^{Cre/+}$;Eed$^{fl/fl}$.

Genotyping procedures for all transgenic mice were as follows. DNA was extracted from mouse earclips with E.Z.N.A. Tissue DNA Kit (Omega bio-tek, D3396-02). For polymerase chain reaction (PCR), 5µl of 50µl extracted DNA was mixed with primers, 2µl 10x REDTaq PCR Reaction Buffer, 0.5µl deoxynucleotide Mix (10mM each, Roche 11 581 295 001), 0.5µl 50mM $MgCl_2$ (Invitrogen P/N y02016), 2µl REDTaq DNA Polymerase (Sigma D4309) and nuclease-free water (Qiagen 1039498).

The primers (Invitrogen) for PCR were as follows:

Table 2. 1 Primer list for genotyping

Primer name	Primer sequence
For Ezh2$^{fl/fl}$	
Reverse 1 (Marc.) 3'of loxp	5'-AGGGCATCAGCCTGGCTGTA-3'
Forward 2 5' of loxp	5'-TTATTCATAGAGCCACCTGG-3'
Forward 3 left loxp 5	5'-ACGAAACAGCTCCAGATTCAGGG-3'
For Eed$^{fl/fl}$	
F	5'-CTACGGGCAGGAGGAAGAG-3'
R1	5'-GGGGGAGAGGGAGTTGTC-3'
R2	5'-CCACATAGGCTCATAGAATTG-3'
For Nestin-CreERT2	
oIMR1084	5'-GCGGTCTGGCAGTAAAAACTATC-3'

oIMR1085	5'-GTGAAACAGCATTGCTGTCACTT-3'
oIMR7338	5'-CTAGGCCACAGAATTGAAAGATCT-3'
oIMR7339	5'-GTAGGTGGAAATTCTAGCATCATCC-3'
For GLAST-CreERT2	
GLAST F8	5′-GAGGCACTTGGCTAGGCTCTGAGGA-3′
GLAST R3	5′-GAGGAGATCCTGACCGATCAGTTGG-3′
CER1	5′-GGTGTACGGTCAGTAAATTGGACAT-3′
For gender	
Forward SRY F	5′-TTGTCTAGAGAGCATGGAGGGCCATGTCAA-3′
Reverse SRY R	5′-CCACTCCTCTGTGACACTTTAGCCCTCCGA-3′

PCR program for genotyping: 94°C 4min, 94°C 30sec, 60°C 1min, 72°C 1min (35 cycles), 72°C 10min, 4°C hold. PCR products were separated by agarose gel electrophoresis (2.5% agarose for $Ezh2^{fl/fl}$ mice or 1% agarose for other mice in 1x TAE buffer with 5μg ethidium bromide/100 mL) at 100V for 60min. Results were visualized under ultraviolet light and images were taken with a Bio-Rad UV transilluminator.

2.2 Tamoxifen and BrdU administration

Tamoxifen (Sigma T-5648) was dissolved in corn oil (Sigma C-8267) with 5% ethanol at 37°C for several hours to prepare a 20mg/ml concentration. The tamoxifen solution was warmed to 37°C before injection.

Adult (9 weeks old) mice were given intraperitoneal injections twice daily for 5 days (1mg/day) (Mori et al. 2006).

For young adult mice (4-5 weeks old), one intraperitoneal injection was given per day for 5 days (180mg/kg body weight) (Lagace et al. 2007).

For young postnatal (P0-P1) pups, (1) “P-TMX”, one subcutaneous injection of tamoxifen was administrated (0.2 or 0.6 mg/gram body weight) (Kuo et al. 2006); or (2) “PM-TMX” once subcutaneous injection of tamoxifen (0.2mg/gram body weight) was administrated, followed by once daily 150mg/kg intraperitoneal injection given to the dam for two days (Petrik et al. 2013). Mice were sacrificed at indicated time points after the last injection.

5-bromo-2'-deoxyuridine (BrdU, Sigma B5002) was dissolved in 0.9% normal saline (10mM NaOH) at 37°C to final stock concentration of 10mg/ml. For mouse injections, 50mg/kg (5ul/g) of BrdU solution was injected intraperitoneally (Comte et al. 2011). The injection frequency and times were indicated elsewhere in every experiment.

2.3 Traumatic brain injury model

Cortical lesion was used for traumatic brain injury model (Szele et al. 1995). Adult mice were anaesthetized with an intraperitoneal injection of 1mg/10mg body weight of Ketamine with 0.1mg/10mg body weight of Xylazine. 10-15mins later, anaesthesia was confirmed by the degree of retraction to foot pinching. After shaving the head over the entire dorsal surface of the skull, the mouse was placed into the stereotactic apparatus with ear bars coated with lignocaine (lignocaine ointment 5%). Lacri-lube eye ointment was applied to the mouse eyes to avoid desiccation. The surgery area on the head was sterilized by applying 70% ETOH with cotton tip applicator followed by betadine (betadine dry powder spray) three times.

Using a scalpel blade (No 11), I made a rostral to caudal incision along the midline of the skull and using small hemostats retracted the skin to expose the skull.

Using a cotton tip applicator and 70% ETOH, the fascia was rubbed away; and with a fine tip felt pen, the area of the skull to be removed over the left frontoparietal motor cortex was marked (Figure 2.1). The marked area of the skull was then cut and removed with a scalpel and fine forceps.

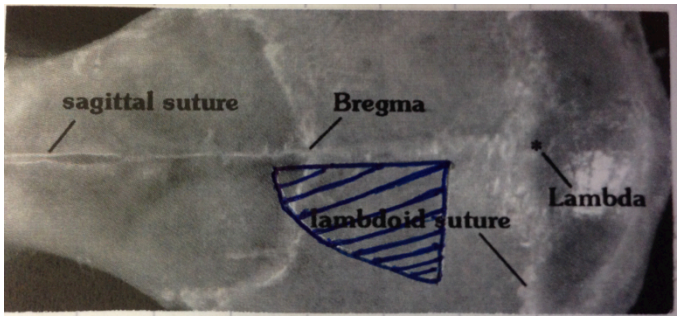

Figure 2. 1 Example of targeted skull area

The dorsolateral prefrontal cerebral cortex underneath the craniotomy was slowly and carefully removed with a fire-polished Pasteur pipet attached to a mild vacuum until the white of the corpus callosum became apparent. The skin incision was sutured and betadine applied. The mice were then placed in a heated box for recovery. For post-surgery analgesic management, the mice were injected subcutaneously with 0.1mg/kg Vetergesic when the mice start to move and another dose of vetergesic was given ~4-6hrs later.

Mouse body weight was monitored every day post-surgery and the mice were culled when the body weight dropped by more than 20%.

Solutions:

Ketamine/ Xylazine: 1ml Ketamine + 0.5 ml Xylazine +8.5 ml normal saline

Ketamine: Vetalar V Ketamine 100mg/ml

Xylazine: Rompun SOLN 2% w/v (20mg/ml)

Vetergesic: Vetergesic Multidose Buprenorphine, 0.3mg/mL

2.4 Middle cerebral artery (MCAO) model of stroke

I used sections obtained from mice that had received a standard middle cerebral artery (MCAO) model of stroke which was carried out by a former Szele lab DPhil student, Dr. Christopher Young (Young et al. 2012).

2.5 Stereotactic lateral ventricle injection

Adult mice were anaesthetized with intraperitoneal injection of 1mg/10mg Ketamine with 0.1mg/10mg Xylazine. After shaving the head over the dorsal surface of the skull, the mouse was placed onto the stereotactic frame. The surgery area was sterilized by applying 70% ETOH with a cotton tip applicator followed by betadine application three times. A rostral to caudal incision was made along the midline of the scalp and using small hemostats the skin opened to expose the skull. The mediolateral (ML), dorsoventral (DV) and anteroposterior (AP) positions for bregma and lambda were determined and the dorsoventral levels equalized to bring the skull horizontal. The injection coordinates from Bregma were as follows: ML +0.75mm, DV -2.6mm, AP +0.5mm. The microinjection was performed with a Hamilton syringe (ID: 0.485mm). 1-2μl of solution was injected at the speed of 0.3ul/min. 2mins after injection, the needle was slowly retracted from the brain and the scalp incision was sutured and daubed with betadine. The post-surgery operation was the same as traumatic brain injury model.

2.6 Electroporation

Plasmids used for postnatal electroporation were prepared by Endofree Plasmid Maxi Kit. Before use, 1% fast green in PBS (filtered through a 0.22μm filter) was mixed

with the plasmid solution at 1:10 for tracing. For the postnatal electroporation procedure, P0-P2 pups were anesthetized by hypothermia. ~2µl of plasmid solution (4µg/µl) was injected into the lateral ventricle via a pulled glass capillary. Pups were then subjected to electrical pulses (-100V, 50ms ON with 850ms intervals for 5 cycles) (BTX ECM 830) by tweezer electrodes coated with conductive gel (Boutin et al. 2008; Chesler et al. 2008; Fernandez et al. 2011). After surgery, pups were kept in a 37°C-warming box for recovery and then returned to the dam.

For adult electroporation, adult mice were anesthetized by intraperitoneal injection of 1mg/10mg Ketamine with 0.1mg/10mg Xylazine. Stereotaxic injection was performed according to the following coordinates from Bregma: dorsoventral= -2.6mm, anteroposterior= +0.5mm, mediolateral= +0.75mm. 2µl of DNA (4µg/µl) was injected into the lateral ventricle at a speed of 0.25µl/min and then electrical pulses (-200V, 50ms ON with 950ms intervals for 5 cycles) were applied (Barnabe-Heider et al. 2008). The surgery area was sutured and mice were then placed in heated box for recovery. For post-surgery analgesic management, the mice were injected subcutaneously with vetergesic when the mice start to move (0.1mg/kg) and another dose of vetergesic was given ~4-6hrs later.

2.7 Histology and immunohistochemical staining

Mice were injected with pentobarbital and perfused with normal saline and 4% PFA. Brains were dissected and kept in 4% PFA at 4°C overnight. On the second day, brains were transferred into 30% sucrose in PB and kept at 4°C for 48 hrs. Brains were frozen down on dry ice and sectioned into cryoprotectant solution on Leica sliding microtome.

Brain sections were washed 3x10min in PBS (pH 7.4), 1x15min in 50mM glycine in PBS, 3x10min in PBS and then blocked in PBS+(10% donkey serum, 0.1%

Triton-X in PBS) for 1hr. Sections were then incubated in primary antibodies at 4°C overnight. The next day, sections were washed with PBS 3x10min, and incubated in secondary antibodies (1:500 in PBS+) for 1hr in dark and washed again 3x10min in PBS. Then brain sections were treated with 4',6-diamidino-2-phenylindole (DAPI, 1:1000) for 15min and washed with 0.1M PB for 3x10min. Sections were mounted on SuperFrost Plus microscope slides with FluorSave Reagent.

For BrdU, Eed and Ezh2 immunohistochemistry, an antigen retrieval step was applied before primary antibody incubation. Brain sections were first washed with 10min PBS three times and incubated in 2M HCl at 37°C for 1hr. The rest of the steps were the same as the immunohistochemistry described above. Biotinylated and streptavidin-conjugated secondary antibodies were used to amplify the fluorescence signal.

The following is a list of primary antibodies used for immunohistochemistry (Table 2.2). AlexaFluor dye conjugated antibodies from Invitrogen were used as secondary antibodies.

Table 2. 2 List of primary antibodies

Antigen	Dilution	Host	Manufacturer Cat.
BrdU	1:400	mouse	Dako M0744
BrdU	1:500	sheep	Abcam Ab1893
Caspase-3	1:1000	rabbit	Cell Signaling 9661
CD45	1:100	rat	Millipore CBL1326
Dcx	1:100	goat	Santa Cruz SC-8066
Eed	1:100	mouse	Abcam ab126542
EGFR	1:200	rabbit	Santa-Cruz sc-03

Ezh2	1:100	mouse	BD Biosciences 612666
GFAP	1:400	rat	Invitrogen 130300
GFAP	1:5000	chicken	Abcam ab4674
GFP	1:500	chicken	Aves GFP-1010
H3K27me3	1:250	rabbit	Millipore 07-449
Iba1	1:500	goat	Abcam ab5076
Ki67	1:500	rabbit	Abcam ab16667
Mash1	1:100	mouse	BD Biosciences 556604
Nestin	1:200	mouse	Millipore MAB353
NeuN	1:400	mouse	Millipore MAB377
Olig2	1:1000	rabbit	Millipore AB9610
PHi3	1:400	rabbit	Millipore 06-570
S100β	1:200	rabbit	Dako Z031129-2
S100β	1:100	mouse	Sigma S2657
Sox2	1:500	rabbit	Millipore AB5603
Sox2	1:200	goat	R&D systems AF2018

2.8 Constructs and molecular cloning

pCAG-Cre-IRES2-EGFP (26646), pCAG-IRES2-EGFP (pCAGIG, 11159), pLKO.1-puro (8453) and CMV-Cre pLKO.1 (25997) were purchased from Addgene (Woodhead et al. 2006; Matsuda and Cepko 2007; Beronja et al. 2010). pLKO.1-shRNA-turboGFP, psPAX2 and pMD2.G were purchased from Sigma. pCAG_tdTom_2A_H2BGFP and pCS2-memb-tdTomato were kind gifts from Dr.

Shankar Srinivas's lab (Trichas et al. 2008). *CLoNe* constructs were from Prof. Zoltan Molnar's lab. Eed and Ring1B shRNA pLKO.1 constructs were from Prof. Neil Brockdorff's lab (Cooper and Brockdorff 2013).

For the Jarid2 overexpression construct, the cloning procedure was as follows. EGFP and Jarid2 sequences were cloned to exchange the Cre sequence between the restriction enzyme sites *XbaI* and *KpnI* in the CMV-Cre pLKO.1 plasmid. First, EGFP was amplified by PCR (Phusion High-Fidelity DNA Polymerase, New England Biolabs M0530S) from pCAG_tdTom_2A_H2BGFP. PCR products were purified by Quick PCR Purification Kit (Qiagen 28104) and both EGFP PCR amplicon and CMV-Cre pLKO.1 plasmids were digested by restriction enzymes *XbaI* and *KpnI* (New England Biolabs) to produce sticky ends. Digested DNA was separated by agarose gel electrophoresis (1% agarose in 1x TAE buffer with 5μg ethidium bromide/100 mL) and purified by Quick Gel Extraction Kit (Qiagen 28704). To ligate DNA, EGFP amplicon and digested CMV-Cre pLKO.1 plasmid were mixed as 20:1 in copy number with T4 ligase (New England Biolabs M0202S) at 16°C overnight. On the next day, ligation products were transformed into GC5^{TM} competent cells (Sigma G3169). Colonies were verified by PCR and only positive ones (CMV-EGFP pLKO.1 plasmid) were sent for sequencing.

To obtain Jarid2 sequence, a plasmid containing cDNA for Jarid2 was purchased from Sigma and the sequence was amplified by PCR. After purification, both the Jarid2 PCR amplicon and CMV-EGFP pLKO.1 plasmid were digested by restriction enzymes *SalI* and *EcoRV* (New England Biolabs). Ligation and transformation steps were the same as those for CMV-EGFP pLKO.1 cloning.

The primers (Invitrogen) for PCR were as follows:

For EGFP

Forward: 5'-gtcatctagaATGAGCAAGGGCGAGGAGCTGTTCACC-3'

Reverse: 5'-gtcaggtaccttagatatcatcatcccgcggatcatcgtcgacTGATG

ATCTGAGTCCGGACTTGTACAGCTC-3'

For Jarid2

Forward: 5'-gtcagtcgacGAGGGCAGAGGAAGTCTGCTAACATGCGGTGACGTC

GAGGAGAATCCTGGCCCAatgagcaaggaaagacccaagaggaatatcattc-3'

Reverse: 5'-GTCAGATATCTACGTACAAAAACTTGAACAGTTTAATGC-3'

2.9 Cell culture

HEK293FT, 3T3 and HEPA cells were cultured in DMEM+GlutaMax (Gibco 32430-027), 10% FBS (Gibco 16000-044) and 1% Pen/Strep (Gibco 15140122) and maintained in 37°C, 5% CO_2 chamber. Before passaging, cells were washed with PBS twice and incubated with trypsin (EDTA 0.05%, Gibco 25300-054) at 37°C until cells detached. Cells were pelleted by centrifuging for 2min at 1200rpm and washed again with PBS and then plated into new flasks or dishes.

For making cell stocks to freeze down, ~80% confluent cells were washed with PBS and incubated in trypsin (EDTA 0.05%, Gibco 25300-054) until cells detached. Cells were then centrifuged for 2min at 1200rpm and resuspended in 1ml freezing medium (complete medium: FBS: DMSO=6:3:1). The cells were mixed well and aliquot 1ml cells/cryovial and stored in -80°C freezer.

For recovering cells from stocks, cells were quickly transferred from -80°C freezer to 37°C water bath till only a small ball of ice remained in the cryovial. 5ml PBS was mixed with the cells and centrifuged for 2min at 1200rpm. Cells were resuspended in 1ml culture medium and then topped up to the required volume for plating.

2.10 Neurosphere assay

Mice were terminated by intraperitoneal injection of pentobarbital and the brains were immediately dissected out and sectioned in the coronal plane with a McIlwain tissue chopper. The SVZ was then dissected out in ice-cold neurobasal+ (see Table 2.3) in a sterile laminar flow hood. The SVZ strips were transferred by Pasteur pipette into a chilled eppendorf tube and spun for 15sec. I aspirated the supernatant and added 300µl accutase and incubated at 37°C for 10min. I then added 2.5mL neurobasal+ and pipetted well to dissociate the SVZ tissue into single cells and centrifuged at 1200rpm for 10min. I aspirated the supernatant and added 1ml neurobasal+growth factor (see Table 2.4) to resuspend the pellet. I counted the cells using a haemocytometer and adjusted the cell numbers to a final concentration of 100,000 cells per 1ml. I cultured the neurospheres in 12.5mL flasks coated with Poly(2-hydroxyethyl methacrylate) (Poly-HEMA).

Table 2. 3 Components of Neurobasal+

Components	Amount	Final concentration	Catalogue#
Neurobasal medium	500mL	475ml	GiBCO 21103
B27 supplement	50x	10mL	GiBCO 17504
N2	100x	5mL	Invitrogen 17502-048
L glutamine	100x	5mL	Invitrogen 25030
Heparine Sodium	10x	36µL	J.T.Baker M916.00
Pen Strept	100x	5mL	GiBCO 15140-122

Table 2. 4 Components of Neurobasal+growth factor

Components	Amount	Final concentration	Catalogue#

Neurobasal +	25mL		
EGF (100µg/mL)	5µl	20ng/mL	Sigma
bFGF (100µg/mL)	5µl	20ng/mL	R&D system

Neurosphere differentiation was performed in Lab-Tek 8-chamber slides (Thermo Scientific 177402) or 96-well plates. Before use, chamber slides were coated with poly-D-lysine at 4°C overnight and washed 3x 5min with distilled water and then coated with 10µg/mL laminin in PBS for 1hr in 37°C incubator. The laminin was aspirated before plating the neurospheres. Secondary neurospheres were dissociated by accutase for 10min at 37°C and plated in double-coated 8-chamber slides with neurobasal+ (without growth factor for differentiation) for 7d.

For fate potential immunohistochemistry, neurospheres were differentiated in 8-chamber slides and were fixed with 4% paraformaldehyde (PFA) for 15min and washed with PBS for 3x 5min and then blocked with PBS+ (5% donkey serum in PBS) for 1hr. Cells were incubated with anti-O4 primary antibody in PBS+ at 4°C overnight. On the next day, neurospheres were washed with PBS for 3x 5min and incubated with secondary antibody (Alexa 568 anti-Mouse) for 1hr. Chambers were then washed with PBS for 3x 5min and blocked again with PBS+ (5% donkey serum, 0.1% Triton-X in PBS) for 1hr and incubated with anti-Tuj1 and anti-GFAP primary antibodies in PBS+ at 4°C overnight. On the third day, chambers were washed with PBS for 3x 5min and incubated with secondary antibodies (Alexa 488 anti-Rat and Alexa 647 anti-Rabbit) for 1hr. Then chambers were washed 3x 5min in PBS and treated with 4',6-diamidino-2-phenylindole (DAPI, 1:1000) for 15min and washed with 0.1M PB for 3x 5min. Chambers were mounted with FluorSave Reagent (Calbiochem 345789).

The following are the primary antibodies used in the fate potential immunohistochemistry (Table 2.5). Alexa Fluor dyes from Invitrogen were used for secondary antibodies.

Table 2. 5 List of primary antibodies

Antigen	Dilution	Host	Manufacturer Cat.
GFAP	1:400	rat	Invitrogen 130300
Tuj1	1:1000	rabbit	COVANCE MMS-435p
O4	1:100	mouse	Millipore MAB345

For BrdU administration, BrdU stock solution (10mg/ml) was diluted as 1:30 with culture medium to the working concentration of 1mM. Cells were incubated with 1mM BrdU for 2hrs (proliferative assay) and fixed by 4% PFA.

2.11 Lentivirus packaging and titration

Lentivirus packaging

The pLKO.1-based second-generation lentiviral system was used in the experiments. $1x10^5$ HEK 293 FT cells were seeded in a 100mm plate and cultured 2 days to reach a confluency of about 80%. The medium was DMEM+GlutaMax (Gibco, 32430-027), 10% FBS (Gibco, 16000-044) and 1% Pen/Strep (Gibco, 15140122). 4hrs before transfection, the medium was replaced with 9ml of fresh DMEM+GlutaMAX+10% FBS (without Pen/Strep). To prepare DNA for transfection, 4.5ug psPAX2, 1.5ug pMD2.G, 6ug transfer plasmid (cDNA/shRNA), and 80µl 2.5M $CaCl_2$ were mixed in H_2O to a final volume of 500ul. 500ul of 2X HEBS (pH 7.05) was then slowly added dropwise to the DNA while vortexing the tube. The solution was left for a few minutes for crystal precipitates to form. 1ml of the precipitated solution was then

slowly added dropwise to the 9ml medium covering the cells while constantly swirling the plate. At 9 AM the next day, the medium was changed with 8ml of DMEM+GlutaMAX+10% FBS+1% Pen/Strep. 48hrs later, the supernatant was collected and replaced with 8ml of fresh medium. The collected supernatant was then spun down for 7min at 2000rpm, 4°C. The supernatant was filtered through 0.45um filters to exclude 293 cell contamination and spun down with a 32Twi rotor for 1hr 40min at 25,000rpm, 4°C. 30ul of autoclaved PBS was added and the mixture incubated overnight at 4°C.

Lentivirus titration

On Day 1, $1X10^4$ HEK 293 FT cells/well were seeded in a 96-well plate. On the next day, the cells were counted in one representative well to ascertain the target cell number. For each viral preparation, 10 eppendorf tubes were prepared for serial dilutions. 2ul virus was added into 198ul culture medium in the 1st tube. 100µl was taken from the 1st tube and add into 900ul medium in the 2nd tube and pipeted to mix well. The serial dilutions were repeated until 10 dilutions were obtained (Table 2.6). 100µl medium with virus was added into each well. Another 100µl medium was added the next day. On Day 5, fluorescent cells were counted in the last two wells before the dilution in which no fluorescent cells could be seen, and the titration was calculated according to the following method.

TU/ul=(P*N/100)/V

P=%GFP^+ cells, N=target cell number, V=volume of virus added in that well. e.g. 1µl gives you 10% of positive cells and starting with 50,000 cells on Day 2, yielded 5,000TU/µl --> 5 x 10^6 TU/ml

Table 2. 6 Virus volume in serial dilution

Tube number	1	2	3	4	5	6	7	8	9	10
Virus volume (µl)	1	10^{-1}	10^{-2}	10^{-3}	10^{-4}	10^{-5}	10^{-6}	10^{-7}	10^{-8}	10^{-9}

2.12 Neural stem cell nucleofection

Neurosphere cell nucleofection was carried out according to the protocol of LONZA (VPG-1004). In brief, 3-4 x 10^6 dissociated cells were mixed with 100µl nucleofection solution (82µl of Nucleofector Solution + 18µl of supplement) and 5-10µg DNA and transferred into the certified cuvette. Nucleofector program A-033 was used. 500µl of pre-warmed culture medium was added into the cuvette and the sample was then transferred by the supplied pipette into 1ml medium and centrifuged at 1200rpm for 5min. Cells were then suspended with fresh medium and plated at 4.5-5 x 10^5 cells/ml.

2.13 Cell transfection

Lipofectamine 2000 kit (Invitrogen 11668) was used for adherent cell line transfection.

2.14 Neurosphere fluorescent immunocytochemistry

For floating neurosphere staining, cells were fixed with 4% PFA for 10min and washed with PBS for 3X5mins. The cells were then blocked with PBS+ (10% donkey serum and 0.1%Triton-X) and incubated with primary antibodies at 4°C, overnight. On Day 2, cells were washed again with PBS for 3X5min and incubated with

secondary antibodies. Nuclei were counterstained with DAPI. All procedures were performed in Netwell inserts.

2.15 Imaging and quantifications

For imaging fluorescent staining slides, epi-fluorescent or confocal microscopy was used. Zeiss 710 or Olympus laser scanning confocal microscopes were used for Z-stack imaging using 40X oil immersion (Zeiss Plan-NeoFluar 40X1.3 Oil DIC) and 20X (Zeiss Plan-Neofluar 20X/0.50) objectives. To excite DAPI, Alexa Fluo 488, Alexa Fluro 568, Alexa Fluro 647 flurophores, excitation wavelengths with 405nm, 488nm, 568nm and 647nm were used respectively. 2µm intervals were used for generating Z-stacks. Confocal images were analysed with LSM Image Brower and ImageJ.

For in vivo analysis, 4-5 representative sections from anterior to posterior SVZ of young adult brains (approximately Bregma +1.70mm to -0.58mm) were imaged and quantified. In every brain section, dorsal, lateral and ventral areas of SVZ (both sides) were analysed to represent the whole SVZ extension. For double and triple staining analysis, at least 6 optical layers of Z stack were imaged. The co-localisation was examined in single optical planes through the Z-axis of every individual image. Brain sections from Bregma +2.22mm to +1.98mm were used for RMS size quantification. For olfactory bulb analysis, at least 10 images with 6 optical layers each, per animal, were acquired to represent anterior to posterior OB of both sides. The same method was also applied to postnatal brain studies. During imaging and quantifications, the primary investigators were blind to genotyping and the data were selectively examined by a second investigator.

2.16 RT-PCR

Total RNA was obtained from the sample with RNeasy Mini Kit following manufacturer instructions. DNA was removed with TURBO DNA-free kit (Invitrogen AM1907) or RNase-Free DNase Set (Qiagen 79254) and reverse transcription was performed by SuperScript III RT kit (Invitrogen 18080). For first-strand cDNA synthesis reaction, 1μg RNA was mixed with 1μl 250ng/μl random primers, 1μl 10mM dNTP and RNase free H_2O, and the mixture was incubated at 65°C for 5min and then on ice for 1min. The following were added into the reaction mixture: 4μl 5x First-Strand Buffer, 1μl 0.1M DTT, 1μl RNaseOUT Recombinant RNase Inhibitor and 1μl SuperScript III RT and then the 20μl final mixture was incubated at 25°C for 5min, 55°C for 1hr, and 70°C for 15min. The cDNA was subjected to real-time quantitative PCR with SYBR Green PCR Master Mix. The target mRNAs were normalized relative to 18S ribosomal RNA. Primers for RT-PCR are listed in Table 2.7.

Table 2. 7 Primer list of RT-qPCR

Gene	Sequence (5'-3')
Gata6	CTTGCGGGCTCTATATGAAACTCCAT
	TAGAAGAAGAGGAAGTAGGAGTCATAGGGACA
Sox17	GCCAAAGACGAACGCAAGCG
	TTCTCTGCCAAGGTCAACGCCT
Hoxa11	TTCCGGCCACACTGAGGACAAG
	ACTCTCGCTCCAGCTCTCGGATCT
Olig2	CGCAGCGAGCACCTCAAATCTAA
	CCCAGGGATGATCTAAGCTCTCGAA
Ngn1	ATCACCACTCTCTGACCC
	GAGGAAGAAAGTATTGATGTTGCCTTA
Ezh2	TTACTGCTGGCACCGTCTGATGTG
	TGTCTGCTTCATCCTGAGAAATAATCTCC
Ezh1	AATATGGGAGCAAAGGCTCTGTATGTG
	CACGAAGTTTCTTCCACTCTTCATTGAG
Eed	GCACAGAGATGAAGTTCTGAGTGCTG
	ATAAGACTCCTTAATTGCATTCATCATCCT

18s	GTAACCCGTTGAACCCCATT
	CCATCCAATCGGTAGTAGCG
Mash1	GCAACCGGGTCAAGTTGGT
	GTCGTTGGAGTAGTTGGGGG
Id2	ATGAAAGCCTTCAGTCCGGTG
	AGCAGACTCATCGGGTCGT
Dcx	CATTTTGACGAACGAGACAAAGC
	TGGAAGTCCATTCATCCGTGA
Bmp4	CACTGTGAGGAGTTTCCATCACGAAG
	GGATGCTGCTGAGGTTGAAGAGGA
Bmp6	GCCATCTCGGTTCTTTACTTCGAT
	GTGGTTTAAGGCAGATGTTGTTGTT
Ngn2	TCGCCAGGGACTGTATCT
	CTGTGAAGTGGAGTCCG
p21 (Cdkn1a)	CCTGGTGATGTCCGACCTG
	CCATGAGCGCATCGCAATC
p27 (Cdkn1b)	TCAAACGTGAGAGTGTCTAACG
	CCGGGCCGAAGAGATTTCTG
p57 (Cdkn1c)	CGAGGAGCAGGACGAGAATC
	GAAGAAGTCGTTCGCATTGGC
Cdkn2a	CAGACCGACGGGCATAGCTTCA
	GGATTTAGCTCTGCTCTTGGGATTGG
Bmp7	TTCCTGGTAACCGAATGCTGA
	CCTGAATCTCGGCGACTTTTT

2.17 Western blot

Proteins were run on a 12% SDS-PAGE gel at 100V and transferred into PVDF membrane at 100V for 90min. The membrane was blocked in 5% skim milk in PBST (PBS+0.1% Tween-20) and incubated with the primary antibody at 4°C overnight. On the second day, the membrane was washed in PBST for 10min, 3 times. The membrane was incubated with the secondary antibody for 1hr. It was then washed in PBST for 20min, 3 times. Lumigen PS-3 kit was used for chemofluorescence development.

2.18 Co-immunoprecipitation assay

μMACS Protein A/G MicroBeads kit (Miltenyi Biotec 130-042-601) were used for the co-immunoprecipitation assay. Cells were first washed with pre-cooled PBS and centrifuged at 300g for 5min, 4°C. 1ml of lysis buffer was added to the pellet and incubated on ice for 30mins with occasional mixing. The sample was then centrifuged at 10,000g for 10min at 4°C. The supernatant was divided into two tubes (IgG tube and Antibody tube). 2μg of monoclonal antibodies with 50μl of MicroBeads, or 4μg of polyclonal antibodies with 100μl of MicroBeads were added and the mix incubated for 30min on ice. To prepare the μColumn, 200μl of lysis buffer was loaded to rinse the column. The cell lysate was then applied to the column and this non-bound fraction was collected as run through. The columns were then rinsed with 4X200μl of lysis buffer and 1X100μl of low salt wash buffer. To elute the bound fraction, 20μl of pre-heated (95°C) 1XSDS gel loading buffer was applied onto the column and incubated for 5min at room temperature. Then columns were eluted with 50μl of pre-heated (95°C) 1XSDS gel loading buffer. The run-through and the elutions for IgG and antibodies were used for western blot to detect protein-protein binding.

2.19 Chromatin-immunoprecipitation assay

Neurospheres or tissues were cross-linked by 0.9% formaldehyde (fresh 9% formaldehyde: 2ml of 37% formaldehyde stock + 6.2ml PBS) and rotated gently at room temperature for 10min. Crosslinking was stopped by adding 2.5M glycine to a final concentration of 0.125M for 5min. Cells were then rinsed twice with cold PBS and spun down for 10min, at 1500rpm, 4°C. The cells were resuspended with 350ul cell lysis buffer and incubate on ice for 10min. Lysates were sonicated on ice at power level 5 for 6 times with 10s on and 10s off every time. They were spun at

12,000rpm for 10min at 4°C and the supernatant transferred to fresh tubes. 10ul was taken from the supernatant as input control with 180ul of TE buffer, 10ul of 5M NaCl to a final concentration of 0.25M, and 2ul RNaseA (4mg/ml). The rest of the fragmented-chromatin was diluted 5 fold in ChIP dilution buffer (e.g. 800ul ChIP dilution buffer into 200ul sonicated supernatant). 5-10ug IP antibody was added and incubated overnight at 4°C with rotation. The next day, 50ul of blocked Protein A/G beads* was added and incubated for 3hrs at 4°C with rotation. The beads were pelleted and the supernatant carefully removed. Beads were then washed with 10min/wash by rotation with: low salt IP wash buffer, high salt IP wash buffer, LiCl IP wash buffer and TE buffer (X2). To elute the complex from the antibody, 140ul freshly prepared elution buffer was added to the pelleted beads and vortexed to mix and incubate at 65°C for 20min. The beads were then spun down and the eluate was transferred to a fresh tube. The elution was repeated once with 100ul elution buffer to get a final volume of 240ul eluates. To reverse crosslinks, proteinase K was added to 10mg/ml and the samples were incubated at 65°C overnight. DNA was purified with Quick PCR Purification Kit (Qiagen 28104).

(*Beads preparation: Beads were washed in PBS and spun at 2000rpm, 1min at 4°C for twice. Beads were then blocked by incubation with 0.1% BSA in PBS for twice (10-15min each time at 4°C) and 0.1% BSA in dilution buffer (10-15min at 4°C). Beads were washed again in dilution buffer and kept in 4°C.)

To run ChIP-qPCR, 1ul DNA was mixed with 1ul primers (2uM stock for forward and reverse primers), 10ul Syber Green and 8 ul H_20 to final volume of 20ul. qPCR was run with standard program and the results were calculated by $2^{-\Delta\Delta Ct}$ relative to input. The primers for qPCR were as follows (Table 2.8).

Table 2. 8 Antibody list for ChIP

Antibody	Host	Catalogue
H3K27me3	rabbit	Millipore 07-449
Eed	mouse	Millipore 05-1320
Ezh2	mouse	Cell Signaling 3147

Table 2. 9 List for ChIP-qPCR primers

Gene	Sequence (5'-3')
Olig2	GCCTGACGCTACAGTGACAA
	GGCTAATTCCGCTCAATGAA
Gata6	CGGTCCTTCGCTTTAGAAGATTGTAGG
	ACACAGACCCAGGCAAGATAGCAAGA
Ngn1	CATTGTTGCGCGCCGTA
	GCGATCAGATCAGCTCCT
Ngn2	GATTGTTTTCTTGGTGGTATATAAGGG
	GACTCCAAGGCACTCCAGTTAAA
Sox2	CCTAGGAAAAGGCTGGGAAC
	GTGGTGTGCCATTGTTTCTG
Actin (promoter)	CCCAACACACCTAGCAAATTAGAACCAC
	CCTGGATTGAATGGACAGAGAGTCACT
Actin (intron I)	CGTATTAGGTCCATCTTGAGAGTACACAGTATT
	GCCATTGAGGCGTGATCGTAGC
Hoxa11	GCTGCGAAGAAGGTGCTGAACG
	CGGTGGGTGAGGGATACTCTCTGG
Sox17	CCACTCACTCTGAGGCTCGCTGTAG
	CCAAAGCAGACCTGAGGCTCGAA

2.20 Microarray

A total of three experiments were conducted on different days. All experiments used 12 weeks old CD-1 male mice. Experiment1: n=5 lesioned, n=5 anaesthetic controls; Experiment 2: n=5 lesioned, n=4 anaesthetic controls; Experiment 3: n=4 lesioned, n= 4 anaesthetic controls. All reagents and instruments were RNase free. Two days post

cortical lesion or anaesthetic control, mice were anesthetized with isoflorane, and placed 5min on ice before excising brain into ice cold aCSF (artificial cerebral spinal fluid) for 2min with gentle swirling. The brain was placed into an RNase free, cold coronal brain mould and three sections/brain of upper third ipsilateral hemisphere were sliced with an RNase free scalpel blade into RNase free microcentrifuge tubes (1.5ml) on dry ice/95% ETOH slush. Microcentrifuge tubes were weighed prior to collecting tissue. RNA isolation was performed using the RNeasy Kit (Qiagen). RNA preparations from all samples had a minimal ratio of 1.7 and 97% purity. All samples were stored at -80. Microarray analysis on all samples was conducted by the Microarray Facility at CMRC, Northwestern University, USA.

2.21 Statistics

Biological replicate numbers were indicated as n number in every experiment in different chapters. For in vivo experiments, n indicates the animal numbers per each group; for in vitro experiments, n indicates the independent culture numbers. Numerical data were presented as mean ± standard error of the mean, except for ChIP-qPCR with mean ± standard deviation. Student's t-test was used to assess the differences between two groups. For significant difference, $p<0.05$ was marked as *, $p<0.01$ as **, $p<0.001$ as ***. Statistical analysis was performed with Graphpad and graphic representations were produced with Mac Numbers.

Chapter 3

PRC2 expression in the healthy and injured brains

3.1 Introduction

3.1.1 PRC2 components

Since the discovery of Polycomb proteins about 70 years ago (Grimaud et al. 2006), several components of PRC2 have been identified and studied till now (Margueron and Reinberg 2011). Unlike PRC1, the histone ubiquitination modifier that is present in more diverse forms, PRC2 is relatively conserved (Margueron and Reinberg 2011; Schwartz and Pirrotta 2014). It is generally believed that PRC2 contains four core subunits: Ezh1/Ezh2, Eed, Suz12 and Rbbp family (Figure 3.1). Additionally, other components can also be found in this complex, including Jarid2, Aebp2, Pcl and non-coding RNA (Figure 3.1A).

Ezh1 and Ezh2 belong to the histone lysine methyltransferase family with the SET domain, which has enzymatic activity and is able to catalyse the di-/tri-methylation of H3K27 (Margueron and Reinberg 2011). The SET domain can also serve as a target for pharmacological inhibitors (Knutson et al. 2012; Liu et al. 2014b). Though Ezh1 and Ezh2 are in the same protein family, a few differences have also been documented: (1) different expression and chromatin binding mechanisms and (2) Ezh1 has much lower enzymatic abilities compared to Ezh2 (Margueron et al. 2008; Margueron and Reinberg 2011). Besides, mutations in human *EZH2* are linked with Weaver syndrome, characterized as overgrowth, macrocephaly, facial gestalt, etc (Gibson et al. 2012; Tatton-Brown et al. 2013). The functions of Ezh2 in the neurogenic niche have just started to be explored (Hwang et al. 2014; Zhang et al. 2014). One controversy arising from these two studies is whether Ezh2 is expressed in adult NSC. This question will be studied in this chapter. Also from the functional perspective, the existence of Ezh1 may interfere with the phenotypes of Ezh2

knockout (Shen et al. 2008). Thus, to circumvent this issue, other PRC2 subunits, like Eed should also be investigated in postnatal/adult SVZ (Xie et al. 2013). Eed is indispensable for the PRC2 formation (Shen et al. 2008; Margueron et al. 2009).

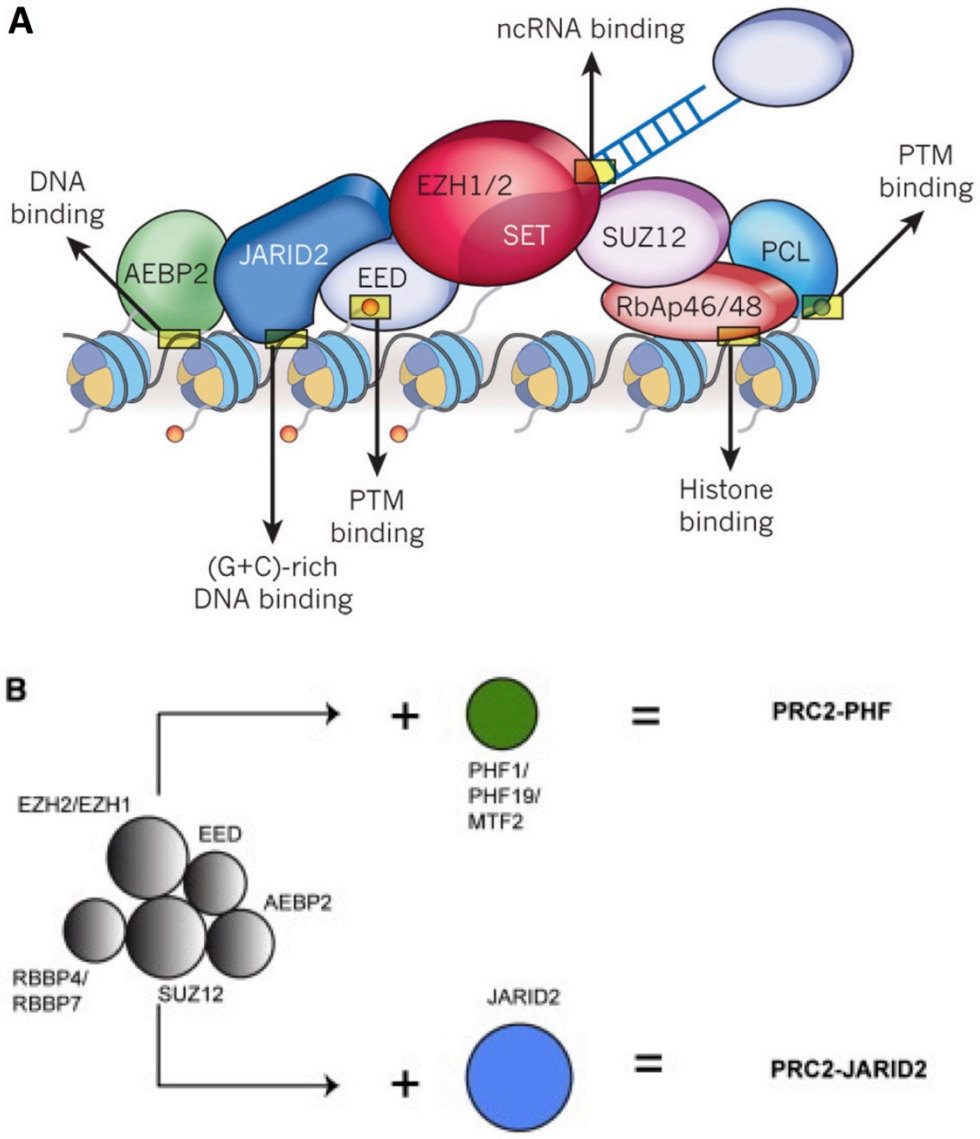

Figure 3. 1 PRC2 components

(A) The components of PRC2 are illustrated. Besides the core subunit (EZH1/EZH2, EED and SUZ112), other components, including JARID2, PCL and ncRNA, are also associated with PRC2 (modified from Margueron and Reinberg 2011). (B) PRC2 can form different variants with either Jarid2 or Phf1/19/Mtf2 (modified from Schwartz and Pirrotta 2014).

Impressively, a new study points out that Eed may link PRC1 and PRC2. These two complexes are capable and will compete to bind with Eed (Cao et al. 2014). Except for the biochemical features of Eed, nothing is known about its functions in neural development. I will start to examine Eed function in the postnatal/adult SVZ here.

Jarid2 is a member of Jumonji family. It was discovered that Jarid2 associates with PRC2 and regulates the binding of the latter to target genes (Figure 3.1B) (Shen et al. 2009; Pasini et al. 2010). Jarid2 was first reported to control the enzymatic ability of PRC2 and to fine-tune its activity (Peng et al. 2009; Shen et al. 2009). Furthermore, Jarid2 and Aebp2-containing PRC2 can read H2A ubiquitylation and be recruited to H2Aub for the next-step H3K27 methylation (Kalb et al. 2014; Schwartz and Pirrotta 2014). Our lab previously found that Jarid2 is expressed in SVZ neural stem/progenitor cells and regulates their proliferative ability. The relevance of Jarid2 with PRC2 in SVZ neurogenesis will be discussed in detail in Chapter 4.

LncRNAs (over 200 nucleotides) have been referred as transcriptional noise or junk for a long time, although this idea has been challenged recently (Mattick and Makunin 2006; Ponting and Belgard 2010; Bassett et al. 2014). Limited information claimed a set of lncRNAs could bind with and then recruit PRC2 in *cis* to repress nearby gene expression. Examples are *XIST* and *HOTAIR* (Rinn et al. 2007; Zhao et al. 2008; Wu et al. 2010). The involvement of PRC2 is one of the most favourable mechanisms for lncRNA research, although opposite observations between RNA immunoprecipitation and super-resolution microscopy make the story more mysterious (Zhao et al. 2008; Cerase et al. 2014). The expression profile of lncRNAs in different cell types in the SVZ has been described recently, and identified a large number of lncRNAs at distinct neurogenic lineage stages (Ramos et al. 2013). Further study of lncRNA in postnatal SVZ neurogenesis will be discussed in Chapter 6.

3.1.2 Gene expression dynamics in SVZ neurogenic lineage

The cytoarchitecture of the postnatal/adult SVZ has been studied extensively. Cell markers for different neurogenic stages have also been discovered for cell type identification, cell sorting and lineage tracing (Ihrie and Alvarez-Buylla 2011; Ming and Song 2011). Briefly, type B stem cells express GFAP and Sox2, type A transit amplifying cells express Mash1 and type C neuroblasts express Dcx (Figure 3.2) (Ming and Song 2011). Nevertheless, a few questions still remain elusive.

Quiescent NSC vs. active NSC The primary difference between quiescent and active stem cells is the cell cycle state. Therefore the identification of quiescent stem cells mainly replies on the incorporation and retaining of thymidine analogue (e.g. BrdU, EdU) (Cheung and Rando 2013). The development of fluorescent protein fused H2B offers an alternative for this purpose (Tumbar et al. 2004; Cheung and Rando 2013). However, they are not feasible in non-thymidine analogue treated or non-transgenic animals. In the SVZ, EGFR is used to distinguish active NSC from quiescent NSC (Codega et al. 2014). With this marker, more gene expression differences have been described between these two NSC groups (Codega et al. 2014). Bothe Glast and Nestin have been stained for NSC and their promoters were also used to label NSC (Mori et al. 2006; Lagace et al. 2007). But current research revealed Glast is expressed preferentially in quiescent NSC whereas Nestin in active NSC (Decarolis et al. 2013; Codega et al. 2014). Based on this comparison, one interesting question is whether PRC2 regulates quiescence vs. activation in SVZ NSC via its involvement in the repression of cell cycle inhibitors (Shen et al. 2008; Pereira et al. 2010; Xie et al. 2013; Hwang et al. 2014).

Adult NSC vs. niche astrocytes The glial nature of adult NSC is reflected from its related molecular signatures with niche astrocytes. The combination of GFAP and prominin1 (CD133) seems promising to distinguish them (Beckervordersandforth et al. 2010; Beckervordersandforth et al. 2014). But the most reliable characteristics of adult NSC are their location in pinwheel-like structure and primary cilium (Mirzadeh et al. 2008; Ihrie and Alvarez-Buylla 2011).

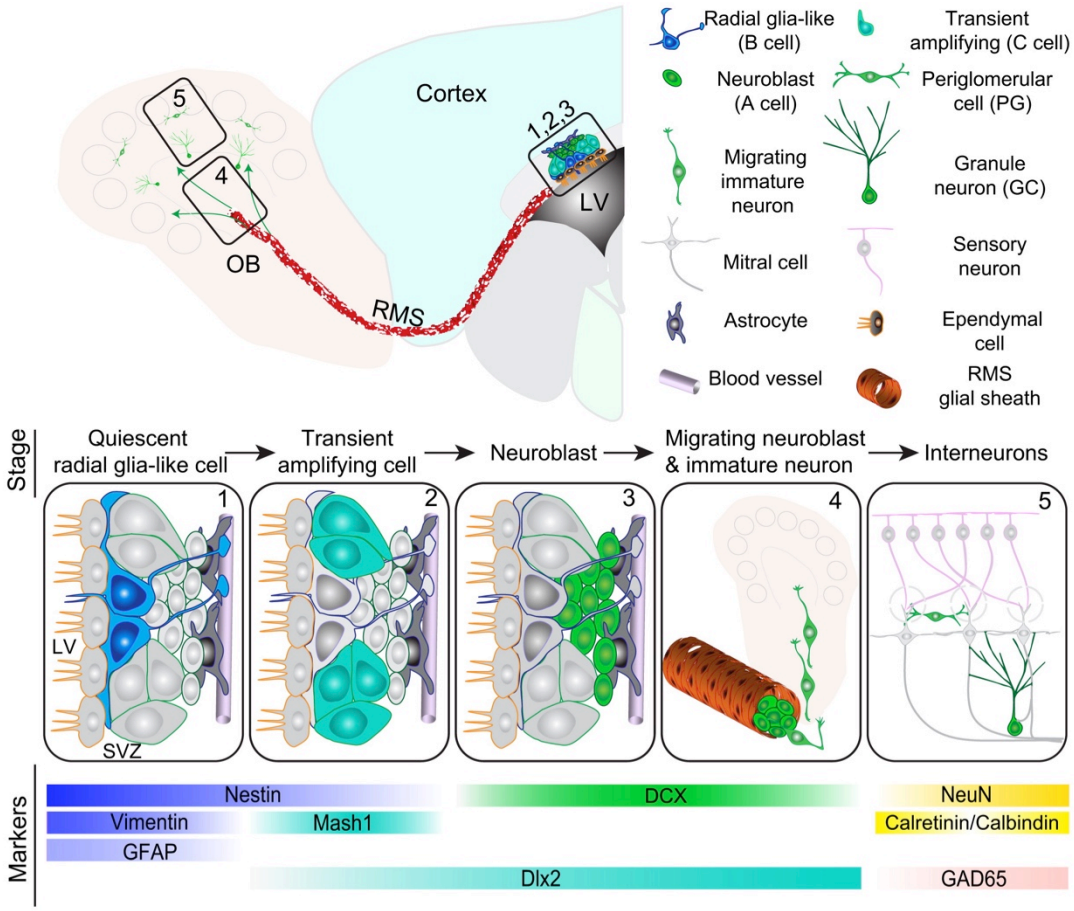

Figure 3. 2 The organization of the adult SVZ

A number of different cell types can be found in the adult SVZ/RMS/OB. (modified from Ming and Song 2011). The neurogenic lineage includes quiescent NSC (radial glia-like), transit amplifying cells and neuroblasts. These individual cell types possess unique cell markers during lineage progression. Moreover, ependymal cells, blood vessels and astrocytes also reside in the adult SVZ.

On the epigenetic level, it is not yet confirmed of any variation in histone or DNA modification among these cell types. Thus I will start the thesis with the expression analysis in the SVZ by immunohistochemistry.

3.1.3 Cell plasticity and dynamics in brain injury

The low regeneration capacity limits self-repair after brain injury. The discovery of cell plasticity in the adult brain, especially the SVZ, provides new insights into the therapeutic potential (Szele and Chesselet 1996; Goings et al. 2002; Goings et al. 2004; Zhang et al. 2004; Gotts and Chesselet 2005). Additionally, reprogramming is another option, although more work is still in need (Guo et al. 2013; Su et al. 2014; Niu et al. 2015).

Cell plasticity in SVZ In the healthy brains, neuroblast migration is restricted in RMS (Ihrie and Alvarez-Buylla 2011). Increased neuroblast numbers and altered migratory stream have been noticed after different injury models (Szele and Chesselet 1996; Young et al. 2011; Young et al. 2012; Young et al. 2014). One proposed therapeutic idea is to guide these neuroblasts towards injury area for cell replacement, but its shortcoming is the majority of SVZ neuroblasts differentiate into GABAergic neurons in OB. For now no evidence can prove that these ectopic migratory neuroblasts are able to differentiate into a spectrum of neuronal subtypes in various brain areas (Liu et al. 2009). The consistent epigenetic modification may explain this long-term lineage commitment, which unfortunately is still unknown to us.

Cell plasticity in lesion Self-renewable and multipotent neurospheres can be generated from the injured cerebral cortex and striatum, the non-neurogenic regions in the adult brains (Buffo et al. 2008; Sirko et al. 2009; Shimada et al. 2012; Grande et al. 2013). Reactive astrocytes are considered as the source for these injury-induced

stem cells (Buffo et al. 2008; Buffo et al. 2010; Sirko et al. 2013). Intriguingly, Lundberg et al reported traumatic brain injury can cause the subcellular relocalization of the DNA methyltransferase, Dnmt1 in reactive astrocytes (Lundberg et al. 2009). We do not know whether this is relevant to the stem cell properties, but it indicates epigenetic mechanisms may underlie astrocyte activation.

In this chapter, I am going to answer the following questions: (1) Whether PRC2 is expressed in SVZ quiescent NSC? (2) Whether PRC2 has a dynamic expression during the SVZ neurogenic lineage progression? (3) What is the expression pattern of PRC2 after brain injury?

3.2 Results

3.2.1 Ezh1 and Ezh2 expression in postnatal and adult SVZ

In situ hybridization of Ezh2 in P56 brain (data from Allen Brain Atlas) had shown its high and dense expression in the SVZ and RMS, with several expressing cells around the brain (Figure 3.3A). In consistent with this mRNA expression pattern, immunohistochemistry also showed the restricted expression of Ezh2 in P42 RMS/SVZ (Figure 3.3B), with few Ezh2+ cells in the striatum and corpus callosum (n=3). In the SVZ, most GFAP+/Sox2+ neural stem cells were Ezh2- (only 6.45±2.75% GFAP+/Sox2+ cells were Ezh2+, n=3) (Figure 3.3C). In the RMS/OB, Ezh2+ nuclei could be detected mainly in the doublecortin (Dcx)+ neuroblasts; while H3K27me3+ nuclei could be found throughout the OB, including RMS and the granular layer (n=3, Figure 3.3D-E). In contrast to Ezh2, RT-qPCR (n=2, Figure 3.3F) indicated the broad expression of Ezh1 across the P56 brain areas, including OB (0.00203±0.00248), cerebral cortex (0.000876±0.000889), striatum (0.000116±0.0000932), septum (0.000136±0.000121) and SVZ (0.000481±0.000484). In situ hybridization of Ezh1 in P56 brain was similar to the RT-qPCR result (data from Allen Brain Atlas, Figure 3.3G).

To confirm the absence of Ezh2 in SVZ quiescent NSC in vivo, I then used the BrdU-label retaining technique (Ferron et al. 2007). BrdU was given twice daily in P42 mice for 5 consecutive days (10 injections in total), and the mice were sacrificed 5 weeks after the last injection. Because of the low cell division frequency, only quiescent SVZ NSC could retain BrdU after the 5-week dilution period. BrdU-label retaining cells (LRC) were costained with Ezh2 and only 7.58±1.96% LRC had

Ezh2+ nuclei in SVZ (n=3, Figure 3.4A, C), which is similar to the GFAP+/Sox2+ cells (Figure 3.3C). However, 97.37±1.96% actively proliferating cells identified by

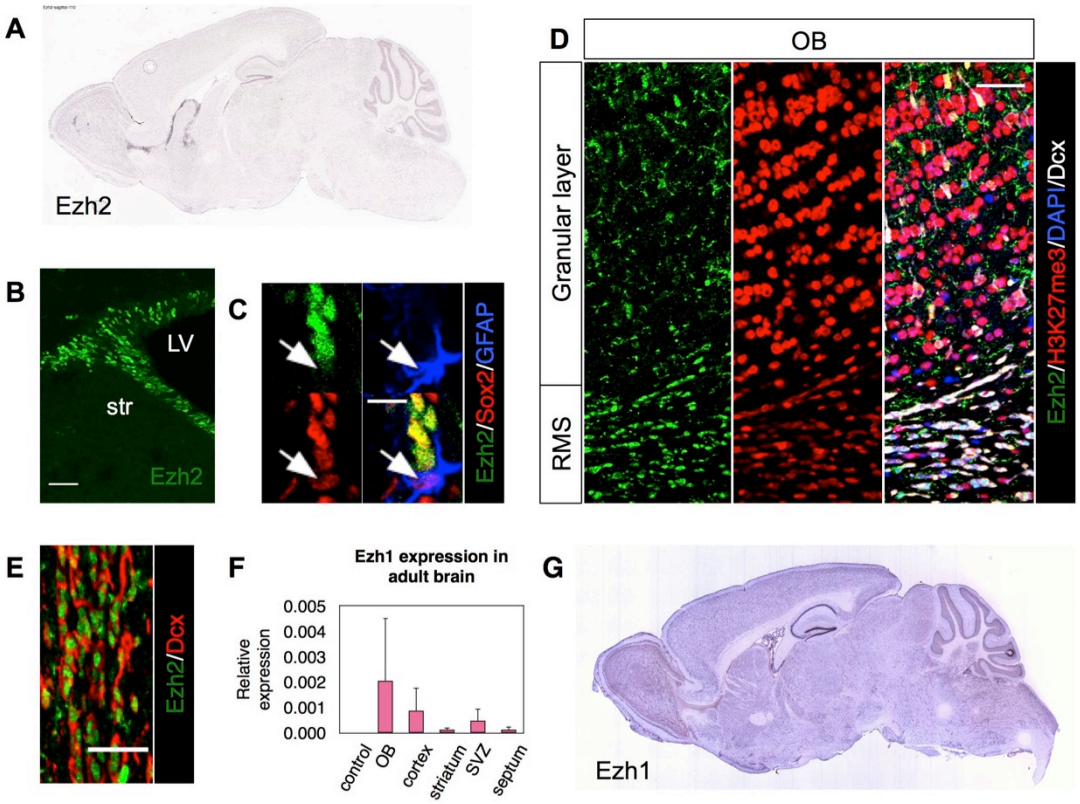

Figure 3. 3 Ezh2 and Ezh1 expression in adult brain

(A) In situ hybridization of Ezh2 in the adult brain (data from Allen Brain Atlas).
(B) Immunostaining shows the restricted expression of Ezh2 in the P42 SVZ (n=3).
(C) Costaining of Ezh2 with GFAP and Sox2 in the P42 SVZ. The white arrows indicate Sox2+/Ezh2- cells (n=3).
(D-E) Costaining of Ezh2 with Dcx and H3K27me3 in the P42 RMS and OB (n=3). (E) shows the high magnification of RMS.
(F) qPCR analysis of Ezh1 expression in different brain areas in the adult brain (n=2). The expression is normalized to the internal control 18s.
(G) In situ hybridization of Ezh1 in the adult brain (P56) (data from Allen Brain Atlas).
LV, lateral ventricle; str, striatum. Scale bar: (B)=40um, (C)=10um, (D)=30um, (E)=20um.

2hrs-BrdU labelling (n=3, Figure 3.4B, C) expressed Ezh2. This could be further confirmed with costaining of Ezh2 and Phospho-histone 3 (PHi3), which labels proliferating cells in M-phase (Figure 3.4D).

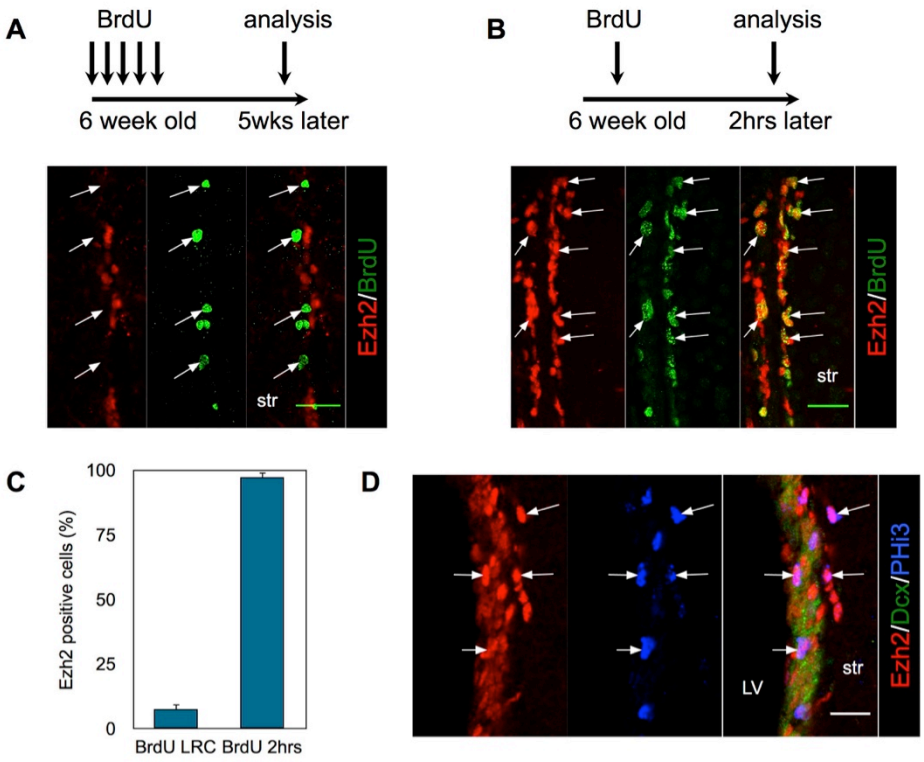

Figure 3. 4 Ezh2 in proliferating cells and quiescent SVZ stem cells

(A) Immunostaining of Ezh2 in the BrdU label-retaining cells. The arrows indicate the examples of BrdU+ cells (n=3).

(B) Costaining of Ezh2 and BrdU after 2hrs BrdU labelling. The arrows indicate the examples of BrdU+ cells (n=3).

(C) Quantification of Ezh2+/BrdU+ cells in total SVZ BrdU+ cells (mean±SD, n=3).

(D) Costaining of Ezh2 and cell proliferative marker PHi3 in the adult SVZ (n=3).

LV, lateral ventricle; str, striatum. Scale bar: (A)=30um, (B)=30um, D=20um.

Neurospheres, in vitro cultured from postnatal SVZ in exposure to EGF and FGF, showed a high level of Ezh2, which had costainings with 2hrs-BrdU, Olig2 and Sox2 (Figure 3.5A-B). In the differentiation condition, Ezh2 could also be detected in 24hrs-BrdU+ nuclei, but not BrdU- nuclei (Figure 3.5C). These together suggest Ezh2

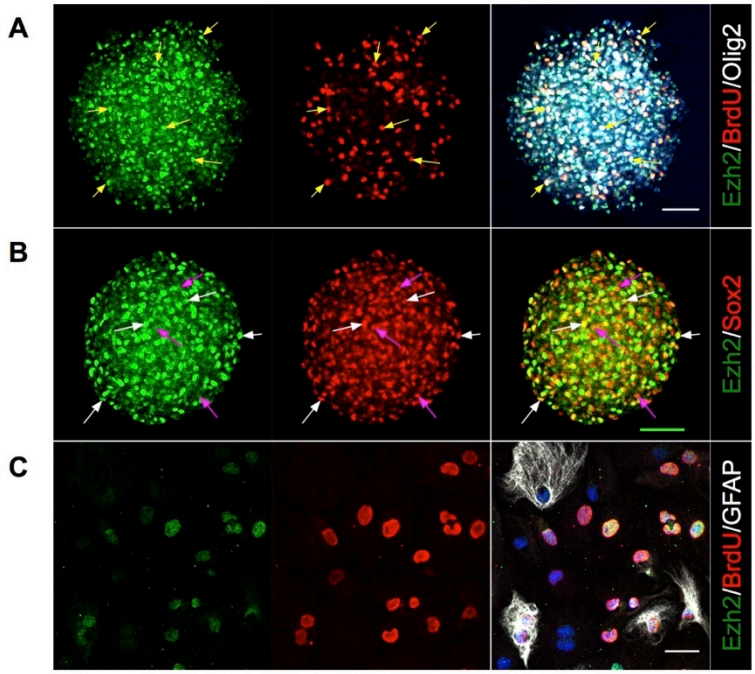

Figure 3. 5 Ezh2 expression in postnatal SVZ neurospheres

(A) Coimmunostaining of Ezh2 with BrdU (2hrs) and Olig2 in postnatal neurospheres. The arrows (yellow) indicate Ezh2+/BrdU+ cells. Nuclei are counterstained with DAPI (blue).
(B) Coimmunostaining of Ezh2 with Sox2 in postnatal neurospheres. The white arrows indicate Ezh2+/Sox2+ cells, while the magenta arrows indicate Ezh2-/Sox2+cells.
(C) Coimmunostaining of Ezh2 with BrdU and GFAP in monolayer cultured neural stem cells from postnatal SVZ (differentiation condition without EGF and FGF). Cells were incubated with BrdU for 24hrs and counterstained with DAPI (blue).
Scale bar: (A)=60um, (B)=60um, (C)=30um.

is not expressed by SVZ quiescent NSC until the NSC get activated and enter the lineage development.

3.2.2 Eed expression in postnatal and adult brains

Eed is another core subunit of PRC2, which is found in both Ezh1/PRC2 and Ezh2/PRC2. To examine the expression of Eed in postnatal brain, western blot was performed on tissues from P4 mouse brains, which showed Eed was expressed in OB, cerebral cortex, cerebellum, striatum and SVZ neurospheres (n=1, Figure 3.6A). Similarly, immunohistochemistry of Eed in P42 brains indicated the broad expression of Eed in cerebral cortex, striatum and OB; while surprisingly in the white matter, i.e. corpus callosum, only weak immunostaining of Eed could be detected (n=3, Figure 3.6B, C). Different cell markers were then costained with Eed to analyse the Eed expression on cellular levels. In SVZ, both Ki67+ actively proliferating cells and BrdU-LRC (in all examined cells) were Eed+ (n=3, Figure 3.6D). GFAP+ niche astrocytes (n=3, Figure 3.6E) and EGFR+GFAP- transit amplifying cells (n=3, Figure 3.6F) were also Eed+. In RMS/OB, Eed+ nuclei could be observed in Dcx+ neuroblasts, neurons in granular layers (n=3, Figure 3.6G-H) and GFAP+ parenchymal astrocytes (n=3, Figure 3.6I). These data suggest, different from Ezh2, Eed is expressed in the entire SVZ lineage including quiescent NSC.

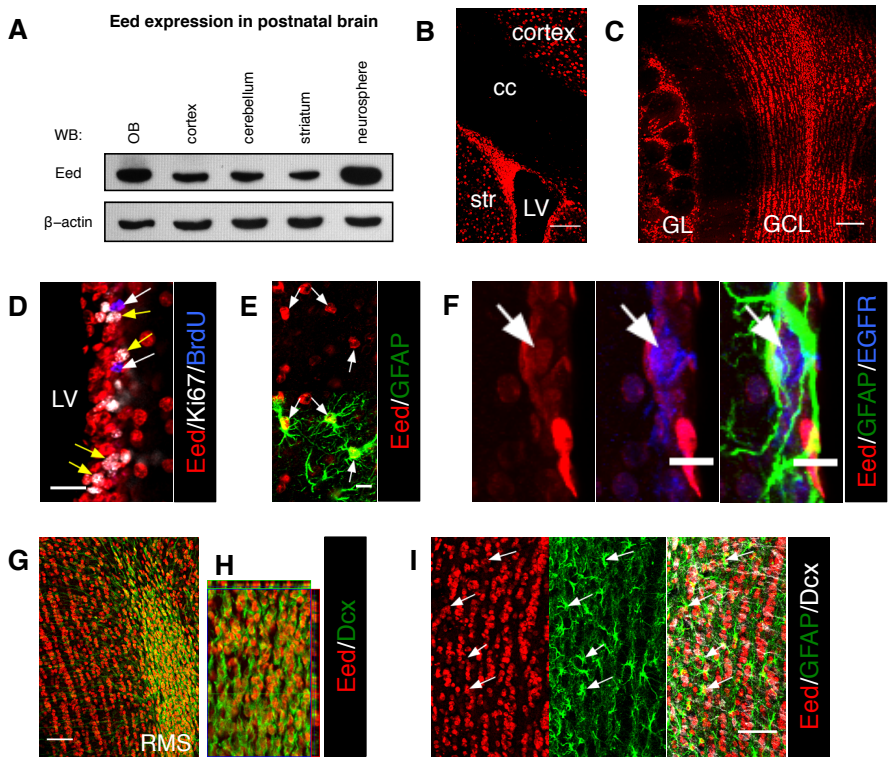

Figure 3. 6 Eed expression in postnatal and adult brains

(A) Western blot of Eed in different brain areas in the postnatal brain (P4) (n=1).

(B-C) Immunostaining of Eed in the adult brain (P57) (n=3).

(D) Costaining of Eed with Ki67 and BrdU in adult SVZ. BrdU indicated LRC cells (n=3). The yellow arrows show Ki67/Eed double positive cells. The white arrows show BrdU/Eed double positive cells.

(E) Costaining of Eed and GFAP in the adult SVZ (n=3). The arrows show GFAP/Eed double positive cells.

(F) Costaining of Eed with GFAP and EGFR in the adult SVZ (n=3). The arrows show EGFR+GFAP- cells.

(G-H) Costaining of Eed and Dcx in the adult OB (n=3). (H) shows the high magnification of RMS.

(I) Costaining of Eed and GFAP in the adult OB (n=3). The arrows indicate GFAP/Eed double positive cells.

Cc, corpus callosum; str, striatum; LV, lateral ventricle; GL, glomerular layer; GCL, granular cell layer. Scale bar: (B)=100um, (C)=100um, (D)=20um, (E)=10um, (F)=10um, (G)=50um, (I)=50um.

3.2.3 H3K27me3 in postnatal and adult brains

Immunostaining of H3K27me3 in P4 brain showed the broad distribution of this mark throughout brain with weak reactivity in the corpus callosum (n=3, Figure 3.7A). Cell type analysis in SVZ indicated Dcx+ neuroblasts had relatively lower H3K27me3 staining, compared to the neighbouring cells (n=3, Figure 3.7B). H3K27me3 was

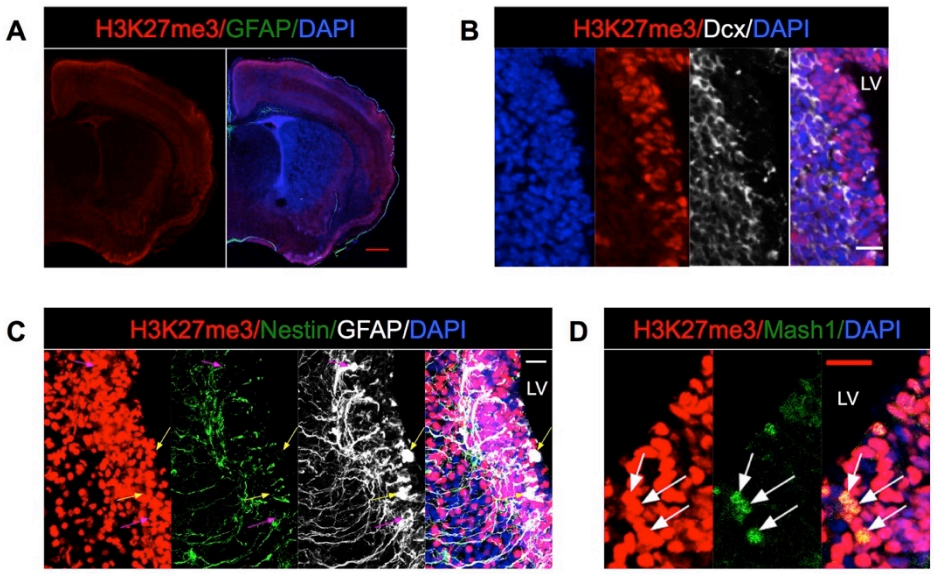

Figure 3. 7 H3K27me3 in different cell types in postnatal brain

(A) Costaining of H3K27me3 and GFAP in the postnatal brain (P4).
(B) Costaining of H3K27me3 with Dcx in the SVZ.
(C) Costaining of H3K27me3 with GFAP and Nestin in the SVZ. The yellow arrows indicate GFAP+/Nestin- astrocytes and the magenta arrows indicate GFAP+/Nestin+ stem cells.
(D) Costaining of H3K27me3 with transit amplifying cell marker Mash1 in the SVZ. The arrows indicate examples of Mash1+ cells.
LV, lateral ventricle. Scale bar: (A)=500um, (B-D)=20um.

expressed in GFAP+/Nestin+ neural stem/progenitor cells, GFAP+/Nestin- niche astrocytes (n=3, Figure 3.7C) and Mash1+ transit amplifying cells (n=3, Figure 3.7D).

In the adult SVZ (P42), H3K27me3 could also be detected in GFAP+/Nestin+ NSC, as well as GFAP+/Nestin- niche astrocytes (n=3, Figure 3.8A). Mash1+ transit amplifying cells and Dcx+ neuroblasts (n=3, Figure 3.8B) also expressed H3K27me3 with a lower level in the neuroblasts. Importantly, variations of global H3K27me3 could be observed among individual postnatal and adult SVZ stem cells, transit amplifying cells and neuroblasts (n=3, Figure 3.7-3.8). However in more quiescent and homogeneous cells, including S100β+ ependymal cells in adult SVZ (n=3, Figure 3.8C) and NeuN+ mature neurons in cortex (n=3, Figure 3.8D), H3K27me3 was more comparable among individual cells. In the Iba1+ microglia, only very weak to absent H3K27me3 could be detected (n=3, Figure 3.8E).

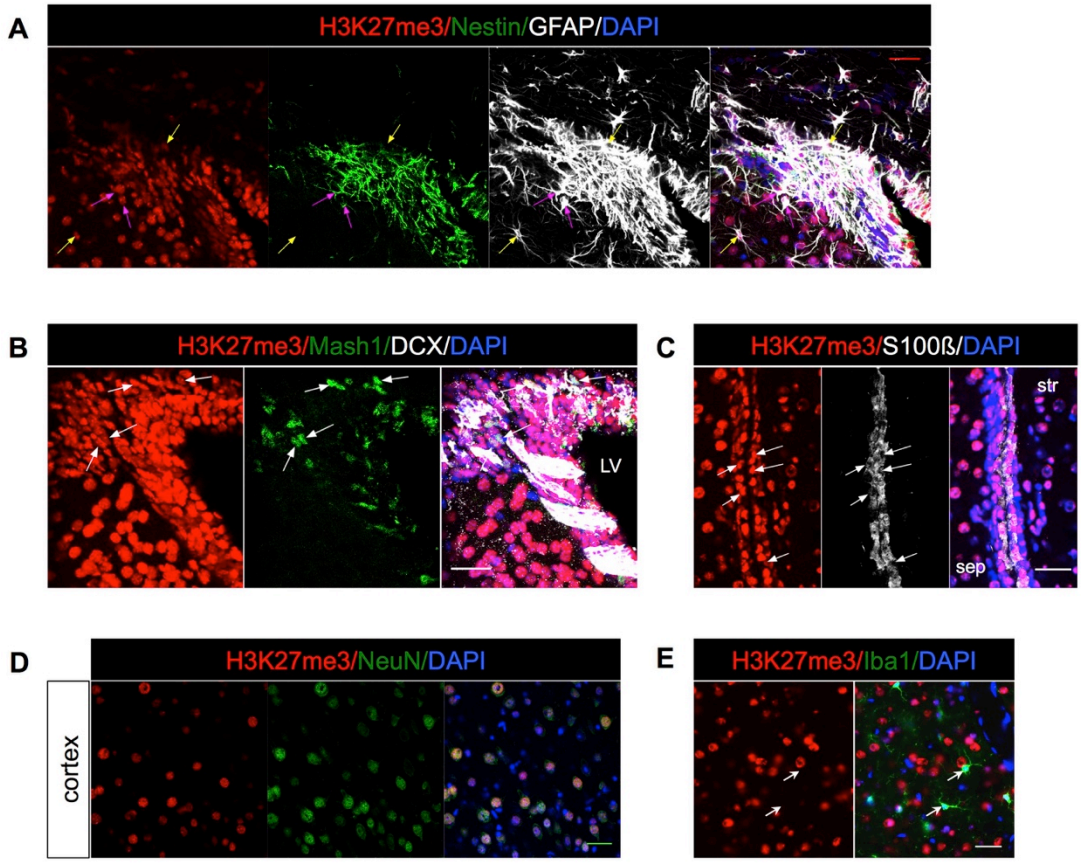

Figure 3. 8 H3K27me3 in different cell types in adult brain

(A) Costaining of H3K27me3 with GFAP and Nestin in the SVZ. The yellow arrows indicate GFAP+/Nestin- astrocytes and the magenta arrows indicate GFAP+/Nestin+ stem cells.

(B) Costaining of H3K27me3 with the neuroblast marker Dcx and the transit amplifying cell marker Mash1 in the SVZ. The arrows indicated the examples of Mash1+ cells.

(C) Costaining of H3K27me3 and the ependymal cell marker S100ß in the SVZ. The arrows indicate examples of S100ß+ cells.

(D) Costaining of H3K27me3 and the neuronal marker NeuN in the cerebral cortex.

(E) Costaining of H3K27me3 and the microglia marker Iba1 in the SVZ. The arrows indicated Iba1+ cells.

LV, lateral ventricle; str, striatum; sep, septum. Scale bar: (A-E)=30um.

A summary of PRC2 expression was given in Figure 3.9.

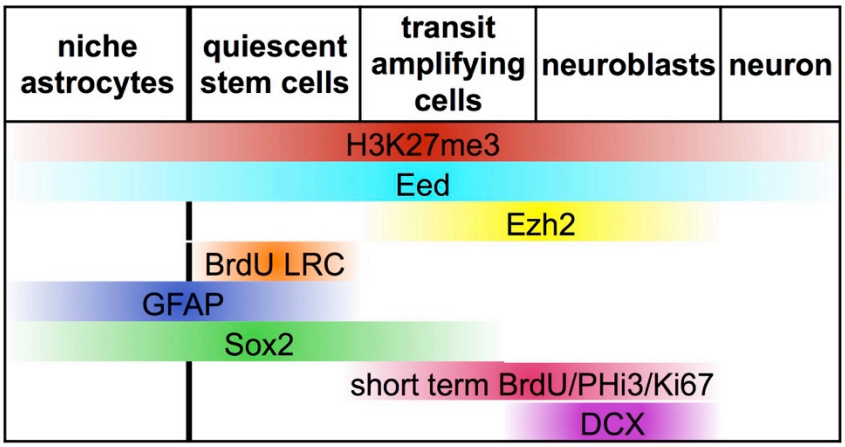

Figure 3. 9 Summary of PRC2 expression in different cell types in adult brain

3.2.4 PRC2 expression in traumatic brain injury

In response to traumatic injury, the parenchymal astrocytes may enter different physiological dynamics. To understand the expression of PRC2 in the pathological condition, I then used the cortical lesion model. 10 injections of BrdU were given to label the actively dividing cells after traumatic brain injury (TBI) as the schematic diagram (n=3, Figure 3.10A). As expected, GFAP+ reactive astrocytes could be identified as BrdU+ proliferative (n=3, Figure 3.10B-C). Also these reactive astrocytes were Sox2+ (n=3, Figure 3.10D). However no Ezh2 expression could be detected by western blot in either ipsilateral or contralateral cerebral cortex (n=1, Figure 3.10E). Blotting for Eed showed no obvious difference between ipsilateral and contralateral cortical tissues (n=1, Figure 3.10E). This indicated Ezh2 might be dispensable for astrocyte activation after invasive brain injury.

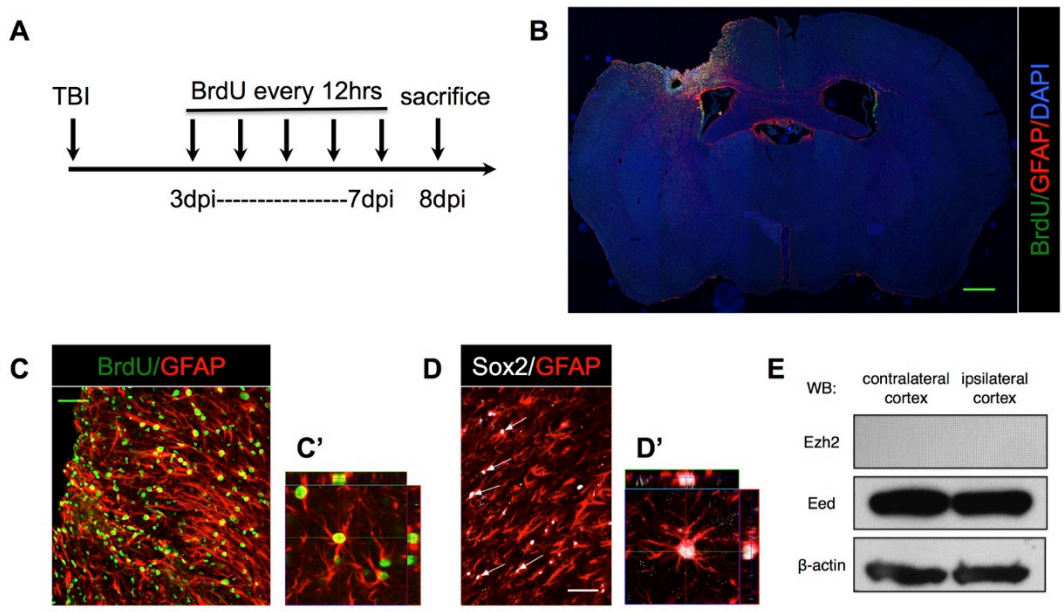

Figure 3. 10 PRC2 in cerebral cortex injury model

(A) A schematic diagram of the experimental design.
(B-C) Costaining of GFAP and BrdU in cortical lesions (n=3). (C-C') Image is shown at higher magnification.
(D) Costaining of GFAP and Sox2 in cortical lesions (n=3). (D') Image is shown at higher magnification. The arrows indicate examples of GFAP+/Sox2+ cells in the cortex.
(E) Western blot for Eed in contralateral (contra) and ipsilateral (ipsi) tissues of the TBI brain.
Scale bar: (B)=600um. (C-D)=60um.

3.2.5 H3K27me3 in MCAO brains

To understand how PRC2 functions and changes in stroke, I stained for H3K27me3 in the 7-day MCAO model of stroke. A broad loss of H3K27me3 in the infarct region could be observed, where GFAP (representing reactive astrocytes) was increasingly expressed (Figure 3.11A). At higher magnification, I found reactive astrocytes had

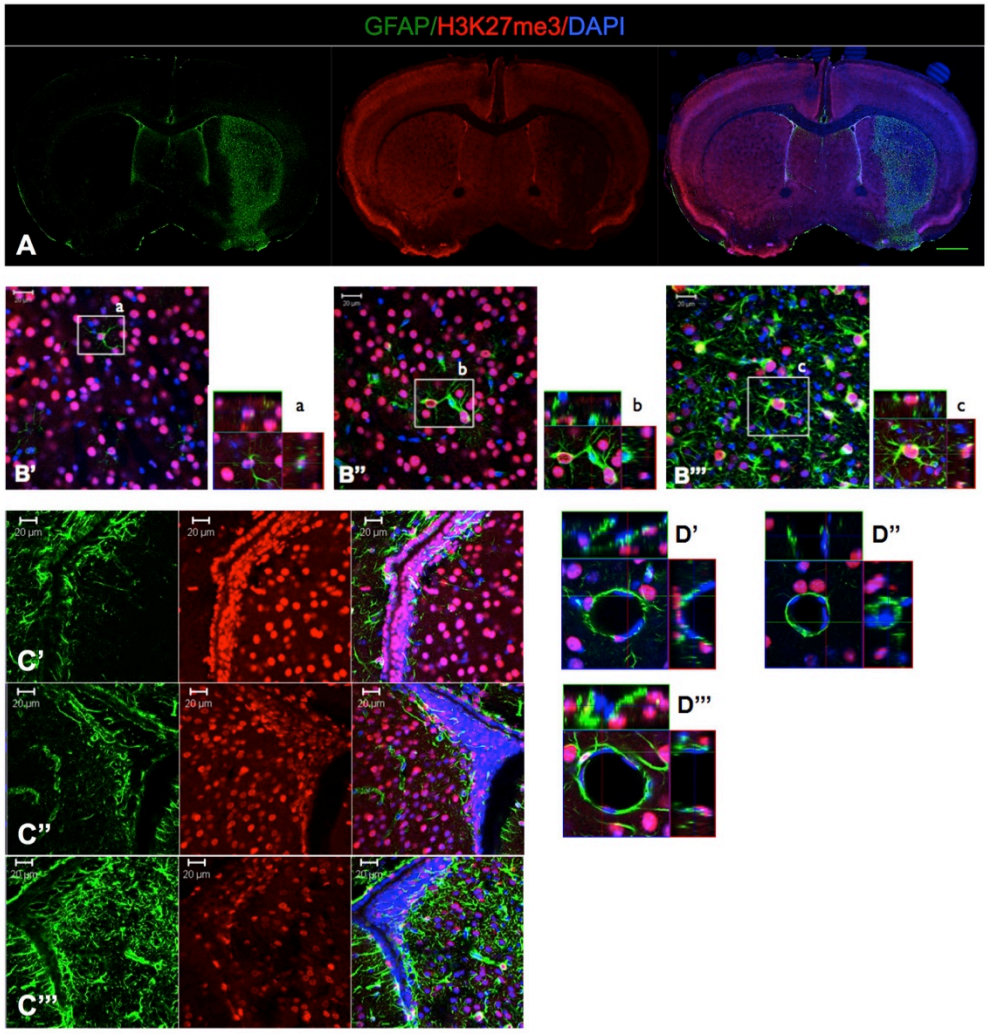

Figure 3. 11 H3K27me3 in MCAO model of stroke

(A-D) Costaining of GFAP and H3K27me3 in 7 days after MCAO (n=3).

(B) Activated astrocytes in the striatum after stroke have high levels of the H3K27me3 mark.

(C) Ependymal cells in 2 out of 5 brains broadly lost H3K27me3 ipsilateral and contralateral to stroke.

(D) Endothelial cells had no obvious change in H3K27me3 immunohistochemical levels before and after stroke (n=3).

B'C'D', sham; B''C''D'', contralateral; and B'''C'''D''', ipsilateral side of MCAO brain. Scale bar: (A)=800um, (B-D)=20um.

high levels of H3K27me3 expression (Figure 3.11B'-B''') and therefore assumed the loss of tri-methylation may result from the death of neurons in the striatum after stroke. I also observed that some ependymal cells (n=2 out of 5 mice) had absent H3K27me3 expression on both the ipsilateral and contralateral sides after stroke (Figure 3.11C'-C'''). The Szele laboratory also previously showed that after ischaemia more endothelial cells proliferate and angiogenesis is activated. I could not, however, find changes in H3K27me3 expression in the endothelial cells in the ipsilateral striatum (n=3) (Figure 3.11D'-D''').

3.3 Discussion

Here, I investigated the expression of different PRC2 components in the brain, especially in the SVZ. The study showed distinct expression patterns of two PRC2 core subunits, i.e. Ezh2 and Eed, with Eed already expressed in quiescent NSC, while after the stem cells become activated and enter the neurogenic program, Ezh2 would start to be expressed. The distribution of global H3K27me3 is similar to the expression pattern of Eed in the healthy brain. In two brain injury models: (1) In cortical lesion, Ezh2 expression will not be activated in the injured cerebral cortex, although astrocytes and microglia are at a high proliferative rate. This suggests the dispensable role of Ezh2 in the activation of glial cells in response to invasive injury. (2) In MCAO, the H3K27me3 shows a more diverse change in different cell types, including ependymal cells.

3.3.1 PRC2 components are differentially expressed in SVZ stem and progenitor cells

PRC2 complex consists of multiple subunits, including Eed, Suz12, Aebp2, Rbbp and the methyltransferases, Ezh2 and Ezh1 (Margueron and Reinberg 2011; Schwartz and Pirrotta 2014). In embryonic stem cells and skin stem cells, Ezh1 was first identified to partially compensate the functions of Ezh2 in the maintenance of H3K27me3 (Shen et al. 2008; Ezhkova et al. 2011). This finding explained the maintenance of H3K27me3 in Ezh2 knockout cells (Shen et al. 2008). In postnatal and adult brains, I found the broad distribution of H3K27me3 mark in various regions and cell types. This is not surprising considering PRC2 as one of the most fundamental gene repressive mechanisms. In contrast, the expression of Ezh2 is more restricted,

especially in the adult brain (Hwang et al. 2014), to the neurogenic niche. This difference can be due to the broad expression of Ezh1 in brain regions outside SVZ. Interestingly, in postnatal brains, both my western blot analysis of different brain regions and published literature (Hwang et al. 2014) suggest more broad expression of Ezh2 around the brain. This age-dependent expression pattern of Ezh2 may result from the maturation of neurons and glial cells. A similar pattern can be noticed in Dcx immunostaining experiment. At the young postnatal age, Dcx is also not limited to the SVZ/RMS as what it is in adult brain. This expression similarity indicates Ezh2 may be involved in the terminal differentiation and maturation of neuroblasts/neurons in non-neurogenic regions, like cerebral cortex, striatum, etc. On the other hand, besides the broad distribution of global H3K27me3, I also observed: (1) weak immunostaining in corpus callosum. Axons and glial cells are the major components of corpus callosum. H3K27me3 is present in the cell nucleus so it means glial cells, especially oligodendrocytes, in corpus callosum have lower levels of global H3K27me3 compared to the cells in the grey matters. Multiple sclerosis is a demyelinating disease, which could affect corpus callosum. Cuprizone treatment in diet is used as a mouse model for multiple sclerosis (Matsushima and Morell 2001; Kipp et al. 2009). Demyelinating in corpus callosum can cause the neighbouring progenitor cells to invade the white matter during cuprizone treatment and recovery periods. Using this model, our lab previously found more H3K27me3+ nuclei in corpus callosum after 3 and 6 weeks of cuprizone treatment. Similarly, published study also shows Ezh2+ cells start to appear in corpus callosum of mice on cuprizone diet (Sher et al. 2012). In addition, oligodendrocyte precursor cells and immature oligodendrocytes, but not mature myelinating oligodendrocytes, will express Ezh2 (Sher et al. 2008). So it seems during oligodendrocyte differentiation, the activity of

Jmjd3, the H3K27 demethylase (Swigut and Wysocka 2007), may surpass PRC2 and erase a substantial proportion of global H3K27me3 in the genome. (2) Variations of H3K27me3 in the same cell types. This could be because of the heterogeneity of SVZ cells during development and also the subtypes of cells with the same markers. For example, in adult striatum GFAP+ cells were reported to perform at least two different morphologies and physiological characteristics (Wang et al. 2008a). (3) Relatively weak staining in the neuroblasts compared to other cell types in SVZ/RMS. Current data I generated is not enough to demonstrate the dynamic changes of global H3K27me3 in SVZ neurogenic lineage. This question can be answered by introduction of Fab-based live endogenous modification labelling (FabLEM) or other engineered sensors into SVZ and live-image the brain slices to monitor the H3K27me3 change during lineage progression (Lin et al. 2004; Kimura et al. 2010; Hayashi-Takanaka et al. 2011; James et al. 2011). One weakness underlying H3K27me3 immunohistochemistry I applied is its low resolution for functional prediction and analysis. Global H3K27me3 staining is not informative enough to tell the genome binding sites, which exert the biological functions. To examine the expression or binding of H3K27me3 at gene resolution, there are two major techniques available at the moment: (1) Chromatin-immunoprecipitation (ChIP) based techniques allow us to analyse H3K27me3 for both specific genes and whole genome from tissues or sorted cells (Shen et al. 2008; Shen et al. 2009; Collas 2010). In Chapter 5, I applied ChIP-qPCR for H3K27me3 binding analysis in both SVZ tissue and cultured neural stem/progenitor cells, which will be described later. However, considering the heterogeneity of most cells, the current ChIP is not feasible for high-resolution study on individual cell level, so the development of single cell ChIP-seq may add to our understanding of histone modifications in the heterogeneous tissues

(Gilfillan et al. 2012). An alternative now is (2) the proximity ligation assay (PLA) based detecting technique (Soderberg et al. 2006; Gomez et al. 2013). In combination of in situ hybridization and PLA, the binding of H3K27me3 at single-cell and single-gene resolution in brain section can then be visualized.

Further studies of PRC2 indicate Ezh1 and Ezh2 have several independent and unique features: Firstly, Ezh1 can repress gene expression through compacting chromatin structure, besides its role in catalysing H3K27 methylation (Margueron et al. 2008). Moreover, Ezh1/PRC2 is more abundant in post-mitotic cells, while Ezh2 is enriched in proliferative cells (Margueron et al. 2008; Stojic et al. 2011; Cheung and Rando 2013). In postnatal/adult SVZ, the NSC exhibit low proliferative dynamics and rest in the quiescent state, which is necessary for the stem cell population maintenance (Kippin et al. 2005; Kriegstein and Alvarez-Buylla 2009; Ihrie and Alvarez-Buylla 2011; Ponti et al. 2013). Recently several labs tried to isolate quiescent and active NSC separately with different cell markers for molecular and behaviour comparisons (Codega et al. 2014; Mich et al. 2014). With GFAP+CD133+ for quiescent NSC and GFAP+CD133+EGFR+ for active NSC, Codega et al sorted these two cell populations from adult SVZ and analysed the gene expression. Based on the microarray data, we could notice the enrichment of Ezh1 in quiescent NSC, while Ezh2 in active NSC (Codega et al. 2014). However Hwang et al reported Ezh2 is expressed in the entire neurogenic cell lineage, including SVZ type B1 astroglial cells (Hwang et al. 2014). This study relies simply on costaining of Ezh2 and GFAP, but unfortunately no quantification was provided by the authors. Although GFAP is used widely as a neural stem cell marker in SVZ, high level of heterogeneity in GFAP+ cells has been documented (Pastrana et al. 2009; Beckervordersandforth et al. 2010; Giachino et al. 2013). Now the lack of Ezh2 in quiescent NSC has been

confirmed by my immunohistochemistry data. Both GFAP/Sox2 double positive cells and BrdU-LRC shown a low percentage of Ezh2+ nuclei, which could represent activated stem cells. Published work on another neurogenic niche in adult brain, the subgranular zone (SGZ) also illustrated that Ezh2 is not expressed in quiescent NSC (Zhang et al. 2014). These imply Ezh2 is either essential for stem cell activation, or for the relatively late lineage progression. Previous studies in embryonic stem cells revealed the functions of Ezh2 in stem cell self-renewal and terminal differentiation (O'Carroll et al. 2001; Chamberlain et al. 2008; Margueron and Reinberg 2011). It is also suggested that Ezh2 is required for NSC differentiation through inhibition of transcription factors including Olig2 and cell cycle inhibitors (Pereira et al. 2010; Sher et al. 2012; Hwang et al. 2014). However, since quiescent NSC do not express Ezh2, the function of PRC2 in SVZ is more elusive. To solve this question, I then analysed the expression of another PRC2 core subunit Eed. Eed is present in both Ezh1- and Ezh2-containing PRC2 (Shen et al. 2008; Margueron and Reinberg 2011). It has been shown Eed functions in PRC2 formation, recruitment and histone methylation (Margueron et al. 2009; Kim et al. 2013; Cao et al. 2014). Cancer research also shed lights on Eed in brain tumour and leukaemia development (Kim et al. 2013; Lee et al. 2014). In the adult SVZ, I found, unlike Ezh2, Eed is in both quiescent and active NSC. At the moment the lack of reliable antibody for Ezh1 in vivo staining precludes Ezh1 expression analysis on the cell type level. However, the difference between Ezh2 and Eed in NSC suggests Eed might form PRC2 with Ezh1 in the quiescent NSC and repress gene expression, although I cannot rule out the possibility that Eed may have PRC2-independent functions.

One question I have not addressed directly in this chapter is whether transit amplifying cells express Ezh2 or not. This is due to the same antibody host species for

Mash1, the transit amplifying cell maker and Ezh2. I yet can conclude that Ezh2 is expressed in transit amplifying cells based on (1) 97.37±1.96% actively proliferating cells are Ezh2+ in my study; (2) in the adult SVZ, transit amplifying cells (54.01±3.22% for Mash1) and neuroblasts (53.32±2.54% for Dcx) make up the Ki67+ proliferating cell pool with a very small proportion of stem cells (3.30±0.95% for GFAP) (Ponti et al. 2013); (3) 89.15±1.72% Mash1+ cells are Ki67+ (Ponti et al. 2013). This is supported by costaining of Dlx2 and Ezh2 by Hwang et al (Hwang et al. 2014).

3.3.2 PRC2 expression in injured brains

Considering the expression of Ezh2 in the actively proliferating cells, I had hypothesized that reactive astrocytes in response to brain injury may start to express Ezh2 for reactive astrocytes share a few key stem-cell characteristics with SVZ NSC (Buffo et al. 2008; Robel et al. 2011; Bardehle et al. 2013; Grande et al. 2013; Sirko et al. 2013). However, unfortunately by western blot I cannot detect any Ezh2 signal from the injured cerebral cortex in the cortical lesion model. Zamanian et al. previously compared the genomic expression of astrocytes sorted from either healthy or ischemic striatum (Zamanian et al. 2012). Same with my data, their microarray also showed no difference of Ezh2 expression in reactive astrocytes (Zamanian et al. 2012). This is interesting as reactive astrocytes can proliferate in vivo but only acquire multipotency, especially neuronal differentiation in vitro. Interestingly, my preliminary data suggested Ezh2 is expressed in the neurospheres cultured from the injured cerebral cortex (Supplemental Figure 3). So it seems Ezh2 is not involved in cell proliferation of reactive astrocytes but may regulate their differentiation ability. Olig2 is a transcriptional factor expressed in both SVZ NSC and also reactive

astrocytes (Hack et al. 2004; Buffo et al. 2005; Marshall et al. 2005; Cai et al. 2007; Chen et al. 2012). It is reported that in SVZ, Ezh2 is necessary to repress Olig2 expression when the stem cells differentiate into neuronal lineage (Hwang et al. 2014). Therefore, the consistent expression of Olig2 in reactive astrocytes in vivo may be one of the reasons that limit the neuronal potential in these cells. This idea has been further pursued by overexpression of a domain-negative form of Olig2 in reactive astrocytes in vivo (Buffo et al. 2005). This mutant Olig2 can antagonize the functions of endogenous Olig2 and has successfully turned a proportion of reactive astrocytes towards the neuronal fate identified by Dcx or Pax6 (Buffo et al. 2005). Hence, the next question is whether overexpression of Ezh2 in these astrocytes could induce their neuronal differentiation ability. Sher et al. forced expression of Ezh2 in the cultured astrocytes and obtained neurosphere-like cell aggregates, but the multipotency is not examined in this study (Sher et al. 2011). So it is still a remaining experiment to carry out in the future. Because no Ezh2 overexpression knock-in mouse is available for now, virus-based technique would be the suitable choice.

One possible mechanism, which enhances the stemness in the reactive astrocytes, is the in vitro culture condition. EGF and FGF are known to regulate NSC proliferation and differentiation (Ihrie and Alvarez-Buylla 2011). The recent studies in reactive astrocyte differentiation in vitro are all following expansion of the cells with EGF and FGF (Buffo et al. 2008; Grande et al. 2013; Sirko et al. 2013). Both EGF and FGF are able to modify the epigenetic modification in cells, which can then have long-term effects on the cell behaviours (Song and Ghosh 2004; Kottakis et al. 2011; Yang et al. 2012). Of note, it is reported that FGF can upregulate Ezh2 mRNA translation through NDY1/miR101 pathway (Kottakis et al. 2011). This study demonstrated a negative feedback loop between FGF and Ezh2, but it remains to be

examined whether a similar mechanism also contributes to multipotency induction in reactive astrocytes in vitro.

On the other hand, I found no obvious change of Eed expression between ipsilateral and contralateral hemispheres from cortical lesion model. I cannot conclude from this that Eed is dispensable for astrocyte activation as its binding sites may change after the stimuli of cortical lesion. A further study of Eed in astrocyte activation will be described in Chapter 4.

In MCAO, a general decrease of global H3K27me3 can be noticed in where the GFAP+ reactive astrocyte reside. As I can detect high level of H3K27me3 in reactive astrocytes at the high magnification, it suggests this decrease should result from the general cell death and loss of neurons in the striatum. And the low level of H3K27m3 in microglia can be another reason.

In adult mice, I found all ependymal cells are positive for H3K27me3. That might simply reflect the requirement of PRC2 in their maturation, or its role in adult ependymal cell properties and behaviours such as quiescence maintenance. In my MCAO experiments, 2 out of 5 MCAO brains lost this mark in the ependyma. Several reasons might explain this inconsistency: (1) the reproducibility of the MCAO model is difficult and there may be different distances between the SVZ and infarct; (2) the heterogeneity of SVZ and ependymal cells: although the activation and neurogenic ability of ependymal cells after brain injury is still not well confirmed (Carlen et al. 2009; Young et al. 2012; Devaraju et al. 2013), in stroke some of the ependymal cells were reported to express GFAP (Young et al. 2012), and I assume the global H3K27me3 may change gradually in individual ependymal cell which can be reflected as the different levels of H3K27me3 in different samples, while more detailed work is still needed. Until now the molecular machinery regulating how

ependymal cells develop and maintain quiescence as they differentiate from radial glia is poorly understood. Marie et al reported that Notch signalling is important for maintaining the quiescence in mature ependymal cells (Carlen et al. 2009). Work in paediatric ependymoma, the third most common brain tumour in children (Mack and Taylor 2009), however, showed overexpression of Notch1 and repression of the Notch inhibitor Fbxw7 (Puget et al. 2009), indicating the involvement of Notch signalling in the progression of paediatric ependymoma. One can hypothesize that the intracellular epigenetic modification might explain this seemingly opposite functions of Notch in ependymal cell quiescence maintenance. To address this question, we can knock out Eed specifically in the adult ependymal cells before or after brain injury with the aid of inducible Cre/LoxP technique. S100β is used as a cell marker for mature ependymal cells (Ihrie and Alvarez-Buylla 2011), but it is not specific enough to activate Cre only in ependymal cells (Raponi et al. 2007; Andreu-Agullo et al. 2012). Another option is Foxj1, a protein which regulates multicilia formation and ependymal development (Jacquet et al. 2009; Devaraju et al. 2013). However fate mapping of Foxj1 in adult healthy rat SVZ with *piggyBac* labelling showed Foxj1-expressing cells would contribute to new neuron generation in the olfactory bulb. This may be due to (1) non-specific labelling of NSC or (2) expression of Foxj1 in a subtype of NSC as it is generally believed that mature ependymal cells in adult brain do not have the neurogenic ability (Ihrie and Alvarez-Buylla 2011). So a more reliable marker for ependymal cells and the development of the transgenic mice are still in need for further study of PRC2 in ependyma.

From the translational and clinical perspective, traumatic brain injury is the leading cause of death and disability around the world. Because of the limited regeneration capacity in the adult brain, endogenous repair with SVZ NSC has little

benefit for the therapeutic purpose nowadays. Besides cell transplantation, there is now another promising method, in vivo reprogramming of astrocytes into neurons for replacement. Inductions of Sox2 and NeuroD1 have successfully achieved this purpose in the labs recently (Guo et al. 2013; Niu et al. 2013; Niu et al. 2015). Interestingly, Niu et al. found in combination of Sox2, valproic acid (VPA), a histone deacetylase inhibitor is capable to enhance the neuronal differentiation of astrocytes in vivo (Niu et al. 2013; Niu et al. 2015). In view of the potential functions of ectopic expression of Ezh2 in astrocyte reprogramming, it may be worthwhile to test whether H3K27 demethylase inhibitors, for instance GSKJ1 (Kruidenier et al. 2012), would have a similar effect. In the broad sense, a systematic screen of small molecules or drugs targeting different epigenetic regulators in vivo is crucial.

3.4 Conclusion

In this chapter, I have demonstrated different expression of two key PRC2 components, Ezh2 and Eed in normal postnatal/adult SVZ neurogenic lineage. Quiescent NSC in SVZ will only express Eed but not Ezh2. Therefore it would be essential to compare the biological functions of Eed and Ezh2 in SVZ NSC lineage progression. In cortical lesion, Ezh2 will not be activated in the cortex and may not participate in astrocyte activation process. These findings provide insights into the further functional analysis of PRC2 in SVZ neurogenesis in both healthy and injured brains.

Chapter 4

PRC2 in postnatal and adult SVZ neurogenesis

4.1 Introduction

The postnatal/adult SVZ harbours the largest population of NSC in the brain (Ihrie and Alvarez-Buylla 2011). Self-renewal and multipotency are two features of SVZ NSC, the dysfunction of which may contribute to gliomagenesis (Sanai et al. 2005). However, the regulating mechanisms are still not fully uncovered. PRC2 is implicated in several steps of stem cell development, serving as a potential master regulator in SVZ NSC.

4.1.1 PRC2 in regulating cell self-renewal and proliferation

The role of PRC2 in stem cell proliferation has been studied extensively because Ezh2 is enriched in active stem cells while Ezh1 is enriched in quiescent stem cells (Cheung and Rando 2013). Ezh2 generally represses *Ink4b-Arf-Ink4a* locus in proliferative stem cells/progenitors of solid tissues and thereby promotes cell division (Ezhkova et al. 2009; Hwang et al. 2014). This is consistent with the observation that a high level of Ezh2 is always associated with solid tumours in breast, colon, liver, pancreas, etc (Kleer et al. 2003; Fluge et al. 2009; Chen et al. 2010; Fussbroich et al. 2011). Interestingly, in human T-cell acute lymphoblastic leukaemia (T-ALL) samples, the expression of Ezh2 is decreased and Ezh2 knockout will lead to T-ALL in mice (Ntziachristos et al. 2012; Simon et al. 2012; Lund et al. 2014). Correspondingly, Eed loss-of-function heterozygous mutant increases the proliferation of hematopoietic stem cell in adult animals, while complete knockout of Eed exhausts the HSC populations (Lessard et al. 1999; Xie et al. 2013). It seems that the complicated role of PRC2 in cell proliferation includes both oncogenic and tumour-suppressor factors.

Self-renewal is one special type of cell proliferation that generates two daughter cells with full stemness (He et al. 2009b). Compared to PRC2, the positive

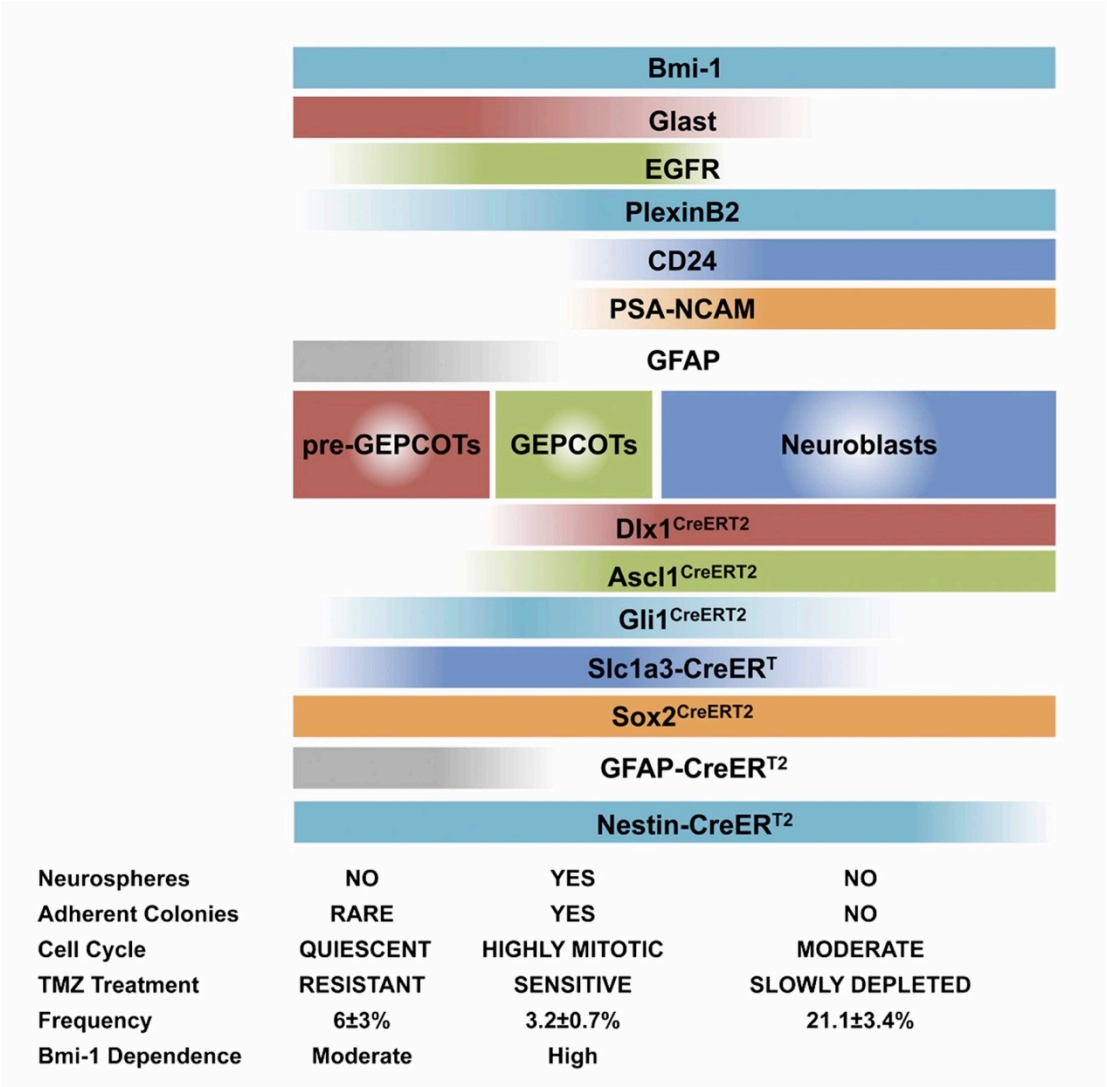

Figure 4. 1 The diversity of SVZ cell types and dynamics

Pre-GEPCOTs for quiescent NSC and GFPCOTs for neurosphere-initiating cells can be isolated from adult SVZ based on the combination of cell markers. Various Cre-lines are able to target these two cell populations at different stages. Sphere forming ability and cell cycle dynamics are summarized for SVZ lineage cells. Quiescent NSC are resistant to the DNA-alkylating agent temozolomide (TMZ) due to their low proliferative rate. In contrast, both GFPCOT cells and neuroblasts can be depleted by TMZ. The proliferative ability of GFPCOT cells is also highly dependent on the PRC1 component Bmi1. (Figure is modified from Mich et al., 2014).

role of the PRC1 component Bmi1 is much better understood in maintaining NSC self-renewal (Molofsky et al. 2003; Fasano et al. 2009; He et al. 2009a; Mich et al. 2014). A recent interesting study compared the role of Bmi1 in the quiescent NSC (pre-GEPCOTs) and neurosphere-initiating cells (GFPCOT) in adult SVZ (Mich et al. 2014). Long-lived quiescent NSC could be sorted based on the combinations of Glast, EGFR, PlexinB2, CD24, O4/PSA-NCAM, Ter199/CD45 (Figure 4.1). Unexpectedly, loss of Bmi1 activated the cell cycle inhibitor p16 only in these quiescent NSC but not in the active cells (neurosphere-initiating cells) (Mich et al. 2014). This is critical in regard to SVZ as no other work has yet compared the epigenetic regulations between quiescent and active NSC.

Since PRC1 and PRC2 usually cooperate in gene silencing, I then hypothesize that Eed may also be involved in SVZ NSC maintenance. This is probably achieved by Eed balancing NSC quiescence versus activation in SVZ. In contrast, Ezh2 should be less important in this process.

4.1.2 PRC2 in regulating stem cell pluripotency and differentiation

Although both ChIP-chip and ChIP-Seq have proved that PRC2 can target differentiation transcription factors in stem cells, there is as yet no working model able to explain the regulations of PRC2 in stem cell pluripotency (Boyer et al. 2006; Mikkelsen et al. 2007; Shen et al. 2008; Shen et al. 2009; Margueron and Reinberg 2011). It has been suggested that PRC2 can maintain the pluripotency in ES cells through the repression of differentiation transcription factors. An alternative model is that PRC2 can guarantee the proper expression of pluripotent transcription factors in ES cells (Figure 4.2A). However, experimental observations in various labs could not confirm either model (Chamberlain et al. 2008; Leeb et al. 2010; Riising et al. 2014).

By virtue of a less essential job in gene silencing, PRC2 may instead function to secure epigenetic memory on the genome-wide rather than exerting direct transcriptional control (Riising et al. 2014).

In somatic stem cells, loss of PRC2 will cause defects in the terminal differentiation and lineage commitment (Figure 4.2B) (Sher et al. 2008; Ezhkova et al. 2009; Hirabayashi et al. 2009; Pereira et al. 2010; Sher et al. 2012; Hwang et al. 2014). For example, during late embryonic cortical development, Ezh2 and PRC1 can inhibit the neurogenic transcriptional factors to promote astrogenesis; while in postnatal/adult SVZ, Ezh2 will target Olig2 to drive neuronal differentiation (Hirabayashi et al. 2009; Hwang et al. 2014). As SVZ NSC and astrocytes share a variety of features, one question is whether PRC2 has any role in determining or inhibiting the neuronal differentiation in either NSC or niche astrocytes. The absence of Ezh2 in either SVZ NSC or astrocytes suggests it may be associated with terminal differentiation but not with the initial step. Pax6 is one of the most important transcription factors for neuronal differentiation in adult SVZ (Hack et al. 2004; Ninkovic et al. 2013). So it is expected that human NSC have no H3K27me3 on *Pax6* locus while in human astrocytes H3K27me3 and H3K4me4 bivalent domains could be found (Rheinbay et al. 2013). On the other hand, Id1 is considered as a marker for rodent adult SVZ NSC (Nam and Benezra 2009). This association is more elusive in human NSC, in which *ID1* locus has the bivalent domain; whereas H3K27me3 is absent on the same locus in human astrocytes (Rheinbay et al. 2013). This difference may result from distinct environmental cues from tissue culture and in vivo stem cell niche. In SVZ both NSC and niche astrocytes express Eed, making it a suitable target candidate for functional studies.

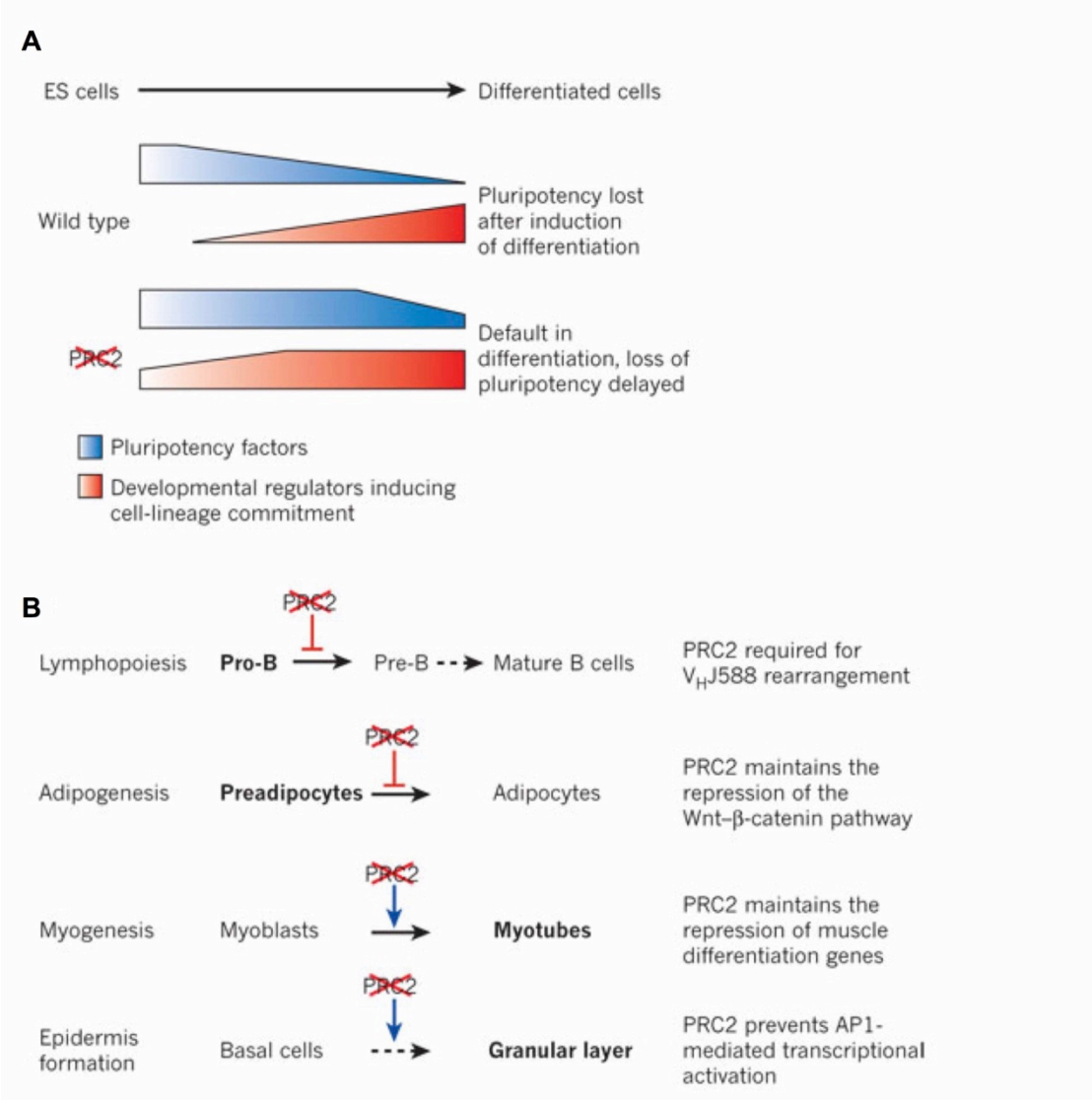

Figure 4. 2 PRC2 in stem cell pluripotency and differentiation

(A) Expression of pluripotency factors and developmental regulators during ES cell differentiation. During ES cell differentiation, PRC2 has dual roles. On the one hand, loss of PRC2 will prolong the expression of pluripotency genes; on the other hand, the differentiation related genes will be misexpressed at an earlier time point.

(B) Various functions of PRC2 in somatic stem cell differentiation. In lymphopoiesis and adipogenesis, PRC2 is required for cell differentiation. However, in myogenesis and epidermal development, PRC2 functions to maintain the stem and progenitor cells. Similarly, low and high EZH2 activities have been reported in leukaemia and solid tumours, respectively.

(Figure is modified from Margueron and Reinberg 2011).

In this chapter, I aim to study the following questions: (1) whether loss of Eed will affect postnatal SVZ NSC proliferation? (2) Whether Eed regulates the stemness in SVZ NSC and astrocytes? (3) What is the difference between Ezh2 and Eed in SVZ neurogenesis?

4.2 Results

4.2.1 Generation of Ezh2 conditional knockout mice

Considering the early embryonic lethality of Ezh2 constitutive knockout mice (O'Carroll et al. 2001), I chose to use the tamoxifen-induced conditional knockout (cKO) approach (Nagy 2000). $Ezh2^{fl/fl}$ mice were as previously reported (Su et al. 2003; Pereira et al. 2010). Genotyping of $Ezh2^{fl/fl}$ mice showed the floxed band at 736bp, and the wild-type band at 681bp (Figure 4.3A). To knockout Ezh2 specifically in the postnatal/adult SVZ neural stem cells, GLAST-CreERT2 was used to induce Cre recombination activity in the astroglial cells (Mori et al. 2006). Genotyping of GLAST-CreERT2 mice showed the Cre band at around 400bp and the wild-type band at around 700bp (Figure 4.3B). $Ezh2^{fl/fl}$ mice were then crossed with GLAST-CreERT2 mice to generate GLAST-CreERT2;$Ezh2^{fl/fl}$ mice (The detailed breeding approach was described in Chapter 2 Material and Methods). Pups were given tamoxifen by subcutaneous injection with different paradigms to test the efficiency and toxicity. I found 0.6mg/kg body weight of tamoxifen injected at P1 would cause moderate to severe swelling in the genital areas, and a higher mortality rate than non-injected pups. These pups were also smaller than non-injected ones. 0.2mg/kg body weight of tamoxifen injection at P1 was then used to induce Cre activity. At this dose, pups were healthy, with occasionally mild swelling in the genital areas. Genotyping of GLAST-CreERT2;$Ezh2^{fl/fl}$ pups (receiving 0.2mg/kg body weight of tamoxifen) showed the deleted band (625bp) as reported (Figure 4.3C) (Su et al. 2003). To avoid tamoxifen contamination in the breeding cage, male GLAST-CreERT2;$Ezh2^{fl/fl}$ was mated with female $Ezh2^{fl/fl}$ producing both GLAST-CreERT2;$Ezh2^{fl/fl}$ (cKO) and $Ezh2^{fl/fl}$ (littermate control) (Figure 4.3D). To verify the knockout, SVZ tissues were

collected at P14 and analysed by

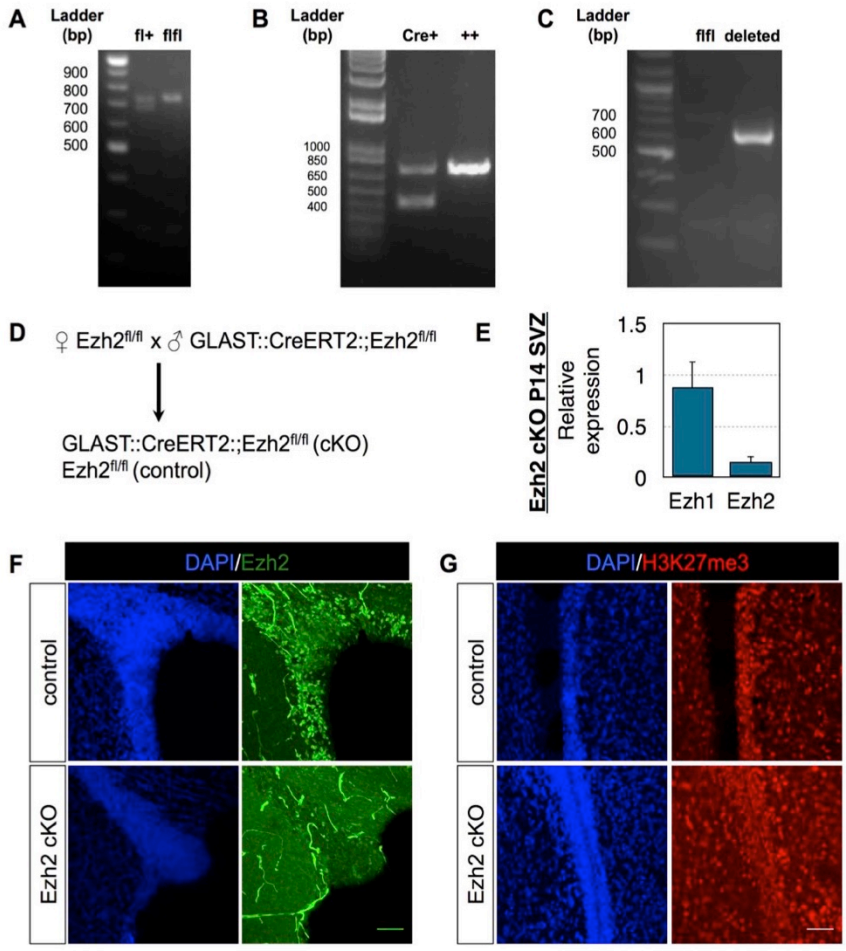

Figure 4. 3 Conditional knockout of Ezh2 in postnatal SVZ

(A, B and C) Examples of PCR genotyping of different mouse strains. (A and C) are for Ezh2 flox, and the sizes for floxed, wt and deleted are 736, 681 and 625bp. (B) is for GLAST::CreERT2. The Cre band is around 400bp.

(D) Breeding scheme for the generation of tamoxifen inducible knockout mice.

(E) qPCR analysis of P14 SVZ shows Ezh2 but not Ezh1 mRNA decreases. Relative expression was normalized to littermate controls. Error bars represent SEM (n=3 for control and n=4 for cKO).

(F) 2 weeks after tamoxifen injection, immunostaining of Ezh2 in SVZ to confirm the knockout efficiency. In cKO, fewer Ezh2+ nuclei were found in the SVZ (n=3).

(G) 2 weeks after tamoxifen injection, immunostaining of H3K27me3 in SVZ (n=3).

Scale bars: (F)=50um, (G)=50um.

RT-qPCR for the expression of Ezh2. Compared to the control (expression normalized to 1), cKO SVZ has a reduction of Ezh2 mRNA expression to 0.144±0.0579 (normalized to control, n=3 for control and n=4 for cKO) with the Ezh1 expression unaffected (0.879±0.257) (Figure 4.3E). To further confirm the knockout at the protein level, pups were sacrificed 2 weeks post tamoxifen injection and brain coronal sections were then immunostained with Ezh2 antibody. A significant decrease of Ezh2+ nuclei would be observed in the cKO SVZ (n=3, Figure 4.3F). Nonetheless, no obvious changes of global H3K27me3 staining could be found after the loss of Ezh2 in SVZ (n=3, Figure 4.3G).

4.2.2 Mild cell proliferation defects in SVZ after the loss of Ezh2

SVZ cytoarchitecture was then analysed to study the function of Ezh2 in postnatal SVZ neurogenesis. At P14 when the decrease of Ezh2 could be observed (Figure 4.3E-F), no significant difference in cell proliferation identified by PHi3 could be found between control (133.39±39.15/section) and cKO (144.14±34.70/section) (n=3 for control and n=5 for cKO) (Figure 4.4A). Olig2 is expressed in oligodendrocyte lineage cells in SVZ and can also direct astrocyte development (Marshall et al. 2005; Menn et al. 2006; Cai et al. 2007). Previous reports also showed that Olig2 is a direct target of PRC2 (Shen et al. 2008; Hwang et al. 2014); but the number of Olig2+ nuclei had no significant difference after the loss of Ezh2 (control: 1336.25±137.79/section versus cKO: 1416.92±107.85/section. n=3 for control and n=5 for cKO) (Figure 4.4B). RT-qPCR of P14 SVZ tissues could not detect obvious change in the expression of Mash1 (cKO: 0.885±0.170), Dcx (cKO: 0.809±0.185) and Id2 (cKO: 1.209±0.260) (n=3, Figure 4.4C), which is consistent with the immunostaining results. However, 28 days post tamoxifen treatment, an

approximately 2-fold reduction would be observed in cKO SVZ tissue for Mash1, Dcx and Id2 expression (Mash1: 0.306±0.0781; Dcx: 0.503±0.128; Id2: 0.496±0.0839) (n=3, Figure 4.4C). Immunohistochemistry of proliferating marker Ki67 also showed a mild but significant decrease of Ki67+ nuclei in cKO SVZ (1983373.34±86528.55/mm^3) compared to control (1574307.19±64531.47/mm^3) (p=0.0193, n=4 for control and n=3 for cKO, Figure 4.4D). In postnatal/adult brains, Mash1+ transit amplifying cells and Dcx+ neuroblasts constitute the majority of SVZ

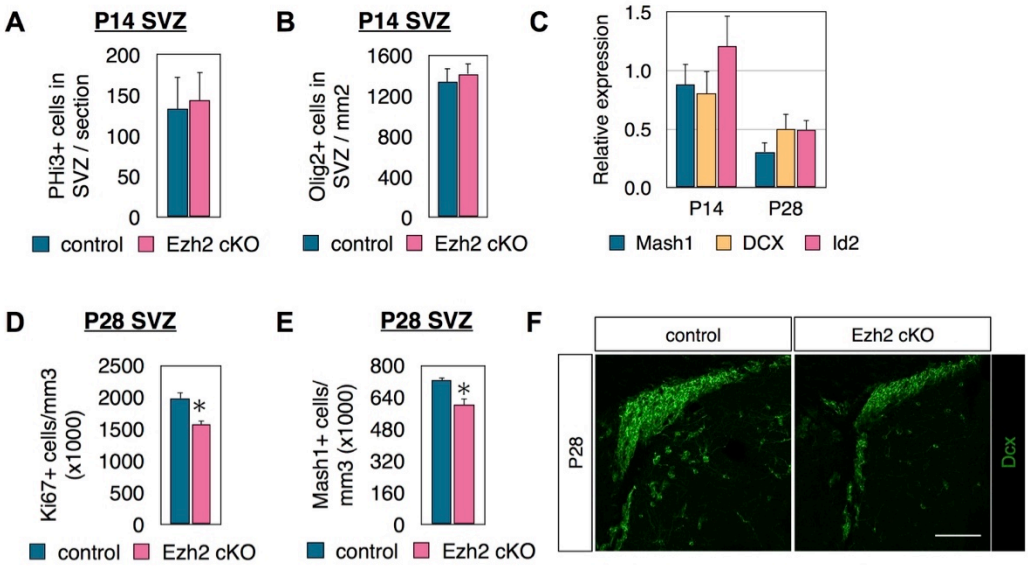

Figure 4. 4 Loss of Ezh2 impairs SVZ cell proliferation

(A-B) Quantifications reveal PHi3+ proliferating cells and Olig2+ oligodendrocyte-lineage cells are not affected in P14 SVZ after loss of Ezh2 (n=3 for controls and n=5 for cKO).

(C) qPCR analysis of P14 and P28 SVZ. Although not affected in P14 SVZ, the expression of Mash1, Dcx and Id2 reduces in P28 SVZ. Relative expression was normalized to littermate controls (n=3).

(D-E) Quantifications show that both Ki67+ proliferating cells and Mash1+ transit amplifying cells decrease in P28 SVZ (n=4 for controls and n=3 for cKO).

(F) Immunostaining of doublecortin (Dcx) in P28 SVZ shows fewer Dcx+ neuroblasts in P28 SVZ after loss of Ezh2 (n=4 for controls and n=3 for cKO).

Error bars represent SEM. *p<0.05. Scale bar: (F)=60um.

actively proliferating cells (Ponti et al. 2013). In agreement with the Ki67 quantification, fewer Mash1+ could be detected in the cKO SVZ (control: 724016.97±14653.38/mm^3. cKO: 599452.26±32574.98/mm^3) (p=0.0252, n=4 for control and n=3 for cKO, Figure 4.4E). Weaker Dcx immunostaining was also observed in SVZ after the loss of Ezh2 (n=4 for control and n=3 for cKO, Figure 4.4F).

4.2.3 Ezh2 is required for postnatal/adult SVZ neurogenesis

To study the neurogenesis ability in postnatal/adult Ezh2 cKO SVZ, 10 doses of BrdU were injected from P29 to P33 to label the proliferating cells in SVZ and to trace the newborn neurons in OB (Figure 4.5A). 6 weeks after the last injection, fewer BrdU+/NeuN+ newborn neurons could be found in the Ezh2 cKO OB (Figure 4.5B-C). Quantifications showed a significant decrease of BrdU+/NeuN+ cells in both granular layers (control: 1279.38± 43.86/mm^2 versus cKO: 944.54± 8.71/mm^2) (p=0.0017, n=3 for controls and n=4 for cKO, Figure 4.5D) and glomerular layers (control: 285.53±21.07/mm^2 versus cKO: 179.43±9.80/mm^2) (p=0.0103, n=3 for controls and n=4 for cKO, Figure 4.5E).

A smaller RMS in OB identified by Dcx staining could also be found in the Ezh2 cKO (n=3 for controls and n=4 for cKO, Figure 4.5F). Analysis of the surface areas of RMS showed a significant decrease in cKO (11774.88±618.86 μm^2), compared to control (17176.76±1211.80 μm^2) (p=0.0076, n=3 for controls and n=4 for cKO, Figure 4.6A-B). There was no difference in cell death (Caspase3) in neuroblasts between control and cKO (control: 0.970±0.0303/RMS. cKO: 1.161±0.286/RMS)

(n=3 for controls and n=4 for cKO, Figure 4.6C-D), which indicates that the reduced neurogenesis is not due to increased cell death after the loss of Ezh2.

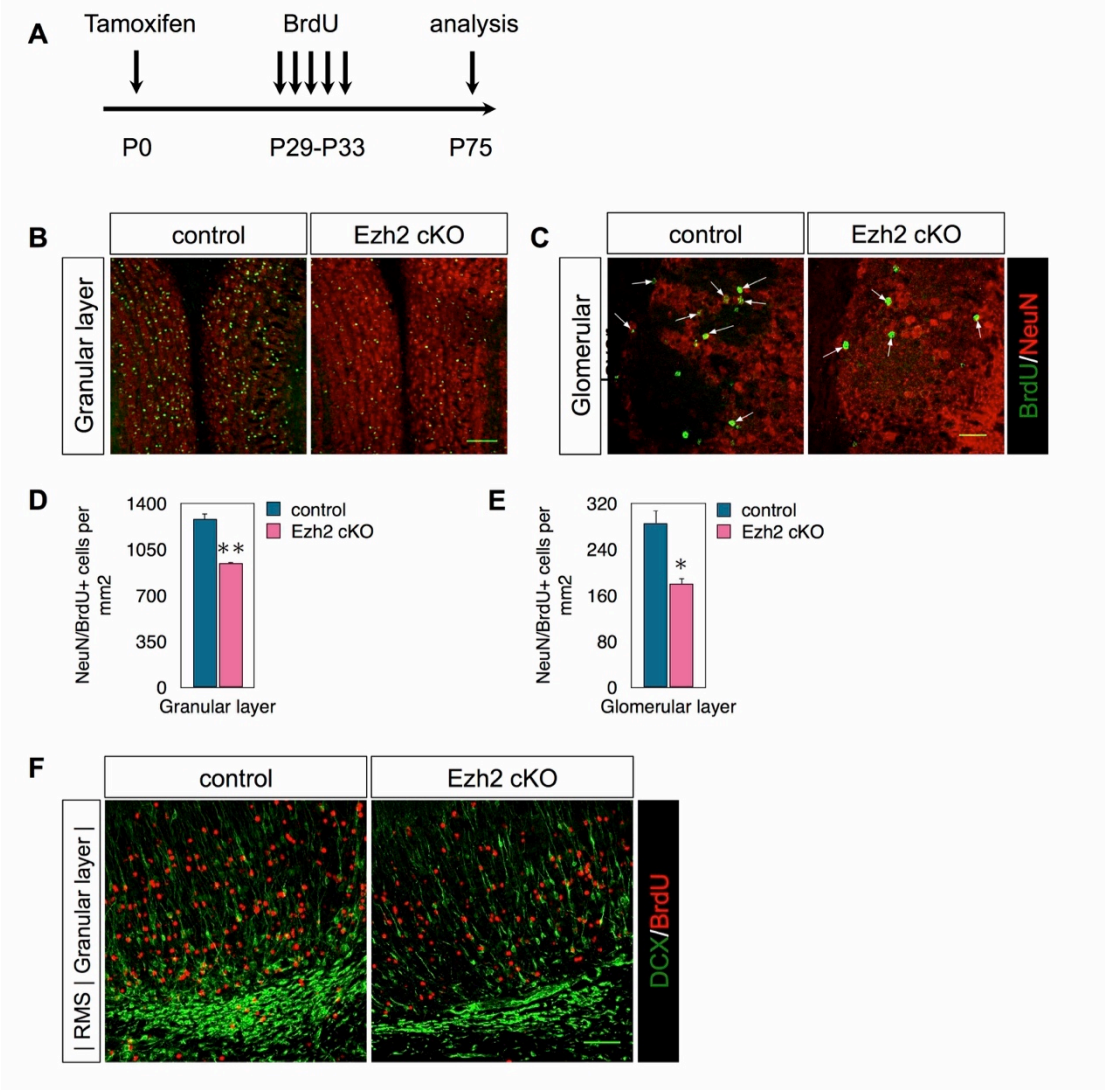

Figure 4. 5 Neurogenesis decreases in OB after Ezh2 knockout

(A) A schematic diagram of the experimental design.

(B and C) Coimmunostaining of BrdU and NeuN in OB reveals many fewer newborn neurons in the OB after loss of Ezh2. The arrows indicate NeuN+/BrdU+ cells.

(D and E) Quantification of NeuN+/BrdU+ cells in the granular layer (C) and glomerular layer (D) (n=3 for controls and n=4 for cKO).

(F) Immunostaining of Dcx and BrdU in P75 OB demonstrates RMS size decreases after loss of Ezh2 (n=3 for controls and n=4 for cKO).

Error bars represent SEM. **p<0.01. Scale bar: (B)=100um, (C)=30um, (F)=60um.

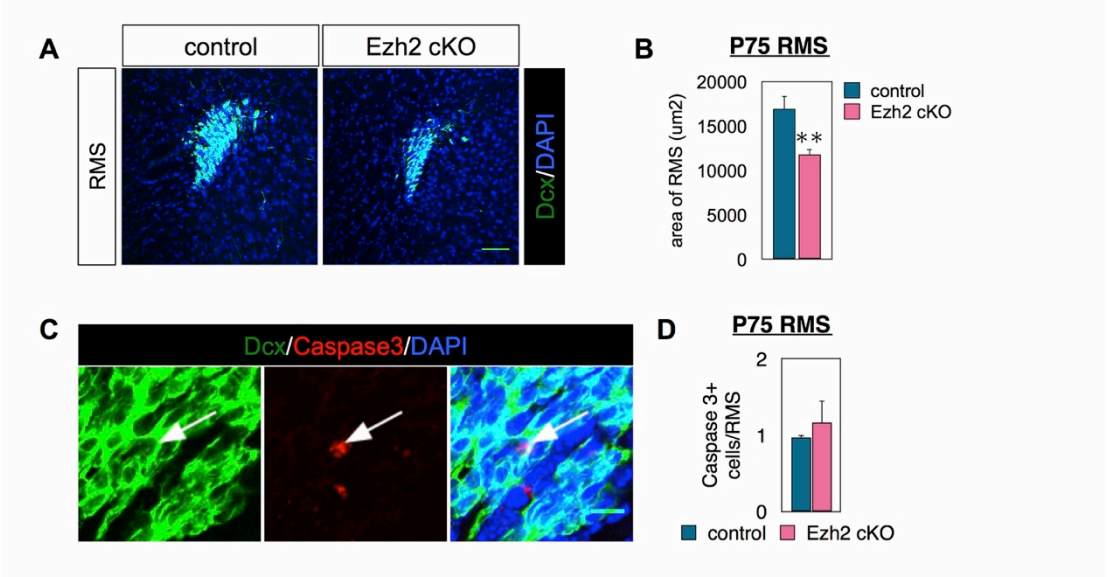

Figure 4. 6 Neuroblasts in RMS decrease after Ezh2 knockout

(A-B) Immunostaining and quantification of Dcx in P75 reveal the RMS size decreases after loss of Ezh2 (n=3 for controls and n=4 for cKO).

(C) Immunostaining of Caspase3 in P75 RMS (n=3 for controls and n=4 for cKO). The arrow indicated Caspase3+/Dcx+ cells.

(D) Quantification of Caspase3+ cells in P75 RMS shows cell viability is not affected after Ezh2 knockout (n=3 for controls and n=4 for cKO).

Error bars represent SEM. **p<0.01. Scale bar: (A)=60um, (C)=10um.

4.2.4 Ezh2 is dispensable for SVZ neural stem cell maintenance

Although in P28 SVZ there was a decrease in the Mash1+ cells in Ezh2 cKO (Figure 4.4C, E), this change could not be detected in P75 SVZ anymore (Figure 4.7A). Quantifications of Mash1+ nuclei in SVZ indicated no difference between control (285.96±3.31(x1000)/mm^3) and cKO (265.97±20.92(x1000)/mm^3) (n=3 for controls and n=4 for cKO, Figure 4.7B). Moreover, immunostaining of PHi3 showed no difference between control (95.30±15.53/section) and cKO (82.36±3.20/section) (n=3 for controls and n=4 for cKO, Figure 4.7C). GFAP+ neural stem cells/niche

astrocytes, S100β+ ependymal cells and Dcx+ neuroblasts had no obvious change after the loss of Ezh2 in P75 SVZ as well (Figure 4.7D-E, H). Previous report suggested Ezh2 is dispensable for the maintenance of long-term hematopoietic stem cells (Xie et al. 2013). Similarly, in the Ezh2 cKO SVZ, the BrdU-LRC pool was not affected as well (control: 11.65±1.58/section versus cKO: 12.16±2.91/section) (n=3 for controls and n=4 for cKO, Figure 4.7F). There was no difference in cell death (Caspase3) in SVZ between control and cKO (control: 1.15±0.200/RMS. cKO: 1.38±0.184/RMS) (n=3 for controls and n=4 for cKO, Figure 4.7G). These data show the minor role of Ezh2 in long-term maintenance of SVZ NSC.

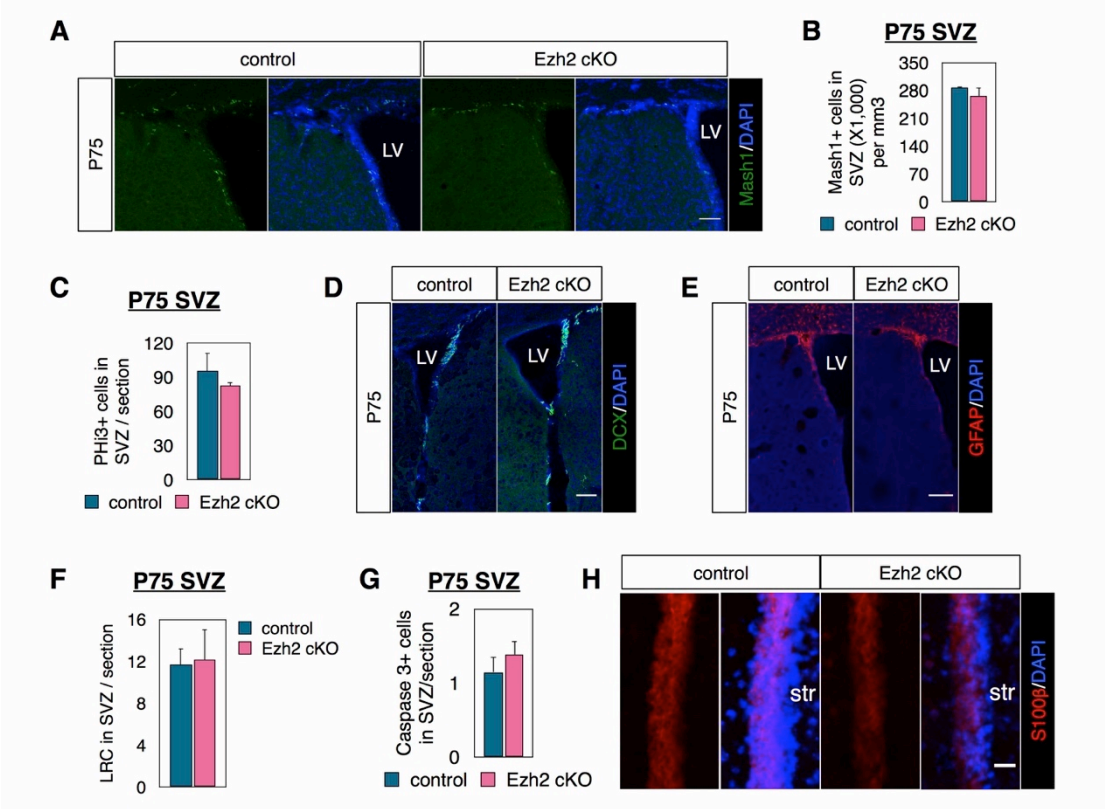

Figure 4. 7 Ezh2 is dispensable for SVZ stem cell maintenance

(A-B) Immunostaining and quantification of Mash1+ cells in P75 SVZ show the transit amplifying cells are not affected after Ezh2 knockout (n=3 for controls and n=4 for cKO).

(C) Quantification of PHi3+ proliferating cells in P75 SVZ (n=3 for controls and n=4 for cKO).

(D-E) Immunostaining shows comparable GFAP and Dcx expression between P75 control and Ezh2 cKO SVZ (n=3 for controls and n=4 for cKO).
(F) Quantification of LRC cells in P75 SVZ (n=3 for controls and n=4 for cKO).
(G) Quantification of Caspase3+ cells in P75 SVZ (n=3 for controls and n=4 for cKO).
(H) Immunostaining shows S100β expression is comparable between P75 control and Ezh2 cKO SVZ (n=3).
Error bars represent SEM. Scale bar: (A)=60um, (D)=100um, (E)=100um, (H)=20um.

4.2.5 Verification of the postnatal electroporation technique

Postnatal electroporation has been used to study gene functions in SVZ development (Boutin et al. 2008; Chesler et al. 2008; Lacar et al. 2010). To verify this technique, multiple different plasmids were used for postnatal electroporation. 1 day post electroporation (dpe) of pCAG-IRES-GFP, GFP+ cells could be detected at the lateral ventricular wall (Figure 4.8A). These cells had radial glia morphology, which is a feature of neonatal SVZ stem cells (Kriegstein and Alvarez-Buylla 2009). Using pCAG-tdTom-2A-H2BGFP, cell membrane and nucleus could be monitored with different fluorescences (Trichas et al. 2008). In 5dpe sagittal sections, the labelled RMS could be seen; and in the OB, cells with the morphologies of neuroblasts or neurons could be found (Figure 4.8B-C). A long-term examination is not available with either pCAG-IRES-GFP or pCAG-tdTom-2A-H2BGFP because of the dilution effect resulting from cell proliferation. For further characterization, CLoNe construct cocktail was electroporated (Garcia-Moreno et al. 2014). Unlike other plasmids used before, a *piggyBac* transposase-expressing construct was co-electroporated with reporter constructs, which can be inherited by the stem cell progenies. This technique allows lineage tracing and clonal analysis. 10 weeks post electroporation; cells in different lineages (neurons, astrocytes and oligodendrocytes) were labelled with

different fluorescent protein expression patterns (Figure 4.8D-G). In this experiment, I could see labelled astrocytes in both deep and superficial cortical layers as well as oligodendrocytes (Figure 4.8D). Distinct fluorescent hues in these cells reveal the different stem cell origins from SVZ. In the meantime, the

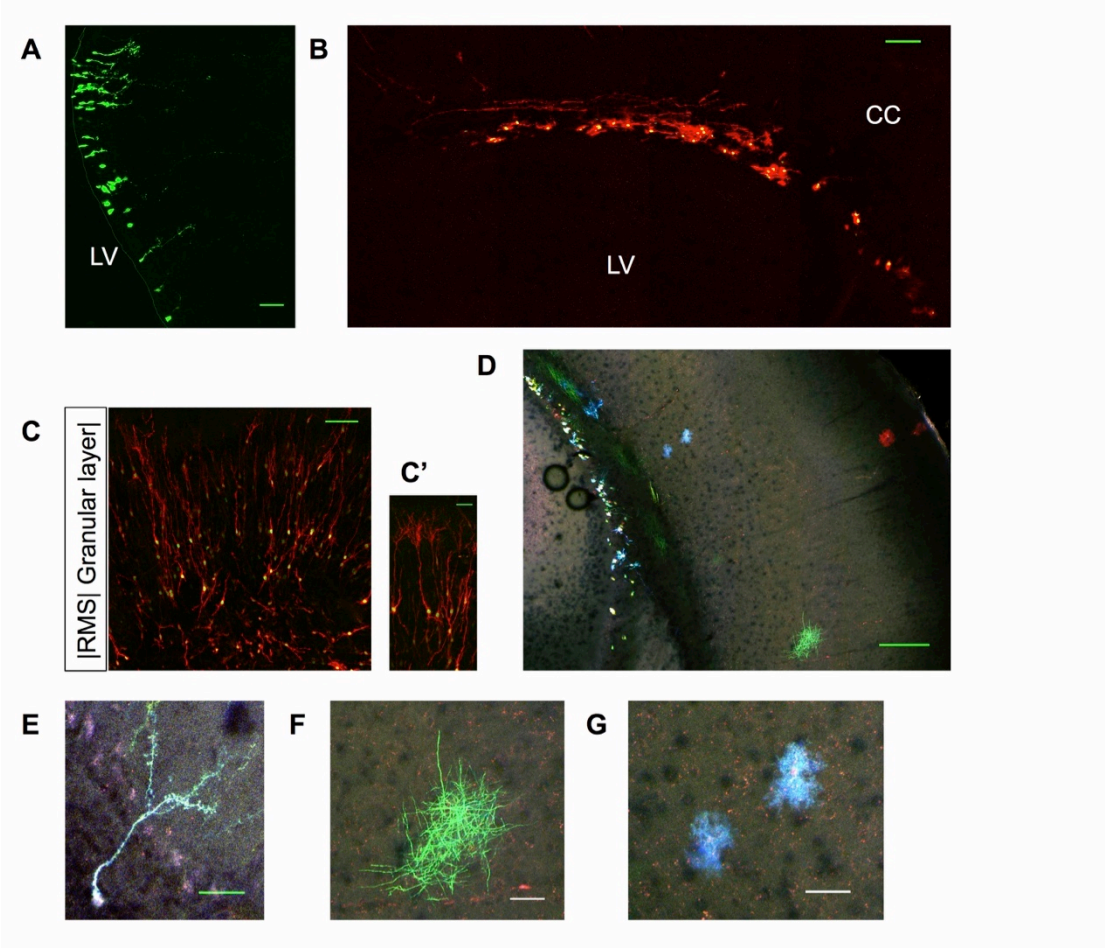

Figure 4. 8 Postnatal electroporation in the SVZ

(A) GFP encoding plasmid can label radial glial cells in SVZ 1dpe (day post electroporation).

(B-C) Electroporation with plasmid, which labels membrane with TdTomato and nucleus with GFP (5dpe). (B) Sagittal view of the SVZ and (C) coronal view of olfactory bulb. (C') shows differentiated neurons at the higher magnification.

(D-G) 10wpe (week post electroporation) of electroporation with CLoNe plasmids. (E-G) show different cell types at higher magnification. (E) neurons, (F) oligodendrocytes and (G) astrocytes.

Scale bar: (A)=60um, (B)=100um, (C)=80um, (C')=40um, (D)=200um, (E-G)=40um.

infrequent generation of cortical astrocytes from postnatal SVZ is consistent with the note that these astrocytes are locally generated (Ge et al. 2012). All these results together proved the feasibility of postnatal electroporation for further study in this thesis.

4.2.6 Generation of Eed conditional knockout mice

As Ezh1 can compensate Ezh2's function in H3K27 di- and tri-methylation (Shen et al. 2008; Ezhkova et al. 2009; Ezhkova et al. 2011; Margueron and Reinberg 2011), I then tried to knockout Eed so as to disrupt the whole PRC2 complex and avoid the issue of redundancy between Ezh1 and Ezh2. $Eed^{fl/fl}$ mice have loxP knock-in locations as previous reported (Figure 4.9A) (Xie et al. 2013). Genotyping of $Eed^{fl/fl}$ mice showed the wild-type band between 150-200bp and the floxed band between 200-300bp (Figure 4.9B). $Eed^{fl/fl}$ mice were then crossed with GLAST-CreERT2 mice to generate GLAST-CreERT2;$Eed^{fl/fl}$ mice (The detailed breeding approach was described in Chapter 2 Material and Methods) (Figure 4.9C). To induce the Cre recombination, 0.2mg/kg body weight of tamoxifen was injected in pups at P1. SVZ tissues were then collected at P14 for RT-qPCR analysis. Compared to the controls (expression normalized to 1), cKO SVZ has a reduction of Eed mRNA expression to 0.652±0.0691 (normalized to control, n=3) (Figure 4.9D). So GLAST-CreERT2;$Eed^{fl/fl}$ mice can be used as a model for functional analysis of Eed in SVZ.

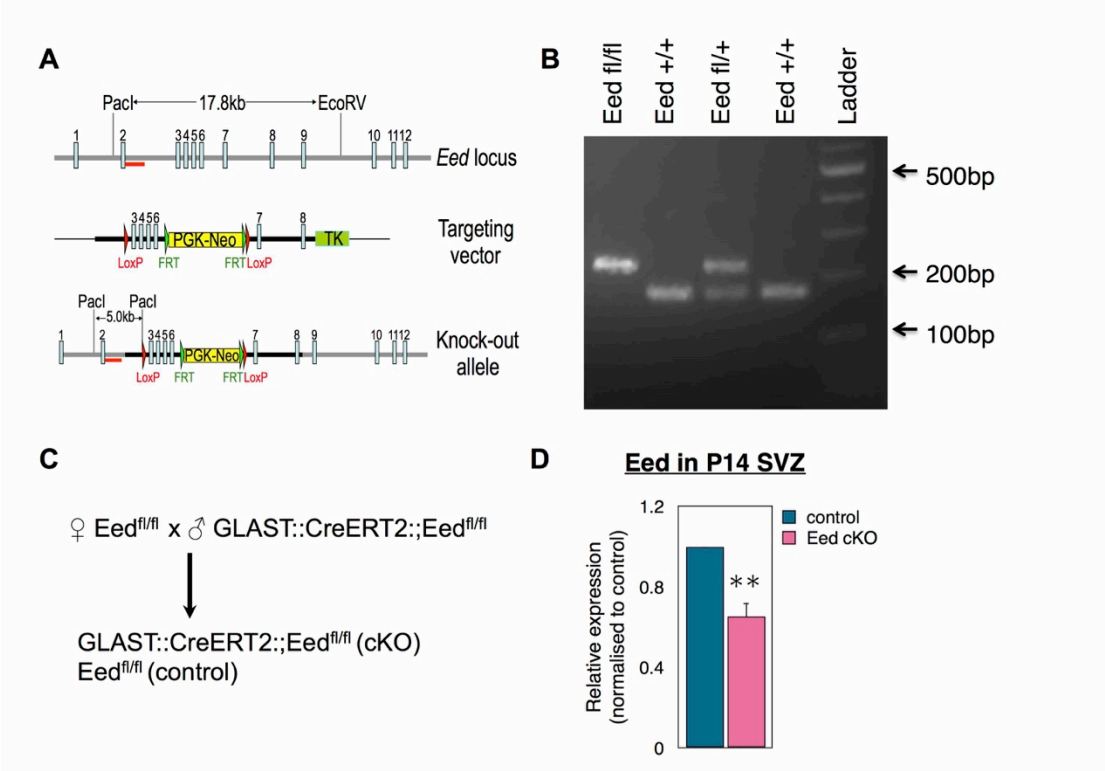

Figure 4. 9 Conditional knockout of Eed in postnatal SVZ

(A) A schematic diagram shows the targeting of the Eed$^{fl/fl}$ transgenic mice (modified from Xie et al., 2014).

(B) Examples of PCR genotyping of different mouse strains. The floxed band is around 220bp and the wildtype band is around 180bp.

(C) A schematic diagram of the experimental design.

(D) qPCR analysis of P14 SVZ shows Eed mRNA decreases. Relative expression was normalized to littermate controls. Error bars represent SEM (n=3). **p<0.01

4.2.7 Eed is required for postnatal/adult SVZ neurogenesis

To study the role of Eed in postnatal SVZ neurogenesis, I first co-electroporated control or Eed shRNA with CAG-IRES-GFP to trace the newborn neurons in the OB. Pup brains were collected at 5dpe and 14dpe. Analysis of the OB showed a dramatic decrease of GFP+ cells in the Eed knockdown groups (KD) (Figure 4.10A). In 5dpe, most GFP+ cells were still in the core of OB, where mostly neuroblasts reside.

Quantification indicated significantly fewer GFP+ cells in the Eed KD OB (77.62±2.28(x1000)/mm^3), compared to the control (122.30±15.74(x1000)/mm^3) (p=0.0129, n=5 for control and n=6 for KD, Figure 4.10A, C). Fewer GFP+ cells in RMS in 5dpe also led to fewer mature neurons in the granular layers in 14dpe (Figure 4.10B). 83.82±7.80(x1000)/mm^3 GFP+ cells could be found in the control OB, while

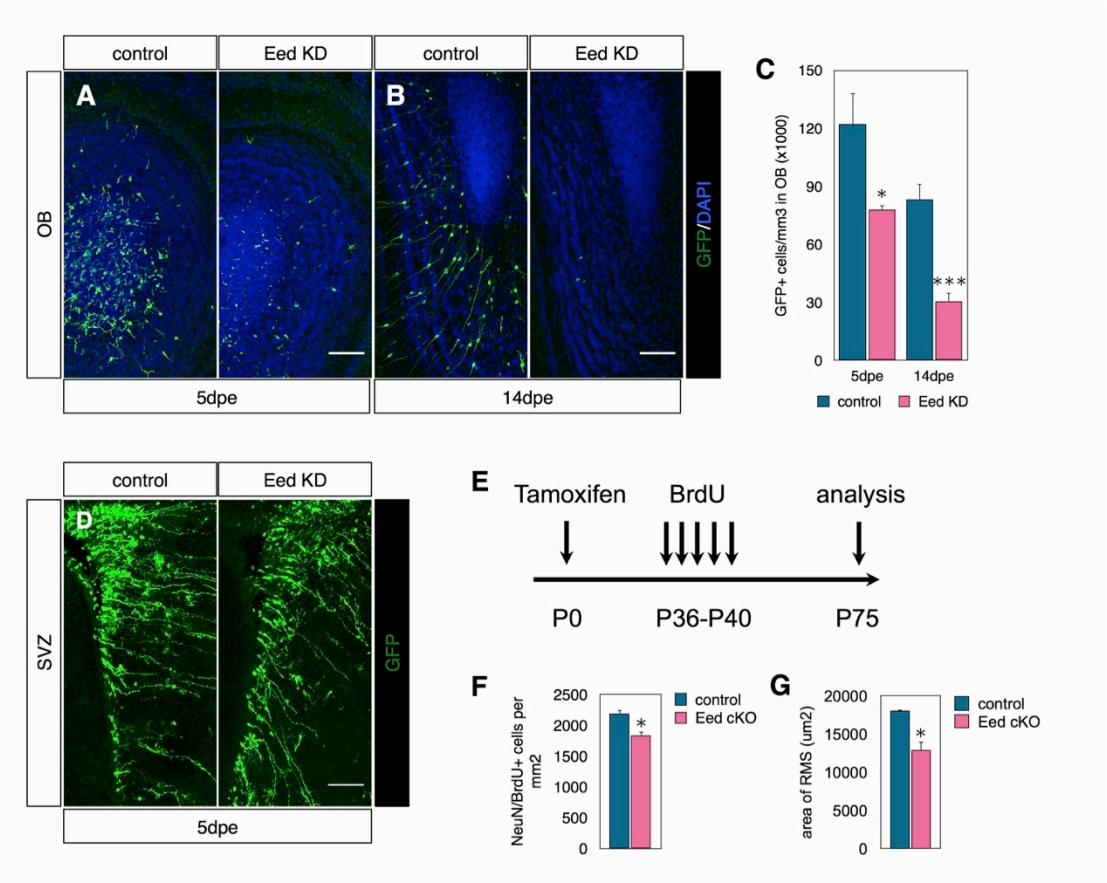

Figure 4. 10 OB neurogenesis is impaired after the loss of Eed in SVZ

(A-B, D) Postnatal electroporation of control or Eed shRNA with GFP. Staining of GFP in OB and SVZ at different time points after electroporation reveals fewer newborn cells are found in the OB after Eed KD.

(C) Quantification of GFP+ cells in the OB (For 5dpe, n=5 for control and n=6 for KD. For 14dpe, n=6 for control and n=6 for KD).

(E) A schematic diagram of the experimental design.

(F) Quantification of NeuN+/BrdU+ newborn neurons in OB (n=3).

(G) Quantification of Dcx staining demonstrates that the RMS size reduces after Eed cKO(n=3).

Error bars represent SEM. *p<0.05, ***p<0.001. Scale bar: (A, B, D)=100um.

in the KD animals there was about 63.2% decreased to 30.66±4.37(x1000)/mm^3 (p=0.0002, n=6, Figure 4.10C). The comparable GFP signals in the SVZ in at 5dpe suggests theis reduced GFP+ cells in the OB is was not due to different electroporation efficiencies between control and KD (Figure 4.10D).

As both Eed shRNA and CAG-IRES-GFP could not be replicated during cell division, there could be a possible dissociation of shRNA and GFP in electroporated cells. GLAST-CreERT2;$Eed^{fl/fl}$ mice were then used. Tamoxifen was administered at P1 and 10 doses of BrdU were injected from P36 to P40 to trace newborn neurons. In P75 mice, neurogenesis was analysed. In agreement with the results from postnatal electroporation, after the loss of Eed, there was a significant decrease of BrdU+/NeuN+ cells in cKO OB (1836.43±55.44/mm^2), compared to the control mice (2191.31±57.07/mm^2) (p=0.0112, n=3, Figure 4.10E). The surface area of the RMS was also reduced from 18020.00±186.51 μm^2 in control to 12855.47±1184.65 μm^2 in Eed cKO (p=0.0126, n=3, Figure 4.10F). Taken together, this suggested Eed is required for postnatal/adult SVZ neurogenesis.

4.2.8 Eed is involved in NSC activation and identity maintenance

At P14, no difference could be found in general cell proliferation by PHi3 in Eed cKO mice. This might be because that the time is not enough for the developmental defects

to be detected. So I chose to examine at a later time point. Meanwhile, I tried to boost

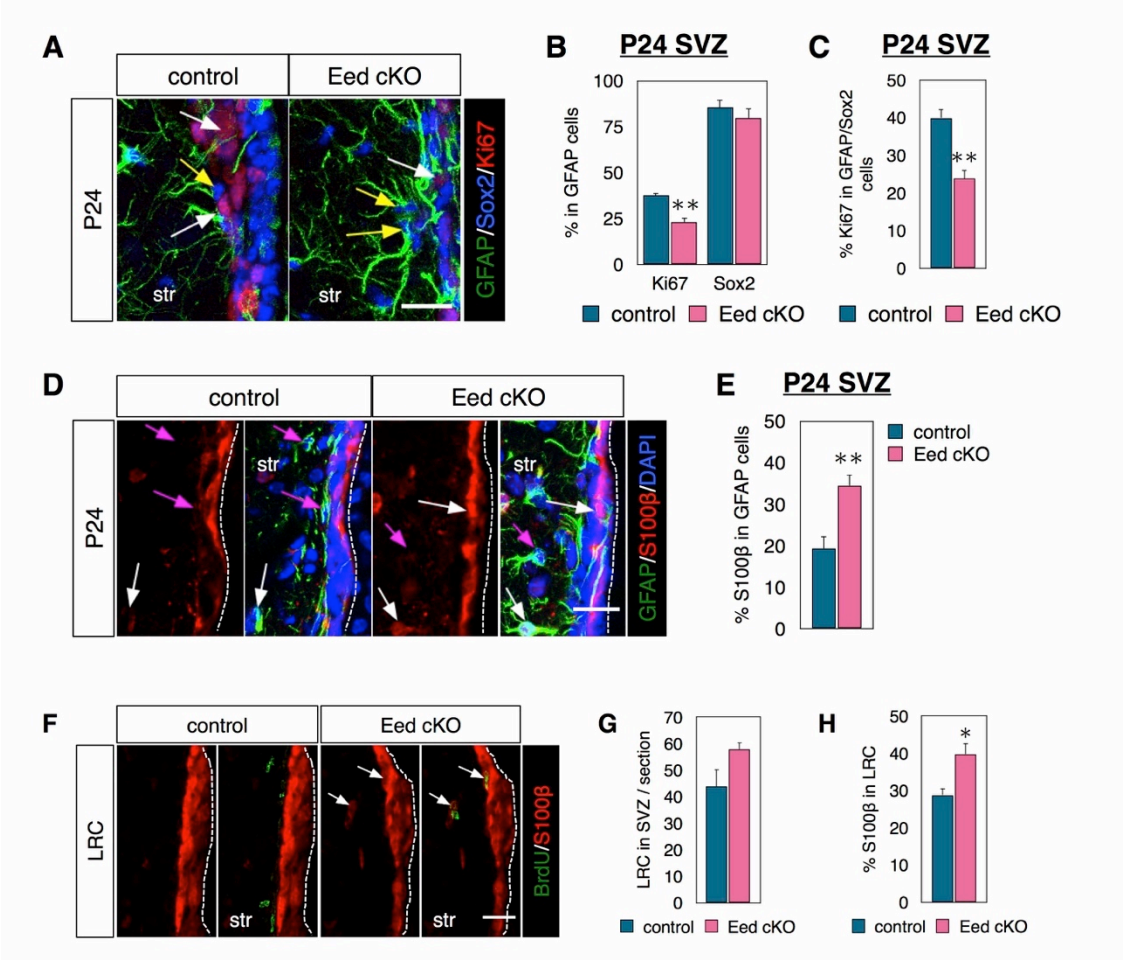

Figure 4. 11 Eed is required for stem cell activation and identity maintenance in the postnatal SVZ

(A) Costaining of GFAP, Sox2 and Ki67 in the P24 SVZ after Eed knockout. The white arrows indicate GFAP+/Sox2+/Ki67+ cells and the yellow arrows indicate GFAP+/Sox2+/Ki67- cells. It reveals mutant NSC are unable to proliferate.
(B-C) Quantification of Ki67, Sox2 in GFAP cells and Ki67 in GFAP/Sox2 cells (n=3).
(D) Costaining of GFAP, S100β in P24 SVZ after Eed knockout. The white arrows indicate GFAP+/S100β+ cells and the magenta arrows indicate GFAP+/S100β- cells. The staining indicates NSC acquire mature astrocytic features after knockout.
(E) Quantification of S100β in GFAP+ cells (n=3).
(F) Costaining of S100β in BrdU/LRC in SVZ after Eed knockout suggests mutant NSC differentiate into astrocytes. The arrows indicated BrdU+/S100β+ cells.
(G) Quantification of total SVZ BrdU/LRC and the percentage of S100β in BrdU/LRC. Error bars represent SEM. **p<0.001. Scale bar: (A)=20um, (D, F)=20um.

the Cre recombination with two doses of tamoxifen in the lactating mother following one dose in the pups (Lagace et al. 2007; Petrik et al. 2013). At P24, I firstly analysed the cell proliferation in the NSC (Figure 4.11A). Ki67/GFAP reduced in Eed cKO SVZ (23.00±2.39%) (p=0.0061, n=3, Figure 4.11B) compared to control (37.58±1.35%), with Sox2/GFAP not affected (control: 85.48±3.87% versus cKO: 79.89±5.10%) (n=3, Figure 4.11B). GFAP+ cells may be either stem cells or niche astrocytes. So I then compared Ki67 in GFAP+/Sox2+ NSC. A significant decrease of about 50% can be found (control: 39.92±2.27% versus cKO: 23.87±2.17%) (p=0.007, n=3, Figure 4.11C). This may arise due to two biological explanations: (1) that the NSC cannot be activated properly, (2) that the cell identity shifts from stem cells to mature astroglial cells. To pursue this question, I then costained S100β in GFAP cells. S100β defines astroglia maturation stage in NSC (Raponi et al. 2007). In Eed cKO SVZ, S100β/GFAP (34.45±2.52%) significantly increased (control: 19.30±2.98%) (p=0.0178, n=3, Figure 4.11D-E).

To further understand the stem cell maintenance in SVZ, I then characterized the BrdU/LRC in SVZ. 10 doses of BrdU were injected from P36 to P40 and 5 weeks were given for diluting out BrdU in the fast proliferating cells (Ferron et al. 2007). Surprisingly, at P75 total number of BrdU/LRC did not change after the loss of Eed (control: 43.75±6.51/section versus cKO: 57.92±2.42/section) (n=3, Figure 4.11F-G). However, among this BrdU/LRC pool in SVZ, more cells exhibited mature astroglia marker S100β (39.79±5.15%) in cKO compared to control (28.73±1.85%) (p=0.0343, n=3, Figure 4.11F, H).

4.2.9 Loss of Eed impaired the neurosphere generation from SVZ

To confirm Eed is involved in SVZ NSC activation and identity maintenance, the neurosphere assay was performed to analyse stem cell properties (Pastrana et al. 2011). Eed shRNA was packaged into lentivirus and dissociated neurospheres were then transduced to knockdown Eed in vitro. Cells were cultured for 3 days and sphere numbers were then counted. There was a significant decrease in the neurosphere frequency per 200,000 starting cells from 3552±329 in control to 2030±363 in Eed KD ($p<0.01$, n=3, Figure 4.12A).

To rule out the possibility of sphere fusion and analyse the sphere-forming ability at the individual cell level, SVZ cells were cultured at the clonal density (10 cells/μl) (Singec et al. 2006; Pastrana et al. 2011). To be consistent with the in vivo experiment, I started with P15 SVZ. Although no general effects on cell proliferation could be found at P14 SVZ in vivo, ~50% fewer neurospheres were generated from the P15 cKO SVZ (33.71±5.49 per 2000 cells) in comparison with controls (56.87±7.66 per 2000 cells) ($p=0.0329$, Figure 12B-C). The average neurosphere diameter analysis however showed no obvious change (control: 116.08±4.11μm versus cKO: 114.00±2.06μm) (n=2) (Figure 12D). The mixing of NSC and neural progenitors results in the heterogeneity of neurospheres which can be observed from the diversity of individual neurosphere size (Pastrana et al. 2011). At P15 loss of Eed did not change the sphere number distribution according to size (n=2) (Figure 12E). The BrdU/LRC experiment started from P35. For consistency, I then cultured P38 SVZ cells at the clonal density for generating neurospheres. The neurosphere yielding ability decreased in Eed cKO (29.91±12.44 per 2000 cells) (control: 64.85±1.13 per 2000 cells) ($p=0.0490$, Figure 12F) as seen at P15. The size of neurosphere was again

not altered based on the preliminary analysis (average size for control: 177.87μm versus cKO: 156.17±7.18μm) (n=1 for control and n=2 for cKO, Figure 12G-H).

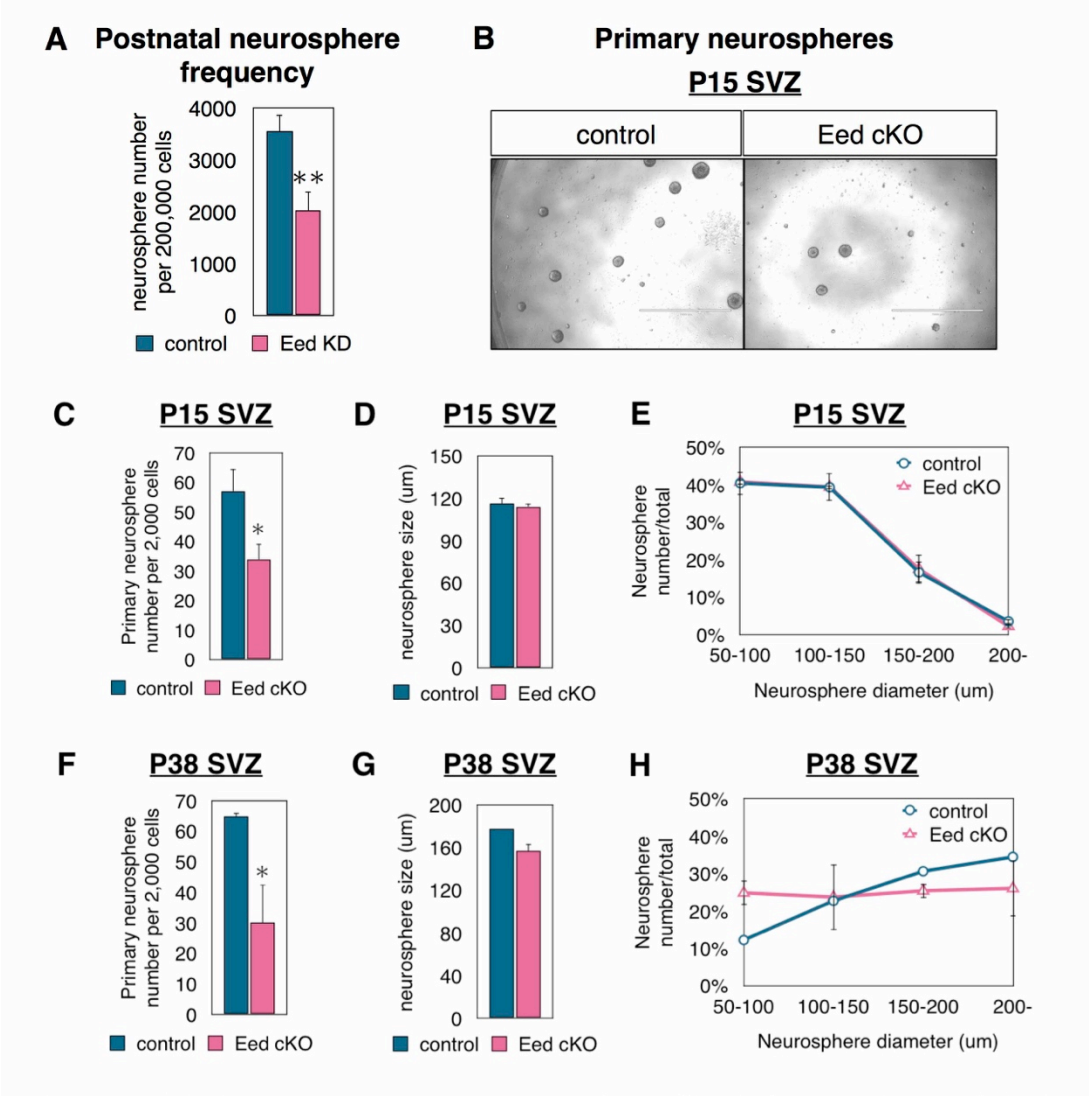

Figure 4. 12 Loss of Eed decreases the neurosphere generation ability in SVZ

(A) In vitro knockdown of Eed by lentivirus infection decreases neurosphere number after 3 days in culture (n=3).

(B-C) Fewer primary neurospheres can be generated from P15 SVZ after in vivo knockout of Eed (n=5 for control and n=6 for cKO).

(D-E) The diameter of primary neurospheres from P15 SVZ is not affected (n=2).

(F) Fewer primary neurospheres can be generated from P38 SVZ after in vivo knockout of Eed (n=3).

(G-H) The diameter analysis of primary neurosphere generated from P38 SVZ (n=1 for control and n=2 for cKO).

Error bars represent SEM. *p<0.05, **p<0.01. Scale bar: (B)=1000um.

4.2.10 Eed is dispensable for astrocyte activation in cortical lesion

To assess the functions of Eed in brain injury, I performed cortical lesions in Eed cKO mice. 5 week old GLAST-CreERT2;Eed$^{fl/fl}$ mice were injected with tamoxifen daily for 5 days. 4 weeks after the last injection, cortical lesion was carried out and the mice were allowed to survive for 5 days before analysis (Figure 4.13A). Sox2 or Ki67 was costained with GFAP in the ipsilateral cortex as an indicator for reactive astrocytes (Figure 4.13B). For proliferative astrocytes, no significant difference could be found between control and Eed cKO cortex (control: 11374.88±2152.01/μm^3 versus cKO: 13342.98±1401.60/μm^3) (n=3, Figure 4.13C). Similarly, GFAP+/Sox2+ cells were not affected after loss of Eed either (control: 65915.60±7848.52/μm^3 versus cKO: 79907.31±3886.10/μm^3) (n=3, Figure 4.13D).

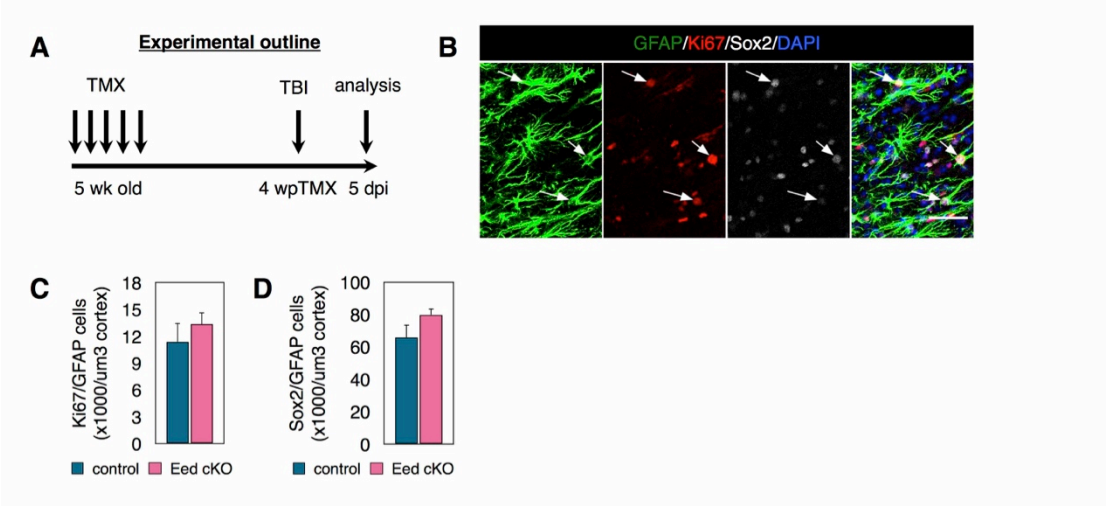

Figure 4. 13 Eed is not required for astrocyte activation after cerebral cortex injury

(A) A schematic diagram for the experiment design.

(B) Costaining of GFAP, Ki67 and Sox2 in the injured cortex. The arrows indicated GFAP+/Sox2+/Ki67+ cells.

(C-D) Quantifications of Ki67+/GFAP+ cells and Sox2+/GFAP+ cells in the injured cortex suggest reactive astrogliosis is not affected after the loss of Eed.

Error bars represent SEM (n=3). Scale bar: (B)=50um.

4.3 Discussion

In this chapter, I have characterized SVZ phenotypes of both Ezh2 and Eed knockout animals. In summary I found Ezh2 is dispensable for NSC maintenance. In contrast, Eed regulates NSC activation and identity maintenance.

4.3.1 Inducible conditional knockout mice for Ezh2 and Eed

Constitutive knockout is a permanent genetic inactivation or disruption in every cell of the animal. Both $Ezh2^{-/-}$ and $Eed^{-/-}$ ES cells have been used extensively to characterize the structure and functions of PRC2 (Boyer et al. 2006; Shen et al. 2008; Shen et al. 2009; Leeb et al. 2010; Ura et al. 2011). Nevertheless because of the essential role of PRC2 in early embryonic development, $Ezh2^{-/-}$ mouse embryos could not survive E8.5 (O'Carroll et al. 2001; Shen et al. 2008). Similarly, disrupted primitive streak could be observed in Eed null and few embryos are able to reach the late-streak stage (Schumacher et al. 1996). The introduction of conditional knockout technology bypasses the problem of embryonic lethality. Previously, several research groups chose hGFAP-Cre line for postnatal SVZ NSC study (Lim et al. 2009; Andreu-Agullo et al. 2012; Hwang et al. 2014; Park et al. 2014). This choice was based on the fact that hGFAP-Cre can induce recombination in precursors of SVZ NSC at E13.5 (Lim et al. 2009). On the other hand, recent cell cycle analysis indicates postnatal/adult NSC are determined between E13.5 and E15.5 (Furutachi et al. 2015). So with this line, one argument should be taken into account: whether the knockout affects either the generation of postnatal/adult SVZ NSC, or the actual behaviours of postnatal/adult SVZ NSC? In consideration of the experimental questions, I crossed

GLAST-CreERT2 with either $Ezh2^{fl/fl}$ or $Eed^{fl/fl}$ mice. Tamoxifen was then injected at around P1. In this way, the spatiotemporal controlled knockout is accomplished.

4.3.2 Both Ezh2 and Eed are required for SVZ neurogenesis

Postnatal/adult SVZ keeps generating new neurons and adds into OB neural circuits (Ihrie and Alvarez-Buylla 2011). I used the BrdU label retaining technique to study the neurogenesis ability after the loss of Ezh2 or Eed. It is based on the fact that cell proliferation is limited to the postnatal/adult SVZ and the cells incorporated with BrdU can migrate and differentiate into OB neurons before the dilution of BrdU in genomic DNA (Ferron et al. 2007). I demonstrated that in both knockout models, the number of BrdU/LRC costained with neuronal marker NeuN in OB decreased significantly. This technique is widely used to study SVZ neurogenesis (Comte et al. 2011; Andreu-Agullo et al. 2012; Feng et al. 2013; Delgado et al. 2014). However the weakness of this application is also obvious: (1) due to the efficiency of tamoxifen-induced recombination, GLAST promoter targeted NSC pool will be comprised of both homozygous and heterozygous knockouts as well as wild type cells. BrdU/LRC in OB will therefore also have a mosaic population. So it is not feasible to study individual BrdU/LRC because of its low specificity to the homozygous knockout cells. To solve this issue, the introduction of fluorescent protein fused reporter transgene would be necessary. With this tamoxifen-induced reporter, the knockout cells can then be distinguished and traced by the fluorescent protein (Ninkovic et al. 2013). (2) Eed is expressed throughout SVZ/RMS/OB and GLAST-CreERT2 mediated recombination could happen in astrocytic cells within and outside of SVZ. Hence one cannot rule out the possibility that loss of Eed in the niche astrocytes or the RMS glial tube would not change the origin of BrdU/LRC in OB. To trace the fate of

the SVZ NSC directly, I used postnatal electroporation in SVZ. Reduced GFP+ cells in Eed KD OB confirmed that Eed is required for neurogenesis.

The generation of Nestin-CreERT2;Ai9;Eed$^{fl/fl}$ mice would circumvent both issues. One advantage of Nestin-CreERT2 is that exclusively SVZ NSC lineage cells are targeted and with this line, I can also examine the gliogenesis versus neurogenesis by tracing the fates of tdTomato positive cells inside and outside SVZ.

4.3.3 Evaluation of electroporation in SVZ

As an efficient and rapid technique, electroporation is extensively applied in embryonic cortical and retinal neurogenesis study. To perform a loss of function study, Cre can be electroporated to induce recombination (Matsuda and Cepko 2007; Franco et al. 2011; Hartman et al. 2013). But I had not considered it as the priority because Cre induced recombination and degradation of the protein may take a few weeks while GFP labelled cells are invisible at 3-4 weeks post electroporation in postnatal SVZ and RMS (Lacar et al. 2010). Therefore GFP-Cre may not be practical in consideration of this temporal issue.

Another argument one may raise is that the comparison of absolute GFP cell number in OB may not be appropriate and instead the percentage of GFP in OB per total GFP cells should be used. I had not chosen the latter because (1) the electroporation efficiencies between control and Eed KD were comparable, and (2) the GFP signals in both SVZ were also similar. Thus it is sufficient to conclude Eed is required for neurogenesis simply by quantification of absolute GFP cell numbers in OB. The same method has also been used by other labs on electroporation-based postnatal SVZ study (Feliciano et al. 2013; Hartman et al. 2013).

Hartman et al reported around 95% colabelling for two-construct co-electroporation in the postnatal SVZ (Hartman et al. 2013). To potentially improve this rate, I increased the shRNA concentration over GFP vector and assumed every GFP labelled cell would be transfected with the shRNA vector. However, I cannot guarantee 100% colabelling for two constructs in all cells.

Furthermore, it is believed mitosis is required for successful electroporation, especially in the adult brains, and researchers have tried to enhance electroporation in non-mitotic cells with the aid of nuclear permeabilising agents (Barnabe-Heider et al. 2008; De la Rossa et al. 2013). But in my electroporation in adult SVZ, I was clearly able to identify labelled ependymal cells as well as NSC based on the cell morphology (Supplemental Figure 2). So more work should be conducted to explore the role of mitosis in electroporation.

4.3.4 PRC2 in SVZ NSC maintenance

The SVZ NSC maintenance is a long-standing question in the field. Several labs have tried to address it from different aspects. At the moment, two key biological processes are considered to be fundamental to maintain the stem cell pool: (1) cell cycle and (2) cell identity between NSC and niche astrocytes (Ihrie and Alvarez-Buylla 2011). Interestingly, it seems Eed, but not Ezh2 is involved in both processes.

As discussed in Chapter 3, SVZ NSC is at a low proliferating rate and this is achieved by the orchestration of multiple cell cycle promoters and inhibitors (Cheung and Rando 2013). For example, p21 is a cyclin-dependent kinase inhibitor (CDKI) which antagonizes the activities of Cdk1 and Cdk2. p21 is expressed in the SVZ NSC and is required for stem cell quiescence maintenance (Kippin et al. 2005; Porlan et al. 2013). Loss of p21 would activate NSC and accelerate neurogenesis at the exhaustion

of stem cell pool. As a result, for the long term fewer NSC could continually generate new neurons (Kippin et al. 2005). The expression of p16Ink4a and p19Arf, another two CDKIs, will limit self-renewal of SVZ NSC (Nishino et al. 2008). On the other hand, Cdk2, in contrast, promotes adult NSC self-renewal capacity (Jablonska et al. 2007). Intriguingly, it seems PRC2 can repress a number of cell cycle regulators. In hematopoietic stem cells, loss of Eed activates Cdkn1a (p21), Cdkn2a (p16Ink4a and p19Arf), Cdkn2b (p15), HoxC4, Ccnd1, Ccng1, etc (Xie et al. 2013). In SVZ, it is reported that Ezh2 can inhibit p16Ink4a directly through H3K27 methylation and then control cell proliferation (Hwang et al. 2014). However, as I cannot detect Ezh2 in SVZ NSC, it indicates Ezh2/p16Ink4a regulation should be more predominant in transit amplifying cells and neuroblasts. In my experiments, the proliferation phenotype after Ezh2 knockout was very limited to P28, but neither P14 nor P75 SVZ. This can be explained by the overlapping functions of Ezh1 and the acute proliferation decrease at P28 were then repaired, as the NSC was not affected by the loss of Ezh2. With Eed knockout, I found fewer GFAP+/Sox2+ NSC were proliferative, which means the stem cells could not be activated properly anymore. This can be also confirmed by in vitro neurosphere culture. Adult NSC stays quiescent mostly but will enter cell cycle in pathological conditions. Infusion of cytosine β-D-arabinofuranoside (AraC) in SVZ with mini-osmotic pump can eliminate fast proliferating cells and quiescent NSC will then divide to regenerate the SVZ cytoarchitecture (Doetsch et al. 1999). By this approach, it is illustrated that deletion of Patched, the main SHH receptor, blocks the NSC activation (Ferent et al. 2014). Moreover, SVZ exposure to exogenous PDGF-AA is able to activate NSC through PDGFRα and induce glioma-like growth (Jackson et al. 2006). In the future

work, it would be informative to test whether, on the Eed knockout background, AraC or PDGF-AA is capable of promoting the NSC to exit from the quiescent stage.

The mystery of adult NSC and niche astrocytes still remains elusive. Transcriptome comparison reveals gene expression signatures for adult NSC, like lgals-3 (Gal3) (Beckervordersandforth et al. 2010). Gal3 can regulate neuroblast migration in SVZ but its role in NSC is still unclear (Comte et al. 2011). Additionally, of note, several CDKIs seem to participate in regulate the neurogenic competence of adult NSC as well. Apart from its function in cell cycle inhibition, p21 is believed to maintain NSC through cell cycle independent manners. Loss of p21 in SVZ increases Bmp2 expression, which leads to premature astrocytic differentiation of NSC. This is archived by direct binding of p21 to Bmp2 promoter with the aid of E2F (Porlan et al. 2013). Furthermore, p21 is also able to directly inhibit Sox2 expression and thereby regulate NSC self-renewal and multipotency (Marques-Torrejon et al. 2013). Besides p21, it is documented that p16Ink4a and p19Arf suppress neuronal differentiation of NSC and loss of function could enhance the neurogenic competence (Price et al. 2014). Similar phenotypes were observed in Eed cKO SVZ, i.e. increased S100β in GFAP cells and BrdU/LRC in SVZ.

The association of p21/p16/p19 with NSC maintenance raises an interesting question, whether PRC2 functions in SVZ through orchestrating different CDKIs? Hwang et al has described loss of Ezh2 could increase the expression of p16Ink4a (Hwang et al. 2014). But it seems p19Arf is not regulated by Ezh2 and the relationship between PRC2 or Ezh2 and p21 is still enigmatic. Cdkn2a (p16Ink4a/p19Arf) null astroglia have reduced p21 expression while loss of p21 will increase p19Arf but not p16Ink4a, indicating a potential CDKI network (Marques-

Torrejon et al. 2013; Price et al. 2014). I am going to talk about whether and how Eed can regulate this CDKI network in Chapter 5.

4.3.5 Neurosphere assay for NSC analysis

Neurosphere assay is widely used as a method to identify NSC and examine the self-renewal and differentiation abilities of NSC (Pastrana et al. 2011). In this chapter, I also applied primary neurosphere assay to characterize the activation of NSC isolated from SVZ. Nonetheless several points should be considered and argued when explaining the data from this assay:

(1) Sphere forming after serial passage is the key indicator for self-renewal ability in NSC (Pastrana et al. 2011). To evaluate the stem cell population in vitro, I also tried to passage the primary neurospheres from control or Eed cKO SVZ. Unfortunately qPCR analysis of the primary spheres showed no significant difference and genotyping also confirmed the heterogeneity in Eed cKO neurosphere. This should be caused by incomplete knockout of Eed in SVZ NSC by the inducible approach. Hence, it is not reasonable to continue serial passage of the primary neurospheres. But on the other hand, I can also estimate only the non-knockout cells from Eed cKO SVZ formed the neurospheres while the homozygous knockout cells lost this ability, which still supports my conclusion.

(2) Starting cell number will interfere with the final sphere forming ability. The concept of self-renewal is that a single stem cell can generate one sphere (Pastrana et al. 2011). As single cell per well culture is not practical in vitro, a proper starting cell number should be used. In the first neurosphere assay in this chapter, high cell density ($1x10^5$/ml) was used, offering us estimation

about general proliferation ability. One weakness of this experiment is that we were unable to examine sphere-forming ability of individual cells, as there is strong evidence for sphere fusion (Singec et al. 2006; Pastrana et al. 2011). 10 cells/μl for primary neurospheres or 1 cell/μl for secondary neurospheres is usually recommended for clonal density culture (Pastrana et al. 2011). I then cultured the cells at a density of 10 cells/μl for the following experiments. But one can still argue the potential of fusion, as neurospheres have high motility (Singec et al. 2006). An alternative method to circumvent this problem is soft agar assay, by which spheres are immobilized in culture (Shi et al. 2008; Wang et al. 2012; Hwang et al. 2014).

(3) The interpretation of neurosphere size could be problematic. Traditionally, large neurospheres are believed to derive from NSC as founder cells while small ones from neural progenitors (Pastrana et al. 2011; Marques-Torrejon et al. 2013). This is based on the theory that NSC can keep proliferating while progenitors can only divide limited times. Experimental observations however confound this theory. On the one hand, quiescent SVZ NSC will not form neurospheres in vitro (Codega et al. 2014). On the other hand, no difference could be determined by serial passage for small or larger neurospheres (Pastrana et al. 2011). In my experiments, no neurosphere size was unchanged after Eed knockout. This could be due to the less essential role of Eed in cell proliferation, or as I discussed above only wildtype or incomplete knockout cells generate neurospheres.

(4) Differentiation analysis in neurospheres. One question I have not answered in this chapter directly is whether loss of Eed will influence neurosphere differentiation. Future work should involve the following two experiments: 1)

Single cell differentiation. An overall analysis of neuronal/astrocytic/oligodendrocytic differentiation of NSC after Eed knockout. 2) Sphere clonal differentiation. Multipotency of individual NSC can be examined by differentiating clonal derived neurospheres.

4.3.6 PRC2 in regulating neuroblast migration

Loss of Ezh2 or Eed reducing neurogenesis could also partially be a consequence of deficient neuroblast migration. In cell culture studies, Ezh2 is shown to regulate migration and invasion of multiple cancer cell lines (Kottakis et al. 2011; Shin and Kim 2012; Xu et al. 2013; Ferraro et al. 2014; Liu et al. 2014a; Gunawan et al. 2015). Far less has been characterized about PRC2 regulating cell migration during brain development. Sonic hedgehog signalling (SHH) is essential for tangential migration in the hindbrain. Interestingly, Ezh2 can maintain proper migration of precerebellar pontine nuclei by repressing Netrin1, which coordinates with SHH as a chemoattractant (Charron et al. 2003; Di Meglio et al. 2013). To study whether Ezh2 or Eed has any function in SVZ neuroblast migration, two experiments can be proposed for future work: (1) In vitro, explant assay (Comte et al. 2011). Using RMS explants from Ezh2 or Eed cKO mice, neuroblast migration can be monitored directly. Nevertheless, one disadvantage of this assay is the lower estimation of the complicated environmental effect. For example, the SHH-dependent Ezh2 role in cell migration may not be reflected properly in explant assays due to the lack of relevant ligands in the culture system. (2) Live-imaging in brain slices would be an alternative to solve this problem. 2-photon time-lapse microscopy can reduce photobleaching and phototoxicity, which enables long term imaging of neuroblast migration (James et al.

2011). The development of gradient index (GRIN) lens provides another choice for deep imaging in intact brains of live mice (Murray and Levene 2012).

4.3.7 Eed is not required for post-injury reactive astrocytosis

In Chapter 3, I described the expression of PRC2 components in the cortex after cortical lesion. Ezh2 is absent in both ipsilateral and contralateral hemispheres, while the expression of Eed remains consistent. As Eed is involved in postnatal/adult SVZ NSC activation, I then tried to answer whether Eed has any role in reactive astrocytosis.

Adult GLAST-CreERT2;Eed$^{fl/fl}$ mice were given tamoxifen to rule out the possibility that loss of Eed may affect cortical astrocyte expansion at early postnatal stages (Ge et al. 2012). At 5 days post injury, reactive astrocytes, featured with GFAP expression, were found in the ipsilateral cortex. For both control and cKO cortices, the morphologies of reactive astrocytes were comparable: hypertrophic and high levels of GFAP (Robel et al. 2011). No significant difference could be found in the quantifications of GFAP+/Ki67+ or GFAP+/Sox2+ cells in cortex after injury, as well. All these data together suggest Eed may not perform a fundamental role in reactive astrocytosis. Soon after brain injury, protoplasmic astrocytes in the cortex upregulate several NSC markers, including Nestin, Vimentin, BLBP, etc. And within a week post injury, about half of these astrocytes will proliferate, with the highest rate at around 5-7 days (Robel et al. 2011). However, these two features were not disrupted after loss of Eed. Reactive astrocytes and SVZ NSC share a few similar signals, so it is interesting to speculate why the functions of Eed seem to be limited to the neurogenic niche and not seen in more general astroglia.

One possibility is that distinct BMP signalling in two areas sets up diverse epigenetic modifications. In the SVZ niche, deletion of Smad4 or infusion of BMP antagonist Noggin will limit neurogenesis but promote oligodendrogenesis (Colak et al. 2008). On the other hand, addition of BMP will however inhibit neurogenesis (Lim et al. 2000). This might be due to the dose response of BMP at different levels (Robel et al. 2011). In brain injury, Noggin will be upregulated, especially in reactive astrocytes, and convert oligodendrocyte precursor cells to astrocytes (Hampton et al. 2007). In the future, it would be informative to study whether BMP signalling and PRC2-dependent epigenetic modification can regulate each other's function to distinguish reactive astrocytes and SVZ NSC.

4.4 Conclusion

In this chapter, I uncovered that PRC2 is essential in postnatal SVZ neurogenesis. For cell proliferation, Ezh2 plays a minor role, which may be compensated by Ezh1. In contrast, Eed is indispensable for SVZ NSC maintenance, which involved two aspects: activation of NSC and the stem cell identity maintenance. Eed is able to protect the SVZ NSC from mature astrocytic fate in SVZ. The function of Eed in parenchymal astrocytes outside SVZ is less important and it is not required for astrocyte activation in response to traumatic brain injury.

Chapter 5

Molecular mechanisms underlying PRC2 regulation

5.1 Introduction

It is well established that PRC2 is involved in the suppression of gene expression (Margueron and Reinberg 2011). Hwang et al previously reported that postnatal loss of Ezh2 could activate p16Ink4a and Olig2 (Hwang et al. 2014). As SVZ NSC do not express Ezh2, this misexpression should affect transit amplifying cells and neuroblasts rather than NSC directly. The noncanonical PRC1 component Bmi1 is required for NSC self-renewal and proliferation by the repression of p16Ink4a, p19Arf and p21 (Molofsky et al. 2003; Fasano et al. 2007; He et al. 2009a). However, this knowledge contradicts the fact that the majority of SVZ NSC remain in the quiescent state in vivo. Therefore it is very possible that these studies actually characterized functions of PRC1/PRC2 in neural progenitors but not NSC. Moreover there is evidence that p21 is expressed in SVZ NSC in vivo (Porlan et al. 2013). So it is still a remaining question how loss of PRC2, especially Eed, in NSC will cause defects in stem cell activation and identity maintenance. As follows, two other features of PRC2 regulatory mechanisms need to be taken into account.

5.1.1 Context-dependent functions of PRC2

With the development of next-generation sequencing methods, PRC2 targets have been identified and studied in various tissues (Mikkelsen et al. 2007; Shen et al. 2009; Sher et al. 2012; Rheinbay et al. 2013; Xie et al. 2013; Hwang et al. 2014). Systematic comparisons of the sequencing data have uncovered that the binding of PRC2 is context-dependent. Olig2, for instance, has H3K27me3 and H3K4me3 bivalent chromatin domain in ESC-derived human neural stem cells while its H3K27me3 mark is lost in glioblastoma cancer stem cells (Rheinbay et al. 2013). ChIP-Seq for Ezh2 in

NSC from E14 embryonic telencephalon also revealed that Olig2 is targeted (Sher et al. 2012). In SVZ derived neurospheres, however, Ezh2 will only target Olig2 when the cells enter differentiation program (Hwang et al. 2014). This precise fine-tuning of individual gene expression could be attributed to the environment/context specific recruiting pathways and the balance between methyltransferase versus demethylase. In addition, as a master regulator, PRC2 orchestrates molecular machineries simultaneously driving opposite cell behaviours (Xie et al. 2013). An unaddressed question raised from this observation is how cells will determine which behaviour direction to select?

5.1.2 Diverse effects of Ezh2 and Eed on target genes

While both Ezh2 and Eed participate in PRC2-dependent gene silencing, their actual effects on target genes are very diverse. For instance, Eed knockout in hematopoietic stem cells led to activation of several genes, including Id2, Dlk1, Sox7, and Bmp7, while the expression of these genes actually decreased after loss of Ezh2 (Xie et al. 2013). There is no evidence yet about mechanisms contributing to these contradicting effects. One possibility is that Ezh2 could have H3K27me3-independent functions. Firstly, as a methyltransferase, Ezh2 can methylate more than just histone (He et al. 2012; Wurm et al. 2014). One example is Gata4, the transcription activity of which can be controlled by Ezh2 direct methylation of Lys299 (He et al. 2012). Secondly, more methyltransferase-independent functions have recently been discovered for Ezh2. It is shown Ezh2 and PAF can form a complex with β-catenin to enhance Wnt signalling mediated gene expression (Jung et al. 2013).

In spite of the extensive study on Ezh2, PRC2-dependent and independent regulation by Eed are far less characterized.

In this chapter, I am going to (1) compare the downstream genes of Ezh2 versus Eed, and (2) examine whether any of these genes could explain the phenotypes I observed in the knockout SVZ.

5.2 Results

5.2.1 PRC2 occupancy in SVZ NSC

To understand how PRC2 regulates SVZ neurogenesis on the molecular level, I analysed PRC2 binding to gene targets in the SVZ. I first did chromatin-immunoprecipitation with either H3K27me3 or control IgG antibody in the SVZ tissues from P4 and P56 mouse brains. Quantitative PCR analysis of precipitated DNA showed enrichment of H3K27me3 on canonical PRC2 targets, i.e. Gata6, Olig2, Ngn1 and Ngn2 (Figure 5.1). Surprisingly, SVZ cell markers like Nestin, EGFR and Sox2 also have H3K27me3 binding, which may be due to the heterogeneity of SVZ tissues (Figure 5.1). Yamanaka factors (Oct4, Sox2, Klf4, c-Myc) and Nanog have been used to induce embryonic-like pluripotency in adult differentiated cells (Takahashi and Yamanaka 2006). The previous data in our lab indicated the absence of Oct4 and Klf4 expression in SVZ tissues; however I could only detect H3K27me3 binding on Oct4 but not Klf4 (Figure 5.1).

Because multiple cell types co-exist in the SVZ, I then examined the PRC2 occupancy in cultured neurospheres. The enrichments of both Eed and H3K27me3 could be found on PRC2 targets (Gata6, Hoxa11, Ngn1, Ngn2, Sox17) (Figure 5.2). In contrast to SVZ tissues, neither Sox2 nor Olig2 was occupied by Eed or H3K27me3 in cultured neurospheres (Figure 5.2). CyclinD1 and Notch1 can be modulated by the PRC2 component Jarid2 (Shirato et al. 2009; Mysliwiec et al. 2011), but no Eed or H3K27me3 could be found on them (Figure 5.2). No PRC2 binding was observed on the Yamanaka factors (Figure 5.2).

In addition, I also performed chromatin-immunoprecipitation with Ezh2 and Jarid2 antibodies in P4 neurospheres. Unfortunately both experiments failed to generate any positive signal. This may be attributed to poor antibody quality.

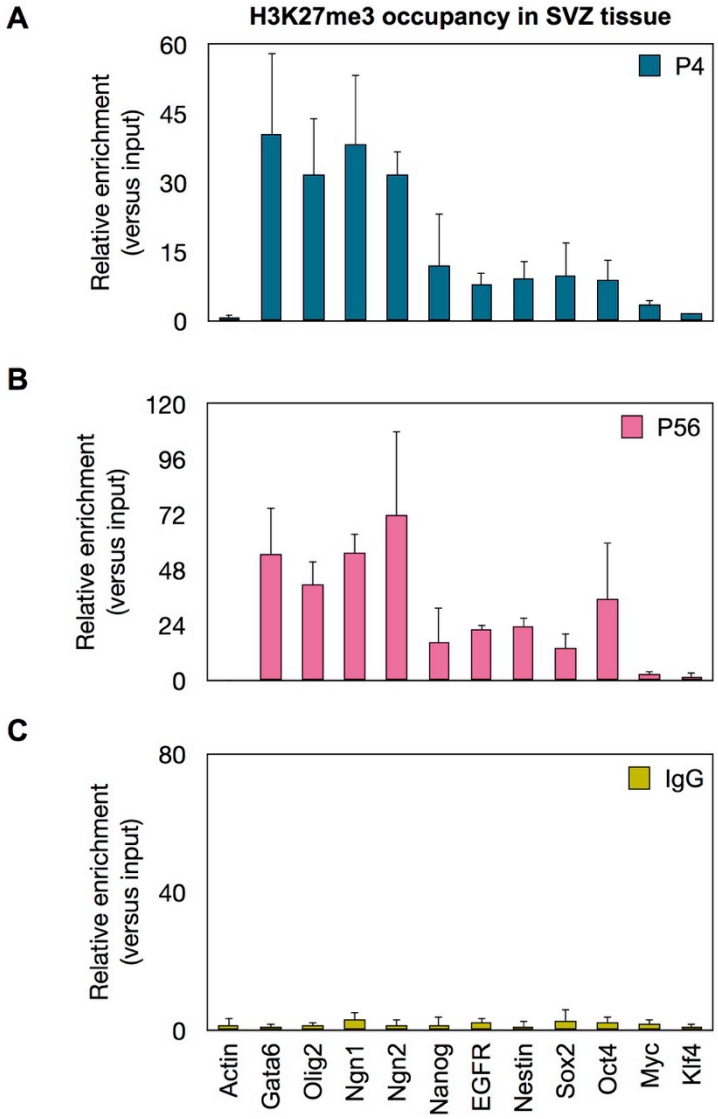

Figure 5. 1 The occupancy of H3K27me3 in SVZ cells at different ages

(A) ChIP-qPCR of H3K27me3 in P4 SVZ (n=3).

(B) ChIP-qPCR of H3K27me3 in P56 SVZ (n=3).

(C) ChIP-qPCR of IgG in SVZ as the negative control (n=3).

Error bars represent SD.

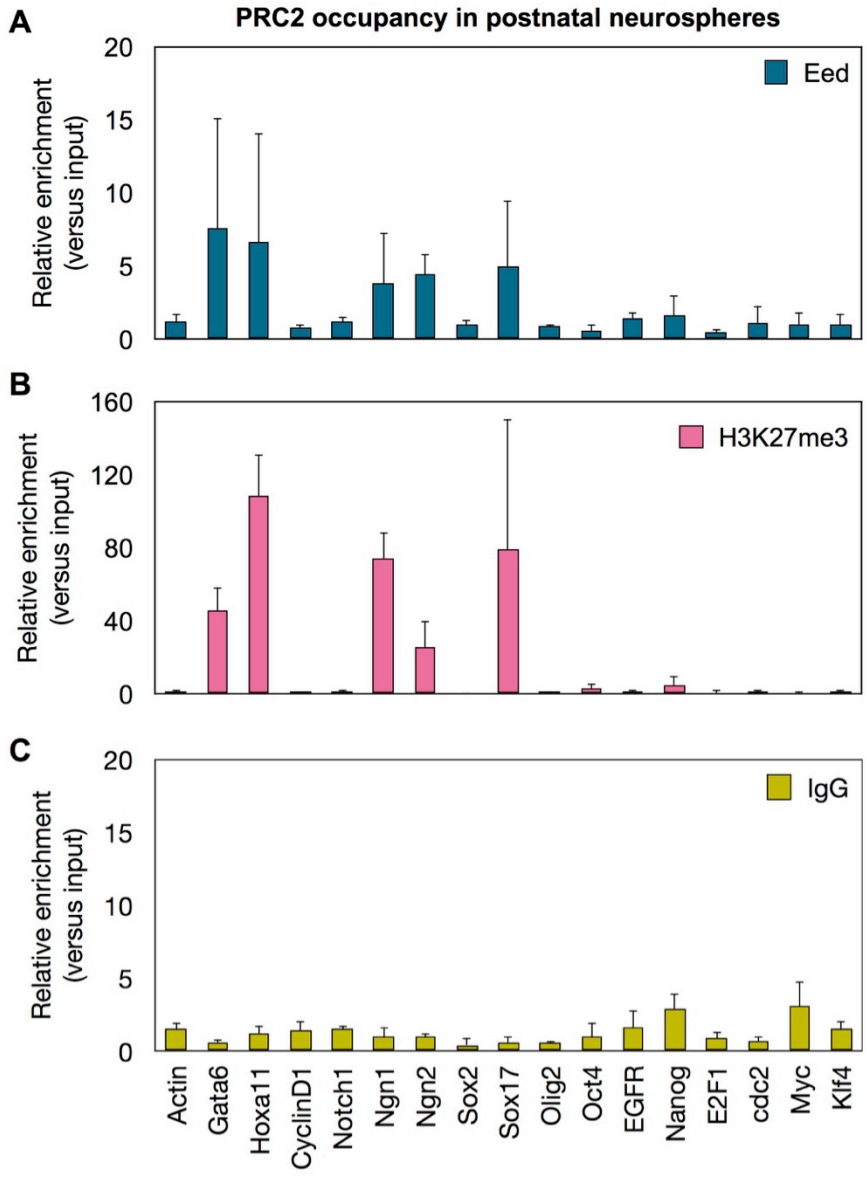

Figure 5. 2 The occupancy of PRC2 in postnatal neurospheres

(A) ChIP-qPCR of Eed in P4 neurospheres (n=3).

(B) ChIP-qPCR of H3K27me3 in P4 neurospheres (n=3).

(C) ChIP-qPCR of IgG in neurospheres as the negative control (n=3).

Error bars represent SD.

5.2.2 Selective activation of gene expression after loss of Eed in SVZ NSC

I then investigated gene expression following Eed knockout. Cyclin-dependent kinase inhibitor Cdkn2a is one of the best-characterized targets of PRC2 during development (Shen et al. 2008; Xie et al. 2013; Hwang et al. 2014). Quantitative PCR analysis of SVZ tissue from P14 mouse brains showed over 11-fold activation of Cdkn2a in Eed cKO (Figure 5.3A). Two transcripts can be expressed from the locus of *Cdkn2a*, p16Ink4a and p19Arf. Loss of Eed led to a 20-fold increase of p16Ink4a and a 5-fold increase of p19Arf, indicating no preferential activation of either transcript (Figure 5.3A). Then I compared the expression of other PRC2 targets. Unexpectedly, only Gata6 among four examined PRC2 targets (Gata6, Olig2, Hoxa11 and Sox17) was dramatically activated in the Eed cKO SVZ (Figure 5.3B). As Eed was shown to control NSC activation and identity maintenance, I checked the expression of genes relevant to cell cycle inhibition. No upregulation could be detected in BMP signalling related genes (Bmp4/6/7/Id1/Id2) or other cyclin-dependent kinase inhibitors (p21/p27/p57) (Figure 5.3C).

To rule out the potential confounding effects of SVZ cell heterogeneity, I cultured neurospheres from P4 mouse SVZ with the $Eed^{fl/fl}$ transgene. Cells dissociated from neurospheres were nucleofected with constructs expressing either GFP or GFP-Cre. 7 days post nucleofection, cells were collected and subjected to qPCR analysis. At this time point, the partial knockout was confirmed with 35% decreased expression of Eed (Figure 5.3D). Consistent with my in vivo data, induction of Eed knockout in vitro was only able to activate a few, but not all, PRC2 targets, i.e. Cdkn2a, Gata6 and Ngn1 (Figure 5.3D). These data together describe an interesting phenomenon that Eed actively represses selective PRC2 targets.

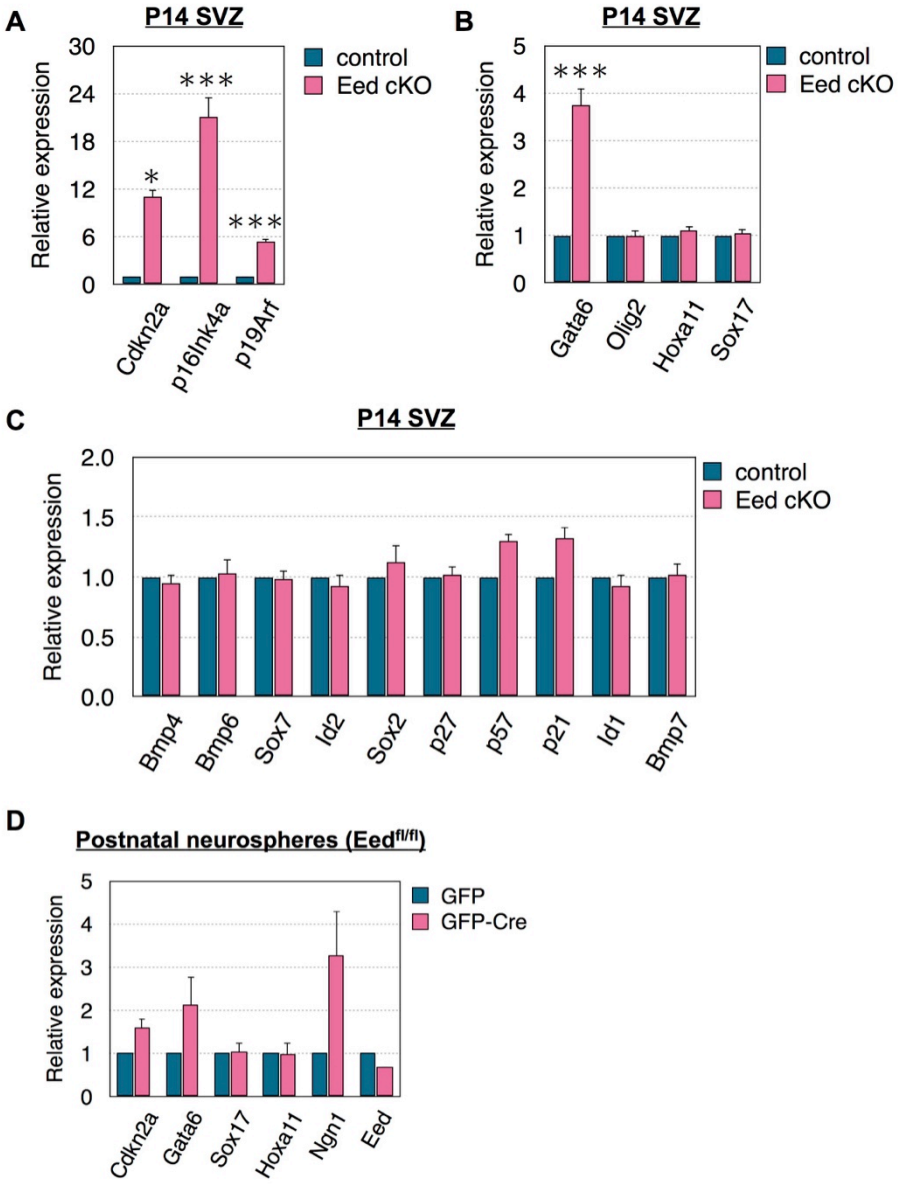

Figure 5. 3 Loss of Eed selectively activates PRC2 targets

(A-C) qPCR of gene expression in Eed cKO SVZ tissues (n=3).

(D) qPCR of $Eed^{fl/fl}$ neurospheres 7 days post nucleofection with either GFP or GFP-Cre (n=3).

Error bars represent SEM. *p<0.05, ***p<0.001.

5.2.3 Gene expression changes after loss of Ezh2 in SVZ

Microarray comparisons from Xie et al illustrated different downstream gene regulations of Ezh2 and Eed in hematopoietic stem cells (Xie et al. 2013). Similarly, loss of Ezh2 in the SVZ altered the expression of Id2, Dlk1, Sox7, Ngn4, Foxc1, Klf2 and Bmp7 to various degrees (Figure 5.4A-B). In P28 SVZ, Foxc1, Id2 and Sox7 were significantly downregulated. Although not statistically significant, a trend in expression decrease could be observed in Bmp7 and Nrg4 as well (Figure 5.4A). In contrast, only Nrg4 reduced significantly in RMS at this time point (Figure 5.4B). These data suggest Ezh2 may target downstream genes in an environment- and context-specific way.

To examine the difference between Ezh2 and Eed in SVZ, I analysed the expression of Cdkn2a and Gata6, both of which were upregulated after loss of Eed (Figure 5.3). Intriguingly, only Cdkn2a but not Gata6 was activated after Ezh2 knockout in P14 SVZ (Figure 5.4C). This could be further confirmed in neurosphere cultures. 9 days post nucleofection of GFP or GFP-Cre in $Ezh2^{fl/fl}$ cells, Cdkn2a was still the only gene activated; while no effect could be found on either Gata6 or Olig2 (Figure 5.4D).

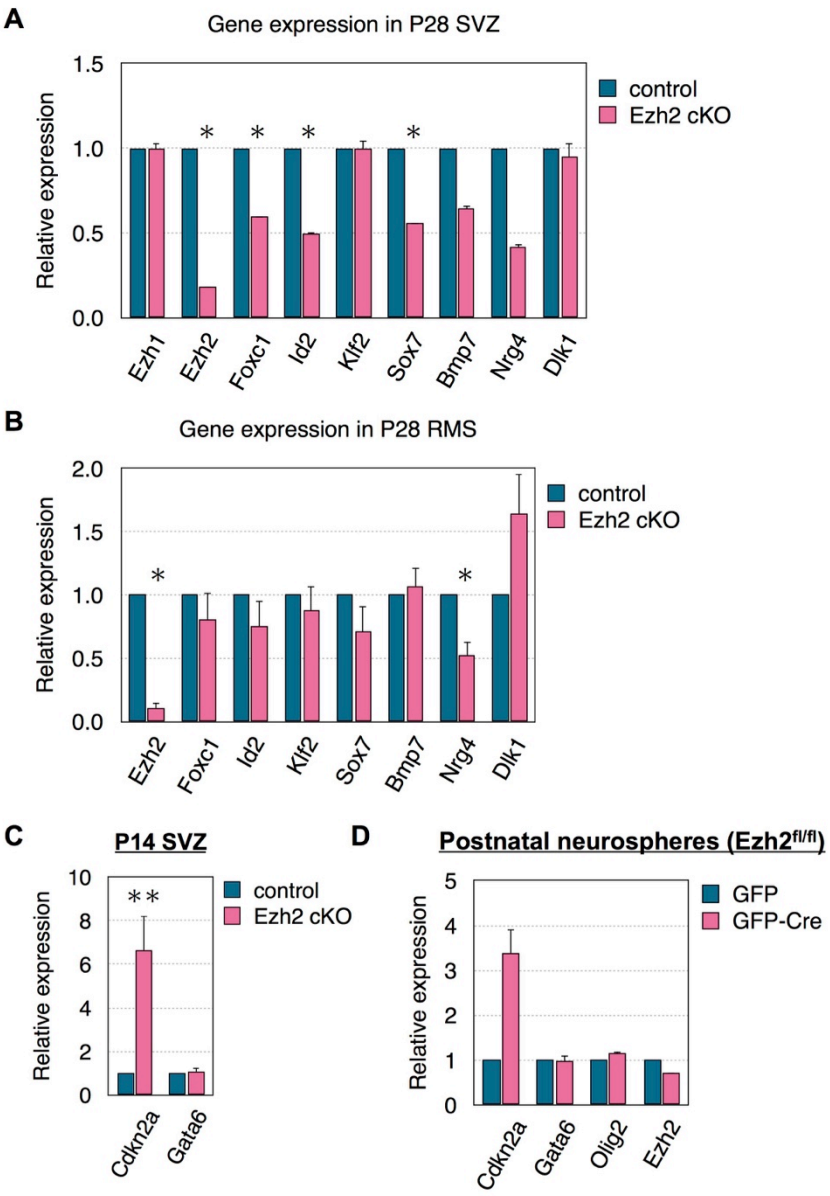

Figure 5. 4 Loss of Ezh2 activates Cdkn2a

(A-B) qPCR of gene expression in Ezh2 cKO SVZ (n=3) and RMS tissues (n=4).

(C) qPCR of Ezh2 cKO SVZ at P14 (n=3).

(D) qPCR of $Ezh2^{fl/fl}$ neurospheres 9 days post nucleofection with either GFP or GFP-Cre (n=2).

Error bars represent SEM. *p<0.05, **p<0.01.

5.2.4 Gata6 inhibits neurogenesis in vitro

Because Gata6 could be activated only after loss of Eed, I then tried to address whether the activation of Gata6 alone would partially phenocopy Eed cKO SVZ.

Neurospheres from wildtype P4 SVZ were nucleofected with GFP and Gata6 overexpression constructs or GFP alone as control. 24 hours post nucleofection, cells were dissociated and plated onto slides coated with poly-D-lysine and laminin, and were then allowed to adhere as a monolayer for another 24 hours. Significantly fewer NSC were proliferative after Gata6 overexpression (control: 15.06±0.91% versus OE: 9.65±1.70%) (n=3, p=0.035) with no obvious increase in cell death (control: 2.94±0.33% versus OE: 3.09±0.71%) (n=3) (Figure 5.5A-B, H). At the same time, GFP labelled cells in the Gata6 overexpression group seemed to display a flat morphology rather than the typical bipolar one for NSC. I had hypothesized that this may be due to fate shift from NSC towards astrocytes. To test this idea, I stained the cells with NSC marker Nestin and astrocyte marker GFAP. Virtually all cells, including the ones with flat morphology, expressed Nestin (Figure 5.5E). 47.86±2.24% of GFP+ cells in Gata6 overexpression were GFAP+, which was comparable to control (42.63±2.84%) (n=3, Figure 5.5 F-G). This means fate shift may not be the primary reason for the morphology change.

I next tested differentiation after Gata6 overexpression in NSC. 48 hours post nucleofection, cells were dissociated and cultured without EGF and FGF for 7 days. As the CAG-GFP construct I used does not integrate into the genome and would therefore be diluted out after multiple cell division, very few and dim GFP signals could be detected at this time point. Hence, I analysed the neuronal marker Tuj1 among total cells identified by DAPI. Preliminary data showed a dramatic decrease in neuronal differentiation from 12.50±1.75% in control to 5.09±1.56% in Gata6

overexpression cells (n=2, Figure 5.5C-D). Taken together, these showed that Gata6 is a negative regulator of in vitro neurogenesis.

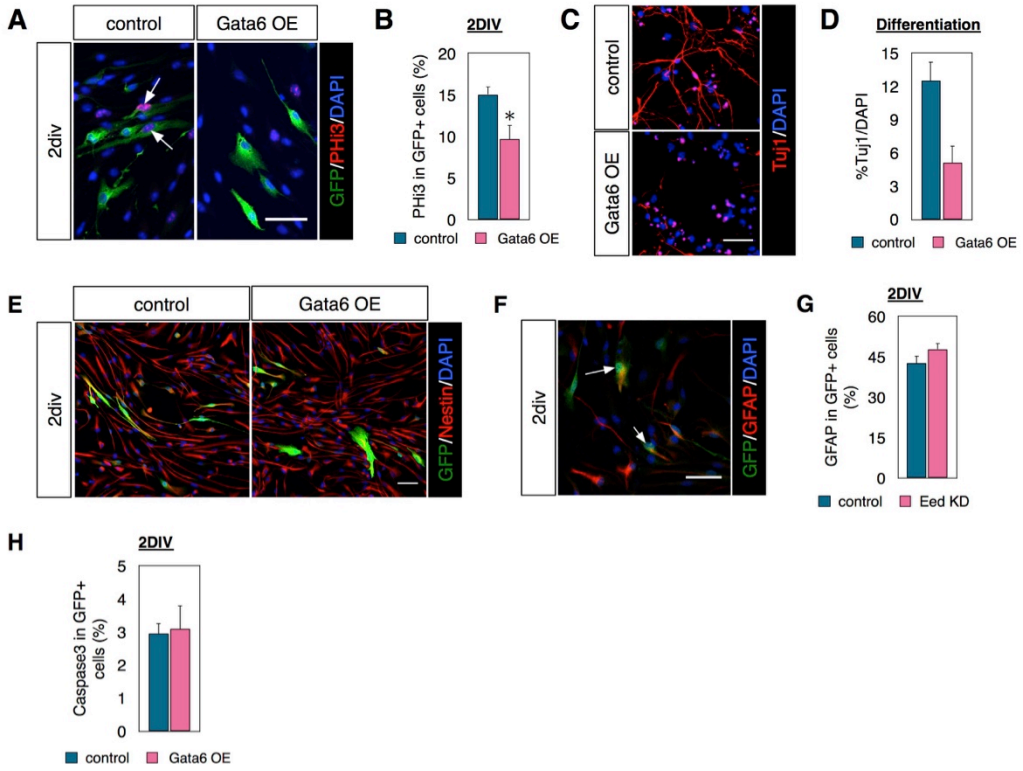

Figure 5. 5 Gata6 inhibits neurogenesis in vitro

(A-B) Neurospheres are nucleofected with Gata6 cDNA and cultured as monolayer cells for 2 days in vitro (n=3). PHi3 staining reveals reduced cell proliferation after Gata6 overexpression. Arrows in (A) indicate PHi3+/GFP+ cells.

(C-D) Nucleofected cells are cultured for differentiation for 7 days in vitro and Tuj1 staining demonstrates Gata6 overexpression leads to deficiency in neuronal differentiation (n=3).

(E-G) Nestin or GFAP staining and quantifications in Gata6 overexpression 2 days in vitro (n=3). Arrows in (F) indicate GFAP+/GFP+ cells.

(H) Quantification of Caspase3 in Gata6 overexpression 2 days in vitro (n=3).

Error bars represent SEM. *p<0.05. Scale bar: (A, C, E, F)=50um.

5.2.5 Gata6 inhibits postnatal SVZ neurogenesis in vivo

To confirm the function of Gata6 misexpression in the neurogenic niche, I electroporated constructs expressing either Gata6 with GFP or GFP alone as control into the SVZ of P1 mouse. Brains were collected 3 days post electroporation (dpe) for analysis. In general, the GFP signals were comparable between control and Gata6 groups and the morphology of radial glia with ectopic expression was also similar to control. However, staining with the transit amplifying cell marker, Mash1 showed a significant decrease in this cell population among total GFP cells (control: 13.26±1.02% versus Gata6 OE: 8.02±0.83%) (n=3, Figure 5.6A.C). This is consistent with the neuronal differentiation deficiency observed in vitro. On the other hand, Gata6 overexpression also reduced the percentage of GFP+ cells that expressed Ki67 from 27.32±1.76% in control to 19.69±1.95% in OE (n=3, Figure 5.6B.C). This confirmed the function of Gata6 in neurogenesis is not limited to in vitro cultures.

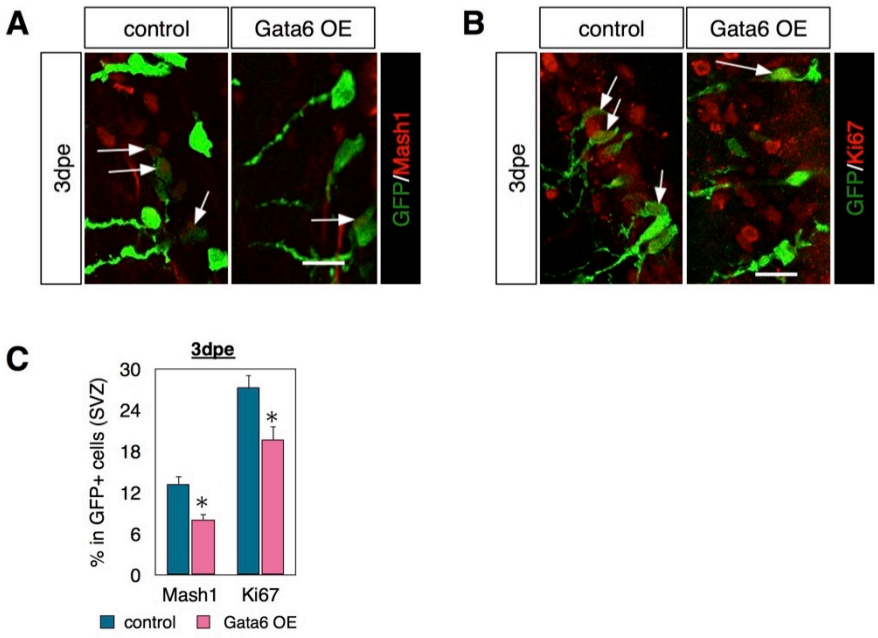

Figure 5. 6 Gata6 inhibits neurogenesis in vivo

(A-B) Immunostaining of Mash1 and Ki67 together with GFP in the SVZ, 3 days post electroporation (n=3). Arrows in (A) indicate Mash1+/GFP+ cells and in (B) indicate Ki67+/GFP+ cells.

(C) Quantifications show Gata6 overexpression reduces Mash1 and Ki67 in GFP cells, 3 days post electroporation (n=3).

Error bars represent SEM. *p<0.05. Scale bar: (A-B)=20um.

5.2.6 Gata6 inhibits p21 post-transcriptionally

Considering the dual roles of Gata6 in cell proliferation and neuronal differentiation, I asked whether this is achieved by regulating p21 as a downstream gene. p21 can control SVZ neurogenesis in both cyclin-dependent and independent manners. At 2 days post nucleofection, although there was a substantial increase in Gata6 expression, no obvious difference could be found on p21 mRNA (Figure 5.7A). This meant Gata6 did not directly regulate p21 expression in SVZ NSC. But when performing western blot on both samples, I found unlike mRNA, the protein of p21 reduced after Gata6 overexpression (Figure 5.7B). These data suggested posttranscriptional regulation of p21 by Gata6. It was previously reported that Gata6 is able to induce microRNAs, which can act as posttranscriptional regulators of multiple genes (Tian et al. 2011). To test this possibility, I examined the expression of microRNA from two clusters: miR-290 and miR-302/367, which are complementary to 3'UTR in p21 mRNA. Unfortunately, no difference could be detected in the expression of these microRNAs after Gata6 overexpression (Figure 5.7C).

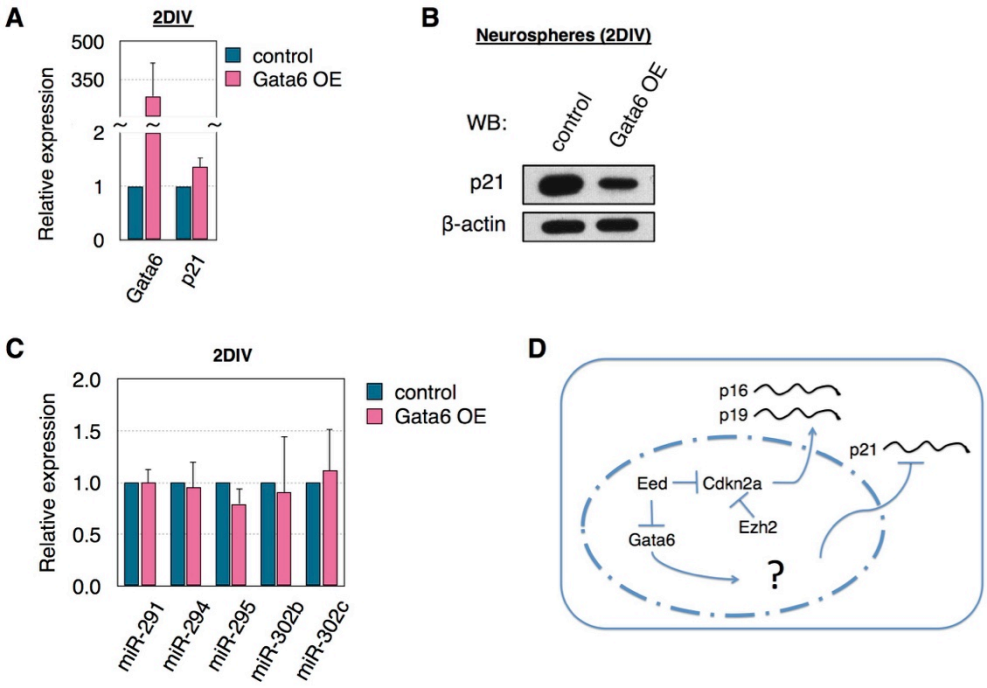

Figure 5. 7 Gata6 regulates p21 posttranscriptionally

(A-B) Expression analysis for p21 mRNA and protein Gata6 overexpression 2 days in vitro. Although p21 mRNA is not dramatically affected, p21 protein decreases after Gata6 overexpression.
(C) Expression of microRNA after Gata6 overexpression in vitro.
(D) Summary of molecular mechanisms underlying PRC2 regulation of SVZ neurogenesis.
Error bars represent SEM.

5.2.7 Gene expression analysis after brain injury

To understand the injury induced-influence on SVZ development, acute gene expression profiles in response to controlled cortical lesions were analysed. 2 days post injury, ipsilateral tissues were collected and analysed via microarray. In total 211 genes were upregulated and 11 genes were down regulated in the cortex (Supplemental Table 1-2). Among the upregulated genes, inflammatory response related genes (like Ifi202b, CD44, Tlr2, Msr2, Ly86, etc) constituted the largest

proportion (35%) (Figure 5.8A). Both microglia and astrocytes will be activated after brain injury. So it is not surprising that a large number of cell cycle regulators (e.g. Ccnb2 and Ccna2) and cytoskeleton related genes (e.g. Nestin, Vimentin, GFAP) were also upregulated (Figure 5.8A,C). Lgals1 and Lgals3 are extracellular matrix proteins that regulate several cell behaviours, including migration and proliferation. Injury induced upregulation of both genes could also be found in the cortex (Figure 5.8C). In contrast, cell death and survival were the most enriched category among downregulated gene group (Figure 5.8B,D).

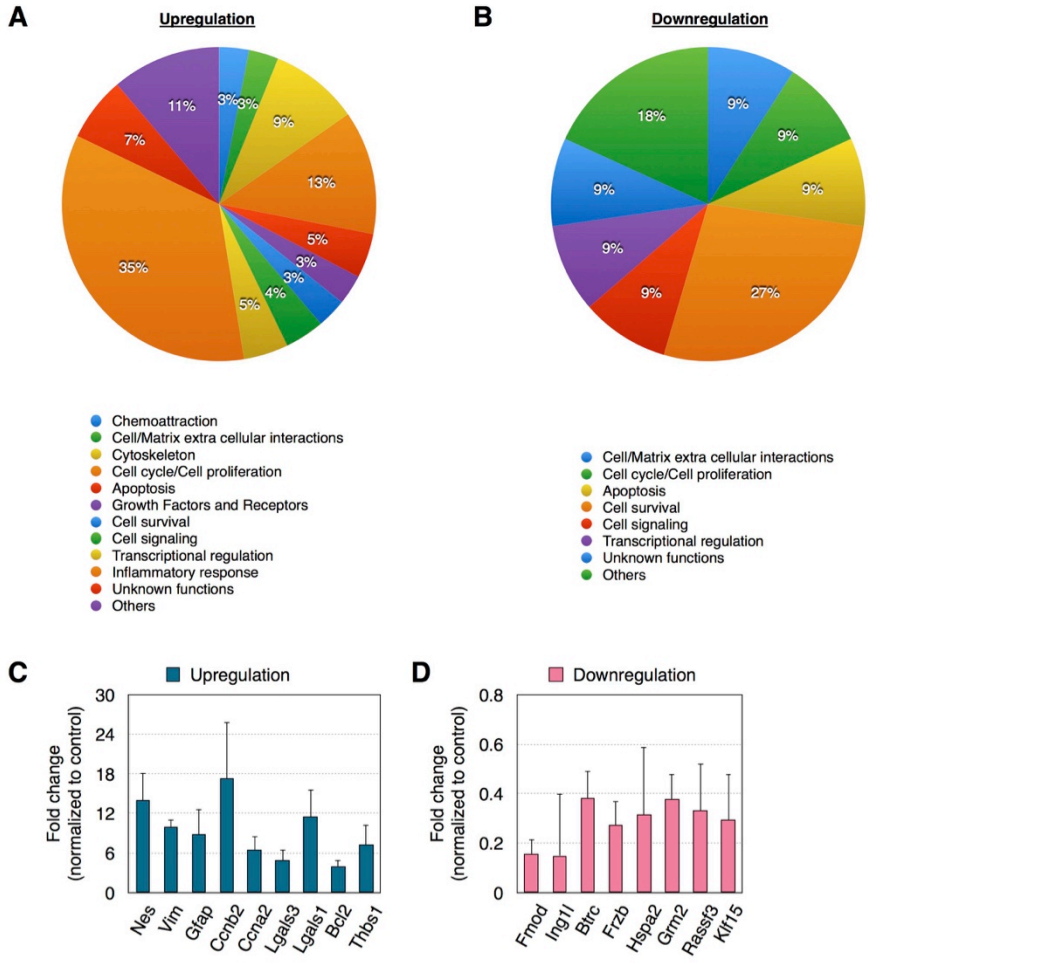

Figure 5. 8 Microarray analysis of cerebral cortex tissue after traumatic injury

(A-B) Gene ontology analysis of differently expressed genes.

(C-D) Examples of upregulated and downregulated genes.

Error bars represent SEM.

5.3 Discussion

In this chapter, I tried to explain the molecular mechanisms underlying SVZ phenotypes after Ezh2 or Eed knockout. I found Ezh2 and Eed can orchestrate the levels of different cyclin-dependent kinase inhibitors.

5.3.1 Selective activation of target genes after loss of PRC2

In this chapter, I determined the binding of H3K27me3 and PRC2 components in the SVZ and studied the expression of target genes after Ezh2 or Eed knockout. Interestingly, I found only a selective number of PRC2 targets were activated, which has not been discussed in the majority of the literature on PRC2 function in organ development.

It is known PRC2 catalyses the di-/tri-methylation of H3K27 and prevents acetylation at the same site, which antagonizes the gene repression function of PRC2 (Margueron and Reinberg 2011). But the PRC2 or H3K27me3 mediated gene silencing mechanisms still remains elusive. Till now there is no direct evidence describing how H3K27me3 can modify chromatin structure, except the fact that PRC2/Ezh1 is able to compact chromatin in an H3K27me3 independent manner (Margueron et al. 2008; Margueron and Reinberg 2011). Instead, the recruiting role of H3K27me3 has been documented extensively (Margueron and Reinberg 2011). The simple and classic pathway is H3K27me3 will recruit PRC1, which can then mono-ubiquitinate H2AK119 (Schuettengruber et al. 2007). H2AK119 is shown to interfere with RNA polymerase II and thereby inhibit the elongation of transcription (Zhou et al. 2008). If this model is applied to all PRC1/PRC2 mediated gene repression, one can expect loss of PRC2 will result in the activation of all target genes considering the

fundamental role for PRC2 in recruiting PRC1. However, both my data as well as studies from other groups indicate that this is not true in most situations (Leeb et al. 2010; Riising et al. 2014). Basically, there are several flaws in this classic pathway:

(1) None of the canonical PRC2 core subunits have sequence specific DNA binding domains (Schuettengruber et al. 2007). Hence PRC2 alone is insufficient to be the first step of PRC serial recruitment. Binding with proteins like Pleiohomeotic (Pho) partially solves this question (Mohd-Sarip et al. 2005; Schuettengruber et al. 2007). Interaction with lncRNAs also directs the *cis*-binding of PRC2 (Rinn et al. 2007; Zhao et al. 2008). Intriguingly, the discovery of PRC1 variants reversed the classic model. Unlike PRC2, multiple PRC1 variants have been reported, among which the KDM2B containing noncanonical PRC1 is believed to bind to DNA directly without H3K27me3 (Gil and O'Loghlen 2014; Schwartz and Pirrotta 2014). KDM2B is a histone demethylase with specific recognition of non-methylated CpG islands (Farcas et al. 2012). Based on this, the new proposed recruiting model would be: KDM2B containing noncanonical PRC1 first binds to non-methylated CpG islands and catalysing H2AK119ub1, which provides the binding sites for PRC2 with the aid of Jarid2 and Aebp2. The canonical PRC1 will then be recruited to H3K27me3 deposited by PRC2 (Farcas et al. 2012; Blackledge et al. 2014; Kalb et al. 2014; Schwartz and Pirrotta 2014).

(2) The necessity of H3K27me3 in gene silencing is being questioned. It is well accepted that H3K27me3 is associated with silent genomic regions, but it seems this association is not indispensable for the expression repression (Ringrose and Paro 2004; Margueron and Reinberg 2011; Tavares et al. 2012; Schwartz and Pirrotta 2014). Neither Eed nor Ring1b knockout alone in ES

cells is adequate to activate PRC target genes and would leave the other protein binding to the same gene unaffected. This offers one scenario that PRC1 and PRC2 may function in a redundant way (Leeb et al. 2010). Further work demonstrated that less than 0.08% target genes could be derepressed after PRC2 knockout, much fewer compared to PRC1 knockout, in ES cells (Riising et al. 2014). If this mechanism is applied to SVZ NSC, the selective gene activation in Eed cKO SVZ can be explained. So a necessary experiment for confirmation will be the comparison between Eed/Ring1a/Ring1b triple knockout and Ring1a/Ring1b double knockout animals. Additionally, compared to the noncanonical PRC1, canonical PRC1 has very low H2AK119 ubiquitination ability (Schwartz and Pirrotta 2014). Hence from an evolutionary perspective, why would PRC2 and canonical PRC1 be recruited in the newly proposed model described above? One possibility is the involvement of H3K27me3 in epigenetic inheritance and memory (Ringrose and Paro 2004; Martin and Zhang 2007; Margueron and Reinberg 2010). In the genome, H3K27me3 has broader binding regions than H2AK119ub1 and may be partially maintained during DNA replication. This correlates with the high expression of Ezh2 in fast proliferating cells and also provides new insights into the function of PRC2 in these cells.

(3) One often-neglected fact is the diversity of PRC1/PRC2 like complexes in plants. Three homologs of Ezh2, two Ring1-like and three Bmi1-like proteins have been identified in Arabidopsis (Hennig and Derkacheva 2009; Merini and Calonje 2015). However no plant homolog of H2Aub has been found, raising the question about the repression and recruiting model of polycomb (Zhang et al. 2007a; Merini and Calonje 2015). Importantly, Bmi1-like

protein AtBMI1 in Arabidopsis seems to regulate the H3K27me3 mark; and at different gene loci, PRC1 and PRC2 follow distinct working mechanisms (Yang et al. 2013; Merini and Calonje 2015). Therefore, it would be informative to test whether in SVZ various PRC pathways regulate gene expression, which causes a selective activation after the loss of Eed.

5.3.2 PRC2 has diverse roles in transcription regulation

The analysis of Ezh2 knockout SVZ/RMS tissues showed upregulation (Cdkn2a) as well as downregulation (Foxc1, Id2, Sox7, Nrg4) of different transcripts. This is interesting considering the repressive functions of PRC2 in a general sense (Margueron and Reinberg 2011). This may be due to PRC2 inhibiting the repressors of certain genes. For instance, in ES cells, Eed and Sox2 can positively regulate each other via Eed repression of COUP-TFII, which would suppress Sox2 by binding to SRR1 regulatory region of Sox2 (Ura et al. 2011). Similar mechanisms may exist in Ezh2 regulation in SVZ/RMS.

Moreover, further works indicate preferential occupancies of distinct H3K27 methylation forms in genomes. H3K27 can be mono-, di- and tri- methylated but it has been questionable whether Ezh1/Ezh2 is responsible for H3K27me1 (Montgomery et al. 2005; Margueron et al. 2008; Shen et al. 2008; Margueron and Reinberg 2011; Ferrari et al. 2014). Recently, Ferrari et al has proposed a new model: PRC2 binds transiently to H3K27me0 and H3K27me1 to catalyse methylation but the deposition of H3K27me3 instead requires stable binding (Ferrari et al. 2014). It is essential to know that H3K27me1, H3K27me2 and H3K27me3 can be found in different genomic regions and importantly, H3K27me1 overlaps with H3K36me3 at transcriptionaly active genes and the expression of these genes decreases after loss of

H3K27me1 (Steiner et al. 2011; Ferrari et al. 2014). Thus it would be interesting to know whether this mechanism applies to the SVZ/RMS as well. To answer this question, a comparison among H3K27me1, H3K27me2 and H3K27me3 in the SVZ/RMS by ChIP-qPCR on gene loci of Foxc1, Id2, Sox7, Nrg4 would be necessary.

Both in vivo and in vitro knockout experiments confirmed that upregulation of Gata6 expression could only be observed after loss of Eed, but not after loss of Ezh2 in SVZ NSC. Similar regulation was previously reported in ES cells and the presence of PRC2/Ezh1 could be considered as the complementary factor for Ezh2 (Shen et al. 2008). Besides this relatively well-accepted explanation, the recent discovery of Eed in PRC1 provides an alternative insight (Cao et al. 2014). In this study, Cao et al found both N- and C-terminals of Eed are essential for PRC2 interaction while the N-terminal is also involved in PRC1 binding. In the recruiting process, PRC1 and PRC2 will compete to interact with Eed, regulating their enzymatic activities. So the loss of Eed could not only affect the functions of PRC2, but also those of PRC1 in gene expression regulation (Cao et al. 2014). In addition to H2A modification, PRC1 is able to control chromatin compaction independent of its histone ubiquitination ability and PRC2/H3K27me3 (Eskeland et al. 2010a; Eskeland et al. 2010b; Endoh et al. 2012; Steffen and Ringrose 2014). At the moment, we do not know whether different PRC1 variants perform these diverse functions or whether Eed preferentially interacts with specific PRC1 variants. Nevertheless, it is likely Eed may regulate transcription in PRC2-independent manners.

5.3.3 Gata6 in regulating SVZ neurogenesis

Gata6 belongs to a transcription factor family regulating different developmental processes. In SVZ NSC, I found Eed knockout can induce Gata6 expression and it seems Gata6 alone can inhibit neurogenesis through reducing stem cell proliferation and neural differentiation. Besides this, little is reported in the literature till now about the role of Gata6 in neural development.

Six different Gata transcription factors exist in mammals. Generally, Gata1/2/3 are responsible for hematopoietic lineage development and Gata4/5/6 for heart and gut development, while tissue-specific roles of each individual Gata transcription factor are also described (Burch 2005). Among them, Gata3 is particularly interesting in regard to neurogenesis. In adult zebrafish, brain injury can induce the expression of Gata3 and this is necessary for the NSC activation during regeneration (Kizil et al. 2012). No evidence has shown upregulation of Gata3 in the rodent SVZ after brain injury (Yoshiya et al. 2003). However, in neuroblastoma, Gata3 is reported to activate Cyclin D1 and promote proliferation. Silencing of Gata3 will instead induce differentiation (Molenaar et al. 2010; Peng et al. 2015). The work in neuroblastoma stem cell lines however described an opposite relationship between Gata3 and Cyclin D1 (Shi and Ding 2009). This may be attributed to the heterogeneity of tumour cells and the diversity of cancer cell lines. The role for Gata6 in brain tumours is less well defined. DNA methylation analysis in glioblastoma identified hypermethylation of CpG islands in the *Gata6* promoter (Martinez et al. 2009; Skiriute et al. 2012). This is consistent with the fact that stable DNA methylation will replace the more dynamic PRC2 modification in target genes in cancer, but it is still not clear whether the repression of Gata6 by DNA methylation is necessary for glioblastoma tumorigenesis.

The study of Gata6 in the cardiovascular system suggests its overexpression can inhibit cell proliferation due to a deficiency in S-phase entry (Perlman et al. 1998; Morrisey 2000). Intriguingly, G1 cell cycle arrest was also observed in astrocyte cultures after the induction of Gata6 and Gata6 may actually function as a tumour suppressor in the brain, which fits the DNA methylation profiles (Kamnasaran et al. 2007). My data and these publications together indicate a general role for Gata6 in cell proliferation.

However, one essential difference between astrocytes/vascular smooth muscle cells and SVZ NSC is that the latter can both proliferate and differentiate. Hence the decreased cell proliferation in SVZ NSC after misexpression of Gata6 could be caused by loss of stemness instead of a direct cell cycle effect. My staining of Nestin unfortunately was unable to detect any change in stemness, while I cannot rule out the possibility that the residual Nestin protein has not degraded at 2 days post transfection, because of the potential long half-life.

Another interesting observation in Gata6 overexpressed NSC is that more flat rather than bipolar cells were found, while the expression of the glial marker GFAP was comparable. Both cell type transition and cell morphology change can contribute to this phenotype. In cardiomyocytes, it is revealed that Gata4 and Gata6 promote cell hypertrophy (Liang et al. 2001). One can hypothesize the flat NSC may be hypertrophic after induction of Gata6. In medulloblastoma, voltage-gated potassium channel EAG2 links changes in cell volume to cell proliferation (Huang et al. 2012). Knockdown of EAG2 increased the cell volume, which then led to G2 phase arrest (Huang et al. 2012). Further work is still needed to investigate whether Gata6 controls cell proliferation in NSC in the same way.

5.3.4 Posttranscriptional regulation of p21 by Gata6

In my in vitro experiments of Gata6 overexpression, I found the protein level of p21 decreased without induction in mRNA, indicating a posttranscriptional regulation of p21 by Gata6. Two relatively well-established posttranscriptional regulation mechanisms were then examined to understand how Gata6 controls p21 mRNA translation.

MicroRNA (miRNA) is a kind of small noncoding RNA consisting of around 22 nucleotides. By base-pair matching, miRNA can form RNA-induced silencing complexes with target mRNAs and processing-related proteins, such as Dicer (Wilson and Doudna 2013). Multiple miRNAs have been described to regulate p21 protein levels in ES cells. Members of the miR-290 and miR-302/367 families have been shown to control p21 by recognition of its specific mRNA 3'UTR (Wang et al. 2008b). Of note, although overexpression of both miRNA clusters is able to reduce p21 protein, the influence on mRNA is more diverse (Wang et al. 2008b). This is possibly due to different miRNA mechanisms of action: translational repression or deadenylation-dependent decay of mRNA (Wilson and Doudna 2013). On the other hand, during lung development, miR-302/367 cluster is a direct target of Gata6 and its temporal expression is controlled by Gata6 precisely in lung endoderm progenitors (Tian et al. 2011). I found, however that overexpression of Gata6 was unable to induce the expression of either miR-290 or miR-302/367 families in SVZ NSC. Although I did not examine all miRNAs in either cluster, it is less possible that untested miRNAs will be upregulated considering clustered members share the same in *cis* regulatory regions. Besides these two clusters, sequence comparisons provide more candidates for p21 upstream miRNAs, including miR-375, miR-17, miR-106, miR-93, miR-20, miR-134, etc (Data from www.microrna.org). So in the future, I

plan to examine the expression of these miRNAs and test whether Gata6-induced miRNA mechanisms regulate p21 posttranscriptionally.

RNA binding proteins (RBP) also play an essential role in posttranscriptional regulation of mRNA. Unlike miRNA, the action of RBP covers more aspects of RNA function: maturation, splicing, stability, translation and so on (Gerstberger et al. 2014). In cell stress and inflammatory conditions, p21 is often posttranscriptionally upregulated. To uncover the mechanism, several RBPs have been identified to regulate p21 in different manners. The half-life and stability of p21 mRNA can be either enhanced by ZONA, PCBP4, and Rbm24, or reduced by FXR1P through RBP binding to 3'UTR in p21 mRNA (Scoumanne et al. 2011; Nie et al. 2012; Davidovic et al. 2013; Jiang et al. 2014). Additionally, the p53 isoform p53/47 is capable of repressing p21 translation while CEBPA improves the stability of p21 protein (Timchenko et al. 1996; Mlynarczyk and Fahraeus 2014). One of p21 mRNA binding proteins, Musashi-1 (Msi1) is particularly interesting in regard to neural development (Sakakibara and Okano 1997; Kaneko et al. 2000; Okano et al. 2005). It has been shown that Msi1 recognizes p21 mRNA 3'UTR and inhibits the translation step and can regulate neurogenesis by modulating p21 protein level (Battelli et al. 2006). The relationship between Msi1 and p21 still remains to be studied in SVZ neurogenesis, as both proteins seem to be expressed in NSC (Sakakibara and Okano 1997; Porlan et al. 2013). And at the moment, there is no direct evidence suggesting Gata6 can directly control the expression of any RBP mentioned above in various tissues or cells including NSC. So it would be worthwhile to test whether in my experiment, Gata6 induces the expression of RBP to regulate p21 posttranscriptionally in SVZ NSC. To systematically understanding RBP regulation of p21 in NSC, it is necessary to

perform mRNA interactome capture to identify individual RBP bindings with p21 mRNA (Castello et al. 2013).

5.3.5 Gene expression analysis after brain injury

The microarray based gene expression analysis revealed the acute response in injured cortex. As expected, many inflammation and cell-cycle related genes were upregulated, which correlated with the activation of microglia and astrocytes. To study the potential influence of injury on SVZ neuro/gliogenesis and migration, more attention was paid to chemoattraction and growth factor relevant genes.

Ccl12 and Cxcl10 Both Ccl12 and Cxcl10 were upregulated over 26 fold in cortical lesion. These chemokines primarily contribute to recruiting immune cells, like microglia and macrophages. The work in neuroblast migration also indicates the chemoattratic functions of chemokines in injured brains. Emigration of neuroblasts from SVZ can be activated by chemokines in stroke, like CXC4, SDF-1α, CCR2, etc (Young et al. 2011). For therapeutic purposes, it would be informative to characterize the chemoattraction abilities of Ccl12 and Cxcl10 on SVZ neuroblasts.

Thbs1 Thrombospondin 1 (Thbs1) is a member of glycoproteins that forms the extracellular matrix. In brains, Thbs1 can be secreted by immature astrocytes and regulates synaptogenesis (Christopherson et al. 2005; Risher and Eroglu 2012). In MCAO, reactive astrocytes will also upregulate both Thbs1 and Thbs2 (Zamanian et al. 2012). So it is very possible reactive astrocytes are the source for increased Thbs1 in cortical lesions but it has yet to be determined how it functions to control extracellular conditions. Interestingly, Thbs4 is expressed in SVZ astrocytes but not cortical astrocytes and it promotes astrogenesis in SVZ after cortical injury. Neuroblasts in the SVZ will be triggered to migrate towards injury after loss of Thbs4

(Benner et al. 2013). It would be interesting to study: whether Thbs1 secreted by reactive astrocytes in cortical lesions controls neuroblast migration from the SVZ.

Tgfbi Transforming growth factor, beta-induced (Tgfbi) can be induced by TGF-β1 in astrocytes and will be upregulated in reactive astrocytes in MCAO, which matches the microarray data in cortical lesion shown here (Yun et al. 2002; Zamanian et al. 2012). On the other hand, Tgfbi will increase in the SVZ in response to cortical impact injury as well (Logan et al. 2013). Although its expression has been studied in different injury models, the function of Tgfbi and TGF in the SVZ is still unclear. It is only documented that exposure to TGF-α in cultured SVZ slices would decrease neuroblast migration (Kim et al. 2009).

5.4 Conclusion

In summary, I identified a regulatory mechanism in SVZ NSC: on the one hand, Eed and Ezh2 repressed Cdkn2a directly through H3K27me3 and inhibit the expression of p16 and p19. On the other hand, Eed but not Ezh2 maintained the expression level of p21 indirectly in NSC through a Gata6-dependent posttranscriptional mechanism. (Figure 5.7D). Activation of Gata6 reduced p21 protein and inhibited SVZ neurogenesis, i.e. cell proliferation and neuronal differentiation.

Chapter 6

Long non-coding RNA regulates postnatal SVZ neurogenesis

6.1 Introduction

Once considered as transcriptional junk, the importance of long noncoding RNA (lncRNA) has started to be realized recently. The high specificity of lncRNA expression in the brain raises the question of what role it plays in brain development and function (Derrien et al. 2012). With new sequencing technologies and gain-/loss-of-function methods, we have begun to elucidate the role of lncRNA in the brain. This not only offers insight into the basic working mechanisms of lncRNA, but also expands our understanding of the complexity of the brain.

6.1.1 LncRNA expression in the brain

The expression of genome-wide lncRNA in brain has been analysed at different scales. The Allen Brain Atlas is a gene expression database for brain, based on in *situ* hybridization and analysis suggests 849 lncRNAs, such as *Gomafu*, *Rian* and *Sox2ot* are enriched in multiple brain regions (Lein et al. 2007; Mercer et al. 2008). However, this study limits the transcripts to the available probe pool in Allen Brain Atlas and therefore underestimates the total number of lncRNA expressed in the adult brains. Furthermore, the gross categorization of brain regions reduces the spatial resolution. These two issues have been circumvented by the introduction of next-generation sequencing (NGS), microdissection of tissues and cell sorting from specific brain regions. In one study, the transcriptome, including both protein-coding and non-coding transcripts, was profiled from different cortical layers (Belgard et al. 2011). Over 1000 lncRNA loci were identified in the mouse cortex with 77 transcripts distinctly expressed between layers. LncRNA 9130024F11Rik for instance is

preferentially expressed in deep layers while A330023F24Rik is in more superficial cortical layers (Belgard et al. 2011).

The adult SVZ is highly heterogeneous, consisting of a vast array of different cell types. FACS sorting-depended cell type analysis described lncRNA expression during SVZ neural lineage progression (Ramos et al. 2013). Besides spatial and temporal features, the lncRNA signatures can also be found between neuronal versus glial and healthy versus disease cells. Take lncRNA Six3os for example. Knockdown of Six3os promoted astrocytic differentiation at the expense of neuronal and oligodendrocytic differentiations (Ramos et al. 2013). This genome-wide lncRNA study in the SVZ provides a database for further investigation, while false positive signals should be taken into consideration for the lack of expression confirmation by in *situ* hybridization.

6.1.2 LncRNA regulation in the neural development

The first lncRNA functionally characterized in the brain, *Evf-2*, locates antisense to *Dlx6* in the Dlx5/6 cluster (Feng et al. 2006; Bond et al. 2009). In embryonic brains, *Evf-2* is expressed in immature neurons, similar to Dlx5/6, and can be induced by sonic hedgehog protein (Feng et al. 2006). Early work indicated that *Evf-2* could form complex with Dlx2 to activate the Dlx5/6 enhancer (Feng et al. 2006). However, the subsequent work from the same group proposed an opposite regulation mechanism through enhancer methylation (Bond et al. 2009; Bassett et al. 2014). This may be due to the interpretations of different technique-based experiments and the *Evf-2*-rescue work confirmed the effect to be RNA-based but not DNA-based (Berghoff et al. 2013; Bassett et al. 2014).

Aside from in *cis*- or *trans*-regulation of gene expression, the cellular expression of lncRNA is also essential to normal neural development. RNCR2, a lncRNA enriched in retinal progenitor cells, controls cell fate specification (Rapicavoli et al. 2010). This study is based on RNAi and overexpression of domain-negative lncRNA. However, RNAi is unable to regulate the transcription of lncRNA directly, so it is still unknown whether the nuclear specific location of RNCR2 is relevant to any transcriptional regulation mechanism.

A neuronal specific lncRNA, *Pnky* was discovered in the SVZ with the characterization of lncRNA expression in adult SVZ lineage cells (Ramos et al. 2013; Ramos et al. 2015). *Pnky* has been shown to maintain NSC in the SVZ and, in its absence, the NSC pool is depleted and neuronal differentiation enhanced (Ramos et al. 2015). Further work demonstrated *Pnky*, in combination with the RNA splicing regulator PTBP1, controls the expression of transcription factors (Ramos et al. 2015). Nevertheless, similar to RNCR2, the loss of function study for *Pnky* was also based on RNAi, so the combination of knockout and rescue experiment by lncRNA can provide more information on the regulatory mechanism by *Pnky* in SVZ neurogenesis. In comparison to the expression pattern of lncRNA in brain, our understanding of the biological functions of these lncRNAs is still in its infancy. Moreover the knockout animals of many lncRNA, including the cortex enriched *Visc-2*, do not have any obvious phenotype, making traditional investigations more challenging (Bassett et al. 2014; Oliver et al. 2014).

6.3.3 LncRNA Paupar

Paupar is a lncRNA locating entirely within the *Pax6os1* locus, upstream of *Pax6* in the genome (Figure 6.1A). It is conserved during evolution and highly expressed in

the adult brain, but only expressed in ES cells after the treatment with retinoic acid (Figure 6.1B-C) (Vance et al. 2014). This neural specific expression pattern is similar to the transcription factor Pax6, which is essential for neuronal differentiation, especially in the adult SVZ (Hack et al. 2004; Ninkovic et al. 2013). The relationship between *Paupar* and Pax6 has been further deciphered: on the one hand *Paupar* is a negative regulator of Pax6 expression and on the other hand they have common and different downstream gene targets (Vance et al. 2014). Hence *Paupar* is likely to cooperate with Pax6 to regulate a set of neural development related transcription factors in *trans* and also functions in a manner independent of Pax6.

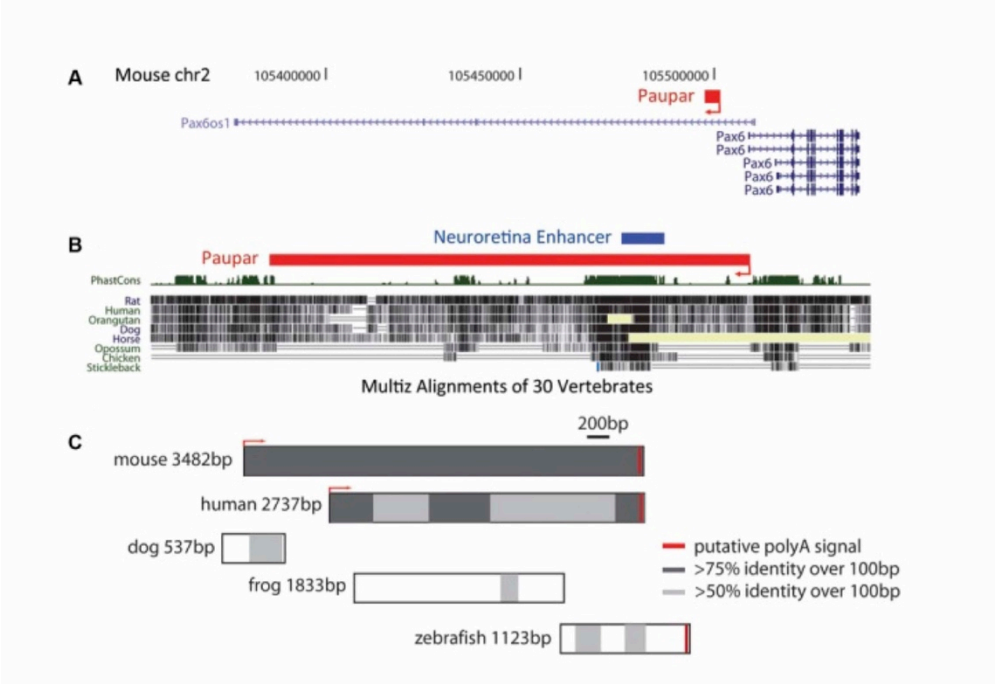

Figure 6. 1 The location and conservation of *Paupar*

(A) *Paupar* locates in the *Pax6os1*, upstream of *Pax6* locus.

(B) The conservation of *Paupar* locus among different species.

(C) The conservation and size of *Paupar* in different species.

(Figure modified from Vance et al. 2014)

Nothing is known about *Paupar* in the SVZ. The expression of *Pax6os1*, however, has been profiled in adult SVZ lineage cells (Ramos et al. 2013). During lineage progression, *Pax6os1* expression gradually increases from SVZ NSC to neuroblasts and SVZ NSC express more *Pax6os*1 transcript than niche astrocytes. Consistent with this notion, in vitro differentiation of SVZ NSC also increase the level of *Pax6os1* (Ramos et al. 2013). Interestingly, in the neuroblastoma cell line N2A, only *Paupar* and Pax6 but not *Pax6os1* are expressed (Vance et al. 2014). Early studies, by lineage tracing and domain-negative methods, found that Pax6 is principally expressed in the dorsolateral SVZ of adult brain and is important in determining dopaminergic neuronal fate (Hack et al. 2005; Weinandy et al. 2011). In addition, recent inducible knockout work indicates Pax6 is able to promote general neuronal over glial fate in the SVZ, in cooperation with a chromatin remodelling factor BAF complex (Ninkovic et al. 2013). This difference might result from distinct loss-of-function techniques applied in the two studies but also reinforces the complicated role of Pax6 in SVZ neurogenesis. For the close relationship between Pax6 and *Paupar*, it would be interesting to test whether *Paupar* has similar functions as Pax6 in the SVZ.

In this chapter, I am going to address the following questions: (1) Which lncRNA are expressed in the adult SVZ based on in *situ* hybridization (ISH)? (2) For the SVZ highly expressed lncRNAs, are there any neighbouring genes relevant for neural development? (3) What is the expression and function of *Paupar* in postnatal SVZ neurogenesis?

6.2 Results

6.2.1 LncRNA expression in the adult SVZ

To understand lncRNA expression in the adult SVZ, I examined the transcripts filtered in the study by Mercer et al 2008. Among 849 lncRNA identified, 181 were either enriched in the olfactory bulb or in the striatum (Mercer et al. 2008). I then compared the gene type information from NCBI and UCSC Genome to rule out protein coding genes such as LOC432449, 2900016G23Rik (Atxn1), 8030498B09Rik and 4930449I04Rik, which were considered as ncRNA in the original study. In total, I found 47 out of 181 lncRNA were highly expressed in the adult SVZ (Figure 6.2, Table 6.1). These included the previously studied lncRNA like *Evf2*, *Gomafu (RNCR2), Sox2ot*, *Kcnq1ot1* (Feng et al. 2006; Sone et al. 2007; Pandey et al. 2008; Amaral et al. 2009; Bond et al. 2009). It is not surprising that the expression of *Evf-2* and *Sox2ot* were highly restricted to adult SVZ considering their close relationship with the NSC transcription factors Dlx5/6 and Sox2, respectively. The remaining lncRNAs, however, were far less known in the brain. Take *Kcnq1ot1* for example. The ISH signal for *Kcnq1ot1* transcript could be detected exclusively in the RMS/SVZ, but not in the OB or cerebral cortex (highlighted in Figure 6.2). In contrast, 9430029A11Rik (*Plxna4os2*) and C130071C03Rik were enriched in both RMS/SVZ and the OB with weaker and sparse signals in the cerebral cortex (highlighted in Figure 6.2). A few other lncRNAs had strong expression across the brain with more dense signals in the SVZ/RMS, such as MGC118427, A130050O07Rik and 5730422E09Rik (Figure 6.2). LncRNAs like B230369F24Rik, 1810026B05Rik and D630010B17Rik, on the other hand, had low overall expression, including in the SVZ/RMS (Figure 6.2).


Evf-2 (P7)
Evf-2 (P56)
Evf-2 (P56)
Gomafu
Gomafu
Sox2ot
Sox2ot
C130071C03Rik
9330175E14Rik
AK021368
2010001K21Rik
9430029A11Rik
C230057M02Rik
D730045B01Rik
1700020I14Rik
D130060J02Rik
E130008D07Rik
Kcnq1ot1
4833414E09Rik
MGC118427
A130050O07Rik
5730422E09Rik
5830411J07Rik
B230369F24Rik
1810026B05Rik
D630010B17Rik
2310014F06Rik

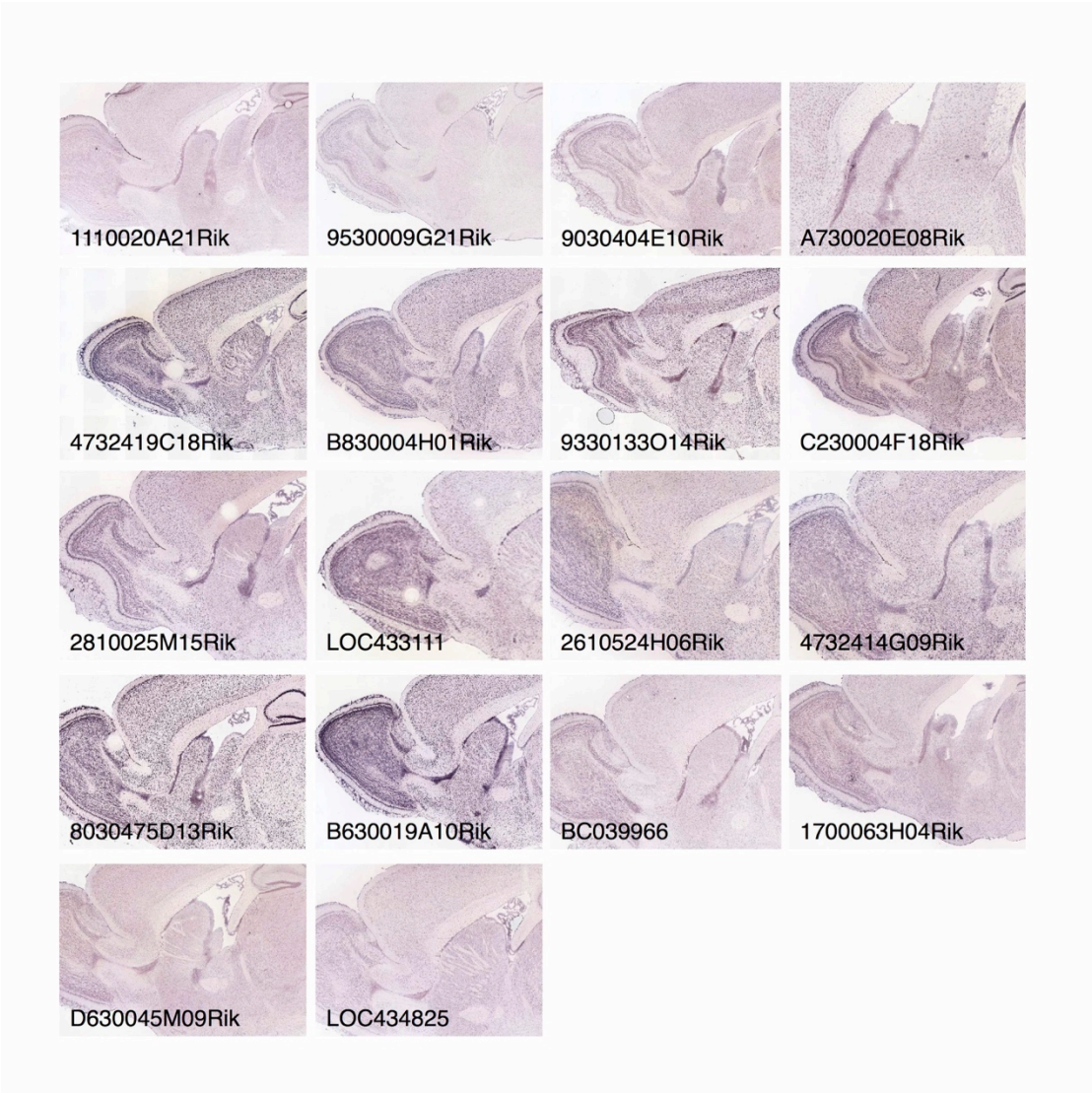

Figure 6. 2 The expression of lncRNA in the adult SVZ

In *situ* hybridization of lncRNAs in P56 brain (Data from Allen Brain Atlas). 47 lncRNA can be found in adult SVZ/RMS/OB, including *Evf-2*, *Gomafu* and *Sox2ot*. Some lncRNAs, like 4732419C18Rik, are expressed more generally in the adult brains; while lncRNAs such as Evf-2 are specifically expressed in the neurogenic region. LncRNAs highlighted with red box are discussed in the main text.

6.2.2 LncRNA locus analysis

A proposed mechanism for lncRNA regulation is in *cis* binding to the neighbouring genes (Vance and Ponting 2014). I therefore characterized the neighbouring genes for the 47 lncRNAs enriched in the SVZ based on USCS Genome mm10. Some lncRNAs were overlapping with or on the opposite strand to known protein coding genes, such as *Sox2ot*, *Kcnq1ot1* and 9430029A11Rik (*Plxna4os2*) (Figure 6.3A-C). *Sox2ot*, for example, was on the sense strand of Sox2 and the entire sequence of the latter located in an intron of *Sox2ot* (Figure 6.3A). Similarly, *Kcnq1ot1* overlapped the protein-coding gene *Kcnq1ot1* on the same strand (Figure 6.3B). In contrast, *Plxna4os2* and a closely related gene *Plxna4os1* were antisense to *Plxna4a* and these lncRNAs were located in two different introns of *Plxna4a* (Figure 6.3C). LncRNA can also serve as precursors or hosts for microRNA (Bassett et al. 2014). Consistent with this notion, miR-1897 and miR-9-2 were in the exons of *Sox2ot* and C130071C03Rik, respectively (Figure 6.3A). I also analysed a group of bidirectional, convergent and divergent, lncRNAs, 1700104B16Rik, 4930563E18Rik and 5730422E09Rik which were all within 1000bp of protein-coding genes (relative to Gtf2e2, Abhd3 and Usp11 individually) (Figure 6.3 D-F).

Among these neighbouring genes, most do not have sufficient functional characterization in neural development. Besides Dlx5/6, Sox2 and miR-9-2, 4732414G09Rik for instance is a bidirectional lncRNA adjacent to CamKK1, and is suppressed during RA induced neuronal differentiation (Feliciano and Edelman 2009).

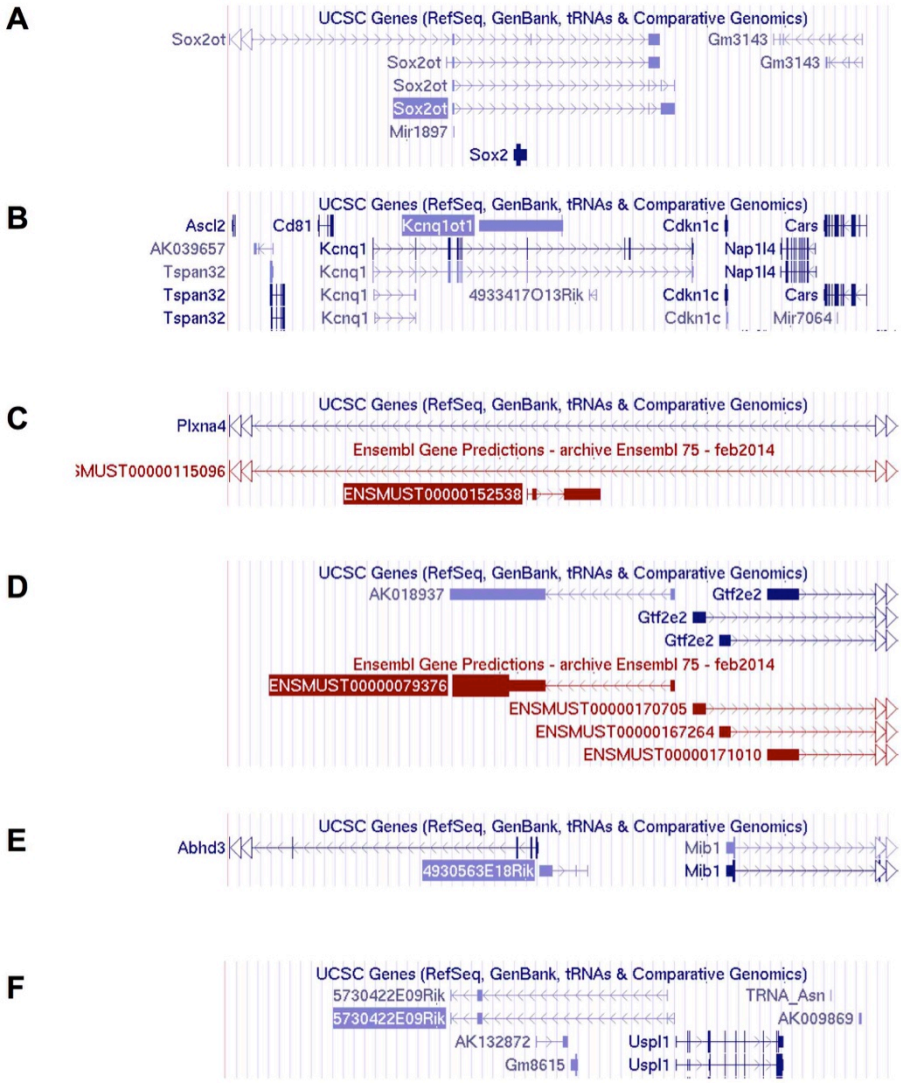

Figure 6. 3 Locus analysis of lncRNA expressed in the adult SVZ

(A-F) Snapshot of lncRNA example loci in the genome (UCSC mm10). (A and B) Both *Sox2*ot and *Kcnq1ot1* overlap with *Sox2* and *Kcnq1* loci, respectively. (C) *Plxna4os2* (*9430029A11Rik* or *ENSMUST00000152538*) locates at the opposite strand of *Plxna4* locus. (D-F) *1700104B16Rik* (*ENSMUST00000079376*) and *Gtf2e2*, *4930563E18Rik* and *Abhd3*, *5730422E09Rik* and *Uspl1* are bidirectional to each other.

Table 6. 1 The neighbouring genes of SVZ enriched lncRNAs

lncRNA	*Neighbouring Gene*
Evf-2	Dlx5, Dlx6
Gomafu	Cryba4
Sox2ot	Sox2, miR1897, Gm3143
C130071C03Rik	Mef2c, miR9-2
9330175E14Rik	Herpud1, Nlrc5
1700028D13Rik	
1700104B16Rik	Gtf2e2
2010001K21Rik	Nhlrc1, Tpmt
9430029A11Rik	Plxna4 (Plexin A4)
1700031A10Rik	Trim31, Rnf39
4930563E18Rik	Abhd3, Mib1
C230057M02Rik	Acsf3
D730045B01Rik	
1700020I14Rik	Oip5, Nusap1, Ndufaf1, Rtf1, Chp1, Exd1
D130060J02Rik	
E130008D07Rik	Tnfrsf21, Gpr110
Kcnq1ot1	Kcnq1, Cdkn1c, Slc22a18, TSSC4, Cd81
4833414E09Rik	
AK034351	
AK038535 (A230028O05Rik)	
MGC118427	St6gal1
A130050O07Rik	miR181a-1
5730422E09Rik	Gnpda1, Usp11
5830411J07Rik	Fam36a, Hnrnpu
B230369F24Rik	Cox20, Hnrnpu
1810026B05Rik	Chd2
D630010B17Rik	Adamts20, Pus71
2310014F06Rik	Tead1, Parva
1110020A21Rik	Ppm1b, Slc3a1, Prep1
9530009G21Rik	Raet1b, Phxr2
9030404E10Rik	Hes1
A730020E08Rik	Ccser1
4732419C18Rik	Rab4a, Rhou
B830004H01Rik	
9330133O14Rik	Snai3, Cyba, Rnf166
C230004F18Rik	Cdr1, Sox3
2810025M15Rik	Rasa12, Sec16b
LOC433111	
2610524H06Rik	

3010003L10Rik	Dmrta2, Faf1
4732414G09Rik	Camkk1, P2rx1, Atp2a3
8030475D13Rik	Ube2d3, Cisd2, Nhedc1, Manba
B630019A10Rik	St6gal1, Adipoq, Eif4a2, Rfc4
BC039966	Dffb, Ajap1
1700063H04Rik	Rimklb, Phc1, M6pr
D630045M09Rik	Ndufs6, Mrpl36, Lpcat1, Slc6a3
LOC434825	Cited1

6.2.3 The expression of lncRNA Paupar in the postnatal SVZ

In the Allen Brain Atlas, there is no probe available for lncRNA *Paupar* in either postnatal or adult brain at the moment. So qPCR was applied to SVZ tissues dissected from the P4 mouse brain to examine the expression level of *Paupar* and another lncRNA *Dali* (Chalei et al. 2014). To rule out the potential contamination of genomic DNA, minus-reverse transcriptase control (Minus RT) was included. In the P4 brain, the Ct values for both lncRNAs were very small (*Paupar*: 25.66, *Dali*: 26.77) relative to the internal control GAPDH (Ct: 16.86); while in Minus RT control, no signal could be detect before cycle 35 (GAPDH: 38.89, *Paupar*: 40.00, *Dali*: 37.73) (Figure 6.4A). This suggested that *Paupar* and *Dali* were highly expressed in the postnatal SVZ, approximately 50-fold higher than that in N2A cells (Vance et al. 2014). Similarly, qPCR for P4 neurospheres also confirmed the expression of *Paupar* and *Dali* in vitro (Figure 6.4B). In general the expression level for *Paupar* was lower in neurospheres compared to SVZ tissue.

To further characterize *Paupar* in brain, the published CHART-Sequencing data was mapped to UCSC Genome to examine *Paupar* binding on *Ezh2* (Vance et al. 2014). The binding site (BS) for *Paupar* located around 55-60kb upstream of the *Ezh2* locus (Figure 6.4C). Importantly, when combing with the histone modification

database, sharp peaks for H3K4me3/H3K27a and weak signal for H3K27me3 could be found at the *Paupar* binding site in cerebellum, cortex and whole brain tissue, suggesting an active chromatin state (Figure 6.4C).

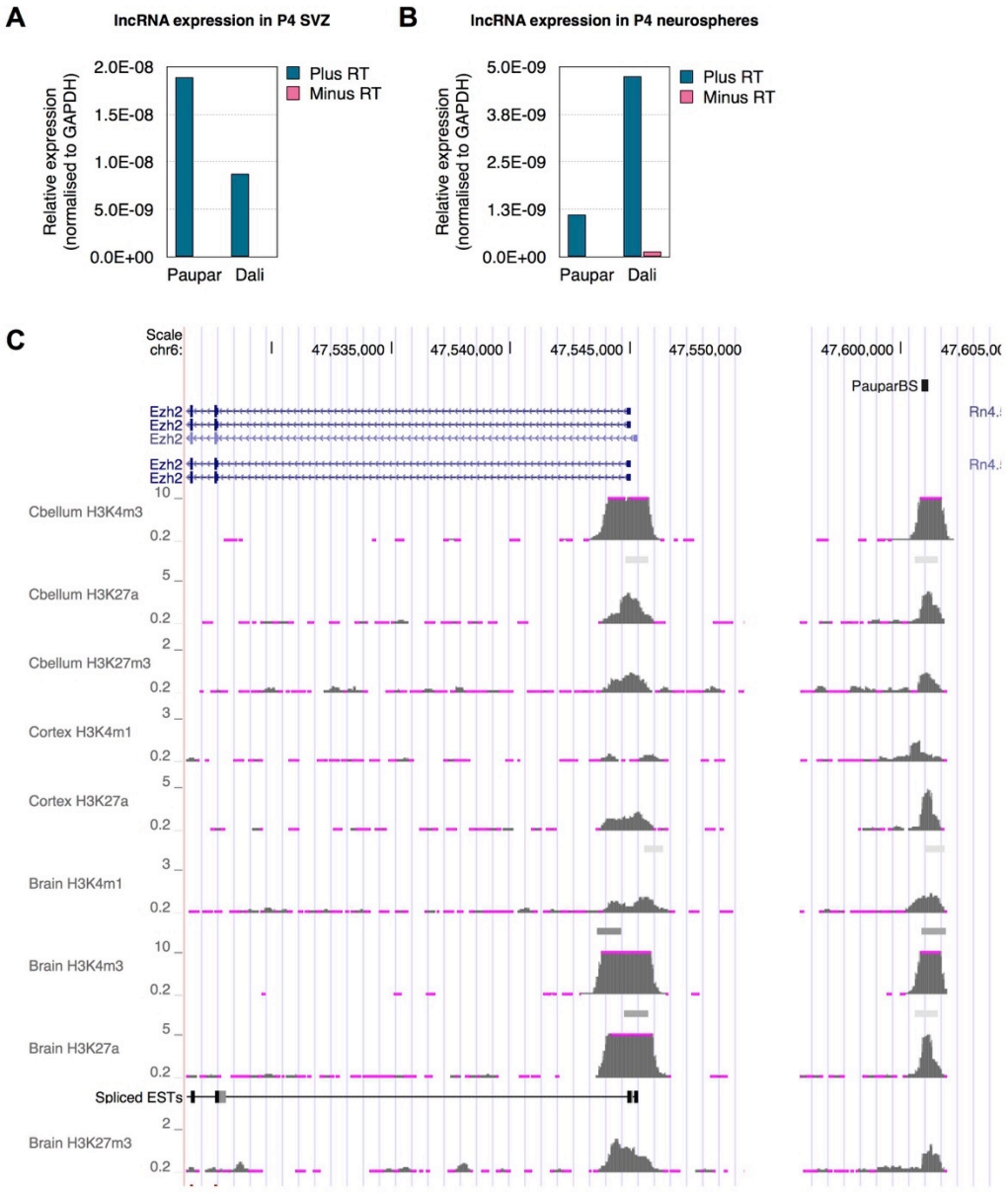

Figure 6. 4 *Paupar* is expressed in SVZ and NSC

(A-B) qPCR analysis of *Paupar* expression in P4 SVZ tissues and P4 neurospheres. The expression is normalised to the internal control GAPDH. Minus reverse transcriptase control is included to determine the contamination of genomic DNA. (C) CHART-Sequence shows that *Paupar* binds to the upstream of *Ezh2* locus and the histone modification analysis at this site (Vance et al. 2014).

6.2.4 The functions of lncRNA Paupar in the postnatal SVZ

To study the functions of *Paupar* in SVZ neurogenesis, two shRNA constructs (sh165 and sh408) were used. The knockdown efficiency of shRNA was first tested in neurospheres in vitro. Cells were nucleofected with scramble, sh165 or sh408 and collected 3 days post nucleofection for qPCR analysis. sh165 gave a much better knockdown efficiency (over 70%) than sh407 (24%) (Figure 6.5A). And with sh165, the expression of Pax6 also decreased about 50%, similar to what was published before; while Ezh2 mRNA level increased approximately 50% (Figure 6.5A) (Vance et al. 2014). To further characterize sh165, cells were also collected 5 days post nucleofection. The knockdown efficiency reduced at 5 days, but it still reached 50% (Figure 6.5B). Correspondingly, Pax6 expression relatively increased while Ezh2 decreased compared to 3 days post knockdown (Figure 6.5B).

Next I determined whether lncRNA *Paupar* is required for postnatal SVZ neurogenesis. I electroporated an individual construct (scramble, sh165 and sh408) into P1 SVZ and pups were allowed to survive for 7 days to enable newborn neuroblasts to reach the OB. At 7dpe, the number of GFP+ cells decreased more than 70% in the OB with sh165 while no significant change could be detected in the sh408 group (scramble: 127754.37±6874.47/mm^3, sh165: 29896.00±4736.20/mm^3, sh408: 110565.68±5895.77/mm^3) (n=3 for scramble, n=5 for sh165 and n=5 for sh408, $p<0.0001$ for scramble versus sh165) (Figure 6.5C-D). The difference in effect between the two knockdown constructs was consistent with in vitro knockdown efficiency test (Figure 6.5A). To understand the mechanism for this reduced neurogenesis, brains were collected at an earlier time point, i.e. 3dpe for analysis in the SVZ. Obviously fewer GFP+ cells were found in the SVZ of the pups electroporated with sh165 (Figure 6.5E). And the majority of labelled cells in sh165

group had weaker GFP signals (Figure 6.5E). Quantification showed 60% reduction in the number of GFP+ SVZ cells that expressed GFAP (scramble: 30.68±1.42% versus sh165: 10.99±1.48%) (n=4 for scramble and n=5 for sh165, p=0.0001, Figure 6.5F-G). Taken together, these preliminary data suggest lncRNA *Paupar* may be necessary for postnatal SVZ neurogenesis.

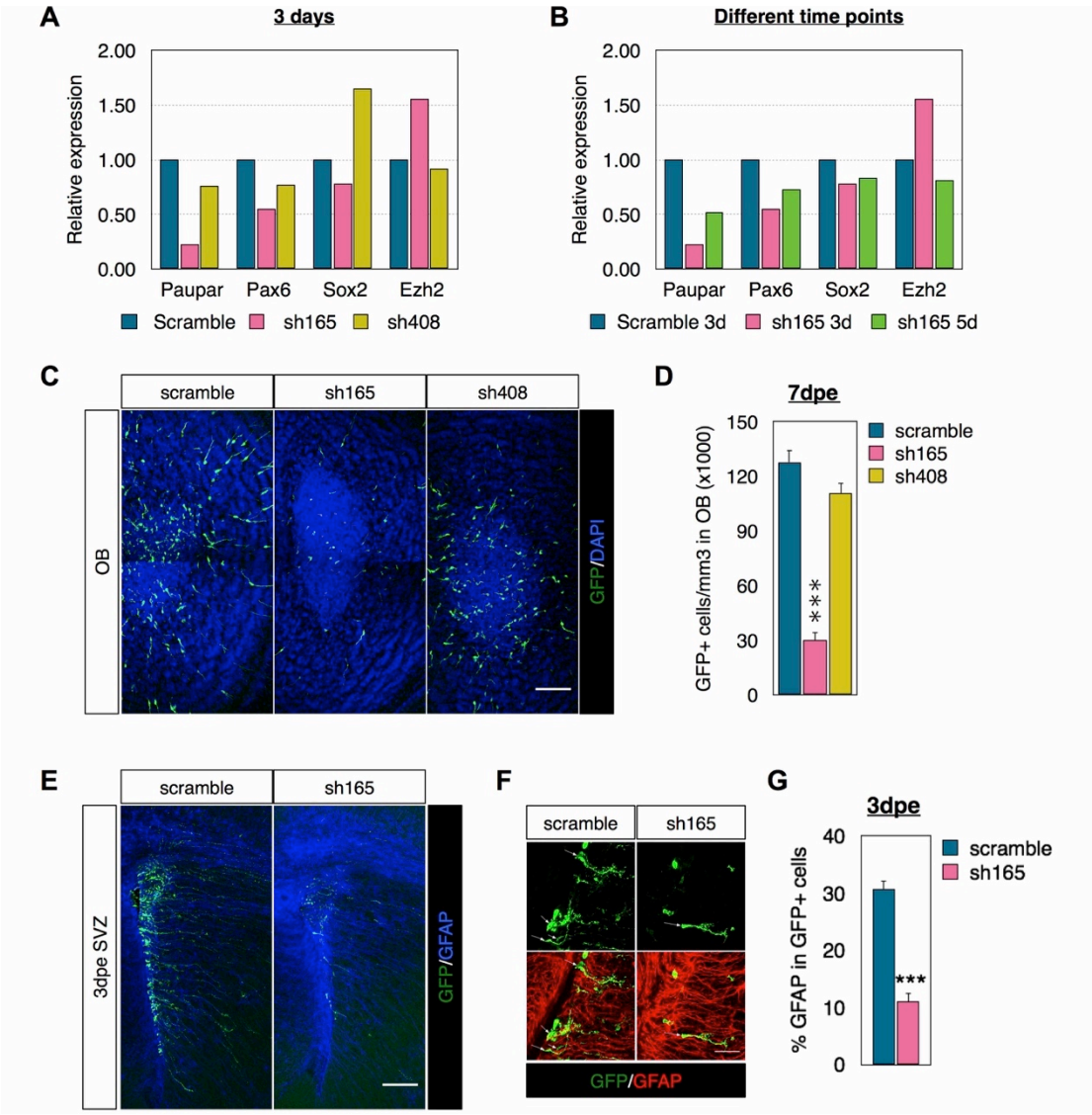

Figure 6. 5 *Paupar* is required for postnatal SVZ neurogenesis

(A-B) qPCR analysis of neurospheres after *Paupar* knockdown by shRNA, sh165 or sh408. Data is normalized to the scramble control (n=1). sh165 reduces *Paupar* transcript more than 70% at 3 days post nucleofection in neurospheres, which leads to decrease Pax6 but increase Ezh2 expression. In contrast, sh408 gives a lower

knockdown efficiency. In the time course analysis, nucleofection of sh165 after 3 days reveals better knockdown efficiency than that after 5 days.

(C-D) Immunostaining and quantification of GFP+ cells in OB 7dpe (n=3 for scramble, n=5 for sh165 and n=5 for sh408). Knockdown with sh165 led to fewer GFP+ newborn cells in the OB; while knockdown with sh408 did not cause a similar phenotype.

(E-G) Immunostaining and quantification of GFP+ and GFAP+ cells in the SVZ 3dpe (n=4 for scramble and n=5 for sh165). Fewer GFP+ cells can be observed in SVZ electroporated with sh165 and fewer of them are GFAP+.

Error bars represent SEM. ***$p<0.001$. Scale bar: (C)=100um, (E)=200um, (F)=50um.

6.3 Discussion

LncRNA is expressed extensively in different cells. However, unlike protein-coding genes, the role of lncRNA during development still remains mysterious. In this chapter, I examined the lncRNA highly expressed in the adult SVZ and the neighbouring genes associated with these loci. Particularly I focused on a lncRNA *Paupar*, upstream of Pax6. *Paupar* was expressed in both postnatal SVZ and neurospheres. Loss of *Paupar* reduced SVZ neurogenesis, possibly due to deficiency in NSC maintenance.

6.3.1 The expression of lncRNA in SVZ

In total, 47 lncRNAs, with confirmation by in *situ* hybridization, were identified in the adult SVZ. This number is a substantial reduction from the 8992 lncRNAs identified in the SVZ by RNA-sequencing (Ramos et al. 2013). Two main reasons could explain this huge difference: firstly, the study based on RNA-sequencing method uncovered a large number of novel transcripts, which constituted almost half of the total number. These transcripts are not included in the database I used, e.g. RefSeq and UCSC Genome. So some may have been excluded from my study. In addition, there is no probe available in Allen Brain Atlas for most of these 8992 lncRNAs at the moment, which also led to a considerable underestimation. Secondly, RNA-Seq can detect weakly expressed lncRNAs, which surpasses the sensitivity limit of in *situ* hybridization. One advantage of the in *situ* hybridization based work is to rule out the false positive signals obtained from RNA-Seq (Roberts et al. 2011). A comparison of these two studies suggests some common loci or lncRNAs, which can be considered as priority candidates for functional analysis in the future.

C130071C03Rik, for example, was identified in both studies. In *situ* hybridization showed the enrichment of this transcript in the SVZ/RMS/OB system. In SVZ NSC, H3K4me3 active domain could be found at this gene locus, in contrast to the bivalent domain in ES cells, and cell type analysis indicated SVZ NSC expressed significantly more C130071C03Rik than neuroblasts (Ramos et al. 2013). It is necessary to confirm this dynamic expression during lineage progression with the combination of in *situ* hybridization and immunofluorescence.

The high expression of an individual lncRNA is not always correlated with essential functions in specific tissues or cells. Unlike the transcripts with protein coding potential, lncRNA can simply be transcriptional noise (Ponting et al. 2009). Since the cells residing in SVZ/RMS are stem cells/progenitors, not the stable cells like neurons found in other brain regions, one can assume the total transcriptional activity would be much higher inside the neurogenic niche. More frequent incorrect transcriptions of RNA with no biological functions are, therefore, expected. This theory is supported by the estimation of RNA polymerase II fidelity and it proves more transcriptional noise than functional mRNA are produced (Struhl 2007). One example, *Visc-2*, is a lncRNA highly expressed in the ventricular and subventricular zone of embryonic telencephalon. Interestingly, *Visc-2* also overlaps with C130071C03Rik; however, no defect in morphology or neurogenesis has been observed after deletion of *Visc-2* (Oliver et al. 2014). It is still too early to conclude *Visc-2* is simply transcriptional noise and its conservation across species indicates *Visc-2* is under evolutionary selection (Ponting et al. 2009; Oliver et al. 2014). It is also possible that lowly expressed lncRNA have essential roles, for instance to fine-tune protein-coding gene expression. Above all, more work is still in need for us to give a general view about the importance of lncRNA.

6.3.2 The potential in cis functions of lncRNA in SVZ

One difficulty in functional prediction for lncRNA is the lack of gene ontology database, which is used widely for protein-coding genes. In *cis* and in *trans* are two basic regulation processes for gene transcription. In this chapter I described the neighbouring genes around lncRNA loci, which may be potential targets or binding partners of lncRNA.

C130071C03Rik miR-9-2 entirely locates in the last exon of C130071C03Rik. Thus, C130071C03Rik may be the precursor of miR-9-2, the immature version of miR-9. It has been reported that miR-9 can control Cajal-Retzius cell differentiation in embryonic telencephalon through transcription factor Foxg1; while in late embryonic VZ/SVZ, miR-9 is able to positively regulate Pax6 and thereby control the proliferation rate (Shibata et al. 2008; Shibata et al. 2011). At approximately 50kb upstream of C130071C03Rik there is another gene *Mef2C*, encoding a neurogenic transcription factor (Cho et al. 2011). Importantly, Mef2c is able to enhance miR-9-2 promoter activity through direct binding (Davila et al. 2014). The importance of C130071C03Rik during this process is still unknown. One model proposed could be that C130071C03Rik recruits Mef2c or facilitates its binding to miR-9-2 promoter in *cis*. Intriguingly, knockout of *Visc-2*, an alternative but shorter transcript from the same locus, led to a reduction of miR-9-2 expression without affecting either C130071C03Rik or Mef2c (Oliver et al. 2014). In the future, it will be interesting to test whether loss of function for C130071C03Rik influences the expression of miR-9-2 in SVZ NSC.

Kcnq1ot1 One relatively established example of in *cis* regulation by lncRNA is to recruit PRC2 to repress the neighbouring genes, such as *Xist* (Zhao et al. 2008).

Among the 47 lncRNAs I examined, *Kcnq1ot1* is known to interact with PRC2 components Ezh2 and Suz12, as well as H3K9 methyltransferase G9a and this interaction correlates with the silent domain of Kcnq1 (Pandey et al. 2008; Kanduri 2011). Kcnq1 is a potassium channel protein and is involved in long QT syndrome (Tester and Ackerman 2014). Besides its role in action potential, Kcnq1 also regulates proliferation and shape in ES cells (Morokuma et al. 2008). In the adult brain, the expression of *Kcnq1ot1* is restricted in SVZ/RMS, which resembles the expression pattern of Ezh2 described in Chapter 3. So it is possible that *Kcnq1ot1* also associates with Ezh2 in this neurogenic niche. Nevertheless, from the Allen Brain Atlas, expression of Kcnq1 could also be detected in the SVZ/RMS. This seems to contradict the scenario that *Kcnq1ot1* represses Kcnq1 in *cis* through PRC2 recruitment. One possibility is that Kcnq1 and *Kcnq1ot1* are expressed in different cell types in the SVZ/RMS, which still needs to be confirmed by higher resolution microscopy. Additionally, there could be unknown functions of *Kcnq1ot1*, independent of PRC2.

9430029A11Rik (Plxna4os2) *Plxna4os2* is antisense to the protein-coding gene *Plxna4*. Plxna4 is involved in semaphorin signalling and regulates axon guidance (Suto et al. 2005; Mlechkovich et al. 2014). Moreover, the migration of oligodendrocyte precursor cells is also controlled by Plxna4 (Okada and Tomooka 2012; Okada and Tomooka 2013). In adult brain, Plxna4 is weak to absent in the SVZ/RMS, which could be a result of posttranscriptional silencing of Plxna4 mRNA by *Plxna4os2* interference (from Allen Brain Atlas). However, this cannot explain the importance of *Plxna4os2* expression in the SVZ/RMS. Further investigation should be taken to understand whether *Plxna4os2* regulates other in *cis* or *trans* processes.

For most other lncRNAs identified in the SVZ, the neighbouring genes do not have reported functions in the nervous system, which adds more difficulties to their functional prediction. Loss of function analysis of these lncRNA by different strategies (e.g. RNAi, transcription terminator insertion, gene deletion, CRISPR/Cas9, etc) is, therefore, a priority (Bassett et al. 2014).

6.3.3 LncRNA Paupar is required for postnatal SVZ neurogenesis

LncRNA *Paupar* regulates cell proliferation and neural differentiation in N2A cells (Vance et al. 2014). Since N2A is a neuroblastoma cell line, the role of *Paupar* may be different from that in the normal situation. The expression of *Paupar* and *Dali* has been confirmed in my work by qPCR in both P4 SVZ and neurospheres. Of note, *Paupar* is more enriched in the SVZ than in neurospheres. This can be due to the inclusion of non-neurogenic cells in dissected SVZ tissues or to the heterogeneity of the SVZ, like quiescent NSC. In contrast, neuroblasts express more lncRNA *Pax6os*1 than do NSC (Ramos et al. 2013). It seems *Paupar* and *Pax6os*1 may have opposing expression patterns. In SVZ, *Paupar* and *Pax6os*1 may coordinate to modulate the protein-coding gene Pax6. In my neurosphere experiment, knockdown of *Paupar* decreased the expression of Pax6 and it was likely a dose response effect, as previously described (Vance et al. 2014). In the next step, I am going to examine whether knockdown of *Pax6os*1 can instead increase the expression of Pax6.

On the other hand, the CHART-Seq analysis suggested *Paupar* binds to the regulatory region of *Ezh2*. Intriguingly, this regulatory region has an active histone state with H3K4me3/H3K27a in the cerebellum, cortex and whole brain, although Ezh2 is not expressed outside the adult SVZ. Therefore, it may be less essential that *Paupar* directs histone modifications to this regulatory region. Instead, *Paupar* and

H3K4me3/H3K27a may function in separate mechanisms, i.e. *Paupar* negatively regulates the expression of Ezh2 in *trans*. Consistent with this hypothesis, knockdown of *Paupar* in neurospheres led to an increase of Ezh2. It is not clear how *Paupar* performed this repressive role, but it could prevent transcription factor binding to the regulatory sequence of *Ezh2*.

In vivo knockdown of *Paupar* by electroporation showed a defect in postnatal SVZ neurogenesis. This study was based on quantification of absolute numbers of GFP+ cells in the OB. One consideration for this method is different electroporation efficiency between control and knockdown groups. I used similar amounts of DNA for individual pups and interestingly the dramatic decrease of GFP+ cells could only be observed in the sh165 group, the one with better knockdown efficiency, but not in sh408 pups. This indicates the phenotype should be a biological effect instead of an artificial result. However, I cannot rule out the possibility that GFP stability and expression were not affected by sh165. To circumvent this issue, I plan to collect the electroporated brains at early time points, i.e. shorter than 24 hours. GFP signal can be visualized as early as a couple of hours post electroporation. So at this early time point, I should be able to dissociate the electroporation efficiency from the biological effects. Moreover at 3dpe, the general GFP signal was also weaker in the sh165 group. Hence, it is also necessary to examine whether cell proliferation is enhanced after knockdown of *Paupar*, which could possibly lead to an accelerated dilution of GFP. Importantly, the GFAP/GFP percentage decreased in the sh165 SVZ. This analysis precluded the issue of electroporation efficiency and suggested that *Paupar* regulates the stem cell population in the postnatal SVZ. Considering the relationship between *Paupar* and Pax6, I hypothesize that *Paupar* may perform this function through Pax6. The indispensable role of Pax6 in neuronal differentiation has already

been characterized in the postnatal and adult SVZ (Jang and Goldman 2011; Ninkovic et al. 2013). However, it is poorly understood whether Pax6 regulates SVZ proliferation directly, although the majority of proliferating cells in SVZ express this transcription factor and Pax6 is required for proliferation in the SGZ (Kohwi et al. 2005; Maekawa et al. 2005). On the other hand, there is evidence that Pax6 inhibits proliferation in the embryonic cortex and astrocytes (Warren et al. 1999; Sakurai and Osumi 2008). In N2A cells, loss of *Paupar* impaired the cell cycle progression and promoted neuronal differentiation (Vance et al. 2014). Thus, it remains to be determined whether loss of *Paupar* or Pax6 in SVZ affects the proliferation and differentiation.

6.4 Conclusion

In this chapter, the expression and function of lncRNA in the SVZ have been explored. The expression of at least 47 lncRNAs was confirmed in the adult SVZ and many of them had neighbouring genes close to the lncRNA loci. Particularly, the lncRNA *Paupar* was expressed in the postnatal SVZ and was necessary for neurogenesis, probably by modulating NSC maintenance. In addition, *Paupar* could bind with regulatory elements to control the expression of Ezh2. Understanding the roles of *Paupar* in SVZ neurogenesis can provide new clues about lncRNA functional mechanisms.

Chapter 7

Discussion

This thesis has focused on the roles of two epigenetic regulators, PRC2 and lncRNA in postnatal/adult SVZ neurogenesis. The core subunits of PRC2, Ezh2 and Eed were shown to be required for SVZ neurogenesis, however in terms of functionality, they behaved differently. Ezh2 repressed Cdkn2a thereby controlling SVZ proliferation. In contrast, Eed was indispensable for SVZ quiescent NSC activation and maintenance of stem cell identity. Moreover, it appeared that this essential role of Eed in NSC activation was limited to the neurogenic niche, with little responsibility for astrocyte reactivation in the injured cerebral cortex. On the molecular level, Eed was also involved in the repression of Cdkn2a; while it could independently control the transcription factor Gata6, and in turn posttranscriptionally modulate p21. Similarly, several lncRNAs were also expressed in the adult SVZ. It has been described that one lncRNA *Paupar* was necessary for postnatal SVZ neurogenesis, possibly by maintaining the stem cell population within the niche. Loss of *Paupar* altered Pax6 and Ezh2 expression, which was also a direct target of *Paupar*. Taken together, these data suggest an integrated function of PRC2 and lncRNA in SVZ neurogenesis.

7.1 Overview of the current work

Although the adult brain is less plastic and relatively stable, neurogenesis can be observed in two major neurogenic niches. Thanks to an in-depth understanding of the adult SVZ, the glial features of SVZ NSC have been well described (Kriegstein and Alvarez-Buylla 2009; Ihrie and Alvarez-Buylla 2011). However, the molecular mechanistic differences between SVZ NSC and astrocytes still remain mysterious. In the healthy brain, both cell types are in a quiescent state. However, SVZ NSC can proliferate occasionally, while parenchymal astrocytes only enter the cell cycle in response to brain injury. The expression of cyclin-dependent kinase inhibitors (CDKIs) appears to be responsible for these activation processes. p16 and p19 are

transcribed from *Cdkn2a* locus, and appear to inhibit the general cell proliferation in SVZ (Hwang et al. 2014). Both transcripts are not typically expressed in SVZ; therefore they do not directly control the quiescent state in SVZ NSC under normal conditions. Similarly, p16 and p19 are not differentially expressed before and after astrocyte activation (Zamanian et al. 2012). Loss of Eed led to decreased NSC proliferation, suggesting misexpression of p16 and p19 would impair NSC activation. However, cortical lesion induced reactive astrocytosis was not.

During the cell cycle, p16 inhibits Cdk4, Cdk6 and Cyclin D, and p19 functions in a p53-dependent manner (Lowe and Sherr 2003). Surprisingly, Cdk6 is upregulated in both active NSC and reactive astrocytes while Cdk4 is only activated in the former, which is also p53 dependent (Zamanian et al. 2012; Codega et al. 2014). These differences may give rise to distinct responses to Eed repression of p16 and p19 in SVZ NSC and mature astrocytes. Recent work on p21 in SVZ proliferation has shown that constitutive loss of p21 would activate NSC (Kippin et al. 2005; Marques-Torrejon et al. 2013). Therefore, the competing mechanisms of p16/19 activation and p21 downregulation after the loss of Eed resulted in deficiency in SVZ NSC activation. Unlike Eed, Ezh2 was not expressed in quiescent SVZ NSC, suggesting it plays minor roles in quiescent NSC maintenance, but could promote cell activation in SVZ. Ezh2 would be less essential in NSC, considering the compensation of Ezh1.

Besides the differences in proliferative dynamics, there was no evidence to demonstrate the neuronal differentiation ability of parenchymal astrocytes outside the SVZ until now. Cell fate stability in mature astrocytes will however be modulated after brain injury (Buffo et al. 2008; Grande et al. 2013; Sirko et al. 2013). In particular, reactive astrocytes acquire multipotency in vitro cultured with EGF and FGF. As I discussed before, Ezh2 drives the neurogenesis in SVZ and hence may also

contribute to the neuronal differentiation ability in parenchymal astrocytes. The discovery of the Eed-Gata6-p21 regulatory pathway in this thesis has contributed to a greater understanding of how PRC2 will enhance the stemness in mature astrocytes. It is in line with the fact that in SVZ p21 could maintain NSC multipotency through BMP signalling, independent of CDKI functions (Porlan et al. 2013). Meanwhile, the pluripotency transcription factor Sox2 is also under the negative regulation of p21 (Marques-Torrejon et al. 2013). Thus, it will be interesting to assess whether the Eed-Gata6-p21 regulatory pathway could contribute to neurogenesis in mature astrocytes. Indeed, p21 is unregulated in reactive astrocytes and overexpression of Sox2 reprograms mature astrocytes into neuroblasts (Zamanian et al. 2012; Niu et al. 2015). However, loss of Eed in reactive astrocytes did not change the GFAP+/Sox2+ cell population in the injured cerebral cortex, indicating the involvement of other mechanisms or functional variations of the Eed-Gata6-p21 regulatory pathway. Likewise, recent work shed light on the negative roles of p16 and p19 in neuronal differentiation, which is consistent with reduced neurogenesis after the loss of either Ezh2 or Eed (Price et al. 2014). Importantly, it has been observed in cortical astrocytes that loss of p16/p19 decreased the expression of p21, while in SVZ cells loss of p21 induced p19 but not p16 expression (Marques-Torrejon et al. 2013; Price et al. 2014). The importance of this potential regulatory loop in SVZ neurogenesis is still under investigation. As Eed represses p16 and p19 expression but maintains p21 expression level, it may balance the effect of this loop and control SVZ homeostasis.

LncRNA is another epigenetic component studied in this thesis. 47 lncRNAs have been confirmed in the adult SVZ. Notably, a postnatal SVZ enriched lncRNA *Paupar* was found to positively regulate Pax6 and negatively regulate Ezh2. *Paupar* may promote Pax6 expression in *cis* while inhibiting Ezh2 in *trans* through binding

with its upstream regulatory region. It has been reported that increased expression of Ezh2 augmented cell proliferation in neurospheres cultured from the SGZ (Zhang et al. 2014). Meanwhile, Pax6 drives neuronal fate against glial differentiation (Ninkovic et al. 2013). Accordingly, reduced neurogenesis was observed after loss of *Paupar* in the postnatal SVZ. These data provide strong evidence for distinct biological activities of lncRNA in neuronal development instead of previously postulated theories of transcriptional noise or junk. The molecular mechanisms underlying *Paupar* regulation of gene expression in SVZ remains to be explored, but it is documented that *Paupar* modulates the transcriptional activity (Vance et al. 2014). Sox2, for instance, is a direct target of *Paupar* with the lncRNA binding to the upstream sequence of the *Sox2* locus, independent of Pax6 (Vance et al. 2014). Further experimental investigation of *Paupar* will elucidate its role in regulating SVZ NSC.

7.2 Limitations

7.2.1 Technical limitations

The functional analysis of Ezh2 and Eed has primarily replied on the inducible Cre/LoxP transgenic mouse model. One consideration of this system should always be borne in mind, especially when conducting stem cell studies, is that this is an incomplete knockout system. The total biological effect may be underestimated in this case and a subtle phenotype may be covered by the surrounding non-knockout normal cells. Additionally, the PRC2 expressing stem cells may remodel and repair the defects in the neurogenic niche at a later time point, similar to the study of Numb knockout in the postnatal SVZ (Kuo et al. 2006). Hence, the negative data observed in Ezh2 cKO mice at P75 may be attributed to this reason rather than a less essential role of Ezh2. Introducing a reporter line has been used as a solution to this problem, but the correlation between knockout and fluorescent marker cannot be 100% guaranteed. The knockout of the floxed-Stop cassette in one allele is sufficient to induce overexpression of a fluorescent protein marker, while recombination of two alleles for the targeted gene is necessary for the functional analysis, although heterozygous knockouts may elicit some phenotypes. To refine this experiment, the Glast-CreERT2;$Eed^{fl/-}$;Ai9 model should be generated to include constitutive knockout in one allele as follows: (1) A universal Cre line, e.g. Rosa26, CAG promoter driving Cre, is crossed with $Eed^{fl/+}$ to knockout one allele of Eed in the whole animal including germ cells. Cre;$Eed^{-/+}$ will be crossed with $Eed^{fl/fl}$ to generate $Eed^{fl/-}$ without the universal Cre knock-in. (2) The mating between $Eed^{fl/-}$ and Glast-CreERT2;$Eed^{fl/fl}$;Ai9 produces Glast-CreERT2;$Eed^{fl/-}$;Ai9. With this line, the fluorescent marker is able to label the homozygous knockout cells at the highest rate.

The development of other genomic editing technologies, such as ZFN, TALEN, CRISPR/Cas9, provides alternative methods to increase knockout efficiency (Gaj et al. 2013; Kim and Kim 2014). Using the CRISPR/Cas9 platform, the guide RNA directs the Cas9 nuclease to induce DNA double-stranded breaks in a sequence-specific manner and the genomic editing could be achieved by DNA repair pathways (Sander and Joung 2014). Thus, this technique circumvents the issue of heterozygous knockout and importantly, reduces the time-scale in generating transgenic animals.

Electroporation and nucleofection are the two techniques I used for in vivo and in vitro genetic manipulations, respectively. However the dilution effect interfered with lineage analysis. For example, Gata6 overexpression induced defects in neuronal differentiation, but this could have been due to a fate shift towards the glial lineage. Clonal differentiation assay is used to test the stem cell pluripotency, which however may not be applicable with nucleofection. Lentivirus or retrovirus mediated overexpression provides stable integration of exogenous constructs into the host cell genome and overcomes the disadvantage of nucleofection in vitro. For in vivo analysis, lentivirus is the priority for its ability to infect quiescent NSC. However I found stereotaxic brain injection led to infections around the needle tract and a single virus is unable to distinguish the pluripotency of individual cells in vivo (Supplemental Figure 1). Brainbow, or its modified versions, and genomic barcodes are two methods available now for this purpose (Szele and Cepko 1996; Szele and Cepko 1998; Livet et al. 2007; Schepers et al. 2012; Garcia-Moreno et al. 2014; Loulier et al. 2014). With multi-fluorescence, brainbow allows for morphology analysis but it is limited by the detecting ability of microscopy. Instead, genomic barcodes permit the classification of individual stem cell lineages in SVZ by PCR or sequencing. Delivered by virus, genomic barcodes would be necessary to determine

whether loss of Eed or activation of Gata6 in vivo affect the neuronal versus glial fate choice.

Cerebral cortical lesion was used as the traumatic brain injury model in this thesis. Although the reproducibility of cortical lesion is generally well accepted, variations in injury size and depth were observed, which may theoretically affect the local cortical and remote SVZ responses. To modify this surgery model, stereotaxic coordinates will be applied in the future to correct the lesion areas in individual mice. Besides, the controlled cortical impact is another model with a higher reproducibility (Romine et al. 2014).

7.2.2 Limitations in data interpretation

I found Eed was necessary for SVZ NSC activation and identity maintenance; however, it was difficult to clearly distinguish the differences between NSC activation and maintenance, for three reasons. Firstly, reduced NSC proliferation and neurosphere frequency can be attributed to loss of stem cell identity, as mature astrocytes do not have sphere-initiating ability. Secondly, recent studies have suggested SVZ quiescent NSC is unable to generate neurospheres in response to EGF and FGF (Codega et al. 2014; Mich et al. 2014). Therefore, fewer neurospheres may not be a biological readout of NSC activation. Instead it could be explained as decreased proliferation in active NSC, transit amplifying cells and neuroblasts, though the alteration in cellular response to mitogens should be taken into consideration. Thirdly, the marker for mature astrocytes, S100β was used in the SVZ NSC. S100β labels ependymal cells and parenchymal astrocytes (Raponi et al. 2007; Ihrie and Alvarez-Buylla 2011). It has been reported that S100β is also enriched in quiescent NSC when compared to active NSC in the adult SVZ (Codega et al. 2014). Thus, one

can argue increased S100β expression in SVZ label-retaining cells may indicate a deficiency in the quiescent state exit, rather than driving NSC into the astroglial lineage. On the other hand, it is still unclear whether loss of Eed in niche astrocytes will activate these cells, which can be detected by label-retaining technique as well. These points are raised from the poor boundary definitions between niche astrocytes and quiescent NSC. In some studies, hGFAP and prominin1 were used together as SVZ NSC markers while hGFAP was used alone for niche and diencephalic astrocytes (Beckervordersandforth et al. 2010; Beckervordersandforth et al. 2014). Nonetheless, these studies replied on neurosphere forming abilities as criteria for NSC, which excludes quiescent NSC and niche astrocytes. Currently, the only difference is the cell morphology and the pinwheel structure (Ihrie and Alvarez-Buylla 2011). The whole mount technique allows exposing the lateral ventricle wall and examining the features of NSC in the core of the pinwheel structure. These will form the basis for future work (Supplemental Figure 4).

The role of PRC2 in initiation versus maintenance of the global transcriptome remains elusive (Margueron and Reinberg 2011; Riising et al. 2014). PRC2 repression of p16 and p19 appears to be responsible for SVZ NSC activation for the inhibitory role of Cdkn2a in the cell cycle. Different models can be proposed to explain this relationship. In the first model, PRC2 functions to maintain the NSC in the active stage and prevent quiescence. This model has led to the suggestion that PRC2 repression of p16 and p19 plays a more important role in the active NSC rather than the quiescent NSC. However, the transcriptome comparisons between active and quiescent NSC or general SVZ NSC and niche astrocytes, are unable to detect any Cdkn2a expression differences (Beckervordersandforth et al. 2010; Codega et al. 2014). This contradiction highlights two other proposed models: (1) PRC2 repression

of p16 and p19 is required for the proliferation in transit amplifying cells and neuroblasts. (2) The cell cycle inhibitory role of p16 and p19 is not involved in maintaining NSC quiescence. In this model, PRC2 represses p16 and p19 in both quiescent and active NSC, which is in keeping with the transcriptome data. The data presented here cannot distinguish between these two models since they could theoretically coexist in SVZ. Analysis of p16 and p19 expression after Eed knockout in individual SVZ cell types should provide more relevant data and insights. On the other hand, PRC2 fine-tuning of p21 protein levels contributes to NSC identity, i.e. neuronal differentiation potential. The cell cycle regulation role of p21 should be less important in stem cell quiescence in this model and its Cdk-independent function determines the neuronal fate of SVZ NSC (Kippin et al. 2005; Porlan et al. 2013). This is consistent with the notion that p21 is not differentially expressed between quiescent and active NSC, i.e. the transcript exists in both cell types (Porlan et al. 2013; Codega et al. 2014). The discovery of posttranscriptional regulation of p21 supports this model but there is no evidence to support the concept that different levels of p21 protein perform distinct functions.

7.3 Future directions

In this thesis, the roles of PRC2 and lncRNA were separately studied in the postnatal SVZ neurogenesis. Their interaction has been described in the study of several lncRNAs such as *Xist* and *HOTAIR* (Rinn et al. 2007; Zhao et al. 2008). In these examples, lncRNA function to recruit PRC2 in *cis* or in *trans* to silence the relevant genes (Brockdorff 2013). For the future work, the following will be carried out.

7.3.1 The interaction of PRC2 and lncRNA in SVZ

The relationship between lncRNA *Paupar* and Ezh2 has been discussed in Chapter 6. Briefly, *Paupar* binds to the upstream regulatory region of Ezh2, where active histone markers can be identified in the brain, suggesting a regulatory relationship between *Paupar* and Ezh2. Firstly, *Paupar* may direct the recruitment of Trithorax complex and histone acetyltransferase CBP for H3K4me3 and H3K27a, respectively. In this case, loss of *Paupar* should rearrange these two histone modifications globally, including the *Ezh2* locus. Secondly, *Paupar* may modulate transcription factors binding to this regulatory region. For example, the oncogenic gene ERG and the tumour repressor gene ESE3 were shown to have opposite regulatory functions with respect to Ezh2 (Kunderfranco et al. 2010). Thus, it is interesting to ascertain if *Paupar* can control the preferentially binding of the Ezh2 regulatory region with either protein. Finally, *Paupar* may prevent PRC2 binding. Currently, there is no genomic comparison relating to *Paupar* and H3K27me3 binding sites, but the *Ezh2* locus suggests *Paupar* may repel PRC2 targeting, a theory requiring further investigation.

Kcnq1ot1 is another interesting lncRNA known to associate with Ezh2 (Pandey et al. 2008; Redrup et al. 2009). Since there are no data on the biological function of *Kcnq1ot1* in SVZ neurogenesis, it is open to speculation, whether *Kcnq1ot1* coordinates Ezh2 in NSC proliferation and differentiation. It needs to be confirmed whether *Kcnq1ot1* binds to Ezh2 in the SVZ and whether they are expressed in the same cell type, as their binding seems to be lineage specific (Pandey et al. 2008). Additionally, *Kcnq1ot1* expression decreases in the OB, indicating it has to be turned off after full neuronal differentiation. Interestingly, in whole brain and neural progenitors, the upstream sequence of its transcription-starting site has

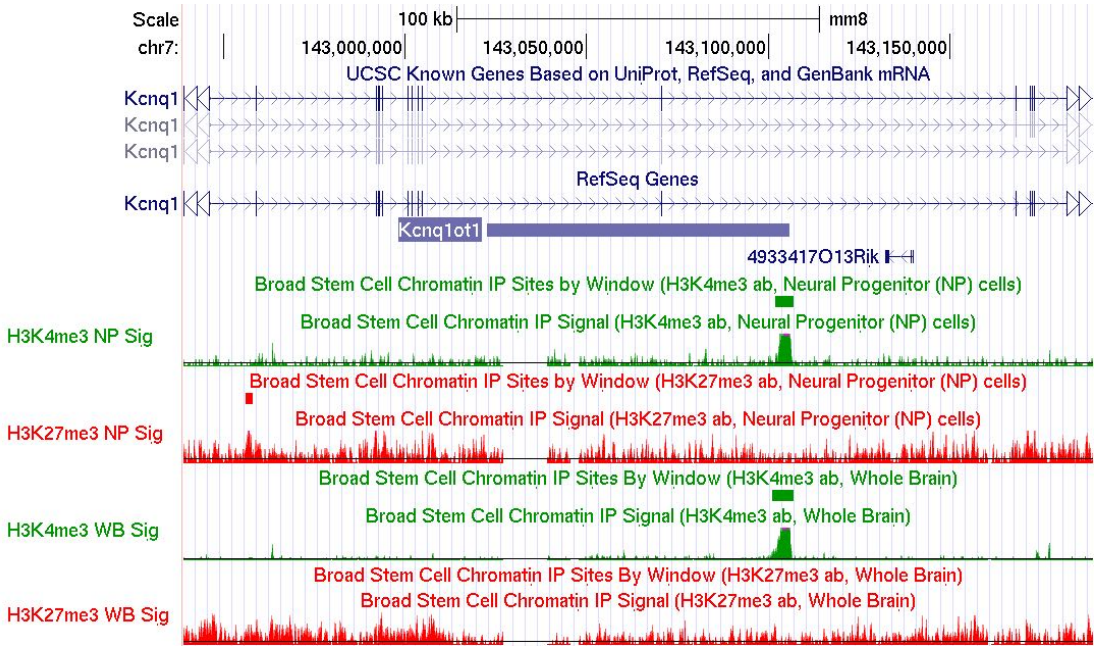

Figure 7. 1 Histone modifications at *Kcnq1ot1* locus in brain and neural progenitors

H3K4me3 and H3K27me3 analysis at the *Kcnq1ot1* locus in the genome (data from UCSC genome). In neural progenitors and whole brain tissues, H3K4me3 but not H3K27me3 peak can be found at the transcription start site of *Kcnq1ot1*.

abundant H3K4me3 but is absent for H3K27me3 (Figure 7.1) (Mikkelsen et al. 2007; Meissner et al. 2008). Instead, the downstream sequence of *Kcnq1ot1*, which corresponds to the gene body of Kcnq1, has obvious H3K27me3 suggesting *Kcnq1ot1* may facilitate the distribution of H3K27me3 in the genome.

7.3.2 PRC2 and lncRNA in glioblastoma

Glioblastoma is a brain tumour closely related to the adult SVZ (Lim et al. 2007). In one mechanistic model, it is believed that glial progenitor cells originated from SVZ NSC may transform into cancer stem cells (CSC) (Sanai et al. 2005). The differences between SVZ NSC and glioblastoma CSC are still poorly understood at the molecular level. Rheinbay et al described the transcriptome and chromatin modification in glioblastoma CSC and NSC (Rheinbay et al. 2013). However in this study, human ES cell-derived NSC were used, which may not represent the features of in vivo NSC. Olig2, for instance, has H3K27me3 and H3K4me3 bivalent domains in this NSC line; while in both CSC and SVZ NSC only H3K4me3 could be detected (Rheinbay et al. 2013). Hence, to understand the role SVZ NSC in tumourigenesis, it is critical to compare the transcriptome and epigenome between CSC and SVZ NSC directly sorted from the brain, to reduce potential influences from in vitro environments.

On the other hand, several lncRNAs, such as *HOTAIR* and *MIAT*, have been identified relevant to glioma grades (Zhang et al. 2013a; Zhang et al. 2013c; Li et al. 2014). Nonetheless, the lncRNA expression analysis in glioblastoma is relatively coarse, i.e. the authors simply compared cancer samples with healthy tissues (Han et al. 2012; Kraus et al. 2015). Indeed, the heterogeneity of glioblastoma compromises lncRNA expression differences in the stem cell populations. A more refined analysis of SVZ NSC and CSC should provide more insights into whether lncRNA is involved

in tumourigenesis. Of note, *HOTAIR* and EZH2 were shown to co-regulate cell proliferation in glioblastoma cells (Zhang et al. 2015). A hypothesis derived from this research suggests that the aberrant H3K27me3 localisation in CSC is due to misexpression of some lncRNA. To give an example, H3K27me3 can be found on *Gata6* locus in both mouse SVZ NSC and human ES cell-derived NSC, but not in CSC (Rheinbay et al. 2013). Intriguingly, the bidirectional lncRNA *1010001N08Rik* in mouse or *GATA6-AS1* in human can be found next to the *Gata6* locus, suggesting a possible in *cis* regulation (Figure 7.2).

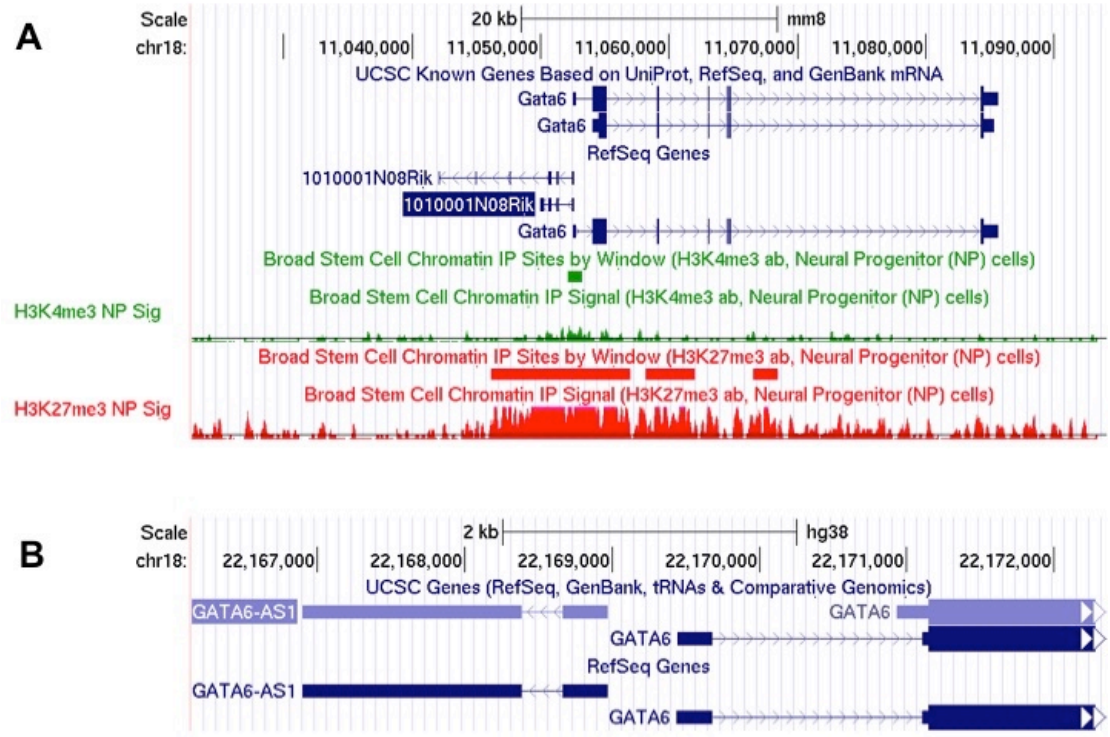

Figure 7. 2 LncRNA in neighbouring of *Gata6* in mouse and human

(A) LncRNA *1010001N08Rik* is bidirectional to *Gata6* in mouse. H3K27me3 is enriched in TSS for both *Gata6* and *1010001N08Rik*.
(B) LncRNA *GATA6-AS1* is bidirectional to *GATA6* in human.
(Data from UCSC Genome)

7.3.3 PRC2 and lncRNA in astrocyte reprogramming

The dynamic expression of lncRNA has started to be explored lately; however, compared to PRC2, our understanding of lncRNA regulation cell reprogramming is still in its infancy (Pasque et al. 2014; Kim et al. 2015). One recent study has demonstrated lincRNA-p21 controls H3K9me3 and DNA methylation in pluripotency genes during reprogramming (Bao et al. 2015). As discussed, Ezh2 may drive the neuronal differentiation in parenchymal astrocytes in vivo. Future experiments will examine whether lncRNA can facilitate this process. Unfortunately, there is no data available now for lncRNA expression in different brain cell types. Therefore, a comprehensive profile of lncRNA in astrocytes and SVZ NSC would need to be undertaken. Following this, it would be interesting to know whether some of these lncRNA may help to recruit Ezh2 to glial transcription factors, like Olig2. These proposed studies would underpin new methods and techniques to help improve astrocyte regenerative ability in astrocytes after traumatic brain injury.

APPENDICES

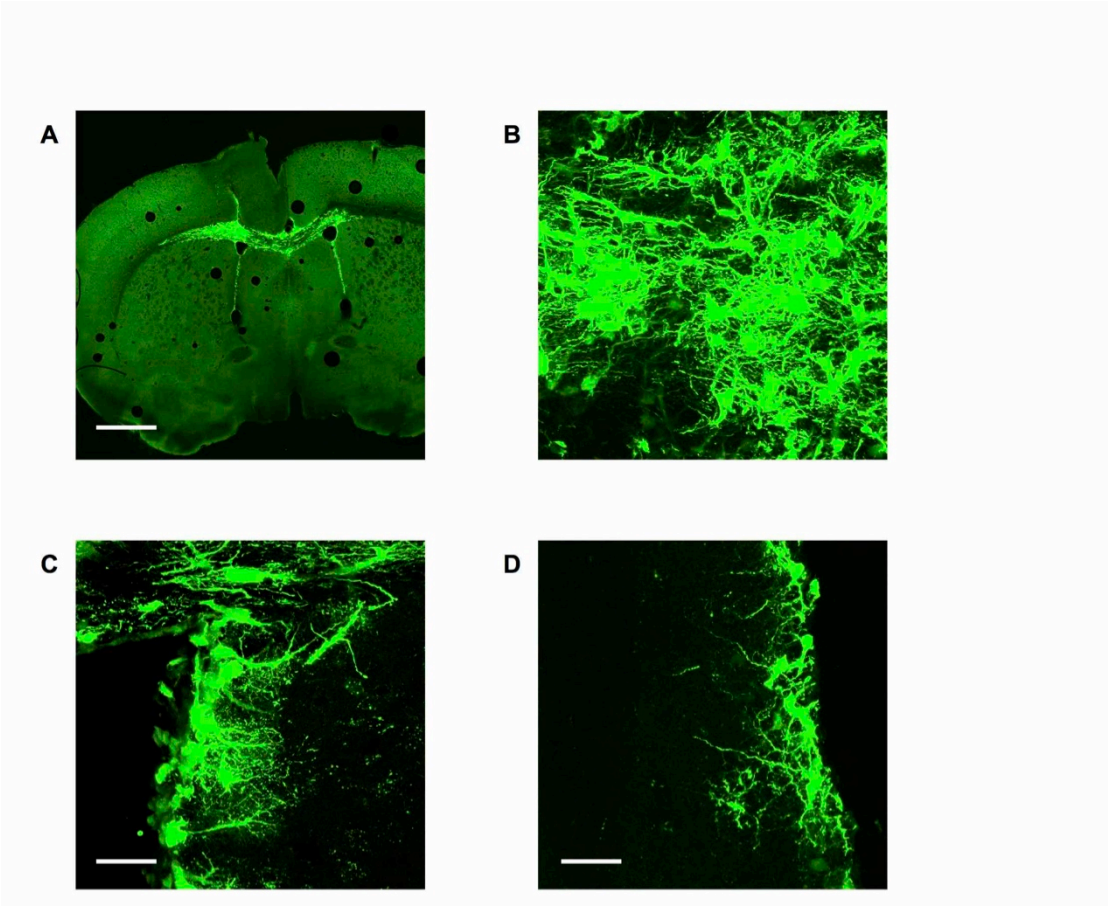

Supplemental Figure 1 Lentivirus injection in adult brain

Lentivirus expressing GFP was injected into the lateral ventricle in adult brain. 7 days later brain was collected.

(A) Injection tract, labelled by GFP, can be found in the cortex.

(B) Cells in the corpus callosum are also infected.

(C-D) Cells infected in the SVZ shows the morphology of NSC.

Scale bar: (A)=1000um, (B-D)=30um.

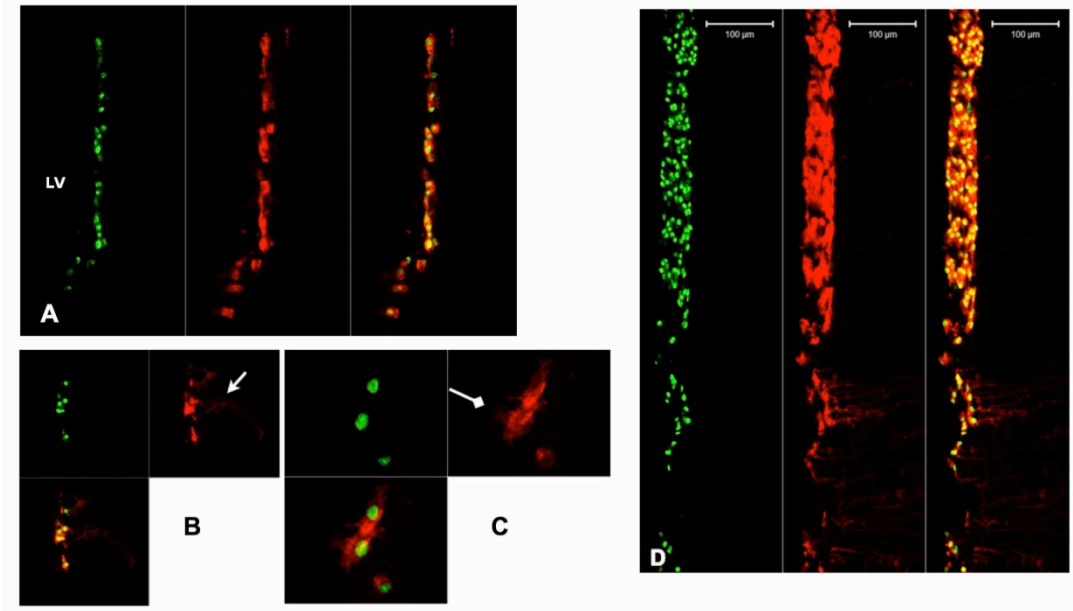

Supplemental Figure 2 Adult electroporation in SVZ

(A-D) Electroporation in adult SVZ with pCAG-tdTomato-2A-H2BGFP. (A) shows the ventral lateral ventricular wall with targeted cells in the ipsilateral side (2dpe). Arrow in (B) indicates the basal process of B cells and (C) shows the multiciliated ependymal cells. (D) Additionally, the cells in the third ventricle also expressed the electroporated DNA. The image is a 70 micron Z-stack.

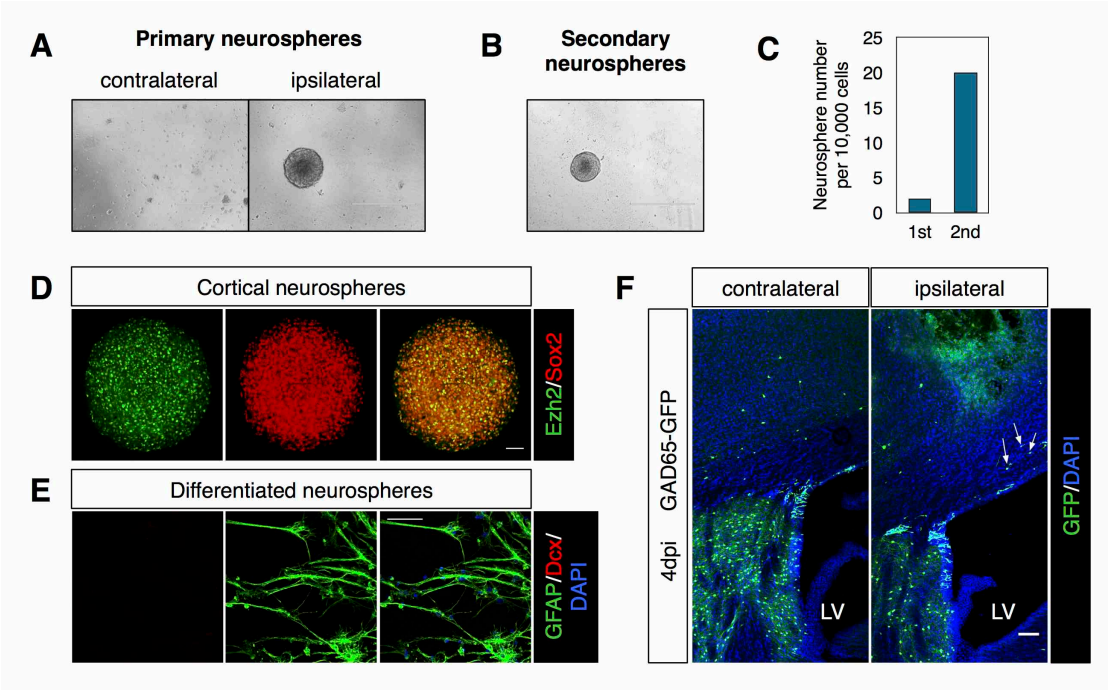

Supplemental Figure 3 Stem cell property characterization after cortical lesion

(A-B) 3 days post cortical lesion surgery, the cerebral cortex tissue around the injury was dissected for neurosphere culture. The primary neurospheres could be found at 7days in culture (A) and could be passaged to form the secondary neurospheres (B).

(C) The neurosphere frequency was quantified 7 days in culture (n=1).

(D) Costaining of Ezh2 and Sox2 in the secondary neurospheres cultured from the injured cerebral cortex.

(E) Immunostaining of the astrocyte marker GFAP and the young neuron marker Dcx in the differentiated neurospheres (7 days in culture).

(F) Cortical lesion was performed in the GAD65-GFP mice. 4 days post injury the GFP+ neuroblasts were analysed.

Scale bar: (A)=1000um, (B)=100um, (D)=(E)=50um, (F)=100um.

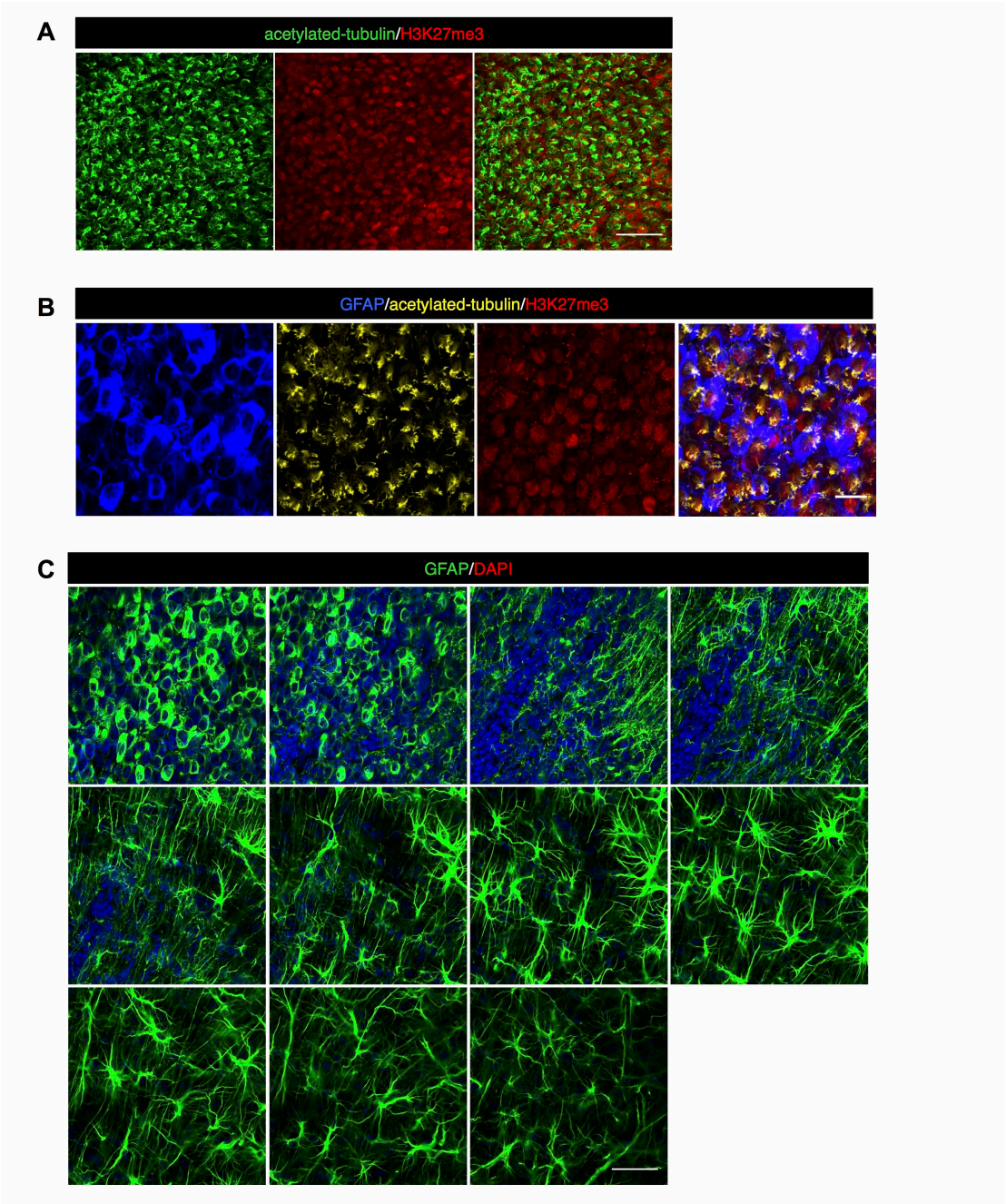

Supplemental Figure 4 The whole mount analysis of the postnatal SVZ

The whole mount assay was performed in P9 mouse brains to reveal the lateral ventrical walls.

(A) The motile cilium marker acetylated-tubulin was costained with H3K27me3.

(B) Costaining of acetylated-tubulin, GFAP and H3K27me3 in the lateral ventrical walls.

(C) Immunostaining of GFAP in the lateral ventrical walls. Images were acquired from apical to basal to show the morphological changes of the GFAP+ cells.

Scale bar: (A)=50um, (B)=20um, (C)=50um.

Supplemental Table 1 Genes upregulated after cortical lesion

Gene	TBI 1	TBI 2	TBI 3
Tubb6	1.61E+07	9779790	7815740
Nes	10.53687866	13.04220493	18.53155429
Vim	10.77053632	10.34500592	8.526450026
Pdlim4	9.437882505	19.33880341	6.126707112
Gfap	13.21021148	7.09575017	6.459850325
Emp1	15.24789929	7.106221296	4.918465072
Msn	7.213583791	5.12874581	4.840514908
Tuba6	5.167111934	4.989413774	3.541469684
Apbb1ip	3.507535724	11.07695818	3.770662335
Prss18	4.883226841	4.184991976	3.997747345
Arpc1b	5.026428903	4.268408902	3.092393333
Tagln2	5.083158921	4.21848963	2.999948978
Iqgap1	3.494938676	3.576944892	4.077570939
Mtmr11	3.684747408	4.041391343	3.036931371
Myo1f	2.35909237	4.611204874	3.954539628
Dab2	2.644681995	2.743070112	2.710579691
Flna	2.399696539	2.538518317	2.040846744
Cotl1	2.201734632	2.239622254	2.063008553
Snip1	4029830	8.818553983	20.59512918
Trim47	6524770	5983450	4154410
Ptx3	14.22713156	12.07529568	7.631311492
Zfpn1a1	5.388533615	8.490080336	4.635727244
Cebpd	5.302267461	5.820264267	4.332672031
	5.471371175	3.113380787	3.9947775
Tax1bp3	4.556999983	3.333900923	3.825453504
Lrrfip1	4.284930856	3.54765717	2.776828822
Tgif2	4.138356263	3.315836389	3.303368569
Ifi202b	1.07E+07	6841970	3183910
Ncf4	5484710	3891530	3347530
Slc15a3	3898910	3764560	3894160
Pik3ap1	8.130790779	3904310	3104670
C3ar1	5955390	14.81918815	54.72153212
Spp1	32.12177101	39.41614143	37.4998558
Cd44	62.75150427	7081150	5.296771166
Capg	18.94602729	8.050229112	30.27148459
Tlr2	9.404989478	50.08890626	13.30218353
Ms4a6d	13.9644232	14.51177142	10.60043166
Lzp-s	13.40724578	132.6227558	6.027291035
Mpeg1	9.380558804	9.357937236	7.825812345
G1p2	14.24635919	5.851261782	4.553563373
Ctsc	8.55046589	7.02452157	7.188314796

Ifi27	8.255128828	7.428023406	6.209360698
Socs3	8.886007412	10.64909773	3.517396076
Cotl1	16.12489628	4.539189168	5.894857856
Lyzs	7.240781499	11.43184992	4.47901018
Msr2	9.029058222	4.185750279	7.203771517
Lcp1	8.397236349	5.429811699	6.251153657
Ly86	8.0248131	6.266620569	5.280664451
Gp49a /// Lilrb4	8.037148127	6.018885564	4.706282263
Msr1	4.746546112	16.34106222	3.212286262
Gusb	5.425018107	6.19722149	5.798141814
Fcgr2b	9.010173343	5.311274527	4.400645298
Cd14	6.381196212	8.239575523	3.886029351
Klhl6	10.64658644	4.056493308	4.221178295
H2-Aa	5.711220322	6.517510559	4.139721257
Apobec1	4.150316525	3.954321278	9.522782964
Fcer1g	5.342892457	5.478901801	3.680196835
Plek	7.250765165	5.20563932	3.486871779
Tlr13	3.6583683	4.081093243	8.310329068
Cd52	4.702900177	6.679393392	3.11313963
Osmr	6.28927463	4.478963292	3.047810514
Ptgs1	5.079068473	4.33333555	3.555467416
Cd68	4.14436006	4.370560135	4.516253972
Lgals9	5.230465232	3.682185469	3.717386099
Fcgr1	5.130759838	3.652169849	3.343555791
Lcn2	5.406940161	4.626527127	2.709516378
Usp18	6.949907552	2.769948448	2.826563159
H2-Ab1	7.855902878	3.586676583	2.405851618
Ifitm3	4.59549022	4.323652763	2.601095223
	3.926975979	4.723988516	2.839843269
H2-Aa	5.050764911	3.687645656	3.001980128
Ctla2a /// Ctla2b	3.609049752	5.163813758	2.448341364
Nckap1l	2.776578561	4.036602109	4.345653175
Bgn	3.991899494	3.507173773	2.77486935
Ii	3.642472681	4.102231544	3.091174112
Csf2rb1	6.481293464	3.60415587	2.037327878
C4	2.891784021	3.692290204	3.443281644
Fcgr3	3.037633917	3.579258342	3.330049319
Prg1	3.555261138	3.281260057	2.512276488
Ctsh	3.702399289	2.889809295	2.722143902
Ucp2	3.618382111	3.081953995	2.470859839
Tyrobp	3.0476338	3.304415828	2.56716043
Ifi30	2.983630421	3.016916881	2.741417359
Slc11a1	2.423523582	3.086347092	3.016803355
Cd53	2.973532091	2.975335553	2.624271989

Ncf1	2.99577908	2.734699381	2.775663646
S100a11	3.287715841	2.891407687	2.037396199
Alox5ap	3.393296841	2.647920419	2.178577071
Aif1	2.83696235	2.760476098	2.329084832
Blnk	3.09013363	2.255455369	2.276679998
Pilra	2.106318497	2.443180757	3.173286942
Hcls1	2.709883344	2.192341349	2.582613597
Ctsz	2.538661843	2.53873494	2.196010322
Fcgr2b	2.954249016	2.306843885	2.214084012
Birc5	41.12912575	5393480	5630530
Ccnb1	5034130	3660140	29.87375658
Cdc2a	13.01005952	82.30173462	15.35255322
Cks1b	49.65933256	7.966888381	20.78705147
Ccnb2	7.529751459	21.2792639	23.11746904
Ccna2	8.801174451	5.02750838	5.461297654
Cdca8	8.198727642	3.557097513	7.385339
Cdca3	7.178869486	10.87336245	2.374770694
Ccnd1	5.20710031	3.087632045	6.712009208
Cks1b	3.891980124	3.72911511	2.904830877
Cks2	3.430013049	2.874708332	2.779700903
Parp3	3.21837979	2.649208873	2.128516507
Smc4l1	2.589236161	2.280939199	2.927514809
Mcm5	2.440465851	2.321850275	2.708460923
Mcm2	4.043247397	2.596132362	2.39380935
Tmem40	6943260	6.917162602	3440330
Adssl1	19.2944966	7698340	2.276094809
Gpnmb	10.88344395	7.446644613	29.90215461
Tgm1	8.136935674	6.913508567	10.62311047
Hal	10.12002272	7.471217408	4.866906136
Cyp1b1	3.993164321	22.71734035	4.894617142
Nupr1	6.89634227	7.930589952	3.142855248
AU020206	4.653261719	5.311618502	6.293958238
Tm4sf1	7.967697907	6.091266757	2.386289624
Dgcr8	2.198989025	10.14280444	6.568246531
Bzrp	6.895135649	5.613702861	3.018422247
A130040M12Rik	3.975658502	4.549520267	4.987151532
1200008O12Rik	8.90264177	3.441775518	3.362629066
Gbp4	4.707335264	3.844656143	4.312455367
2810417H13Rik	4.859879612	3.488743088	4.418031198
0610011I04Rik	3.536195379	4.727150803	4.411715257
Clic1	4.621895415	4.162087624	2.877990663
BC032204	3.915869553	3.234586893	4.137570837
Serpina3n	4.297712714	3.072380888	3.708316143
Olfml3	4.528753727	2.878543792	3.370519984

D17H6S56E-5	2.382524031	4.482640072	4.211560338
Ris2	7.657524871	2.105626435	3.083465789
Mcm3	7.323332611	2.180506774	3.629333658
Slc14a1	3.961172028	3.53386041	2.727025965
2610001E17Rik	3.687097573	3.031785282	2.547631203
Upp1	3.846620724	2.70734794	2.828885758
A530050D06Rik	2.746392696	3.061992711	3.251787647
Aipl1	2.898601516	2.179199184	4.412760527
Rrbp1	2.997303103	3.293986273	2.500012919
Odc1 /// LOC545783 /// LOC546355	2.482105472	3.635921274	2.856077621
Mcm2	4.043247397	2.596132362	2.39380935
Hfe	2.434095144	3.055281434	3.225074727
Pros1	3.464916225	2.35546292	2.647411605
Mcm6	2.835679821	2.585541428	2.845484497
2410004L22Rik	2.161982264	3.849325015	2.362879648
Wfs1	3.203270315	2.535780741	2.148406228
Emr1	2.407231971	2.60057354	2.528222923
Prg4	2.676170997	2.426041238	2.37074455
D11Ertd759e	2.822705661	2.360993141	2.293036994
Slc7a7	2.147666119	2.681979305	2.533647466
Slfn2	2.303467133	2.382601039	2.605897766
Loh11cr2a	2.369966454	2.140798607	2.522916524
2810418N01Rik	2.398954704	2.008289719	2.13993844
Ccl12	122.3128372	1.95E+07	54.24913654
Cxcl10	36.21651444	33.78640777	10.78528691
Cxcl16	9.339830489	4.752220715	3.184769642
Ccl6	3.834890808	4.466600668	6.398686572
Hbegf	3.410671048	2.714720609	2.672969149
Cklfsf3	2.943939394	2.153132007	2.015163983
Ube2c	5504610	14.48671813	5181510
Tgfbi	15.21763335	13.36224154	12.98248828
	5.108287251	7.635152457	3.4884025
Pycard	6.20413934	4.220355985	4.339996082
C1qb	4.482641394	4.578225513	3.300424851
Tax1bp3	4.556999983	3.333900923	3.825453504
Tnfrsf12a	4.621157301	3.25047065	2.720799582
Psmb8	3.41193826	3.933982711	2.503493503
Tgm2	3.544033484	3.200507507	2.51449034
Timp1	49.05327348	15.35295788	8.613319581
Angptl4	6.492544696	26.98116322	3.622870163
Tnc	7.950871793	3.66150992	4.505748111
Lgals3	5.769334808	5.909146792	3.125371332
Prss18	4.883226841	4.184991976	3.997747345
Anxa2	5.960293473	5.077281129	2.505436048

S100a4	5.149359	3.268597326	4.469399755
Chi3l1	3.061268018	4.863407399	4.222308515
Bgn	3.991899494	3.507173773	2.77486935
Itgam	3.945661893	2.735742011	2.302597804
Fn1	2.39887784	2.730201393	3.079163843
Col3a1	2.686441597	2.720334537	2.274551759
Col16a1	3.12425545	2.63905323	2.047638136
Itga7	2.672294552	2.333795336	2.087032811
Lgals1	8.307309723	16.18663961	9.921648207
Top2a	8.406196023	8.52271881	9.381649272
Ms4a11	8.339770411	10.81676886	5.878317101
P2ry6	8.969711879	4.812951881	6.190558264
Mki67	5.377695602	4.192049623	5.980181422
Ddr1	3.566054813	7.096613897	3.254825968
Hist1h2ad	3.660322788	2.819169092	5.660712988
Cks1b	3.891980124	3.72911511	2.904830877
Pbk	4.286190806	2.930091539	2.584992817
Grn	2.291087699	2.480952344	2.253549759
Tgfbi	11.12030406	9.232103466	10.96511437
Thbs1	5.959716803	10.6806701	5.168258866
Tgfb1	7.092821118	4.848941387	2.921018538
Hbegf	3.410671048	2.714720609	2.672969149
Fgfrl1	2.523511496	3.216705257	2.321058629
Igfbp3	2.10525952	2.93931164	2.16151368
Rrm2	11.61967416	5119190	49.10814637
Ptgs1	9.197565868	8.733972149	2.936421534
Hmox1	5.346037883	4.967335563	4.279764507
Bcl2	5.05197914	3.888464689	3.09150376
Hspb6	4.844750202	3.151665163	2.601998831
Glipr2	3.702997921	3.285683001	3.143430143
Rab32	4.712265679	7.200436422	4.885805163
Ptprc	5.211580763	3.741094674	3.600485002
Arhgdib	4.315590092	5.083334751	2.879032742
Rac2	3.358178358	3.956673475	3.113584709
Racgap1	2.45103897	5.71646847	2.76736103
Rhoc	3.676638029	2.872489419	2.53931111
Pttg1	3.683169336	2.653939617	2.124702727
Gpr34	2.157933107	2.100983296	2.689987982

Supplemental Table 2 Genes downregulated after cortical lesion

Gene	TBI 1	TBI 2	TBI 3
Fmod	0.357520359	0.498946941	0.422673641
Ing1l	0.43896872	0.010799486	2.23771E-07
Btrc	0.460801726	0.262744774	0.428492098
Frzb	0.159211143	0.334277041	0.325118926
Hspa2	0.46314242	0.482682265	2.3081E-07
Grm2	0.475289159	0.384297833	0.278945188
Rassf3	0.398957961	0.12402985	0.480357419
Klf15	0.471323448	0.09995309	0.311860854
MGI:1351330	0.218904295	0.444370369	0.338288308
Cacng3	0.375518667	0.322057377	0.476628545
16 days embryo head cDNA	0.37803291	0.492930579	0.461494288

Supplemental recipes for ChIP solutions

Cell Lysis Buffer:	**Stock**	**dilution**	**50 ml solution**
50 mM Tri-Cl, pH8.1	1M	(20x)	2.5 ml
10 mM EDTA	0.5M	(50x)	1 ml
1% SDS	10%	(10x)	5ml
Add fresh:			
1mMDTT	1M	(1000 x)	
1 mM PMSF in EtOH	0.1M	(100x)	
Sigma proteease inhibitor cocktail		(200x)	

ChIP Dilution Buffer:	**Stock**	**dilution**	**50 ml solution**
16.7 mM Tri-Cl, pH8.1	1M	(59.9x)	0.835 ml
167 mM NaCl	5M	(29.9x)	1.67 ml
1.2 mM EDTA	0.5 M	(416.7x)	0.12 ml
1.1% Triton X-100	20%		0.55 ml
Add fresh:			
1 mM PMSF	0.1M	(100x)	
Sigma proteease inhibitor cocktail		(200x)	

Low Salt IP Wash Buffer:	**Stock**	**dilution**	**50 ml solution**
20 mM Tri-Cl, pH8.1	1M	(50x)	1 ml
150 mM NaCl	5M	(33.3x)	1.5 ml
1 mM EDTA	0.5M	(500x)	0.1 ml
1% Triton X-100	20%		2.5 ml
0.1% SDS	20%	(200x)	0.25 ml
0.1% Na-deoxycholate	5%	(50x)	1 ml

High Salt IP Wash Buffer:	**Stock**	**dilution**	**50 ml solution**
20 mM Tri-Cl, pH8.1	1M	(50x)	1 ml
500 mM NaCl	5M	(10x)	5 ml
1 mM EDTA	0.5M	(500x)	0.1 ml
1% Triton X-100	20%		2.5 ml
0.1% SDS	20%	(200x)	0.25 ml
0.1% Na-deoxycholate	5%	(50x)	1 ml

LiCl IP Wash Buffer:	**Stock**	**dilution**	**50 ml solution**
10 mM Tri-Cl, pH8.1	1M	(100x)	0.5 ml
250 mM LiCl	2M	(8x)	6.25 ml
1 mM EDTA	0.5 M	(500x)	0.1 ml
0.5% NP-40 (IGEPAL-CA630)	10%		2.5 ml
0.5% Deoxycholic acid (Na salt)	5%	(10x)	5 ml

TE Buffer:	**Stock**	**dilution**	**50 ml solution**
10 mM Tri-Cl, pH8.1	1 M	(100x)	0.5 ml
1 mM EDTA	0.5 M	(500x)	0.1 ml

IP Elution Buffer (without NaHCO3):	**Stock**	**dilution**	**50 ml solution**
1% SDS	20%	(10x)	2.5 ml
50 mM TrisCl (pH 8.1)	1 M	(10x)	2.5 ml
1 mM EDTA	0.5 M	(500x)	100ul

NaHCO3 solution	1 M
NaCl solution:	5 M

IP Elution solution:

9 v of IP Elution Buffer
1 v of 1 M NaHCO3 solution
1/20 v of 5M NaCl solution
1/250 Protein K (sigma)
(add freshly before use!)

Supplemental recipes for common solutions

PBS 10X 1M pH 7.4		
Sodium chloride	NaCl	80 g
Potassium choloride	KCl	2 g
Potassium dihydrogen phosphate	KH2PO4	2.4 g
Sodium phosphate dibasic anhydrous	Na2HPO4	14.4 g
	dH2O	to 1000 mL

PB 0.1 M pH 7.4		
Monobasic Solution A (0.2 M)		
Sodium phosphate monobasic	NaH2PO4	27.8 g
	dH2O	to 1000 mL
Dibasic Solution B (0.2 M)		
Sodium phosphate dibasic anhydrous	Na2HPO4	28.4 g
	dH2O	to 1000 mL
PB (0.1 M)		
Monobasic Solution A (0.2 M)		140 mL
Dibasic Solution B (0.2 M)		360 mL
	dH2O	to 1000 mL

Cryoprotectant	
Sucrose	300 g
Ethylene glycol	300 mL
PB 0.1 M	to 1000 mL

PFA 4%	
Paraformaldehyde	20 g
PBS 0.1 M	to 1000 mL

REFERENCES

Alvarez-Buylla A, Ling CY, Yu WS. 1994. Contribution of neurons born during embryonic, juvenile, and adult life to the brain of adult canaries: regional specificity and delayed birth of neurons in the song-control nuclei. *J Comp Neurol* **347**: 233-248.

Amaral PP, Neyt C, Wilkins SJ, Askarian-Amiri ME, Sunkin SM, Perkins AC, Mattick JS. 2009. Complex architecture and regulated expression of the Sox2ot locus during vertebrate development. *RNA* **15**: 2013-2027.

Ambasudhan R, Talantova M, Coleman R, Yuan X, Zhu SY, Lipton SA, Ding S. 2011. Direct Reprogramming of Adult Human Fibroblasts to Functional Neurons under Defined Conditions. *Cell Stem Cell* **9**: 113-118.

Andang M, Hjerling-Leffler J, Moliner A, Lundgren TK, Castelo-Branco G, Nanou E, Pozas E, Bryja V, Halliez S, Nishimaru H et al. 2008. Histone H2AX-dependent GABA(A) receptor regulation of stem cell proliferation. *Nature* **451**: 460-U464.

Andreu-Agullo C, Maurin T, Thompson CB, Lai EC. 2012. Ars2 maintains neural stem-cell identity through direct transcriptional activation of Sox2. *Nature* **481**: 195-198.

Bannister AJ, Kouzarides T. 2011. Regulation of chromatin by histone modifications. *Cell Res* **21**: 381-395.

Bao XC, Wu HT, Zhu XH, Guo XP, Hutchins AP, Luo ZW, Song H, Chen YQ, Lai KY, Yin MH et al. 2015. The p53-induced lincRNA-p21 derails somatic cell reprogramming by sustaining H3K9me3 and CpG methylation at pluripotency gene promoters. *Cell Research* **25**: 80-92.

Bardehle S, Kruger M, Buggenthin F, Schwausch J, Ninkovic J, Clevers H, Snippert HJ, Theis FJ, Meyer-Luehmann M, Bechmann I et al. 2013. Live imaging of astrocyte responses to acute injury reveals selective juxtavascular proliferation. *Nat Neurosci* **16**: 580-586.

Barnabe-Heider F, Goritz C, Sabelstrom H, Takebayashi H, Pfrieger FW, Meletis K, Frisen J. 2010. Origin of new glial cells in intact and injured adult spinal cord. *Cell Stem Cell* **7**: 470-482.

Barnabe-Heider F, Meletis K, Eriksson M, Bergmann O, Sabelstrom H, Harvey MA, Mikkers H, Frisen J. 2008. Genetic manipulation of adult mouse neurogenic niches by in vivo electroporation. *Nat Methods* **5**: 189-196.

Bassett AR, Akhtar A, Barlow DP, Bird AP, Brockdorff N, Duboule D, Ephrussi A, Ferguson-Smith AC, Gingeras TR, Haerty W et al. 2014. Considerations when investigating lncRNA function in vivo. *eLife* **3**: e03058.

Battelli C, Nikopoulos GN, Mitchell JG, Verdi JM. 2006. The RNA-binding protein Musashi-1 regulates neural development through the translational repression of p21(WAF-1). *Molecular and Cellular Neuroscience* **31**: 85-96.

Beckervordersandforth R, Deshpande A, Schaffner I, Huttner HB, Lepier A, Lie DC, Gotz M. 2014. In Vivo Targeting of Adult Neural Stem Cells in the Dentate Gyrus by a Split-Cre Approach. *Stem cell reports* **2**: 153-162.

Beckervordersandforth R, Tripathi P, Ninkovic J, Bayam E, Lepier A, Stempfhuber B, Kirchhoff F, Hirrlinger J, Haslinger A, Lie DC et al. 2010. In vivo fate mapping and expression analysis reveals molecular hallmarks of prospectively isolated adult neural stem cells. *Cell Stem Cell* **7**: 744-758.

Belachew S, Chittajallu R, Aguirre AA, Yuan X, Kirby M, Anderson S, Gallo V. 2003. Postnatal NG2 proteoglycan-expressing progenitor cells are intrinsically multipotent and generate functional neurons. *J Cell Biol* **161**: 169-186.

Belgard TG, Marques AC, Oliver PL, Abaan HO, Sirey TM, Hoerder-Suabedissen A, Garcia-Moreno F, Molnar Z, Margulies EH, Ponting CP. 2011. A transcriptomic atlas of mouse neocortical layers. *Neuron* **71**: 605-616.

Benner EJ, Luciano D, Jo R, Abdi K, Paez-Gonzalez P, Sheng H, Warner DS, Liu C, Eroglu C, Kuo CT. 2013. Protective astrogenesis from the SVZ niche after injury is controlled by Notch modulator Thbs4. *Nature*.

Berghoff EG, Clark MF, Chen S, Cajigas I, Leib DE, Kohtz JD. 2013. Evf2 (Dlx6as) lncRNA regulates ultraconserved enhancer methylation and the differential transcriptional control of adjacent genes. *Development* **140**: 4407-4416.

Bergmann O, Liebl J, Bernard S, Alkass K, Yeung MSY, Steier P, Kutschera W, Johnson L, Landen M, Druid H et al. 2012. The Age of Olfactory Bulb Neurons in Humans. *Neuron* **74**: 634-639.

Beronja S, Livshits G, Williams S, Fuchs E. 2010. Rapid functional dissection of genetic networks via tissue-specific transduction and RNAi in mouse embryos. *Nat Med* **16**: 821-827.

Bian EB, Zong G, Xie YS, Meng XM, Huang C, Li J, Zhao B. 2014. TET family proteins: new players in gliomas. *Journal of neuro-oncology* **116**: 429-435.

Blackledge NP, Farcas AM, Kondo T, King HW, McGouran JF, Hanssen LL, Ito S, Cooper S, Kondo K, Koseki Y et al. 2014. Variant PRC1 complex-dependent H2A ubiquitylation drives PRC2 recruitment and polycomb domain formation. *Cell* **157**: 1445-1459.

Bond AM, VanGompel MJW, Sametsky EA, Clark MF, Savage JC, Disterhoft JF, Kohtz JD. 2009. Balanced gene regulation by an embryonic brain ncRNA is

critical for adult hippocampal GABA circuitry. *Nature Neuroscience* **12**: 1020-U1091.

Boutin C, Diestel S, Desoeuvre A, Tiveron MC, Cremer H. 2008. Efficient In Vivo Electroporation of the Postnatal Rodent Forebrain. *Plos One* **3**.

Boyer LA, Plath K, Zeitlinger J, Brambrink T, Medeiros LA, Lee TI, Levine SS, Wernig M, Tajonar A, Ray MK et al. 2006. Polycomb complexes repress developmental regulators in murine embryonic stem cells. *Nature* **441**: 349-353.

Bracken AP, Dietrich N, Pasini D, Hansen KH, Helin K. 2006. Genome-wide mapping of Polycomb target genes unravels their roles in cell fate transitions. *Genes Dev* **20**: 1123-1136.

Brockdorff N. 2013. Noncoding RNA and Polycomb recruitment. *RNA*.

Buffo A, Rite I, Tripathi P, Lepier A, Colak D, Horn AP, Mori T, Gotz M. 2008. Origin and progeny of reactive gliosis: A source of multipotent cells in the injured brain. *Proc Natl Acad Sci U S A* **105**: 3581-3586.

Buffo A, Rolando C, Ceruti S. 2010. Astrocytes in the damaged brain: molecular and cellular insights into their reactive response and healing potential. *Biochem Pharmacol* **79**: 77-89.

Buffo A, Vosko MR, Erturk D, Hamann GF, Jucker M, Rowitch D, Gotz M. 2005. Expression pattern of the transcription factor Olig2 in response to brain injuries: implications for neuronal repair. *Proc Natl Acad Sci U S A* **102**: 18183-18188.

Burch JBE. 2005. Regulation of GATA gene expression during vertebrate development. *Semin Cell Dev Biol* **16**: 71-81.

Cai J, Chen Y, Cai WH, Hurlock EC, Wu H, Kernie SG, Parada LF, Lu QR. 2007. A crucial role for Olig2 in white matter astrocyte development. *Development* **134**: 1887-1899.

Cao Q, Wang X, Zhao M, Yang R, Malik R, Qiao Y, Poliakov A, Yocum AK, Li Y, Chen W et al. 2014. The central role of EED in the orchestration of polycomb group complexes. *Nat Commun* **5**: 3127.

Carlen M, Meletis K, Goritz C, Darsalia V, Evergren E, Tanigaki K, Amendola M, Barnabe-Heider F, Yeung MS, Naldini L et al. 2009. Forebrain ependymal cells are Notch-dependent and generate neuroblasts and astrocytes after stroke. *Nat Neurosci* **12**: 259-267.

Castello A, Horos R, Strein C, Fischer B, Eichelbaum K, Steinmetz LM, Krijgsveld J, Hentze MW. 2013. System-wide identification of RNA-binding proteins by interactome capture. *Nature Protocols* **8**: 491-500.

Cerase A, Smeets D, Tang YA, Gdula M, Kraus F, Spivakov M, Moindrot B, Leleu M, Tattermusch A, Demmerle J et al. 2014. Spatial separation of Xist RNA and polycomb proteins revealed by superresolution microscopy. *Proc Natl Acad Sci U S A*.

Cesana M, Cacchiarelli D, Legnini I, Santini T, Sthandier O, Chinappi M, Tramontano A, Bozzoni I. 2011. A long noncoding RNA controls muscle differentiation by functioning as a competing endogenous RNA. *Cell* **147**: 358-369.

Chalei V, Sansom SN, Kong LS, Lee S, Montiel J, Vance KW, Ponting CP. 2014. The long non-coding RNA Dali is an epigenetic regulator of neural differentiation. *eLife* **3**.

Chamberlain SJ, Yee D, Magnuson T. 2008. Polycomb repressive complex 2 is dispensable for maintenance of embryonic stem cell pluripotency. *Stem Cells* **26**: 1496-1505.

Chan KM, Fang D, Gan H, Hashizume R, Yu C, Schroeder M, Gupta N, Mueller S, James CD, Jenkins R et al. 2013. The histone H3.3K27M mutation in pediatric glioma reprograms H3K27 methylation and gene expression. *Genes Dev*.

Charron F, Stein E, Jeong J, McMahon AP, Tessier-Lavigne M. 2003. The morphogen sonic hedgehog is an axonal chemoattractant that collaborates with netrin-1 in midline axon guidance. *Developmental Biology* **259**: 518-518.

Chen LP, Li ZF, Ping M, Li R, Liu J, Xie XH, Song XJ, Guo L. 2012. Regulation of Olig2 during astroglial differentiation in the subventricular zone of a cuprizone-induced demyelination mouse model. *Neuroscience* **221**: 96-107.

Chen YC, Xie D, Li WY, Cheung CM, Yao H, Chan CY, Chan CY, Xu FP, Liu YH, Sung JJY et al. 2010. RNAi targeting EZH2 inhibits tumor growth and liver metastasis of pancreatic cancer in vivo. *Cancer letters* **297**: 109-116.

Chesler AT, Le Pichon CE, Brann JH, Araneda RC, Zou DJ, Firestein S. 2008. Selective gene expression by postnatal electroporation during olfactory interneuron nurogenesis. *Plos One* **3**: e1517.

Cheung TH, Rando TA. 2013. Molecular regulation of stem cell quiescence. *Nat Rev Mol Cell Biol* **14**: 329-340.

Cho EG, Zaremba JD, McKercher SR, Talantova M, Tu SC, Masliah E, Chan SF, Nakanishi N, Terskikh A, Lipton SA. 2011. MEF2C Enhances Dopaminergic Neuron Differentiation of Human Embryonic Stem Cells in a Parkinsonian Rat Model. *Plos One* **6**.

Christopherson KS, Ullian EM, Stokes CC, Mullowney CE, Hell JW, Agah A, Lawler J, Mosher DF, Bornstein P, Barres BA. 2005. Thrombospondins are astrocyte-secreted proteins that promote CNS synaptogenesis. *Cell* **120**: 421-433.

Codega P, Silva-Vargas V, Paul A, Maldonado-Soto AR, Deleo AM, Pastrana E, Doetsch F. 2014. Prospective identification and purification of quiescent adult neural stem cells from their in vivo niche. *Neuron* **82**: 545-559.

Cohen AS, Tuysuz B, Shen Y, Bhalla SK, Jones SJ, Gibson WT. 2015. A novel mutation in EED associated with overgrowth. *J Hum Genet*.

Colak D, Mori T, Brill MS, Pfeifer A, Falk S, Deng C, Monteiro R, Mummery C, Sommer L, Gotz M. 2008. Adult neurogenesis requires Smad4-mediated bone morphogenic protein signaling in stem cells. *J Neurosci* **28**: 434-446.

Collas P. 2010. The current state of chromatin immunoprecipitation. *Molecular biotechnology* **45**: 87-100.

Comte I, Kim Y, Young CC, van der Harg JM, Hockberger P, Bolam PJ, Poirier F, Szele FG. 2011. Galectin-3 maintains cell motility from the subventricular zone to the olfactory bulb. *J Cell Sci* **124**: 2438-2447.

Cooper S, Brockdorff N. 2013. Genome-wide shRNA screening to identify factors mediating Gata6 repression in mouse embryonic stem cells. *Development* **140**: 4110-4115.

Curtis MA, Kam M, Nannmark U, Anderson MF, Axell MZ, Wikkelso C, Holtas S, van Roon-Mom WM, Bjork-Eriksson T, Nordborg C et al. 2007. Human neuroblasts migrate to the olfactory bulb via a lateral ventricular extension. *Science* **315**: 1243-1249.

Davidovic L, Durand N, Khalfallah O, Tabet R, Barbry P, Mari B, Sacconi S, Moine H, Bardoni B. 2013. A novel role for the RNA-binding protein FXR1P in myoblasts cell-cycle progression by modulating p21/Cdkn1a/Cip1/Waf1 mRNA stability. *PLoS Genet* **9**: e1003367.

Davila JL, Goff LA, Ricupero CL, Camarillo C, Oni EN, Swerdel MR, Toro-Ramos AJ, Li JL, Hart RP. 2014. A Positive Feedback Mechanism That Regulates Expression of miR-9 during Neurogenesis. *Plos One* **9**.

De la Rossa A, Bellone C, Golding B, Vitali I, Moss J, Toni N, Luscher C, Jabaudon D. 2013. In vivo reprogramming of circuit connectivity in postmitotic neocortical neurons. *Nat Neurosci* **16**: 193-200.

Decarolis NA, Mechanic M, Petrik D, Carlton A, Ables JL, Malhotra S, Bachoo R, Gotz M, Lagace DC, Eisch AJ. 2013. In vivo contribution of nestin- and GLAST-lineage cells to adult hippocampal neurogenesis. *Hippocampus*.

Delgado AC, Ferron SR, Vicente D, Porlan E, Perez-Villalba A, Trujillo CM, P DO, Farinas I. 2014. Endothelial NT-3 Delivered by Vasculature and CSF Promotes Quiescence of Subependymal Neural Stem Cells through Nitric Oxide Induction. *Neuron*.

Derrien T, Johnson R, Bussotti G, Tanzer A, Djebali S, Tilgner H, Guernec G, Martin D, Merkel A, Knowles DG et al. 2012. The GENCODE v7 catalog of human long noncoding RNAs: Analysis of their gene structure, evolution, and expression. *Genome Res* **22**: 1775-1789.

Devaraju K, Barnabe-Heider F, Kokaia Z, Lindvall O. 2013. FoxJ1-expressing cells contribute to neurogenesis in forebrain of adult rats: evidence from in vivo electroporation combined with piggyBac transposon. *Experimental cell research* **319**: 2790-2800.

Di Meglio T, Kratochwil CF, Vilain N, Loche A, Vitobello A, Yonehara K, Hrycaj SM, Roska B, Peters AH, Eichmann A et al. 2013. Ezh2 orchestrates topographic migration and connectivity of mouse precerebellar neurons. *Science* **339**: 204-207.

Ding DF, Xu LQ, Xu H, Li XF, Liang QQ, Zhao YJ, Wang YJ. 2014. Mash1 efficiently reprograms rat astrocytes into neurons. *Neural Regen Res* **9**: 25-32.

Dinger ME, Pang KC, Mercer TR, Mattick JS. 2008. Differentiating protein-coding and noncoding RNA: challenges and ambiguities. *PLoS Comput Biol* **4**: e1000176.

Dizon ML, Shin L, Sundholm-Peters NL, Kang E, Szele FG. 2006. Subventricular zone cells remain stable in vitro after brain injury. *Neuroscience* **142**: 717-725.

Doetsch F, Garcia-Verdugo JM, Alvarez-Buylla A. 1999. Regeneration of a germinal layer in the adult mammalian brain. *Proc Natl Acad Sci U S A* **96**: 11619-11624.

Egan CM, Nyman U, Skotte J, Streubel G, Turner S, O'Connell DJ, Rraklli V, Dolan MJ, Chadderton N, Hansen K et al. 2013. CHD5 is required for neurogenesis and has a dual role in facilitating gene expression and polycomb gene repression. *Dev Cell* **26**: 223-236.

Endoh M, Endo TA, Endoh T, Isono K, Sharif J, Ohara O, Toyoda T, Ito T, Eskeland R, Bickmore WA et al. 2012. Histone H2A mono-ubiquitination is a crucial step to mediate PRC1-dependent repression of developmental genes to maintain ES cell identity. *PLoS Genet* **8**: e1002774.

Ernst A, Alkass K, Bernard S, Salehpour M, Perl S, Tisdale J, Possnert G, Druid H, Frisen J. 2014. Neurogenesis in the Striatum of the Adult Human Brain. *Cell*.

Eskeland R, Freyer E, Leeb M, Wutz A, Bickmore WA. 2010a. Histone acetylation and the maintenance of chromatin compaction by Polycomb repressive complexes. *Cold Spring Harb Symp Quant Biol* **75**: 71-78.

Eskeland R, Leeb M, Grimes GR, Kress C, Boyle S, Sproul D, Gilbert N, Fan Y, Skoultchi AI, Wutz A et al. 2010b. Ring1B compacts chromatin structure and represses gene expression independent of histone ubiquitination. *Mol Cell* **38**: 452-464.

Ezhkova E, Lien WH, Stokes N, Pasolli HA, Silva JM, Fuchs E. 2011. EZH1 and EZH2 cogovern histone H3K27 trimethylation and are essential for hair follicle homeostasis and wound repair. *Genes Dev* **25**: 485-498.

Ezhkova E, Pasolli HA, Parker JS, Stokes N, Su IH, Hannon G, Tarakhovsky A, Fuchs E. 2009. Ezh2 orchestrates gene expression for the stepwise differentiation of tissue-specific stem cells. *Cell* **136**: 1122-1135.

Falcao AM, Marques F, Novais A, Sousa N, Palha JA, Sousa JC. 2012. The path from the choroid plexus to the subventricular zone: go with the flow! *Front Cell Neurosci* **6**.

Farcas AM, Blackledge NP, Sudbery I, Long HK, McGouran JF, Rose NR, Lee S, Sims D, Cerase A, Sheahan TW et al. 2012. KDM2B links the Polycomb Repressive Complex 1 (PRC1) to recognition of CpG islands. *eLife* **1**: e00205.

Fasano CA, Dimos JT, Ivanova NB, Lowry N, Lemischka IR, Temple S. 2007. shRNA knockdown of Bmi-1 reveals a critical role for p21-Rb pathway in NSC self-renewal during development. *Cell Stem Cell* **1**: 87-99.

Fasano CA, Phoenix TN, Kokovay E, Lowry N, Elkabetz Y, Dimos JT, Lemischka IR, Studer L, Temple S. 2009. Bmi-1 cooperates with Foxg1 to maintain neural stem cell self-renewal in the forebrain. *Genes Dev* **23**: 561-574.

Favaro R, Valotta M, Ferri ALM, Latorre E, Mariani J, Giachino C, Lancini C, Tosetti V, Ottolenghi S, Taylor V et al. 2009. Hippocampal development and neural stem cell maintenance require Sox2-dependent regulation of Shh. *Nature Neuroscience* **12**: 1248-U1262.

Federation AJ, Bradner JE, Meissner A. 2014. The use of small molecules in somatic-cell reprogramming. *Trends in Cell Biology* **24**: 179-187.

Feliciano DM, Edelman AM. 2009. Repression of Ca2+/calmodulin-dependent protein kinase IV signaling accelerates retinoic acid-induced differentiation of human neuroblastoma cells. *J Biol Chem* **284**: 26466-26481.

Feliciano DM, Zhang S, Quon JL, Bordey A. 2013. Hypoxia-inducible factor 1a is a Tsc1-regulated survival factor in newborn neurons in tuberous sclerosis complex. *Hum Mol Genet* **22**: 1725-1734.

Feng JC, Bi CM, Clark BS, Mady R, Shah P, Kohtz JD. 2006. The Evf-2 noncoding RNA is transcribed from the Dlx-5/6 ultraconserved region and functions as a Dlx-2 transcriptional coactivator. *Gene Dev* **20**: 1470-1484.

Feng W, Khan MA, Bellvis P, Zhu Z, Bernhardt O, Herold-Mende C, Liu HK. 2013. The Chromatin Remodeler CHD7 Regulates Adult Neurogenesis via Activation of SoxC Transcription Factors. *Cell Stem Cell* **13**: 62-72.

Feng W, Liu HK. 2013. Epigenetic regulation of neuronal fate determination: the role of CHD7. *Cell Cycle* **12**: 3707-3708.

Ferent J, Cochard L, Faure H, Taddei M, Hahn H, Ruat M, Traiffort E. 2014. Genetic activation of hedgehog signaling unbalances the rate of neural stem cell renewal by increasing symmetric divisions. *Stem cell reports* **3**: 312-323.

Fernandez ME, Croce S, Boutin C, Cremer H, Raineteau O. 2011. Targeted electroporation of defined lateral ventricular walls: a novel and rapid method to study fate specification during postnatal forebrain neurogenesis. *Neural Dev* **6**.

Fernando RN, Eleuteri B, Abdelhady S, Nussenzweig A, Andang M, Ernfors P. 2011. Cell cycle restriction by histone H2AX limits proliferation of adult neural stem cells. *Proc Natl Acad Sci U S A* **108**: 5837-5842.

Ferrari KJ, Scelfo A, Jammula S, Cuomo A, Barozzi I, Stutzer A, Fischle W, Bonaldi T, Pasini D. 2014. Polycomb-dependent H3K27me1 and H3K27me2 regulate active transcription and enhancer fidelity. *Mol Cell* **53**: 49-62.

Ferraro A, Boni T, Pintzas A. 2014. EZH2 regulates cofilin activity and colon cancer cell migration by targeting ITGA2 gene. *Plos One* **9**: e115276.

Ferron SR, Andreu-Agullo C, Mira H, Sanchez P, Marques-Torrejon MA, Farinas I. 2007. A combined ex/in vivo assay to detect effects of exogenously added factors in neural stem cells. *Nat Protoc* **2**: 849-859.

Fluge O, Gravdal K, Carlsen E, Vonen B, Kjellevold K, Refsum S, Lilleng R, Eide TJ, Halvorsen TB, Tveit KM et al. 2009. Expression of EZH2 and Ki-67 in colorectal cancer and associations with treatment response and prognosis. *Brit J Cancer* **101**: 1282-1289.

Franco SJ, Martinez-Garay I, Gil-Sanz C, Harkins-Perry SR, Muller U. 2011. Reelin regulates cadherin function via Dab1/Rap1 to control neuronal migration and lamination in the neocortex. *Neuron* **69**: 482-497.

Freeman MR. 2010. Specification and morphogenesis of astrocytes. *Science* **330**: 774-778.

Funato K, Major T, Lewis PW, Allis CD, Tabar V. 2014. Use of human embryonic stem cells to model pediatric gliomas with H3.3K27M histone mutation. *Science* **346**: 1529-1533.

Furutachi S, Miya H, Watanabe T, Kawai H, Yamasaki N, Harada Y, Imayoshi I, Nelson M, Nakayama KI, Hirabayashi Y et al. 2015. Slowly dividing neural progenitors are an embryonic origin of adult neural stem cells. *Nat Neurosci* **18**: 657-665.

Fussbroich B, Wagener N, Macher-Goeppinger S, Benner A, Falth M, Sultmann H, Holzer A, Hoppe-Seyler K, Hoppe-Seyler F. 2011. EZH2 Depletion Blocks the Proliferation of Colon Cancer Cells. *Plos One* **6**.

Gaj T, Gersbach CA, Barbas CF, 3rd. 2013. ZFN, TALEN, and CRISPR/Cas-based methods for genome engineering. *Trends in biotechnology* **31**: 397-405.

Garcia-Moreno F, Vasistha NA, Begbie J, Molnar Z. 2014. CLoNe is a new method to target single progenitors and study their progeny in mouse and chick. *Development* **141**: 1589-1598.

Ge WP, Miyawaki A, Gage FH, Jan YN, Jan LY. 2012. Local generation of glia is a major astrocyte source in postnatal cortex. *Nature*.

Gerstberger S, Hafner M, Tuschl T. 2014. A census of human RNA-binding proteins. *Nat Rev Genet* **15**: 829-845.

Ghashghaei HT, Lai C, Anton ES. 2007. Neuronal migration in the adult brain: are we there yet? *Nat Rev Neurosci* **8**: 141-151.

Giachino C, Basak O, Lugert S, Knuckles P, Obernier K, Fiorelli R, Frank S, Raineteau O, Alvarez-Buylla A, Taylor V. 2013. Molecular diversity subdivides the adult forebrain neural stem cell population. *Stem Cells*.

Gibson WT, Hood RL, Zhan SH, Bulman DE, Fejes AP, Moore R, Mungall AJ, Eydoux P, Babul-Hirji R, An J et al. 2012. Mutations in EZH2 cause Weaver syndrome. *American journal of human genetics* **90**: 110-118.

Gil J, O'Loghlen A. 2014. PRC1 complex diversity: where is it taking us? *Trends Cell Biol*.

Gilfillan GD, Hughes T, Sheng Y, Hjorthaug HS, Straub T, Gervin K, Harris JR, Undlien DE, Lyle R. 2012. Limitations and possibilities of low cell number ChIP-seq. *BMC genomics* **13**: 645.

Gleason D, Fallon JH, Guerra M, Liu JC, Bryant PJ. 2008. Ependymal stem cells divide asymmetrically and transfer progeny into the subventricular zone when activated by injury. *Neuroscience* **156**: 81-88.

Goings GE, Sahni V, Szele FG. 2004. Migration patterns of subventricular zone cells in adult mice change after cerebral cortex injury. *Brain Res* **996**: 213-226.

Goings GE, Wibisono BL, Szele FG. 2002. Cerebral cortex lesions decrease the number of bromodeoxyuridine-positive subventricular zone cells in mice. *Neurosci Lett* **329**: 161-164.

Goldberg AD, Allis CD, Bernstein E. 2007. Epigenetics: a landscape takes shape. *Cell* **128**: 635-638.

Goll MG, Bestor TH. 2005. Eukaryotic cytosine methyltransferases. *Annu Rev Biochem* **74**: 481-514.

Gomez D, Shankman LS, Nguyen AT, Owens GK. 2013. Detection of histone modifications at specific gene loci in single cells in histological sections. *Nat Methods*.

Gotts JE, Chesselet MF. 2005. Mechanisms of subventricular zone expansion after focal cortical ischemic injury. *J Comp Neurol* **488**: 201-214.

Grande A, Sumiyoshi K, Lopez-Juarez A, Howard J, Sakthivel B, Aronow B, Campbell K, Nakafuku M. 2013. Environmental impact on direct neuronal reprogramming in vivo in the adult brain. *Nat Commun* **4**: 2373.

Grimaud C, Negre N, Cavalli G. 2006. From genetics to epigenetics: the tale of Polycomb group and trithorax group genes. *Chromosome research : an international journal on the molecular, supramolecular and evolutionary aspects of chromosome biology* **14**: 363-375.

Grote P, Wittler L, Hendrix D, Koch F, Wahrisch S, Beisaw A, Macura K, Blass G, Kellis M, Werber M et al. 2013. The Tissue-Specific lncRNA Fendrr Is an Essential Regulator of Heart and Body Wall Development in the Mouse. *Developmental Cell* **24**: 206-214.

Guibert S, Weber M. 2013. Functions of DNA Methylation and Hydroxymethylation in Mammalian Development. *Epigenetics and Development* **104**: 47-83.

Gunawan M, Venkatesan N, Loh JT, Wong JF, Berger H, Neo WH, Li LY, La Win MK, Yau YH, Guo T et al. 2015. The methyltransferase Ezh2 controls cell adhesion and migration through direct methylation of the extranuclear regulatory protein talin. *Nat Immunol* **16**: 505-516.

Guo Z, Zhang L, Wu Z, Chen Y, Wang F, Chen G. 2013. In Vivo Direct Reprogramming of Reactive Glial Cells into Functional Neurons after Brain Injury and in an Alzheimer's Disease Model. *Cell Stem Cell*.

Gupta N, Hashizume R, Andor N, Zhang ZG, Petritsch C, Mueller S, James CD. 2014. Biologically-Based Therapeutics for the Treatment of Diffuse Intrinsic Pontine Gliomas. *Neuro-Oncology* **16**.

Hack MA, Saghatelyan A, de Chevigny A, Pfeifer A, Ashery-Padan R, Lledo PM, Gotz M. 2005. Neuronal fate determinants of adult olfactory bulb neurogenesis. *Nat Neurosci* **8**: 865-872.

Hack MA, Sugimori M, Lundberg C, Nakafuku M, Gotz M. 2004. Regionalization and fate specification in neurospheres: the role of Olig2 and Pax6. *Mol Cell Neurosci* **25**: 664-678.

Hagey DW, Muhr J. 2014. Sox2 Acts in a Dose-Dependent Fashion to Regulate Proliferation of Cortical Progenitors. *Cell reports*.

Hahn MA, Qiu R, Wu X, Li AX, Zhang H, Wang J, Jui J, Jin SG, Jiang Y, Pfeifer GP et al. 2013. Dynamics of 5-hydroxymethylcytosine and chromatin marks in Mammalian neurogenesis. *Cell reports* **3**: 291-300.

Hampton DW, Asher RA, Kondo T, Steeves JD, Ramer MS, Fawcett JW. 2007. A potential role for bone morphogenetic protein signalling in glial cell fate determination following adult central nervous system injury in vivo. *Eur J Neurosci* **26**: 3024-3035.

Han L, Zhang K, Shi Z, Zhang J, Zhu J, Zhu S, Zhang A, Jia Z, Wang G, Yu S et al. 2012. LncRNA pro fi le of glioblastoma reveals the potential role of lncRNAs in contributing to glioblastoma pathogenesis. *International journal of oncology* **40**: 2004-2012.

Hartman NW, Lin TV, Zhang L, Paquelet GE, Feliciano DM, Bordey A. 2013. mTORC1 targets the translational repressor 4E-BP2, but not S6 kinase 1/2, to regulate neural stem cell self-renewal in vivo. *Cell reports* **5**: 433-444.

Hayashi-Takanaka Y, Yamagata K, Wakayama T, Stasevich TJ, Kainuma T, Tsurimoto T, Tachibana M, Shinkai Y, Kurumizaka H, Nozaki N et al. 2011. Tracking epigenetic histone modifications in single cells using Fab-based live endogenous modification labeling. *Nucleic Acids Res* **39**: 6475-6488.

He A, Shen X, Ma Q, Cao J, von Gise A, Zhou P, Wang G, Marquez VE, Orkin SH, Pu WT. 2012. PRC2 directly methylates GATA4 and represses its transcriptional activity. *Genes Dev* **26**: 37-42.

He S, Iwashita T, Buchstaller J, Molofsky AV, Thomas D, Morrison SJ. 2009a. Bmi-1 over-expression in neural stem/progenitor cells increases proliferation

and neurogenesis in culture but has little effect on these functions in vivo. *Dev Biol* **328**: 257-272.

He S, Nakada D, Morrison SJ. 2009b. Mechanisms of stem cell self-renewal. *Annual review of cell and developmental biology* **25**: 377-406.

Heinrich C, Bergami M, Gascon S, Lepier A, Vigano F, Dimou L, Sutor B, Berninger B, Gotz M. 2014. Sox2-Mediated Conversion of NG2 Glia into Induced Neurons in the Injured Adult Cerebral Cortex. *Stem cell reports* **3**: 1000-1014.

Hendrich BD, Brown CJ, Willard HF. 1993. Evolutionary conservation of possible functional domains of the human and murine XIST genes. *Hum Mol Genet* **2**: 663-672.

Hennig L, Derkacheva M. 2009. Diversity of Polycomb group complexes in plants: same rules, different players? *Trends in genetics : TIG* **25**: 414-423.

Hirabayashi Y, Suzki N, Tsuboi M, Endo TA, Toyoda T, Shinga J, Koseki H, Vidal M, Gotoh Y. 2009. Polycomb limits the neurogenic competence of neural precursor cells to promote astrogenic fate transition. *Neuron* **63**: 600-613.

Hou P, Li Y, Zhang X, Liu C, Guan J, Li H, Zhao T, Ye J, Yang W, Liu K et al. 2013. Pluripotent stem cells induced from mouse somatic cells by small-molecule compounds. *Science* **341**: 651-654.

Huang X, Dubuc AM, Hashizume R, Berg J, He Y, Wang J, Chiang C, Cooper MK, Northcott PA, Taylor MD et al. 2012. Voltage-gated potassium channel EAG2 controls mitotic entry and tumor growth in medulloblastoma via regulating cell volume dynamics. *Genes Dev* **26**: 1780-1796.

Huttner HB, Bergmann O, Salehpour M, Racz A, Tatarishvili J, Lindgren E, Csonka T, Csiba L, Hortobagyi T, Mehes G et al. 2014. The age and genomic integrity of neurons after cortical stroke in humans. *Nat Neurosci* **17**: 801-803.

Hwang WW, Salinas RD, Siu JJ, Kelley KW, Delgado RN, Paredes MF, Alvarez-Buylla A, Oldham MC, Lim DA. 2014. Distinct and separable roles for EZH2 in neurogenic astroglia. *eLife* **3**: e02439.

Ihrie RA, Alvarez-Buylla A. 2011. Lake-front property: a unique germinal niche by the lateral ventricles of the adult brain. *Neuron* **70**: 674-686.

Inta D, Gass P. 2015. Is forebrain neurogenesis a potential repair mechanism after stroke? *J Cereb Blood Flow Metab*.

Jablonska B, Aguirre A, Vandenbosch R, Belachew S, Berthet C, Kaldis P, Gallo V. 2007. Cdk2 is critical for proliferation and self-renewal of neural

progenitor cells in the adult subventricular zone. *J Cell Biol* **179**: 1231-1245.

Jackson EL, Garcia-Verdugo JM, Gil-Perotin S, Roy M, Quinones-Hinojosa A, VandenBerg S, Alvarez-Buylla A. 2006. PDGFR alpha-positive B cells are neural stem cells in the adult SVZ that form glioma-like growths in response to increased PDGF signaling. *Neuron* **51**: 187-199.

Jacquet BV, Salinas-Mondragon R, Liang H, Therit B, Buie JD, Dykstra M, Campbell K, Ostrowski LE, Brody SL, Ghashghaei HT. 2009. FoxJ1-dependent gene expression is required for differentiation of radial glia into ependymal cells and a subset of astrocytes in the postnatal brain. *Development* **136**: 4021-4031.

James R, Kim Y, Hockberger PE, Szele FG. 2011. Subventricular zone cell migration: lessons from quantitative two-photon microscopy. *Front Neurosci* **5**: 30.

Jang ES, Goldman JE. 2011. Pax6 Expression Is Sufficient to Induce a Neurogenic Fate in Glial Progenitors of the Neonatal Subventricular Zone. *Plos One* **6**.

Jiang Y, Hsieh J. 2014. HDAC3 controls gap 2/mitosis progression in adult neural stem/progenitor cells by regulating CDK1 levels. *Proc Natl Acad Sci U S A* **111**: 13541-13546.

Jiang Y, Zhang M, Qian Y, Xu E, Zhang J, Chen X. 2014. Rbm24, an RNA-binding protein and a target of p53, regulates p21 expression via mRNA stability. *J Biol Chem* **289**: 3164-3175.

Jin KL, Wang XM, Xie L, Mao XO, Zhu W, Wang Y, Shen JF, Mao Y, Banwait S, Greenberg DA. 2006. Evidence for stroke-induced neurogenesis in the human brain. *P Natl Acad Sci USA* **103**: 13198-13202.

Juan AH, Kumar RM, Marx JG, Young RA, Sartorelli V. 2009. Mir-214-dependent regulation of the polycomb protein Ezh2 in skeletal muscle and embryonic stem cells. *Mol Cell* **36**: 61-74.

Julian LM, Vandenbosch R, Pakenham CA, Andrusiak MG, Nguyen AP, McClellan KA, Svoboda DS, Lagace DC, Park DS, Leone G et al. 2013. Opposing regulation of Sox2 by cell-cycle effectors E2f3a and E2f3b in neural stem cells. *Cell Stem Cell* **12**: 440-452.

Jung HY, Jun S, Lee M, Kim HC, Wang X, Ji H, McCrea PD, Park JI. 2013. PAF and EZH2 Induce Wnt/beta-Catenin Signaling Hyperactivation. *Mol Cell* **52**: 193-205.

Kalb R, Latwiel S, Baymaz HI, Jansen PW, Muller CW, Vermeulen M, Muller J. 2014. Histone H2A monoubiquitination promotes histone H3 methylation in Polycomb repression. *Nat Struct Mol Biol* **21**: 569-571.

Kamakaka RT, Biggins S. 2005. Histone variants: deviants? *Genes Dev* **19**: 295-310.

Kamao H, Mandai M, Okamoto S, Sakai N, Suga A, Sugita S, Kiryu J, Takahashi M. 2014. Characterization of human induced pluripotent stem cell-derived retinal pigment epithelium cell sheets aiming for clinical application. *Stem cell reports* **2**: 205-218.

Kamnasaran D, Qian B, Hawkins C, Stanford WL, Guha A. 2007. GATA6 is an astrocytoma tumor suppressor gene identified by gene trapping of mouse glioma model. *Proc Natl Acad Sci U S A* **104**: 8053-8058.

Kanduri C. 2011. Kcnq1ot1: a chromatin regulatory RNA. *Semin Cell Dev Biol* **22**: 343-350.

Kaneko S, Bonasio R, Saldana-Meyer R, Yoshida T, Son J, Nishino K, Umezawa A, Reinberg D. 2013. Interactions between JARID2 and Noncoding RNAs Regulate PRC2 Recruitment to Chromatin. *Mol Cell*.

Kaneko Y, Sakakibara S, Imai T, Suzuki A, Nakamura Y, Sawamoto K, Ogawa Y, Toyama Y, Miyata T, Okano H. 2000. Musashi1: an evolutionally conserved marker for CNS progenitor cells including neural stem cells. *Dev Neurosci* **22**: 139-153.

Kang SS, Kook JH, Hwang S, Park SH, Nam SC, Kim JK. 2008. Inhibition of matrix metalloproteinase-9 attenuated neural progenitor cell migration after photothrombotic ischemia. *Brain Res* **1228**: 20-26.

Kaslin J, Ganz J, Brand M. 2008. Proliferation, neurogenesis and regeneration in the non-mammalian vertebrate brain. *Philosophical transactions of the Royal Society of London Series B, Biological sciences* **363**: 101-122.

Kawaguchi D, Furutachi S, Kawai H, Hozumi K, Gotoh Y. 2013. Dll1 maintains quiescence of adult neural stem cells and segregates asymmetrically during mitosis. *Nat Commun* **4**: 1880.

Khuong-Quang DA, Buczkowicz P, Rakopoulos P, Liu XY, Fontebasso AM, Bouffet E, Bartels U, Albrecht S, Schwartzentruber J, Letourneau L et al. 2012. K27M mutation in histone H3.3 defines clinically and biologically distinct subgroups of pediatric diffuse intrinsic pontine gliomas. *Acta Neuropathol* **124**: 439-447.

Kim DH, Marinov GK, Pepke S, Singer ZS, He P, Williams B, Schroth GP, Elowitz MB, Wold BJ. 2015. Single-Cell Transcriptome Analysis Reveals Dynamic Changes in lncRNA Expression during Reprogramming. *Cell Stem Cell* **16**: 88-101.

Kim H, Kim JS. 2014. A guide to genome engineering with programmable nucleases. *Nat Rev Genet* **15**: 321-334.

Kim W, Bird GH, Neff T, Guo G, Kerenyi MA, Walensky LD, Orkin SH. 2013. Targeted disruption of the EZH2-EED complex inhibits EZH2-dependent cancer. *Nature chemical biology*.

Kim Y, Comte I, Szabo G, Hockberger P, Szele FG. 2009. Adult mouse subventricular zone stem and progenitor cells are sessile and epidermal growth factor receptor negatively regulates neuroblast migration. *Plos One* **4**: e8122.

Kim Y, Szele FG. 2008. Activation of subventricular zone stem cells after neuronal injury. *Cell Tissue Res* **331**: 337-345.

Kimura H, Hayashi-Takanaka Y, Yamagata K. 2010. Visualization of DNA methylation and histone modifications in living cells. *Curr Opin Cell Biol* **22**: 412-418.

Kipp M, Clarner T, Dang J, Copray S, Beyer C. 2009. The cuprizone animal model: new insights into an old story. *Acta Neuropathol* **118**: 723-736.

Kippin TE, Martens DJ, van der Kooy D. 2005. p21 loss compromises the relative quiescence of forebrain stem cell proliferation leading to exhaustion of their proliferation capacity. *Genes Dev* **19**: 756-767.

Kizil C, Kyritsis N, Dudczig S, Kroehne V, Freudenreich D, Kaslin J, Brand M. 2012. Regenerative neurogenesis from neural progenitor cells requires injury-induced expression of Gata3. *Dev Cell* **23**: 1230-1237.

Kleer CG, Cao Q, Varambally S, Shen RL, Ota L, Tomlins SA, Ghosh D, Sewalt RGAB, Otte AP, Hayes DF et al. 2003. EZH2 is a marker of aggressive breast cancer and promotes neoplastic transformation of breast epithelial cells. *P Natl Acad Sci USA* **100**: 11606-11611.

Knutson SK, Wigle TJ, Warholic NM, Sneeringer CJ, Allain CJ, Klaus CR, Sacks JD, Raimondi A, Majer CR, Song J et al. 2012. A selective inhibitor of EZH2 blocks H3K27 methylation and kills mutant lymphoma cells. *Nature chemical biology* **8**: 890-896.

Kohli RM, Zhang Y. 2013. TET enzymes, TDG and the dynamics of DNA demethylation. *Nature* **502**: 472-479.

Kohwi M, Osumi N, Rubenstein JLR, Alvarez-Buylla A. 2005. Pax6 is required for making specific subpopulations of granule and periglomerular neurons in the olfactory bulb. *Journal of Neuroscience* **25**: 6997-7003.

Kojima T, Hirota Y, Ema M, Takahashi S, Miyoshi I, Okano H, Sawamoto K. 2010. Subventricular zone-derived neural progenitor cells migrate along a

blood vessel scaffold toward the post-stroke striatum. *Stem Cells* **28**: 545-554.

Koketsu D, Furuichi Y, Maeda M, Matsuoka N, Miyamoto Y, Hisatsune T. 2006. Increased number of new neurons in the olfactory bulb and hippocampus of adult non-human primates after focal ischemia. *Exp Neurol* **199**: 92-102.

Kottakis F, Polytarchou C, Foltopoulou P, Sanidas I, Kampranis SC, Tsichlis PN. 2011. FGF-2 regulates cell proliferation, migration, and angiogenesis through an NDY1/KDM2B-miR-101-EZH2 pathway. *Mol Cell* **43**: 285-298.

Kouzarides T. 2007. Chromatin modifications and their function. *Cell* **128**: 693-705.

Kraus TFJ, Greiner A, Guibourt V, Lisec K, Kretzschmar HA. 2015. Identification of Stably Expressed lncRNAs as Valid Endogenous Controls for Profiling of Human Glioma. *J Cancer* **6**: 111-119.

Kriegstein A, Alvarez-Buylla A. 2009. The glial nature of embryonic and adult neural stem cells. *Annu Rev Neurosci* **32**: 149-184.

Kruidenier L, Chung CW, Cheng Z, Liddle J, Che K, Joberty G, Bantscheff M, Bountra C, Bridges A, Diallo H et al. 2012. A selective jumonji H3K27 demethylase inhibitor modulates the proinflammatory macrophage response. *Nature* **488**: 404-408.

Kunderfranco P, Mello-Grand M, Cangemi R, Pellini S, Mensah A, Albertini V, Malek A, Chiorino G, Catapano CV, Carbone GM. 2010. ETS transcription factors control transcription of EZH2 and epigenetic silencing of the tumor suppressor gene Nkx3.1 in prostate cancer. *Plos One* **5**: e10547.

Kuo CT, Mirzadeh Z, Soriano-Navarro M, Rasin M, Wang D, Shen J, Sestan N, Garcia-Verdugo J, Alvarez-Buylla A, Jan LY et al. 2006. Postnatal deletion of Numb/Numblike reveals repair and remodeling capacity in the subventricular neurogenic niche. *Cell* **127**: 1253-1264.

Lacar B, Young SZ, Platel JC, Bordey A. 2010. Imaging and recording subventricular zone progenitor cells in live tissue of postnatal mice. *Front Neurosci* **4**.

Lagace DC, Whitman MC, Noonan MA, Ables JL, DeCarolis NA, Arguello AA, Donovan MH, Fischer SJ, Farnbauch LA, Beech RD et al. 2007. Dynamic contribution of nestin-expressing stem cells to adult neurogenesis. *J Neurosci* **27**: 12623-12629.

Lander ES Linton LM Birren B Nusbaum C Zody MC Baldwin J Devon K Dewar K Doyle M FitzHugh W et al. 2001. Initial sequencing and analysis of the human genome. *Nature* **409**: 860-921.

Lavado A, Oliver G. 2011. Six3 is required for ependymal cell maturation. *Development* **138**: 5291-5300.

Lee DA, Bedont JL, Pak T, Wang H, Song J, Miranda-Angulo A, Takiar V, Charubhumi V, Balordi F, Takebayashi H et al. 2012. Tanycytes of the hypothalamic median eminence form a diet-responsive neurogenic niche. *Nat Neurosci* **15**: 700-702.

Lee SR, Kim HY, Rogowska J, Zhao BQ, Bhide P, Parent JM, Lo EH. 2006a. Involvement of matrix metalloproteinase in neuroblast cell migration from the subventricular zone after stroke. *J Neurosci* **26**: 3491-3495.

Lee TI, Jenner RG, Boyer LA, Guenther MG, Levine SS, Kumar RM, Chevalier B, Johnstone SE, Cole MF, Isono K et al. 2006b. Control of developmental regulators by Polycomb in human embryonic stem cells. *Cell* **125**: 301-313.

Lee W, Teckie S, Wiesner T, Ran L, Prieto Granada CN, Lin M, Zhu S, Cao Z, Liang Y, Sboner A et al. 2014. PRC2 is recurrently inactivated through EED or SUZ12 loss in malignant peripheral nerve sheath tumors. *Nat Genet* **46**: 1227-1232.

Leeb M, Pasini D, Novatchkova M, Jaritz M, Helin K, Wutz A. 2010. Polycomb complexes act redundantly to repress genomic repeats and genes. *Genes Dev* **24**: 265-276.

Lehtinen MK, Walsh CA. 2011. Neurogenesis at the brain-cerebrospinal fluid interface. *Annual review of cell and developmental biology* **27**: 653-679.

Lehtinen MK, Zappaterra MW, Chen X, Yang YJ, Hill AD, Lun M, Maynard T, Gonzalez D, Kim S, Ye P et al. 2011. The cerebrospinal fluid provides a proliferative niche for neural progenitor cells. *Neuron* **69**: 893-905.

Lein ES Hawrylycz MJ Ao N Ayres M Bensinger A Bernard A Boe AF Boguski MS Brockway KS Byrnes EJ et al. 2007. Genome-wide atlas of gene expression in the adult mouse brain. *Nature* **445**: 168-176.

Lessard J, Schumacher A, Thorsteinsdottir U, van Lohuizen M, Magnuson T, Sauvageau G. 1999. Functional antagonism of the Polycomb-Group genes eed and Bmi1 in hemopoietic cell proliferation. *Genes Dev* **13**: 2691-2703.

Lewis PW, Muller MM, Koletsky MS, Cordero F, Lin S, Banaszynski LA, Garcia BA, Muir TW, Becher OJ, Allis CD. 2013. Inhibition of PRC2 Activity by a Gain-of-Function H3 Mutation Found in Pediatric Glioblastoma. *Science*.

Li R, Qian J, Wang YY, Zhang JX, You YP. 2014. Long noncoding RNA profiles reveal three molecular subtypes in glioma. *CNS neuroscience & therapeutics* **20**: 339-343.

Liang Q, De Windt LJ, Witt SA, Kimball TR, Markham BE, Molkentin JD. 2001. The transcription factors GATA4 and GATA6 regulate cardiomyocyte hypertrophy in vitro and in vivo. *J Biol Chem* **276**: 30245-30253.

Lim DA, Cha S, Mayo MC, Chen MH, Keles E, VandenBerg S, Berger MS. 2007. Relationship of glioblastoma multiforme to neural stem cell regions predicts invasive and multifocal tumor phenotype. *Neuro Oncol* **9**: 424-429.

Lim DA, Huang YC, Swigut T, Mirick AL, Garcia-Verdugo JM, Wysocka J, Ernst P, Alvarez-Buylla A. 2009. Chromatin remodelling factor Mll1 is essential for neurogenesis from postnatal neural stem cells. *Nature* **458**: 529-533.

Lim DA, Tramontin AD, Trevejo JM, Herrera DG, Garcia-Verdugo JM, Alvarez-Buylla A. 2000. Noggin antagonizes BMP signaling to create a niche for adult neurogenesis. *Neuron* **28**: 713-726.

Lin CW, Jao CY, Ting AY. 2004. Genetically encoded fluorescent reporters of histone methylation in living cells. *J Am Chem Soc* **126**: 5982-5983.

Lin N, Dang J, Rana TM. 2015. Haunting the HOXA Locus: Two Faces of lncRNA Regulation. *Cell Stem Cell* **16**: 449-450.

Liu F, You Y, Li X, Ma T, Nie Y, Wei B, Li T, Lin H, Yang Z. 2009. Brain injury does not alter the intrinsic differentiation potential of adult neuroblasts. *J Neurosci* **29**: 5075-5087.

Liu L, Xu Z, Zhong L, Wang H, Jiang S, Long Q, Xu J, Guo J. 2014a. Enhancer of zeste homolog 2 (EZH2) promotes tumour cell migration and invasion via epigenetic repression of E-cadherin in renal cell carcinoma. *BJU international*.

Liu TP, Lo HL, Wei LS, Hao-Yun Hsiao H, Yang PM. 2014b. S-Adenosyl-L-methionine-competitive inhibitors of the histone methyltransferase EZH2 induce autophagy and enhance drug sensitivity in cancer cells. *Anti-cancer drugs*.

Liu XJ, Li F, Stubblefield EA, Blanchard B, Richards TL, Larson GA, He YJ, Huang Q, Tan AC, Zhang DB et al. 2012. Direct reprogramming of human fibroblasts into dopaminergic neuron-like cells. *Cell Research* **22**: 321-332.

Livet J, Weissman TA, Kang H, Draft RW, Lu J, Bennis RA, Sanes JR, Lichtman JW. 2007. Transgenic strategies for combinatorial expression of fluorescent proteins in the nervous system. *Nature* **450**: 56-62.

Logan TT, Villapol S, Symes AJ. 2013. TGF-beta superfamily gene expression and induction of the Runx1 transcription factor in adult neurogenic regions after brain injury. *Plos One* **8**: e59250.

Lopez-Juarez A, Remaud S, Hassani Z, Jolivet P, Pierre Simons J, Sontag T, Yoshikawa K, Price J, Morvan-Dubois G, Demeneix BA. 2012. Thyroid hormone signaling acts as a neurogenic switch by repressing Sox2 in the adult neural stem cell niche. *Cell Stem Cell* **10**: 531-543.

Loulier K, Barry R, Mahou P, Le Franc Y, Supatto W, Matho KS, Ieng S, Fouquet S, Dupin E, Benosman R et al. 2014. Multiplex cell and lineage tracking with combinatorial labels. *Neuron* **81**: 505-520.

Lowe SW, Sherr CJ. 2003. Tumor suppression by Ink4a-Arf: progress and puzzles. *Current opinion in genetics & development* **13**: 77-83.

Lund K, Adams PD, Copland M. 2014. EZH2 in normal and malignant hematopoiesis. *Leukemia* **28**: 44-49.

Lundberg J, Karimi M, von Gertten C, Holmin S, Ekstrom TJ, Sandberg-Nordqvist AC. 2009. Traumatic brain injury induces relocalization of DNA-methyltransferase 1. *Neurosci Lett* **457**: 8-11.

Lv X, Jiang H, Liu Y, Lei X, Jiao J. 2014. MicroRNA-15b promotes neurogenesis and inhibits neural progenitor proliferation by directly repressing TET3 during early neocortical development. *EMBO Rep* **15**: 1305-1314.

Macas J, Nern C, Plate KH, Momma S. 2006. Increased generation of neuronal progenitors after ischemic injury in the aged adult human forebrain. *J Neurosci* **26**: 13114-13119.

Mack SC, Taylor MD. 2009. The genetic and epigenetic basis of ependymoma. *Childs Nerv Syst* **25**: 1195-1201.

Maekawa M, Takashima N, Arai Y, Nomura T, Inokuchi K, Yuasa S, Osumi N. 2005. Pax6 is required for production and maintenance of progenitor cells in postnatal hippocampal neurogenesis. *Genes Cells* **10**: 1001-1014.

Magnusson JP, Goritz C, Tatarishvili J, Dias DO, Smith EM, Lindvall O, Kokaia Z, Frisen J. 2014. A latent neurogenic program in astrocytes regulated by Notch signaling in the mouse. *Science* **346**: 237-241.

Margueron R, Justin N, Ohno K, Sharpe ML, Son J, Drury WJ, 3rd, Voigt P, Martin SR, Taylor WR, De Marco V et al. 2009. Role of the polycomb protein EED in the propagation of repressive histone marks. *Nature* **461**: 762-767.

Margueron R, Li G, Sarma K, Blais A, Zavadil J, Woodcock CL, Dynlacht BD, Reinberg D. 2008. Ezh1 and Ezh2 maintain repressive chromatin through different mechanisms. *Mol Cell* **32**: 503-518.

Margueron R, Reinberg D. 2010. Chromatin structure and the inheritance of epigenetic information. *Nat Rev Genet* **11**: 285-296.

-. 2011. The Polycomb complex PRC2 and its mark in life. *Nature* **469**: 343-349.

Marques-Torrejon MA, Porlan E, Banito A, Gomez-Ibarlucea E, Lopez-Contreras AJ, Fernandez-Capetillo O, Vidal A, Gil J, Torres J, Farinas I. 2013. Cyclin-Dependent Kinase Inhibitor p21 Controls Adult Neural Stem Cell Expansion by Regulating Sox2 Gene Expression. *Cell Stem Cell* **12**: 88-100.

Marshall CA, Novitch BG, Goldman JE. 2005. Olig2 directs astrocyte and oligodendrocyte formation in postnatal subventricular zone cells. *J Neurosci* **25**: 7289-7298.

Marti-Fabregas J, Romaguera-Ros M, Gomez-Pinedo U, Martinez-Ramirez S, Jimenez-Xarrie E, Marin R, Marti-Vilalta JL, Garcia-Verdugo JM. 2010. Proliferation in the human ipsilateral subventricular zone after ischemic stroke. *Neurology* **74**: 357-365.

Martin C, Zhang Y. 2007. Mechanisms of epigenetic inheritance. *Curr Opin Cell Biol* **19**: 266-272.

Martinez R, Martin-Subero JI, Rohde V, Kirsch M, Alaminos M, Fernandez AF, Ropero S, Schackert G, Esteller M. 2009. A microarray-based DNA methylation study of glioblastoma multiforme. *Epigenetics : official journal of the DNA Methylation Society* **4**: 255-264.

Matsuda T, Cepko CL. 2007. Controlled expression of transgenes introduced by in vivo electroporation. *Proc Natl Acad Sci U S A* **104**: 1027-1032.

Matsushima GK, Morell P. 2001. The neurotoxicant, cuprizone, as a model to study demyelination and remyelination in the central nervous system. *Brain pathology* **11**: 107-116.

Mattick JS, Makunin IV. 2006. Non-coding RNA. *Hum Mol Genet* **15 Spec No 1**: R17-29.

Meissner A, Mikkelsen TS, Gu H, Wernig M, Hanna J, Sivachenko A, Zhang X, Bernstein BE, Nusbaum C, Jaffe DB et al. 2008. Genome-scale DNA methylation maps of pluripotent and differentiated cells. *Nature* **454**: 766-770.

Menn B, Garcia-Verdugo JM, Yaschine C, Gonzalez-Perez O, Rowitch D, Alvarez-Buylla A. 2006. Origin of oligodendrocytes in the subventricular zone of the adult brain. *J Neurosci* **26**: 7907-7918.

Mercer TR, Dinger ME, Mattick JS. 2009. Long non-coding RNAs: insights into functions. *Nature Reviews Genetics* **10**: 155-159.

Mercer TR, Dinger ME, Sunkin SM, Mehler MF, Mattick JS. 2008. Specific expression of long noncoding RNAs in the mouse brain. *Proc Natl Acad Sci U S A* **105**: 716-721.

Merini W, Calonje M. 2015. PRC1 is taking the lead in PcG repression. *The Plant journal : for cell and molecular biology*.

Mich JK, Signer RA, Nakada D, Pineda A, Burgess RJ, Vue TY, Johnson JE, Morrison SJ. 2014. Prospective identification of functionally distinct stem cells and neurosphere-initiating cells in adult mouse forebrain. *eLife* **3**: e02669.

Mikkelsen TS, Ku M, Jaffe DB, Issac B, Lieberman E, Giannoukos G, Alvarez P, Brockman W, Kim TK, Koche RP et al. 2007. Genome-wide maps of chromatin state in pluripotent and lineage-committed cells. *Nature* **448**: 553-560.

Ming GL, Song H. 2011. Adult neurogenesis in the mammalian brain: significant answers and significant questions. *Neuron* **70**: 687-702.

Mirzadeh Z, Merkle FT, Soriano-Navarro M, Garcia-Verdugo JM, Alvarez-Buylla A. 2008. Neural stem cells confer unique pinwheel architecture to the ventricular surface in neurogenic regions of the adult brain. *Cell Stem Cell* **3**: 265-278.

Mlechkovich G, Peng SS, Shacham V, Martinez E, Gokhman I, Minis A, Tran TS, Yaron A. 2014. Distinct Cytoplasmic Domains in Plexin-A4 Mediate Diverse Responses to Semaphorin 3A in Developing Mammalian Neurons. *Science signaling* **7**.

Mlynarczyk C, Fahraeus R. 2014. Endoplasmic reticulum stress sensitizes cells to DNA damage-induced apoptosis through p53-dependent suppression of p21(CDKN1A). *Nat Commun* **5**: 5067.

Mohd-Sarip A, Cleard F, Mishra RK, Karch F, Verrijzer CP. 2005. Synergistic recognition of an epigenetic DNA element by Pleiohomeotic and a Polycomb core complex. *Genes Dev* **19**: 1755-1760.

Molenaar JJ, Ebus ME, Koster J, Santo E, Geerts D, Versteeg R, Caron HN. 2010. Cyclin D1 is a direct transcriptional target of GATA3 in neuroblastoma tumor cells. *Oncogene* **29**: 2739-2745.

Molofsky AV, Pardal R, Iwashita T, Park IK, Clarke MF, Morrison SJ. 2003. Bmi-1 dependence distinguishes neural stem cell self-renewal from progenitor proliferation. *Nature* **425**: 962-967.

Montgomery ND, Yee D, Chen A, Kalantry S, Chamberlain SJ, Otte AP, Magnuson T. 2005. The murine polycomb group protein Eed is required for global histone H3 lysine-27 methylation. *Current Biology* **15**: 942-947.

Mori T, Tanaka K, Buffo A, Wurst W, Kuhn R, Gotz M. 2006. Inducible gene deletion in astroglia and radial glia--a valuable tool for functional and lineage analysis. *Glia* **54**: 21-34.

Morokuma J, Blackiston D, Adams DS, Seebohm G, Trimmer B, Levin M. 2008. Modulation of potassium channel function confers a hyperproliferative invasive phenotype on embryonic stem cells. *Proc Natl Acad Sci U S A* **105**: 16608-16613.

Morrisey EE. 2000. GATA-6: the proliferation stops here: cell proliferation in glomerular mesangial and vascular smooth muscle cells. *Circ Res* **87**: 638-640.

Murray TA, Levene MJ. 2012. Singlet gradient index lens for deep in vivo multiphoton microscopy. *Journal of biomedical optics* **17**: 021106.

Mysliwiec MR, Carlson CD, Tietjen J, Hung H, Ansari AZ, Lee Y. 2011. Jarid2 (JUMONJI, at rich interactive domain 2) regulates notch1 expression via histone modification in the developing heart. *J Biol Chem*.

Nagy A. 2000. Cre recombinase: the universal reagent for genome tailoring. *Genesis* **26**: 99-109.

Nam HS, Benezra R. 2009. High levels of Id1 expression define B1 type adult neural stem cells. *Cell Stem Cell* **5**: 515-526.

Neff T, Sinha AU, Kluk MJ, Zhu N, Khattab MH, Stein L, Xie H, Orkin SH, Armstrong SA. 2012. Polycomb repressive complex 2 is required for MLL-AF9 leukemia. *Proc Natl Acad Sci U S A* **109**: 5028-5033.

Nesterova TB, Slobodyanyuk SY, Elisaphenko EA, Shevchenko AI, Johnston C, Pavlova ME, Rogozin IB, Kolesnikov NN, Brockdorff N, Zakian SM. 2001. Characterization of the genomic Xist locus in rodents reveals conservation of overall gene structure and tandem repeats but rapid evolution of unique sequence. *Genome Res* **11**: 833-849.

Nie M, Balda MS, Matter K. 2012. Stress- and Rho-activated ZO-1-associated nucleic acid binding protein binding to p21 mRNA mediates stabilization, translation, and cell survival. *Proc Natl Acad Sci U S A* **109**: 10897-10902.

Ninkovic J, Steiner-Mezzadri A, Jawerka M, Akinci U, Masserdotti G, Petricca S, Fischer J, von Holst A, Beckers J, Lie CD et al. 2013. The BAF Complex Interacts with Pax6 in Adult Neural Progenitors to Establish a Neurogenic Cross-Regulatory Transcriptional Network. *Cell Stem Cell*.

Nishino J, Kim I, Chada K, Morrison SJ. 2008. Hmga2 promotes neural stem cell self-renewal in young but not old mice by reducing p16Ink4a and p19Arf Expression. *Cell* **135**: 227-239.

Nishiyama A, Komitova M, Suzuki R, Zhu XQ. 2009. Polydendrocytes (NG2 cells): multifunctional cells with lineage plasticity. *Nature Reviews Neuroscience* **10**: 9-22.

Niu W, Zang T, Smith DK, Vue TY, Zou Y, Bachoo R, Johnson JE, Zhang CL. 2015. SOX2 Reprograms Resident Astrocytes into Neural Progenitors in the Adult Brain. *Stem cell reports*.

Niu W, Zang T, Zou Y, Fang S, Smith DK, Bachoo R, Zhang CL. 2013. In vivo reprogramming of astrocytes to neuroblasts in the adult brain. *Nat Cell Biol*.

Ntziachristos P, Tsirigos A, Van Vlierberghe P, Nedjic J, Trimarchi T, Flaherty MS, Ferres-Marco D, da Ros V, Tang Z, Siegle J et al. 2012. Genetic inactivation of the polycomb repressive complex 2 in T cell acute lymphoblastic leukemia. *Nat Med* **18**: 298-301.

O'Carroll D, Erhardt S, Pagani M, Barton SC, Surani MA, Jenuwein T. 2001. The polycomb-group gene Ezh2 is required for early mouse development. *Mol Cell Biol* **21**: 4330-4336.

Okada A, Tomooka Y. 2012. Possible roles of Plexin-A4 in positioning of oligodendrocyte precursor cells in developing cerebral cortex. *Neuroscience Letters* **516**: 259-264.

-. 2013. A role of Sema6A expressed in oligodendrocyte precursor cells. *Neuroscience Letters* **539**: 48-53.

Okano H, Kawahara H, Toriya M, Nakao K, Shibata S, Imai T. 2005. Function of RNA-binding protein Musashi-1 in stem cells. *Experimental cell research* **306**: 349-356.

Okita K, Nagata N, Yamanaka S. 2011. Immunogenicity of induced pluripotent stem cells. *Circ Res* **109**: 720-721.

Oliver PL, Chodroff RA, Gosal A, Edwards B, Cheung AF, Gomez-Rodriguez J, Elliot G, Garrett LJ, Lickiss T, Szele F et al. 2014. Disruption of Visc-2, a Brain-Expressed Conserved Long Noncoding RNA, Does Not Elicit an Overt Anatomical or Behavioral Phenotype. *Cereb Cortex*.

Ono K, Tomasiewicz H, Magnuson T, Rutishauser U. 1994. N-CAM mutation inhibits tangential neuronal migration and is phenocopied by enzymatic removal of polysialic acid. *Neuron* **13**: 595-609.

Orr BA, Haffner MC, Nelson WG, Yegnasubramanian S, Eberhart CG. 2012. Decreased 5-Hydroxymethylcytosine Is Associated with Neural Progenitor Phenotype in Normal Brain and Shorter Survival in Malignant Glioma. *Plos One* **7**.

Paez-Gonzalez P, Abdi K, Luciano D, Liu Y, Soriano-Navarro M, Rawlins E, Bennett V, Garcia-Verdugo JM, Kuo CT. 2011. Ank3-dependent SVZ niche assembly is required for the continued production of new neurons. *Neuron* **71**: 61-75.

Pandey RR, Mondal T, Mohammad F, Enroth S, Redrup L, Komorowski J, Nagano T, Mancini-Dinardo D, Kanduri C. 2008. Kcnq1ot1 antisense noncoding RNA mediates lineage-specific transcriptional silencing through chromatin-level regulation. *Mol Cell* **32**: 232-246.

Park DH, Hong SJ, Salinas RD, Liu SJ, Sun SW, Sgualdino J, Testa G, Matzuk MM, Iwamori N, Lim DA. 2014. Activation of Neuronal Gene Expression by the JMJD3 Demethylase Is Required for Postnatal and Adult Brain Neurogenesis. *Cell reports*.

Parras CM, Galli R, Britz O, Soares S, Galichet C, Battiste J, Johnson JE, Nakafuku M, Vescovi A, Guillemot F. 2004. Mash1 specifies neurons and oligodendrocytes in the postnatal brain. *EMBO J* **23**: 4495-4505.

Pasini D, Cloos PA, Walfridsson J, Olsson L, Bukowski JP, Johansen JV, Bak M, Tommerup N, Rappsilber J, Helin K. 2010. JARID2 regulates binding of the Polycomb repressive complex 2 to target genes in ES cells. *Nature* **464**: 306-310.

Pasque V, Tchieu J, Karnik R, Uyeda M, Dimashkie AS, Case D, Papp B, Bonora G, Patel S, Ho R et al. 2014. X Chromosome Reactivation Dynamics Reveal Stages of Reprogramming to Pluripotency. *Cell* **159**: 1681-1697.

Pastrana E, Cheng LC, Doetsch F. 2009. Simultaneous prospective purification of adult subventricular zone neural stem cells and their progeny. *Proc Natl Acad Sci U S A* **106**: 6387-6392.

Pastrana E, Silva-Vargas V, Doetsch F. 2011. Eyes wide open: a critical review of sphere-formation as an assay for stem cells. *Cell Stem Cell* **8**: 486-498.

Paul S, Kuo A, Schalch T, Vogel H, Joshua-Tor L, McCombie WR, Gozani O, Hammell M, Mills AA. 2013. Chd5 requires PHD-mediated histone 3 binding for tumor suppression. *Cell reports* **3**: 92-102.

Peng HW, Ke XX, Hu RJ, Yang LQ, Cui HJ, Wei YQ. 2015. Essential role of GATA3 in regulation of differentiation and cell proliferation in SK-N-SH neuroblastoma cells. *Mol Med Rep* **11**: 881-886.

Peng JC, Valouev A, Swigut T, Zhang J, Zhao Y, Sidow A, Wysocka J. 2009. Jarid2/Jumonji coordinates control of PRC2 enzymatic activity and target gene occupancy in pluripotent cells. *Cell* **139**: 1290-1302.

Pereira JD, Sansom SN, Smith J, Dobenecker MW, Tarakhovsky A, Livesey FJ. 2010. Ezh2, the histone methyltransferase of PRC2, regulates the balance

between self-renewal and differentiation in the cerebral cortex. *P Natl Acad Sci USA* **107**: 15957-15962.

Perlman H, Suzuki E, Simonson M, Smith RC, Walsh K. 1998. GATA-6 induces p21(Cip1) expression and G1 cell cycle arrest. *J Biol Chem* **273**: 13713-13718.

Petrik D, Yun S, Latchney SE, Kamrudin S, LeBlanc JA, Bibb JA, Eisch AJ. 2013. Early postnatal in vivo gliogenesis from nestin-lineage progenitors requires cdk5. *Plos One* **8**: e72819.

Petryniak MA, Potter GB, Rowitch DH, Rubenstein JL. 2007. Dlx1 and Dlx2 control neuronal versus oligodendroglial cell fate acquisition in the developing forebrain. *Neuron* **55**: 417-433.

Piccolo FM, Fisher AG. 2014. Getting rid of DNA methylation. *Trends Cell Biol* **24**: 136-143.

Ponti G, Obernier K, Guinto C, Jose L, Bonfanti L, Alvarez-Buylla A. 2013. Cell cycle and lineage progression of neural progenitors in the ventricular-subventricular zones of adult mice. *Proc Natl Acad Sci U S A* **110**: E1045-1054.

Ponting CP, Belgard TG. 2010. Transcribed dark matter: meaning or myth? *Hum Mol Genet* **19**: R162-168.

Ponting CP, Oliver PL, Reik W. 2009. Evolution and Functions of Long Noncoding RNAs. *Cell* **136**: 629-641.

Porlan E, Morante-Redolat JM, Marques-Torrejon MA, Andreu-Agullo C, Carneiro C, Gomez-Ibarlucea E, Soto A, Vidal A, Ferron SR, Farinas I. 2013. Transcriptional repression of Bmp2 by p21(Waf1/Cip1) links quiescence to neural stem cell maintenance. *Nat Neurosci* **16**: 1567-1575.

Price JD, Park KY, Chen J, Salinas RD, Cho MJ, Kriegstein AR, Lim DA. 2014. The Ink4a/Arf locus is a barrier to direct neuronal transdifferentiation. *J Neurosci* **34**: 12560-12567.

Puget S, Grill J, Valent A, Bieche I, Dantas-Barbosa C, Kauffmann A, Dessen P, Lacroix L, Geoerger B, Job B et al. 2009. Candidate genes on chromosome 9q33-34 involved in the progression of childhood ependymomas. *J Clin Oncol* **27**: 1884-1892.

Quinones-Hinojosa A, Chaichana K. 2007. The human subventricular zone: A source of new cells and a potential source of brain tumors. *Experimental Neurology* **205**: 313-324.

Quinones-Hinojosa A, Sanai N, Soriano-Navarro M, Gonzalez-Perez O, Mirzadeh Z, Gil-Perotin S, Romero-Rodriguez R, Berger MS, Garcia-Verdugo JM,

Alvarez-Buylla A. 2006. Cellular composition and cytoarchitecture of the adult human subventricular zone: a niche of neural stem cells. *J Comp Neurol* **494**: 415-434.

Ramaswamy S, Goings GE, Soderstrom KE, Szele FG, Kozlowski DA. 2005. Cellular proliferation and migration following a controlled cortical impact in the mouse. *Brain Res* **1053**: 38-53.

Ramos AD, Andersen RE, Liu SJ, Nowakowski TJ, Hong SJ, Gertz CC, Salinas RD, Zarabi H, Kriegstein AR, Lim DA. 2015. The long noncoding RNA Pnky regulates neuronal differentiation of embryonic and postnatal neural stem cells. *Cell Stem Cell* **16**: 439-447.

Ramos AD, Diaz A, Nellore A, Delgado RN, Park KY, Gonzales-Roybal G, Oldham MC, Song JS, Lim DA. 2013. Integration of Genome-wide Approaches Identifies lncRNAs of Adult Neural Stem Cells and Their Progeny In Vivo. *Cell Stem Cell* **12**: 616-628.

Rapicavoli NA, Poth EM, Blackshaw S. 2010. The long noncoding RNA RNCR2 directs mouse retinal cell specification. *BMC Dev Biol* **10**: 49.

Raponi E, Agenes F, Delphin C, Assard N, Baudier J, Legraverend C, Deloulme JC. 2007. S100B expression defines a state in which GFAP-expressing cells lose their neural stem cell potential and acquire a more mature developmental stage. *Glia* **55**: 165-177.

Redrup L, Branco MR, Perdeaux ER, Krueger C, Lewis A, Santos F, Nagano T, Cobb BS, Fraser P, Reik W. 2009. The long noncoding RNA Kcnq1ot1 organises a lineage-specific nuclear domain for epigenetic gene silencing. *Development* **136**: 525-530.

Rheinbay E, Suva ML, Gillespie SM, Wakimoto H, Patel AP, Shahid M, Oksuz O, Rabkin SD, Martuza RL, Rivera MN et al. 2013. An Aberrant Transcription Factor Network Essential for Wnt Signaling and Stem Cell Maintenance in Glioblastoma. *Cell reports*.

Riccio A. 2010. Dynamic epigenetic regulation in neurons: enzymes, stimuli and signaling pathways. *Nature Neuroscience* **13**: 1330-1337.

Riising EM, Comet I, Leblanc B, Wu X, Johansen JV, Helin K. 2014. Gene Silencing Triggers Polycomb Repressive Complex 2 Recruitment to CpG Islands Genome Wide. *Mol Cell*.

Ringrose L, Paro R. 2004. Epigenetic regulation of cellular memory by the Polycomb and Trithorax group proteins. *Annu Rev Genet* **38**: 413-443.

Rinn JL, Kertesz M, Wang JK, Squazzo SL, Xu X, Brugmann SA, Goodnough LH, Helms JA, Farnham PJ, Segal E et al. 2007. Functional demarcation of

active and silent chromatin domains in human HOX loci by noncoding RNAs. *Cell* **129**: 1311-1323.

Risher WC, Eroglu C. 2012. Thrombospondins as key regulators of synaptogenesis in the central nervous system. *Matrix biology : journal of the International Society for Matrix Biology* **31**: 170-177.

Robel S, Berninger B, Gotz M. 2011. The stem cell potential of glia: lessons from reactive gliosis. *Nat Rev Neurosci* **12**: 88-104.

Roberts A, Trapnell C, Donaghey J, Rinn JL, Pachter L. 2011. Improving RNA-Seq expression estimates by correcting for fragment bias. *Genome Biology* **12**.

Robins SC, Stewart I, McNay DE, Taylor V, Giachino C, Goetz M, Ninkovic J, Briancon N, Maratos-Flier E, Flier JS et al. 2013. alpha-Tanycytes of the adult hypothalamic third ventricle include distinct populations of FGF-responsive neural progenitors. *Nat Commun* **4**: 2049.

Romine J, Gao X, Chen J. 2014. Controlled cortical impact model for traumatic brain injury. *J Vis Exp*: e51781.

Royo H, Cavaille J. 2008. Non-coding RNAs in imprinted gene clusters. *Biology of the cell / under the auspices of the European Cell Biology Organization* **100**: 149-166.

Sakakibara S, Okano H. 1997. Expression of neural RNA-binding proteins in the postnatal CNS: Implications of their roles in neuronal and glial cell development. *Journal of Neuroscience* **17**: 8300-8312.

Sakurai K, Osumi N. 2008. The neurogenesis-controlling factor, Pax6, inhibits proliferation and promotes maturation in murine astrocytes. *Journal of Neuroscience* **28**: 4604-4612.

Sanai N, Alvarez-Buylla A, Berger MS. 2005. Neural stem cells and the origin of gliomas. *N Engl J Med* **353**: 811-822.

Sanai N, Berger MS, Garcia-Verdugo JM, Alvarez-Buylla A. 2007. Comment on "Human neuroblasts migrate to the olfactory bulb via a lateral ventricular extension". *Science* **318**: 393; author reply 393.

Sanai N, Nguyen T, Ihrie RA, Mirzadeh Z, Tsai HH, Wong M, Gupta N, Berger MS, Huang E, Garcia-Verdugo JM et al. 2011. Corridors of migrating neurons in the human brain and their decline during infancy. *Nature* **478**: 382-386.

Sanai N, Tramontin AD, Quinones-Hinojosa A, Barbaro NM, Gupta N, Kunwar S, Lawton MT, McDermott MW, Parsa AT, Manuel-Garcia Verdugo J et al. 2004. Unique astrocyte ribbon in adult human brain contains neural stem cells but lacks chain migration. *Nature* **427**: 740-744.

Sandberg CJ, Vik-Mo EO, Behnan J, Helseth E, Langmoen IA. 2014. Transcriptional Profiling of Adult Neural Stem-Like Cells from the Human Brain. *Plos One* **9**.

Sander JD, Joung JK. 2014. CRISPR-Cas systems for editing, regulating and targeting genomes. *Nature biotechnology* **32**: 347-355.

Sauvageau M, Goff LA, Lodato S, Bonev B, Groff AF, Gerhardinger C, Sanchez-Gomez DB, Hacisuleyman E, Li E, Spence M et al. 2013. Multiple knockout mouse models reveal lincRNAs are required for life and brain development. *eLife* **2**: e01749.

Schepers AG, Snippert HJ, Stange DE, van den Born M, van Es JH, van de Wetering M, Clevers H. 2012. Lineage tracing reveals Lgr5+ stem cell activity in mouse intestinal adenomas. *Science* **337**: 730-735.

Schuettengruber B, Chourrout D, Vervoort M, Leblanc B, Cavalli G. 2007. Genome regulation by polycomb and trithorax proteins. *Cell* **128**: 735-745.

Schumacher A, Faust C, Magnuson T. 1996. Positional cloning of a global regulator of anterior-posterior patterning in mice. *Nature* **384**: 648.

Schwartz YB, Pirrotta V. 2014. Ruled by Ubiquitylation: A New Order for Polycomb Recruitment. *Cell reports* **8**: 321-325.

Scoumanne A, Cho SJ, Zhang J, Chen X. 2011. The cyclin-dependent kinase inhibitor p21 is regulated by RNA-binding protein PCBP4 via mRNA stability. *Nucleic Acids Res* **39**: 213-224.

Sheikh BN, Dixon MP, Thomas T, Voss AK. 2012. Querkopf is a key marker of self-renewal and multipotency of adult neural stem cells. *Journal of Cell Science* **125**: 295-309.

Shen X, Kim W, Fujiwara Y, Simon MD, Liu Y, Mysliwiec MR, Yuan GC, Lee Y, Orkin SH. 2009. Jumonji modulates polycomb activity and self-renewal versus differentiation of stem cells. *Cell* **139**: 1303-1314.

Shen X, Liu Y, Hsu YJ, Fujiwara Y, Kim J, Mao X, Yuan GC, Orkin SH. 2008. EZH1 mediates methylation on histone H3 lysine 27 and complements EZH2 in maintaining stem cell identity and executing pluripotency. *Mol Cell* **32**: 491-502.

Sher F, Boddeke E, Copray S. 2011. Ezh2 Expression in Astrocytes Induces Their Dedifferentiation Toward Neural Stem Cells. *Cell Reprogram* **13**: 1-6.

Sher F, Boddeke E, Olah M, Copray S. 2012. Dynamic changes in Ezh2 gene occupancy underlie its involvement in neural stem cell self-renewal and differentiation towards oligodendrocytes. *Plos One* **7**: e40399.

Sher F, Rossler R, Brouwer N, Balasubramaniyan V, Boddeke E, Copray S. 2008. Differentiation of Neural Stem Cells into Oligodendrocytes: Involvement of the Polycomb Group Protein Ezh2. *Stem Cells* **26**: 2875-2883.

Shi HL, Ding HF. 2009. GATA3 regulation of human neuroblastoma stem cell activity. *Faseb J* **23**.

Shi L, Cheng ZH, Zhang JX, Li R, Zhao P, Fu Z, You YP. 2008. hsa-mir-181a and hsa-mir-181b function as tumor suppressors in human glioma cells. *Brain Research* **1236**: 185-193.

Shibata M, Kurokawa D, Nakao H, Ohmura T, Aizawa S. 2008. MicroRNA-9 modulates Cajal-Retzius cell differentiation by suppressing Foxg1 expression in mouse medial pallium. *J Neurosci* **28**: 10415-10421.

Shibata M, Nakao H, Kiyonari H, Abe T, Aizawa S. 2011. MicroRNA-9 regulates neurogenesis in mouse telencephalon by targeting multiple transcription factors. *J Neurosci* **31**: 3407-3422.

Shimada IS, LeComte MD, Granger JC, Quinlan NJ, Spees JL. 2012. Self-renewal and differentiation of reactive astrocyte-derived neural stem/progenitor cells isolated from the cortical peri-infarct area after stroke. *J Neurosci* **32**: 7926-7940.

Shin YJ, Kim JH. 2012. The role of EZH2 in the regulation of the activity of matrix metalloproteinases in prostate cancer cells. *Plos One* **7**: e30393.

Shirato H, Ogawa S, Nakajima K, Inagawa M, Kojima M, Tachibana M, Shinkai Y, Takeuchi T. 2009. A jumonji (Jarid2) protein complex represses cyclin D1 expression by methylation of histone H3-K9. *J Biol Chem* **284**: 733-739.

Siebzehnrubl FA, Buslei R, Eyupoglu IY, Seufert S, Hahnen E, Blumcke I. 2007. Histone deacetylase inhibitors increase neuronal differentiation in adult forebrain precursor cells. *Exp Brain Res* **176**: 672-678.

Simon C, Chagraoui J, Krosl J, Gendron P, Wilhelm B, Lemieux S, Boucher G, Chagnon P, Drouin S, Lambert R et al. 2012. A key role for EZH2 and associated genes in mouse and human adult T-cell acute leukemia. *Genes Dev* **26**: 651-656.

Singec I, Knoth R, Meyer RP, Maciaczyk J, Volk B, Nikkhah G, Frotscher M, Snyder EY. 2006. Defining the actual sensitivity and specificity of the neurosphere assay in stem cell biology. *Nat Methods* **3**: 801-806.

Sirko S, Behrendt G, Johansson PA, Tripathi P, Costa M, Bek S, Heinrich C, Tiedt S, Colak D, Dichgans M et al. 2013. Reactive glia in the injured brain acquire stem cell properties in response to sonic hedgehog glia. *Cell Stem Cell* **12**: 426-439.

Sirko S, Neitz A, Mittmann T, Horvat-Brocker A, von Holst A, Eysel UT, Faissner A. 2009. Focal laser-lesions activate an endogenous population of neural stem/progenitor cells in the adult visual cortex. *Brain : a journal of neurology* **132**: 2252-2264.

Skiriute D, Vaitkiene P, Saferis V, Asmoniene V, Skauminas K, Deltuva VP, Tamasauskas A. 2012. MGMT, GATA6, CD81, DR4, and CASP8 gene promoter methylation in glioblastoma. *BMC cancer* **12**: 218.

Soderberg O, Gullberg M, Jarvius M, Ridderstrale K, Leuchowius KJ, Jarvius J, Wester K, Hydbring P, Bahram F, Larsson LG et al. 2006. Direct observation of individual endogenous protein complexes in situ by proximity ligation. *Nat Methods* **3**: 995-1000.

Sone M, Hayashi T, Tarui H, Agata K, Takeichi M, Nakagawa S. 2007. The mRNA-like noncoding RNA Gomafu constitutes a novel nuclear domain in a subset of neurons. *J Cell Sci* **120**: 2498-2506.

Song MR, Ghosh A. 2004. FGF2-induced chromatin remodeling regulates CNTF-mediated gene expression and astrocyte differentiation. *Nat Neurosci* **7**: 229-235.

Spassky N, Merkle FT, Flames N, Tramontin AD, Garcia-Verdugo JM, Alvarez-Buylla A. 2005. Adult ependymal cells are postmitotic and are derived from radial glial cells during embryogenesis. *J Neurosci* **25**: 10-18.

Steffen PA, Ringrose L. 2014. What are memories made of ? How Polycomb and Trithorax proteins mediate epigenetic memory. *Nat Rev Mol Cell Bio* **15**: 340-356.

Steiner LA, Schulz VP, Maksimova Y, Wong C, Gallagher PG. 2011. Patterns of histone H3 lysine 27 monomethylation and erythroid cell type-specific gene expression. *J Biol Chem* **286**: 39457-39465.

Stojic L, Jasencakova Z, Prezioso C, Stutzer A, Bodega B, Pasini D, Klingberg R, Mozzetta C, Margueron R, Puri PL et al. 2011. Chromatin regulated interchange between polycomb repressive complex 2 (PRC2)-Ezh2 and PRC2-Ezh1 complexes controls myogenin activation in skeletal muscle cells. *Epigenetics & chromatin* **4**: 16.

Struhl K. 2007. Transcriptional noise and the fidelity of initiation by RNA polymerase II. *Nat Struct Mol Biol* **14**: 103-105.

Su IH, Basavaraj A, Krutchinsky AN, Hobert O, Ullrich A, Chait BT, Tarakhovsky A. 2003. Ezh2 controls B cell development through histone H3 methylation and Igh rearrangement. *Nat Immunol* **4**: 124-131.

Su Z, Niu W, Liu ML, Zou Y, Zhang CL. 2014. In vivo conversion of astrocytes to neurons in the injured adult spinal cord. *Nat Commun* **5**: 3338.

Sundholm-Peters NL, Yang HK, Goings GE, Walker AS, Szele FG. 2005. Subventricular zone neuroblasts emigrate toward cortical lesions. *J Neuropathol Exp Neurol* **64**: 1089-1100.

Suto F, Ito K, Uemura M, Shimizu M, Shinkawa Y, Sanbo M, Shinoda T, Tsuboi M, Takashima S, Yagi T et al. 2005. Plexin-A4 mediates axon-repulsive activities of both secreted and transmembrane semaphorins and plays roles in nerve fiber guidance. *Journal of Neuroscience* **25**: 3628-3637.

Swigut T, Wysocka J. 2007. H3K27 demethylases, at long last. *Cell* **131**: 29-32.

Szele FG, Alexander C, Chesselet MF. 1995. Expression of molecules associated with neuronal plasticity in the striatum after aspiration and thermocoagulatory lesions of the cerebral cortex in adult rats. *J Neurosci* **15**: 4429-4448.

Szele FG, Cepko CL. 1996. A subset of clones in the chick telencephalon arranged in rostrocaudal arrays. *Curr Biol* **6**: 1685-1690.

Szele FG, Cepko CL. 1998. The dispersion of clonally related cells in the developing chick telencephalon. *Dev Biol* **195**: 100-113.

Szele FG, Chesselet MF. 1996. Cortical lesions induce an increase in cell number and PSA-NCAM expression in the subventricular zone of adult rats. *J Comp Neurol* **368**: 439-454.

Takahashi K, Yamanaka S. 2006. Induction of pluripotent stem cells from mouse embryonic and adult fibroblast cultures by defined factors. *Cell* **126**: 663-676.

Tan JZ, Yan Y, Wang XX, Jiang Y, Xu HE. 2014. EZH2: biology, disease, and structure-based drug discovery. *Acta pharmacologica Sinica* **35**: 161-174.

Tang LL, Nogales E, Ciferri C. 2010. Structure and function of SWI/SNF chromatin remodeling complexes and mechanistic implications for transcription. *Prog Biophys Mol Bio* **102**: 122-128.

Taranova OV, Magness ST, Fagan BM, Wu YQ, Surzenko N, Hutton SR, Pevny LH. 2006. SOX2 is a dose-dependent regulator of retinal neural progenitor competence. *Gene Dev* **20**: 1187-1202.

Tatton-Brown K, Hanks S, Ruark E, Zachariou A, Duarte Sdel V, Ramsay E, Snape K, Murray A, Perdeaux ER, Seal S et al. 2011. Germline mutations in the oncogene EZH2 cause Weaver syndrome and increased human height. *Oncotarget* **2**: 1127-1133.

Tatton-Brown K, Murray A, Hanks S, Douglas J, Armstrong R, Banka S, Bird LM, Clericuzio CL, Cormier-Daire V, Cushing T et al. 2013. Weaver syndrome and EZH2 mutations: Clarifying the clinical phenotype. *Am J Med Genet A*.

Tavares L, Dimitrova E, Oxley D, Webster J, Poot R, Demmers J, Bezstarosti K, Taylor S, Ura H, Koide H et al. 2012. RYBP-PRC1 complexes mediate H2A ubiquitylation at polycomb target sites independently of PRC2 and H3K27me3. *Cell* **148**: 664-678.

Tester DJ, Ackerman MJ. 2014. Genetics of long QT syndrome. *Methodist DeBakey cardiovascular journal* **10**: 29-33.

Tian Y, Zhang Y, Hurd L, Hannenhalli S, Liu F, Lu MM, Morrisey EE. 2011. Regulation of lung endoderm progenitor cell behavior by miR302/367. *Development* **138**: 1235-1245.

Timchenko NA, Wilde M, Nakanishi M, Smith JR, Darlington GJ. 1996. CCAAT/enhancer-binding protein alpha C/EBP alpha inhibits cell proliferation through the p21 (WAF-1/CIP-1/SDI-1) protein. *Gene Dev* **10**: 804-815.

Tomasiewicz H, Ono K, Yee D, Thompson C, Goridis C, Rutishauser U, Magnuson T. 1993. Genetic deletion of a neural cell adhesion molecule variant (N-CAM-180) produces distinct defects in the central nervous system. *Neuron* **11**: 1163-1174.

Tonchev AB, Yamashima T, Chaldakov GN. 2007. Distribution and phenotype of proliferating cells in the forebrain of adult macaque monkeys after transient global cerebral ischemia. *Advances in anatomy, embryology, and cell biology* **191**: 1-106.

Tonchev AB, Yamashima T, Sawamoto K, Okano H. 2005. Enhanced proliferation of progenitor cells in the subventricular zone and limited neuronal production in the striatum and neocortex of adult macaque monkeys after global cerebral ischemia. *J Neurosci Res* **81**: 776-788.

Trichas G, Begbie J, Srinivas S. 2008. Use of the viral 2A peptide for bicistronic expression in transgenic mice. *BMC Biol* **6**: 40.

Tumbar T, Guasch G, Greco V, Blanpain C, Lowry WE, Rendl M, Fuchs E. 2004. Defining the epithelial stem cell niche in skin. *Science* **303**: 359-363.

Tuoc TC, Boretius S, Sansom SN, Pitulescu ME, Frahm J, Livesey FJ, Stoykova A. 2013. Chromatin Regulation by BAF170 Controls Cerebral Cortical Size and Thickness. *Dev Cell* **25**: 256-269.

Ura H, Murakami K, Akagi T, Kinoshita K, Yamaguchi S, Masui S, Niwa H, Koide H, Yokota T. 2011. Eed/Sox2 regulatory loop controls ES cell self-renewal through histone methylation and acetylation. *EMBO J* **30**: 2190-2204.

Vance KW, Ponting CP. 2014. Transcriptional regulatory functions of nuclear long noncoding RNAs. *Trends in genetics : TIG* **30**: 348-355.

Vance KW, Sansom SN, Lee S, Chalei V, Kong L, Cooper SE, Oliver PL, Ponting CP. 2014. The long non-coding RNA Paupar regulates the expression of both local and distal genes. *EMBO J* **33**: 296-311.

Voigt P, Reinberg D. 2013. Putting a halt on PRC2 in pediatric glioblastoma. *Nat Genet* **45**: 587-589.

Waddington CH. 2012. The epigenotype. 1942. *Int J Epidemiol* **41**: 10-13.

Wang C, Liu F, Liu YY, Zhao CH, You Y, Wang L, Zhang J, Wei B, Ma T, Zhang Q et al. 2011. Identification and characterization of neuroblasts in the subventricular zone and rostral migratory stream of the adult human brain. *Cell Res* **21**: 1534-1550.

Wang GG, Allis CD, Chi P. 2007. Chromatin remodeling and cancer, Part II: ATP-dependent chromatin remodeling. *Trends in molecular medicine* **13**: 373-380.

Wang L, Liu ZY, Balivada S, Shrestha T, Bossmann S, Pyle M, Pappan L, Shi JS, Troyer D. 2012. Interleukin-1 beta and transforming growth factor-beta cooperate to induce neurosphere formation and increase tumorigenicity of adherent LN-229 glioma cells. *Stem Cell Res Ther* **3**.

Wang LP, Cheung G, Kronenberg G, Gertz K, Ji SB, Kempermann G, Endres M, Kettenmann H. 2008a. Two Types of Astrocytic Cell in the adult striatum. *2008 International Special Topic Conference on Information Technology and Applications in Biomedicine, Vols 1 and 2*: 546-550.

Wang Y, Baskerville S, Shenoy A, Babiarz JE, Baehner L, Blelloch R. 2008b. Embryonic stem cell-specific microRNAs regulate the G1-S transition and promote rapid proliferation. *Nat Genet* **40**: 1478-1483.

Warren N, Caric D, Pratt T, Clausen JA, Asavaritikrai P, Mason JO, Hill RE, Price DJ. 1999. The transcription factor, Pax6, is required for cell proliferation and differentiation in the developing cerebral cortex. *Cerebral Cortex* **9**: 627-635.

Weinandy F, Ninkovic J, Gotz M. 2011. Restrictions in time and space--new insights into generation of specific neuronal subtypes in the adult mammalian brain. *Eur J Neurosci* **33**: 1045-1054.

Wilson RC, Doudna JA. 2013. Molecular mechanisms of RNA interference. *Annual review of biophysics* **42**: 217-239.

Woodhead GJ, Mutch CA, Olson EC, Chenn A. 2006. Cell-autonomous beta-catenin signaling regulates cortical precursor proliferation. *J Neurosci* **26**: 12620-12630.

Wu G, Broniscer A, McEachron TA, Lu C, Paugh BS, Becksfort J, Qu C, Ding L, Huether R, Parker M et al. 2012. Somatic histone H3 alterations in pediatric diffuse intrinsic pontine gliomas and non-brainstem glioblastomas. *Nat Genet* **44**: 251-253.

Wu SC, Kallin EM, Zhang Y. 2010. Role of H3K27 methylation in the regulation of lncRNA expression. *Cell Res* **20**: 1109-1116.

Wurm S, Zhang J, Guinea-Viniegra J, Garcia F, Munoz J, Bakiri L, Ezhkova E, Wagner EF. 2014. Terminal epidermal differentiation is regulated by the interaction of Fra-2/AP-1 with Ezh2 and ERK1/2. *Genes Dev*.

Xia T, Liao Q, Jiang X, Shao Y, Xiao B, Xi Y, Guo J. 2014. Long noncoding RNA associated-competing endogenous RNAs in gastric cancer. *Scientific reports* **4**: 6088.

Xie H, Xu J, Hsu JH, Nguyen M, Fujiwara Y, Peng C, Orkin SH. 2013. Polycomb Repressive Complex 2 Regulates Normal Hematopoietic Stem Cell Function in a Developmental-Stage-Specific Manner. *Cell Stem Cell*.

Xu CH, Hou ZB, Zhan P, Zhao W, Chang CJ, Zou J, Hu HD, Zhang YQ, Yao X, Yu LK et al. 2013. EZH2 regulates cancer cell migration through repressing TIMP-3 in non-small cell lung cancer. *Med Oncol* **30**.

Xue Y, Ouyang K, Huang J, Zhou Y, Ouyang H, Li H, Wang G, Wu Q, Wei C, Bi Y et al. 2013. Direct conversion of fibroblasts to neurons by reprogramming PTB-regulated microRNA circuits. *Cell* **152**: 82-96.

Yadavilli S, Scafidi J, Becher OJ, Saratsis AM, Hiner RL, Kambhampati M, Mariarita S, MacDonald TJ, Codispoti KE, Magge SN et al. 2015. The emerging role of NG2 in pediatric diffuse intrinsic pontine glioma. *Oncotarget*.

Yadirgi G, Leinster V, Acquati S, Bhagat H, Shakhova O, Marino S. 2011. Conditional activation of Bmi1 expression regulates self-renewal, apoptosis, and differentiation of neural stem/progenitor cells in vitro and in vivo. *Stem Cells* **29**: 700-712.

Yang C, Bratzel F, Hohmann N, Koch M, Turck F, Calonje M. 2013. VAL- and AtBMI1-mediated H2Aub initiate the switch from embryonic to postgerminative growth in Arabidopsis. *Curr Biol* **23**: 1324-1329.

Yang W, Xia Y, Hawke D, Li X, Liang J, Xing D, Aldape K, Hunter T, Alfred Yung WK, Lu Z. 2012. PKM2 phosphorylates histone H3 and promotes gene transcription and tumorigenesis. *Cell* **150**: 685-696.

Yin Y, Yan P, Lu J, Song G, Zhu Y, Li Z, Zhao Y, Shen B, Huang X, Zhu H et al. 2015. Opposing Roles for the lncRNA Haunt and Its Genomic Locus in Regulating HOXA Gene Activation during Embryonic Stem Cell Differentiation. *Cell Stem Cell* **16**: 504-516.

Yoshiya K, Tanaka H, Kasai K, Irisawa T, Shiozaki T, Sugimoto H. 2003. Profile of gene expression in the subventricular zone after traumatic brain injury. *J Neurotrauma* **20**: 1147-1162.

Young CC, Al-Dalahmah O, Lewis NJ, Brooks KJ, Jenkins MM, Poirier F, Buchan AM, Szele FG. 2014. Blocked angiogenesis in Galectin-3 null mice does not alter cellular and behavioral recovery after middle cerebral artery occlusion stroke. *Neurobiology of disease* **63**: 155-164.

Young CC, Brooks KJ, Buchan AM, Szele FG. 2011. Cellular and molecular determinants of stroke-induced changes in subventricular zone cell migration. *Antioxid Redox Signal* **14**: 1877-1888.

Young CC, van der Harg JM, Lewis NJ, Brooks KJ, Buchan AM, Szele FG. 2012. Ependymal Ciliary Dysfunction and Reactive Astrocytosis in a Reorganized Subventricular Zone after Stroke. *Cereb Cortex*.

Yun SJ, Kim MO, Kim SO, Park J, Kwon YK, Kim IS, Lee EH. 2002. Induction of TGF-beta-inducible gene-h3 (betaig-h3) by TGF-beta1 in astrocytes: implications for astrocyte response to brain injury. *Brain Res Mol Brain Res* **107**: 57-64.

Zamanian JL, Xu L, Foo LC, Nouri N, Zhou L, Giffard RG, Barres BA. 2012. Genomic analysis of reactive astrogliosis. *J Neurosci* **32**: 6391-6410.

Zaratiegui M, Irvine DV, Martienssen RA. 2007. Noncoding RNAs and gene silencing. *Cell* **128**: 763-776.

Zhang J, Ji F, Liu Y, Lei X, Li H, Ji G, Yuan Z, Jiao J. 2014. Ezh2 regulates adult hippocampal neurogenesis and memory. *J Neurosci* **34**: 5184-5199.

Zhang JX, Han L, Bao ZS, Wang YY, Chen LY, Yan W, Yu SZ, Pu PY, Liu N, You YP et al. 2013a. HOTAIR, a cell cycle-associated long noncoding RNA and a strong predictor of survival, is preferentially expressed in classical and mesenchymal glioma. *Neuro Oncol* **15**: 1595-1603.

Zhang K, Sridhar VV, Zhu J, Kapoor A, Zhu JK. 2007a. Distinctive core histone post-translational modification patterns in Arabidopsis thaliana. *Plos One* **2**: e1210.

Zhang KL, Sun XT, Zhou X, Han L, Chen LY, Shi ZD, Zhang AL, Ye MH, Wang QX, Liu CY et al. 2015. Long non-coding RNA HOTAIR promotes glioblastoma cell cycle progression in an EZH2 dependent manner. *Oncotarget* **6**: 537-546.

Zhang R, Zhang Z, Zhang C, Zhang L, Robin A, Wang Y, Lu M, Chopp M. 2004. Stroke transiently increases subventricular zone cell division from asymmetric to symmetric and increases neuronal differentiation in the adult rat. *J Neurosci* **24**: 5810-5815.

Zhang RL, Zhang ZG, Wang Y, LeTourneau Y, Liu XS, Zhang X, Gregg SR, Wang L, Chopp M. 2007b. Stroke induces ependymal cell transformation into radial glia in the subventricular zone of the adult rodent brain. *J Cereb Blood Flow Metab* **27**: 1201-1212.

Zhang RR, Cui QY, Murai K, Lim YC, Smith ZD, Jin S, Ye P, Rosa L, Lee YK, Wu HP et al. 2013b. Tet1 regulates adult hippocampal neurogenesis and cognition. *Cell Stem Cell* **13**: 237-245.

Zhang XQ, Sun S, Lam KF, Kiang KM, Pu JK, Ho AS, Lui WM, Fung CF, Wong TS, Leung GK. 2013c. A long non-coding RNA signature in glioblastoma multiforme predicts survival. *Neurobiology of disease* **58**: 123-131.

Zhao J, Sun BK, Erwin JA, Song JJ, Lee JT. 2008. Polycomb proteins targeted by a short repeat RNA to the mouse X chromosome. *Science* **322**: 750-756.

Zhao T, Zhang ZN, Rong Z, Xu Y. 2011. Immunogenicity of induced pluripotent stem cells. *Nature* **474**: 212-215.

Zhou Q, Anderson DJ. 2002. The bHLH transcription factors OLIG2 and OLIG1 couple neuronal and glial subtype specification. *Cell* **109**: 61-73.

Zhou W, Zhu P, Wang J, Pascual G, Ohgi KA, Lozach J, Glass CK, Rosenfeld MG. 2008. Histone H2A monoubiquitination represses transcription by inhibiting RNA polymerase II transcriptional elongation. *Mol Cell* **29**: 69-80.

Ziegler AN, Levison SW, Wood TL. 2015. Insulin and IGF receptor signalling in neural-stem-cell homeostasis. *Nat Rev Endocrinol* **11**: 161-170.